

**The impact of changing anthropogenic emissions on  
European atmospheric aerosols over the second half of the  
20<sup>th</sup> Century**

Steven Thomas Turnock

Submitted in accordance with the requirements for the degree of  
Doctor of Philosophy

The University of Leeds  
School of Earth and Environment

May 2016

## **Declaration of Authorship**

The candidate confirms that the work submitted is his own, except where work which has formed part of jointly-authored publications has been included. The contribution of the candidate and the other authors to this work has been explicitly indicated below. The candidate confirms that appropriate credit has been given within the thesis where reference has been made to the work of others.

Chapter 3 is the publication Turnock, S. T., Spracklen, D. V., Carslaw, K. S., Mann, G. W., Woodhouse, M. T., Forster, P. M., Haywood, J., Johnson, C. E., Dalvi, M., Bellouin, N., and Sanchez-Lorenzo, A.: Modelled and observed changes in aerosols and surface solar radiation over Europe between 1960 and 2009, *Atmos. Chem. Phys.*, 15, 9477-9500, doi:10.5194/acp-15-9477-2015, 2015. The manuscript was written by the candidate with advice from supervisors (D.V. Spracklen, K.S. Carslaw, P.M. Forster and J. Haywood) and comments from co-authors during its preparation. The analysis of model simulations and evaluation against observations was solely undertaken by the candidate. The set-up and running of the model simulations involved collaboration between the candidate, M.T. Woodhouse and G.W. Mann. Development of specific parts of the model version used in the paper was done by C. Johnson, M. Dalvi and N. Bellouin. Observations of surface solar radiation were provided by A. Sanchez-Lorenzo.

Chapter 4 is the draft manuscript Turnock, S. T., Mann, G. W., Woodhouse M.T., Carslaw, K. S. and Spracklen, D. V: The Spatial and Temporal Importance of Cloud Water pH to Global Sulfate Aerosols and their Radiative Effect over the period 1960 to 2009, (in prep), 2016). The manuscript was written by the candidate with advice from supervisors (D.V. Spracklen and K.S. Carslaw). The analysis of model simulations and evaluation against observations was solely undertaken by the candidate. The set-up and running of the model simulations involved collaboration between the candidate, M.T. Woodhouse and G.W. Mann.

Chapter 5 is the publication Turnock, S. T., Butt, E. W., Richardson, T. B., Mann, G. W., Reddington, C. L., Forster, P. M., Haywood, J., Crippa, M., Janssens-Maenhout, G., Johnson, C. E., Bellouin, N., Carslaw, K. S., and Spracklen, D. V: The impact of European legislative and technology measures to reduce air pollutants on air quality, human health and climate, *Environ. Res. Lett.*, 11(2), 024010, doi:10.1088/1748-9326/11/2/024010,

2016. The manuscript was written by the candidate with advice from supervisors (D.V. Spracklen, K.S. Carslaw and J. Haywood) and comments from co-authors during its preparation. The set-up of simulations and modification of input emissions, as well as the analysis of the model output, was solely done by the candidate with advice from G. W. Mann. E. Butt calculated the health impacts from the model output. T.B. Richardson and P.M. Forster provided advice on calculating the climate impact from the radiation changes between the two scenarios. M. Crippa and G. Janssens-Maenhout provided the emissions data for each scenario. Development of specific parts of the model version used in the paper was done by C. Johnson and N. Bellouin. C.L. Reddington provided the code for undertaking calculations of the urban contribution to  $PM_{2.5}$ .

This copy has been supplied on the understanding that it is copyright material and that no quotation from the thesis may be published without proper acknowledgement.

The right of Steven Thomas Turnock to be identified as Author of this work has been asserted by him in accordance with the Copyright, Designs and Patents Act 1988.

© 2016 The University of Leeds and Steven Thomas Turnock

## **Acknowledgements**

I would like to thank my lead supervisor Dominick Spracklen for all the help and advice that he provided to me throughout my PhD as I don't think I would have got this far without it. Also thanks goes to the contributions from my other supervisors Ken Carslaw, Piers Forster and Jim Haywood (at the Met office) for all the different reviews and guidance provided along the way.

Thanks should also go to the members of the aerosol modellers group for providing a good group forum for modelling support and also for reviews of presentations throughout different parts of my PhD. In particular, I would like to thank Graham Mann and Matt Woodhouse who helped me with a lot of different model related issues that I had in setting up and running the model during those early days. Also thanks to Ed Butt for providing the human health calculations and Tom Richardson for help and advice on the climate impacts from air quality legislation.

I would like to acknowledge the funding from NERC for my PhD and also the CASE funding from the Met Office. Also thanks should go to various people within the Met Office and wider modelling support community who have aided me at various points throughout my PhD.

Special thanks go to the members of my PhD year group (Douglas, Leighton, Joey, David and Hannah) for sharing with me the ups and the downs of doing a PhD at Leeds. Also thanks to anyone who has played sport (football, badminton and squash mainly) with me over the years.

Thanks all of my friends and family, especially my parents, for all their encouragement throughout the years. Finally the last and biggest thanks goes to my wife Laura and son Benjamin for all the help and support that you have provided me over the PhD years, as I definitely wouldn't have been able to get this far without you both.

## Abstract

Across Europe anthropogenic emissions have changed substantially over recent decades, due in part to the implementation of air pollution control legislation. It is important to understand the effect that such changes in emissions have on atmospheric aerosols and their impact on air quality and climate.

The composition climate model HadGEM3-UKCA and long term observations of aerosols are used to simulate and evaluate the change in aerosols over the period 1960 to 2009. Simulated sulphate mass, total aerosol mass and aerosol number concentrations from HadGEM3-UKCA were underestimated but temporal trends were in better agreement when compared to observations. The inclusion of aerosols was found to be essential when reproducing the observed brightening trend in surface solar radiation across Europe since 1990. The all-sky aerosol radiative forcing (relative to a 1980-2000 mean) increased by  $>3 \text{ W m}^{-2}$  during the period 1970-2009 due to reductions in aerosol concentrations.

The sensitivity of sulphate aerosol formation and aerosol radiative effects to an increase in cloud water pH were investigated over the period 1970 to 2009. Sulphate aerosol mass increased over regions with large  $\text{SO}_2$  emissions but decreased at other locations. A positive response in the all-sky aerosol radiative effect was simulated due to reductions in aerosol number concentrations. Over Europe the aerosol radiative forcing between 1970 and 2009 varied from  $+1.5$  to  $+7 \text{ W m}^{-2}$  depending on whether an increase or decrease in cloud water pH was assumed. This shows the additional uncertainty that could exist in aerosol radiative effects if temporal changes in such parameters are not considered.

Two emission scenarios have been used to assess the effect of European air quality legislation and technology improvements since the 1970s on particulate air quality, human health and climate. European annual mean  $\text{PM}_{2.5}$  concentrations reduced by 35% and are calculated to have prevented 80,000 premature deaths annually across the European Union, a perceived financial benefit to society of US\$232 billion. A positive response in the all-sky aerosol radiative effect was simulated, which has increased European annual mean surface temperatures by  $0.45 \text{ }^\circ\text{C}$ . The implementation of legislation and technology improvements has improved air quality and human health across Europe but also had an unintended impact on climate.

## Table of Contents

<b>Declaration of Authorship .....</b>	<b>ii</b>
<b>Acknowledgements.....</b>	<b>iv</b>
<b>Abstract.....</b>	<b>v</b>
<b>Table of Contents .....</b>	<b>vi</b>
<b>List of Tables .....</b>	<b>x</b>
<b>List of Figures .....</b>	<b>xii</b>
<b>Abbreviations .....</b>	<b>xix</b>
<b>Chapter 1 Introduction.....</b>	<b>1</b>
1.1 Air Quality and Human Health.....	2
1.1.1 Air Pollutants .....	2
1.1.2 Impacts on Health .....	3
1.1.3 Air Quality Legislation.....	4
1.2 Aerosol Radiative Effects and Climate .....	6
1.3 Anthropogenic Emission Trends .....	11
1.4 Long Term Aerosol Observations and Model Studies .....	14
1.5 Aerosols Processes affected by Emission Changes .....	18
1.5.1 Sources and Emissions.....	18
1.5.2 Chemical Composition .....	19
1.5.3 Microphysical Processes.....	22
1.5.4 Removal .....	23
1.6 Summary and Motivation.....	24
1.7 Thesis Aims and Objectives .....	26
1.8 References.....	28
<b>Chapter 2 Methods .....</b>	<b>40</b>
2.1 Introduction .....	40
2.2 The Chemistry Scheme.....	40
2.3 The Aerosol Model .....	42
2.3.1 Gas Phase and Primary Aerosol Emissions.....	42
2.3.2 Aerosol Microphysics .....	44
2.3.2.1 New Particle Formation .....	44
2.3.2.2 Coagulation .....	45
2.3.2.3 Condensation .....	45

2.3.2.4 In-cloud Oxidation/Cloud Processing .....	46
2.3.3 Removal Processes .....	47
2.3.3.1 Dry Deposition.....	47
2.3.3.2 Wet Deposition.....	47
2.4 The Climate Model .....	48
2.4.1 Aerosol Radiation Interactions .....	48
2.4.2 Aerosol Cloud Interactions .....	49
2.4.3 Set up of radiation scheme.....	50
2.5 Health Impacts .....	50
2.6 The Experiments.....	52
2.6.1 Time varying emissions 1960-2009.....	53
2.6.2 Alternative pH.....	54
2.6.3 European Air Quality Measures .....	54
2.7 Long Term Aerosol Observations over Europe .....	56
2.7.1 EMEP Observations.....	57
2.7.2 Aerosol Size distributions .....	60
2.7.3 AOD .....	61
2.7.4 Surface Solar Radiation .....	62
2.8 References.....	64
<b>Chapter 3 Modelled and Observed Changes in aerosols and surface solar radiation over Europe between 1960 and 2009 .....</b>	<b>73</b>
Abstract.....	74
3.1 Introduction .....	74
3.2 Methods .....	76
3.2.1 Model Description and Simulation.....	76
3.2.1.1 General .....	76
3.2.1.2 Aerosol Radiative Effects .....	77
3.2.1.3 Aerosol Emissions.....	77
3.2.2 Observations .....	78
3.2.2.1 EMEP Observations .....	78
3.2.2.2 Aerosol Size Distribution .....	78
3.2.2.3 AOD .....	78
3.2.2.4 Surface Solar Radiation .....	78
3.2.3 Model Evaluation Metrics .....	80
3.3 Results .....	80

3.3.1 Simulated European aerosols and surface solar radiation from 1960 to 2009 .....	80
3.3.2 Model Evaluation.....	81
3.3.2.1 Sulfate aerosol mass.....	81
3.3.2.2 Total aerosol mass.....	81
3.3.2.3 Aerosol size distribution .....	85
3.3.2.4 Aerosol optical depth.....	87
3.3.2.5 Surface solar radiation .....	87
3.3.2.6 Evaluation Summary .....	90
3.4 European aerosol radiative forcing.....	91
3.5 Conclusions.....	92
References.....	93
<b>Chapter 4 The spatial and temporal importance of pH to sulphate aerosols and radiative forcing over the period 1960 to 2009 .....</b>	<b>98</b>
Abstract.....	100
4.1 Introduction .....	100
4.2 Materials and Methods.....	103
4.2.1 HadGEM3-UKCA composition-climate model.....	103
4.2.2 Sulphate aerosol formation in HadGEM3-UKCA.....	104
4.2.3 Simulations.....	105
4.3 Results and Discussions .....	105
4.3.1 Sulphate Formation.....	105
4.3.2 Model Evaluation.....	107
4.3.3 Climate Implications .....	109
4.4 Conclusions.....	112
Acknowledgments and Data.....	114
References.....	114
<b>Chapter 5 The impact of European legislative and technology measures to reduce air pollutants on air quality, human health and climate .....</b>	<b>120</b>
Abstract.....	121
5.1 Introduction .....	121
5.2 Methods .....	123
5.2.1 HadGEM3-UKCA composition climate model.....	123
5.2.2 Anthropogenic emission scenarios.....	123
5.2.3 Human health and economic impacts .....	123
5.2.4 Climate response .....	124

5.3 Results and Discussion .....	124
5.3.1 Effects on air quality .....	124
5.3.2 Health and economic effects .....	126
5.3.3 Effects on climate .....	127
5.4 Conclusions.....	128
Acknowledgements .....	129
References.....	129
<b>Chapter 6 Discussion and Conclusion.....</b>	<b>131</b>
6.1 Modelled and Observed Changes in aerosols and surface solar radiation over Europe between 1960 and 2009.....	131
6.2 The spatial and temporal importance of pH to sulphate aerosols and radiative forcing over the period 1960 to 2009.....	133
6.3 The impact of European legislative and technology measures to reduce air pollutants on air quality, human health and climate .....	135
6.4 Summary.....	136
6.5 Implications for Future Work .....	139
6.6 References.....	142
<b>Appendix A Supplementary material for Chapter 4.....</b>	<b>148</b>
Supplementary Figures .....	148
Supplementary Tables .....	152
<b>Appendix B Supplementary Material for Chapter 5.....</b>	<b>156</b>

## List of Tables

Table 1.1 List of common air pollutants.....	2
Table 1.2 Calculated long term health impacts from exposure to air pollutants in recent studies.....	4
Table 1.3 Air quality standards set for major air pollutants by the European air quality directive, the WHO air quality guidelines (AQG) and the United States Environmental Protection Agency (US-EPA) National Ambient Air Quality Standards (NAAQS). Values in parenthesis show averaging period for which the standard is defined. ....	5
Table 1.4 Global emission estimates for major aerosol classes (Seinfeld and Pandis, 2006, and references therein).....	19
Table 1.5 Summary of sources, formation and effects of aerosol components (Boucher et al., 2013) .....	21
Table 1.6 Summary of the main microphysical processes influencing the aerosol size distribution .....	23
Table 2.1 Summary of the gas and aqueous phase chemistry used within GLOMAP-mode (Mann et al., 2010).....	42
Table 2.2 Details of the ground based observations and where used within this thesis.....	57
Table 3.1 Details of the ground-based observations used in this study. ....	80
Table 3.2 Statistical summary of modelled and observed annual and seasonal (DJF and JJA) mean sulfate at all long-term (>20 years data) measurement sites (34 sites) between 1978 and 2009. Absolute and relative (%) changes in concentrations are calculated as the difference between the mean of the initial 5 years of data minus the mean of the last 5 years of data. Trends that are above or below the value of twice of the standard error of the trend (95% confidence) are highlighted in bold.....	82
Table 3.3 Statistical summary of modelled and observed annual and seasonal (DJF and JJA) mean SPM concentrations at all long-term (>20 years of data) measurement sites (34 sites) between 1978 and 1998. A similar comparison is presented for PM <sub>10</sub> mass concentrations at all long-term (>10 years of data) measurement sites (16 sites) between 1997 and 2009. Absolute and relative (%) changes in concentrations are calculated as the difference between the mean of the initial 5 years of data minus the mean of the last 5 years of data. Trends that are above or below the value of twice of the standard error of the trend (95% confidence) are highlighted in bold.....	84

Table 3.4 Statistical summary of modelled and observed annual and seasonal (DJF and JJA) mean AOD at all long-term (>7 years of data) measurement sites (13 sites) between 2000 and 2009. A similar comparison is presented at the three measurement locations that contain annual mean observations throughout every year between 2000 and 2009 (AOD, three sites). Absolute and relative (%) changes in concentrations are calculated as the difference between the mean of the initial 5 years of data minus the mean of the last 5 years of data. Trends that are above or below the value of twice of the standard error of the trend (95% confidence) are highlighted in bold. ....88

Table 3.5 Statistical summary of simulated and observed annual mean SSR for three different time periods (1960–1974, 1975–1989 and 1990–2009) at the 20 measurement sites across Europe which have a continuous 50-year data record. Absolute and relative (%) changes in SSR are calculated as the difference between the mean of the initial 5 years of data minus the mean of the last 5 years of data for the time period considered. Trends that are above or below the value of twice of the standard error of the trend (95% confidence) are highlighted in bold.....89

Table 3.6 Global and European shortwave top of atmosphere all-sky and clear-sky aerosol RF, relative to a 1980–2000 mean. Values for 1972 are included as this is when the simulated minimum aerosol RF occurs over Europe. For comparison we include global carbon dioxide RF (relative to 1750) from the IPCC fifth assessment report (Myhre et al., 2013). .....91

Table 5.1 Changes in the European annual mean all-sky aerosol radiative effects due to air pollutant mitigation measures. Clear-sky and cloudy-sky RE at the TOA and surface between the REF and NO-AQ simulations over the European continental land mass within the domain 10°W–36°E and 36°N–61°N. Values in parentheses are changes over the period 1970–2009 from Turnock et al (2015). .....127

## List of Figures

Figure 1.1 Direct and indirect (via modification of cloud properties) interactions of aerosols with radiation; new definitions from the IPCC AR5 report and how they relate to other commonly used definitions (Boucher et al., 2013). .....	7
Figure 1.2 Global effective radiative forcing (ERF) estimates of the main drivers of climate change relative to a 1750 baseline from AR5 (IPCC, 2013). .....	8
Figure 1.3 Annual mean top of atmosphere radiative forcing due to aerosol radiation interactions from different aerosol components over the period 1750 to 2010, as presented in the IPCC AR5 (Boucher et al., 2013). .....	10
Figure 1.4 Whisker plots showing estimates of the indirect effects of aerosol on radiation from Global Climate Model studies involving satellite data of RFari, ERFaci and ERFari+aci from the IPCC AR5 (Boucher et al., 2013). .....	10
Figure 1.5 Time series of the global total land emissions from all sectors for black carbon, organic carbon, ammonia (NH <sub>3</sub> ), sulphur dioxide (SO <sub>2</sub> ) and methane (CH <sub>4</sub> ) from 1850 to present day (Lamarque et al. 2010). .....	11
Figure 1.6 Time series of the European emissions of BC, CO, NO <sub>x</sub> and SO <sub>2</sub> across Western and Central Europe from 1980 to 2010 in different emission inventories (Granier et al., 2011). .....	12
Figure 1.7 Annual mean concentrations of SO <sub>4</sub> <sup>2-</sup> (µg m <sup>-3</sup> ) in aerosols from 1974 to 2009 (Tørseth et al., 2012) .....	15
Figure 1.8 Time series of PM <sub>2.5</sub> (left) and PM <sub>10</sub> (right) in µg m <sup>-3</sup> at selected EMEP sites from 1998 to 2009 (Tørseth et al., 2012) .....	16
Figure 1.9 Schematic of the microphysical and chemical processes that influence the evolution of the atmospheric aerosol (Raes et al., 2000). .....	22
Figure 1.10 Schematic showing the air quality chemistry climate interactions and feedbacks (Jacob & Winner, 2009). .....	24
Figure 2.1 Total annual European emissions of sulphur dioxide (SO <sub>2</sub> ), black carbon (BC) and organic carbon (OC) in 2010 from the MACCity and EDGAR (both the reference and NO-AQ scenarios) emissions inventory. ....	56
Figure 2.2 Spatial location of all the measurement sites used within this thesis from the EMEP network for a) SO <sub>2</sub> , b) sulphate, c) SPM, d) PM <sub>10</sub> and e) rainwater pH. Locations have been colour coded by the sub-regional definition used in Chapter 3: Northern Europe (red), North West Europe (green), Central Europe (blue) , Southern Europe (black) and Eastern Europe (yellow). .....	58

Figure 2.3 Time series of the European observations of a) Sulphur dioxide (SO <sub>2</sub> ), b) sulphate aerosol (SO <sub>4</sub> ), c) total suspended particulate matter (SPM) and d) particulate matter with a diameter of less than 10 µm (PM <sub>10</sub> ) from the EMEP network over the period 1978 to 2010. Coloured lines are observations at each individual measurement location with the solid black lines showing the mean value of all observations for each year.....	59
Figure 2.4 Time series of European observations of rainwater pH from the EMEP network over the period 1972 to 2010. Coloured lines represent observations at each individual monitoring location with the solid black line showing the mean value of all observations for each year. ....	60
Figure 2.5 Annual mean aerosol number concentrations from HadGEM3-UKCA with observations from EUSAAR and GUAN overplotted in 2008 for a) total aerosol number concentrations, b) N30 (particles greater than 30 nm in diameter), c) N50 (>50 nm) and d) N100 (>100 nm) .....	61
Figure 2.6 Location of the AOD monitoring sites from AERONET (colour coded by the sub-regional definition used in Chapter 3: Northern Europe (red), North West Europe (green), Central Europe (blue) , Southern Europe (black) and Eastern Europe (yellow)). .....	61
Figure 2.7 Time series of aerosol optical depth observations from AERONET at 440 nm wavelength over the period 1994 to 2010. Coloured lines represent observations at each individual monitoring location for the months of each year. ....	62
Figure 2.8 Location of the surface solar radiation monitoring sites from GEBA (colour coded by the sub-regional definition used in Chapter 3: Northern Europe (red), North West Europe (green), Central Europe (blue) , Southern Europe (black) and Eastern Europe (yellow)). ....	62
Figure 2.9 Observations of all-sky incident surface solar radiation since 1920 at four individual European measurement locations: G26 – Locarno-Monti (Switzerland), G33 – Potsdam (Germany), G41 – Stockholm (Sweden) and G49 – Wageningen (Netherlands).....	63
Figure 2.10 Observations of a) all-sky incident surface solar radiation across all monitoring sites used within this thesis. b) incident surface solar radiation at each monitoring relative to the 1980-2000 mean value at each site. Thick black line represents mean value across all monitoring locations.....	64
Figure 3.1 Location of measurements used in this study for (a) sulfate aerosol mass (*), total aerosol mass ( ) and sites that have measured both (X), (b) AOD ( ) and surface solar radiation (+). Regional European definitions are north-western Europe (green), northern Europe (red), central Europe (blue), eastern Europe (orange) and southern. ....	79

Figure 3.2 Annual European emissions ( $\text{Gg yr}^{-1}$ ) of aerosols and aerosol precursors from the MACCity inventory over the period 1960–2009. (a) Total European emissions of sulfur dioxide ( $\text{SO}_2$ , orange), organic carbon (OC, light green), black carbon (BC, black), ammonia ( $\text{NH}_3$ , light purple) and oxides of nitrogen ( $\text{NO}_x$ , blue). (b)–(f) show European regional emissions for (b) $\text{SO}_2$ , (c) $\text{NO}_x$ , (d) $\text{NH}_3$ , (e) BC and (f) OC. Regions are as defined in Fig. 1: northern (red), north-western (green), central (blue), eastern (orange), southern (purple).....	79
Figure 3.3 Temporal variation in the number of locations measuring surface solar radiation (SSR), sulfate aerosol mass ( $\text{SO}_4$ ), total suspended particle mass (SPM), $\text{PM}_{10}$ mass and aerosol optical depth (AOD). .....	80
Figure 3.4 Simulated European annual mean (a) $\text{PM}_{10}$ and composition-resolved surface mass concentration; (b) aerosol number concentration for particles with dry diameter $>3$ (total), $>30$ (N30), $>50$ (N50) and $>100$ nm (N100); (c) AOD at 440 nm; and (d) SSR between 1960 and 2009. Mean values are calculated over the European land domain shown in Fig.1.....	82
Figure 3.5 Annual mean sulfate aerosol mass concentrations ( $\mu\text{g S m}^{-3}$ ) from the lowest model level with observations overplotted in circles for (a) 1980, (b) 1990, (c) 2000 and (d) 2009. (e) Time series of annual and seasonal mean observed (solid lines) and modelled (dashed lines) sulfate concentrations averaged across all measurement locations for each particular year. Shaded areas show $\pm 1$ standard deviation of the modelled (light grey) and observed (dark grey) annual mean values, with the hatching identifying areas of overlap.....	83
Figure 3.6 European and sub-regional normalised mean bias factors for summertime (red) and wintertime (blue) sulfate aerosol mass concentrations across all the years that data were available. The solid line shows the median value, the boxes show the 25th and 75th percentile values with the error bars showing the maximum and minimum values and the circles representing outliers (values $>1.5x$ interquartile range).....	84
Figure 3.7 Annual (black), summertime (red) and wintertime (blue) trends in modelled and observed sulfate aerosol mass concentrations ( $\mu\text{g S m}^{-3} \text{ yr}^{-1}$ ) at each individual monitoring location over their operational period between 1978 and 2009. ....	84
Figure 3.8 Annual mean SPM mass concentrations ( $\mu\text{g m}^{-3}$ ) from the lowest model level with observations overplotted in circles for (a) 1980 and (b) 1990. (d) and (e) are the same as (a) and (b) but for $\text{PM}_{10}$ mass concentrations in 2000 and 2009. A time series of annual and seasonal mean observed (solid lines) and modelled (dashed lines) (c) SPM and (f) $\text{PM}_{10}$ concentrations averaged across all measurement locations for each particular year. Shaded areas show $\pm 1$ standard deviation of the modelled (light grey) and observed (dark grey) annual mean values, with the hatching identifying areas of overlap.....	85

Figure 3.9 European and sub-regional normalised mean bias factors for summertime (red) and wintertime (blue) (a) SPM and (b) PM<sub>10</sub> mass concentrations across all the years that data were available. The solid line shows the median value, the boxes show the 25th and 75th percentile values with the error bars showing the maximum and minimum values and the circles representing outliers (values >1.5x interquartile range).....86

Figure 3.10 Calculated annual (black), summertime (red) and wintertime (blue) linear trends in modelled and observed (a) SPM and (b) PM<sub>10</sub> mass concentrations ( $\mu\text{g S m}^{-3} \text{ yr}^{-1}$ ) at each individual monitoring location over their operational period between 1978 and 2002 for SPM and between 1996 and 2009 for PM<sub>10</sub>. .....86

Figure 3.11 Annual mean observed vs. simulated aerosol number concentrations for (a) N30 (particles greater than 30 nm diameter), (b) N50 (>50 nm) and (c) N100 (>100 nm) at monitoring sites across Europe. ....87

Figure 3.12 Annual mean AOD at 440 nm with observations from the AERONET sites overplotted for (a) 2000 and (b) 2009. (c) Time series of monthly and seasonal mean observed (solid lines) and modelled (dashed lines) AOD at 440 nm averaged across all measurement locations. (d) European NMBFs of AOD for annual (orange), summertime (red) and wintertime (blue) across all the years and sites that data were available. The annual NMBF for the three sites with the longest continuous record (>9 years) is shown in yellow. ....88

Figure 3.13 Observed (black line) and simulated (red line) European annual mean all-sky SSR anomalies ( $\text{Wm}^{-2}$ ) relative to a 1980–2000 average. Simulated all-sky SSR not including aerosol radiative effects (ARE) is also shown (orange line). Values are calculated as the average across all measurement locations within Europe (see Fig. 1). The standard deviation of the annual mean for each year is shown by the shaded areas of dark grey for the observations and light grey for the model with the hatching representing where the areas overlap.....89

Figure 3.14 European normalised mean bias factors for sulfate aerosol mass, SPM mass, PM<sub>10</sub> mass, AOD and SSR across all the years where data were available (see Tables 2–5) and separately for the period 2000–2009. The solid line shows the median value, the boxes show the 25th and 75th percentile values with the error bars showing the maximum and minimum values and the circles representing outliers (values >1.5x interquartile range). .....90

Figure 3.15 Taylor diagram comparing simulated and observed European sulfate mass concentrations, SPM, PM <sub>10</sub> , AOD and SSR. Comparisons are made across all the years where observations are available. We additionally show results for the period 2000–2009, where sulfate, PM <sub>10</sub> , AOD and SSR are consistently available. For AOD, we separately plot the three locations with the longest observational record. For SSR we also plot the three different time periods (1960–1974, 1975–1989, 1990–2009). Correlation coefficients are plotted against the observed standard deviations normalised relative to the simulated standard deviation. ....	90
Figure 3.16 European and sub-regional top of atmosphere aerosol radiative forcing (Wm <sup>-2</sup> ), relative to a 1980–2000 average, under (a) all-sky and (b) clear-sky conditions. European regions are as defined in Fig. 1 .....	92
Figure 4.1 Differences between the pH 6.5 and pH 5.0 simulations in column mass burdens of a) sulphur dioxide (SO <sub>2</sub> ) and b) sulphate aerosol (SO <sub>4</sub> <sup>2-</sup> ) for the mid-year of the period, 1985. The temporal evolution of the difference in regional column burdens for c) SO <sub>2</sub> and d) SO <sub>4</sub> over the North Atlantic, NE USA, China and European regions, as defined in Figure A4. ....	107
Figure 4.2 Model evaluation of sulphate aerosol mass concentrations across Europe over the period 1978 to 2009. Annual (black), summertime (JJA, red) and wintertime (DJF, blue) trends in modelled and observed sulphate mass concentrations at each EMEP station for a) pH 5.0 and b) pH 6.5 simulations. European normalized mean bias factors for sulphate aerosol concentrations over the period 1980-1984 and 2005-2009 in summertime (JJA, red (80-84) and orange (05-09)) and wintertime (DJF, blue (80-84) and green (05-09)) in c) pH 5.0 and d) pH 6.5 simulations. Central and north regions of Europe are as defined in Turnock et al. (2015).....	108
Figure 4.3 Percentage difference between pH 6.5 and pH 5.0 simulations for 1985 (mid-year of the period) in surface number concentrations of particles with a dry diameter larger than a) 100 nm (N100) and b) all sizes (N Total). Surface aerosol number size distributions in 1985 averaged across the regions c) Europe (black) and NE USA (pale green), and d) China (red) and North Atlantic (blue), as defined in Figure S4. Solid and dashed lines show the simulated aerosol size distribution using a pH of 5.0 and 6.5 respectively.....	110
Figure 4.4 Differences in all-sky a) and clear-sky b) shortwave top of atmosphere aerosol radiative effects between the pH 6.5 and pH 5 simulations for the year 1985. Hatching in a) shows where the differences in cloud drop number concentrations are more than 40%. Calculated c) all-sky and d) clear-sky aerosol radiative forcings between 1970 and 2009 over Europe, NE USA, China and North Atlantic (regions defined in Fig. A4) using four different start and end point combinations from the pH 5.0 and pH 6.5 simulations. ....	111

Figure 5.1 The impact of European air quality mitigation on annual mean emissions of (a) sulphur dioxide (SO<sub>2</sub>) (b) black carbon (BC), (c) organic carbon (OC). The impact is shown as the difference between the 2010 REF emissions and the NO-AQ emission scenario, calculated as the total of the energy, industry and road transportation sectors. Panel (d) shows the total European emissions (10°W–36°E, 36°N–61°N) in each scenario, as well as those in 1970 from the MACCity and EDGAR inventories. The totals from the NO-AQ and REF scenarios along with the difference between each are also displayed above panels (a)–(c). Within panel (d) the values refer to the percentage difference in the European total emissions of each species between EDGAR REF 1970 and each of the 2010 REF and NO-AQ scenario. .... 124

Figure 5.2 Percentage change in annual mean surface concentrations (averaged over 5 years) of (a) PM<sub>2.5</sub>, (b) sulphate, (c) black carbon (BC) and (d) particulate organic matter (POM) due to the mitigation of air pollution. Percentage changes are calculated as the difference between the REF and NO-AQ simulations relative to the latter simulation (i.e. REF-NOAQ/NOAQ). Stippling indicates regions where the difference is larger than the variability of the annual mean values (i.e. greater than two standard deviations of the annual mean). Above each panel we show the European mean concentrations (calculated as mean values over the continental land mass within the domain 10°W–36°E and 36°N–61°N) for each scenario along with the absolute and percentage change between simulations. We also detail the 1970–2009 simulated change in concentration from Turnock et al (2015). .... 125

Figure 5.3 The impact of air quality mitigation measures on human health and perceived economic benefit in Europe. (a) Number of premature deaths prevented annually due to all causes of disease from the change in PM<sub>2.5</sub> concentrations due to air quality mitigation (REF minus NO-AQ simulations). (b) Same as (a) but per 10 000 population. (c) Total number of premature deaths prevented for all causes of disease across the EU due to air quality mitigation compared to the reduction in premature deaths calculated due to the actual change in PM<sub>2.5</sub> concentrations over the period 1970–2009 simulated by Turnock et al (2015) (error bars represent the 95% confidence intervals of the concentration response functions used for calculating total European annually prevented premature mortality). (d) The perceived economic benefit calculated for air quality mitigation from the number of deaths prevented annually across Europe. The error bars represent the economic savings calculated using the 95% confidence intervals of the total number of European annually prevented premature deaths..... 126

Figure 5.4 Difference between the REF and NO-AQ simulations in annual mean (average over 5 years) aerosol radiative effect at the top of atmosphere for (a) all-sky and (b) clear-sky conditions and incident surface solar radiation for (c) all-sky and (d) clear-sky conditions. Stippling indicates regions where the difference is larger than the variability of the annual mean values (i.e. greater than two standard deviations of the annual mean). European mean concentrations for each scenario are calculated as mean values over the continental land mass within the domain (10°W–36°E and 36°N–61°N, with the change between the two simulations shown above each panel..... 128

## Abbreviations

**ACCMIP** - The **A**tmospheric **C**hemistry and **C**limate **M**odel **I**ntercomparison Project

**AeroCom** – **A**erosol modelling inter**C**omparison project

**AERONET** - **A**erosol **R**obotic **N**ETwork

**AOD** – **A**erosol **O**ptical **D**epth

**AR5** – 5<sup>th</sup> **A**ssessment **R**eport of the **I**PCC

**CCN** – **C**loud **C**ondensation **N**uclei

**CDN** – **C**loud **D**rop **N**umber

**CRF** – **C**oncentration dose-**R**esponse **F**unction

**DMS** – **D**i**M**ethyl **S**ulphide

**EMEP** – **E**uropean **M**onitoring and **E**valuation **P**rogramme

**ERFaci** – **E**ffective **R**adiative **F**orcing from **a**erosol **c**loud interactions

**ERFari** – **E**ffective **R**adiative **F**orcing from **a**erosol **r**adiation interactions

**GLOMAP** – **G**LObal **M**odel of **A**erosol **P**rocesses

**HadGEM3** – 3<sup>rd</sup> generation of the **H**adley Centre's **G**lobal **E**nvironment **M**odel

**IMPROVE** – **I**ntegrated **M**onitoring of **P**ROtected **V**isual **E**nvironment

**IPCC** – **I**ntergovernmental **P**anel on **C**limate **C**hange

**PM<sub>10</sub>** – **P**articulate **m**atter with a diameter less **10** micrometres

**PM<sub>2.5</sub>** – **P**articulate **m**atter with a diameter less **2.5** micrometres

**POPs** – **P**ersistent **O**rganic **P**ollutants

**RCP** – **R**eference **C**oncentration **P**athway

**RR** – **R**elative **R**isk

**RFaci** – **R**adiative **F**orcing from **a**erosol **c**loud interactions

**RFari** – **R**adiative **F**orcing from **a**erosol **r**adiation interactions

**SOA** – **S**econdary **O**rganic **A**erosols

**SSR** – **S**urface **S**olar **R**adiation

**UKCA** – **U**nited **K**ingdom **C**hemistry and **A**erosol programme

**UM** – **U**nified **M**odel

**UNECE** – **U**nited **N**ations **E**conomic **C**ommission for **E**urope

**US-EPA** – **U**nited **S**tates **E**nvironmental **P**rotection **A**gency

**VOCs** – **V**olatile **O**rganic **C**ompounds

**VSL** – **V**alue of a **S**tatistical **L**ife

**WHO** – **W**orld **H**ealth **O**rganization

**WTP** – **W**illingness **T**o **P**ay

## **Chapter 1**

### **Introduction**

The atmospheric aerosol consists of a population of solid and/or liquid particles suspended in air. The size of aerosol particles vary enormously by over several orders of magnitude from 1 nm to 0.1 mm. Aerosol particles can be classified according to their source as either primary (directly emitted from the source) or secondary (formed in-situ via gas to particle conversion). The source of aerosol particles can be anthropogenic (e.g. soot from combustion activities) or natural (e.g. mineral dust) in origin, and affects the concentration and composition of particles at different locations throughout the world. Typical number and mass concentrations of aerosol particles range from  $<10^2 \text{ cm}^{-3}$  and  $<10^1 \mu\text{g m}^{-3}$  in remote regions to  $>10^5 \text{ cm}^{-3}$  and  $>10^2 \mu\text{g m}^{-3}$  in urban areas (Baltensperger & Nyeki, 1998).

The size and physio-chemical properties of aerosol particles are determined by processes such as condensation, evaporation, coagulation, chemical reaction and water uptake. These processes influences the overall properties of aerosol particles in the atmosphere and also their lifetime, primarily determined by wet deposition (Seinfeld & Pandis, 2006). Atmospheric aerosols are highly spatially and temporally variable (in both concentration and composition) due to their short residence time in the troposphere (~1 week), which makes modelling their different interactions and impacts challenging. This is in contrast to the near uniform distribution and relatively long residence time of long-lived greenhouse gases in the atmosphere.

Aerosol particles contribute to a number of environmental problems including acid deposition and damage to ecosystems, reduced visibility, poor air quality and human health issues (Brunekreef & Holgate, 2002; Fowler et al., 2009; Vautard et al., 2009). Additionally, they can influence the radiative balance of the Earth through direct and indirect interactions (Boucher et al., 2013). This thesis specifically focuses on the impact of aerosols (or alternatively referred to as aerosol particles or particulate matter) on air quality, human health and climate, inferred from changes to the radiative balance.

## 1.1 Air Quality and Human Health

### 1.1.1 Air Pollutants

Air pollution can be defined as a build-up of gases or aerosol particles, emitted from anthropogenic or natural sources, in the atmosphere to sufficiently high concentrations that results in damage to ecosystems, human health and the built environment (Jacobson, 2002; Seinfeld & Pandis, 2006). The concentration of air pollutants within an environment is expressed in terms of its air quality.

High levels of air pollutants have been traditionally associated with anthropogenic activity in urban or industrialised areas. However, it is now widely accepted that air pollution is also a transboundary problem, spanning regional and hemispheric scales (depending on the lifetime in the atmosphere of the pollutant considered).

Air pollutants can form from anthropogenic (or natural) emissions of both gas-phase species and particulate matter, being either primary (directly emitted) or secondary (formed via reaction in the atmosphere) in nature. Table 1 shows some of the most common air pollutants, with the focus of this thesis being on particulate air pollutants.

**Table 1.1** List of common air pollutants

<b>Gas-phase</b>	<b>Particulate-phase</b>
O <sub>3</sub> , SO <sub>2</sub> , NO, NO <sub>2</sub> , CO, CH <sub>4</sub> , VOCs, POPs, Hg	PM <sub>10</sub> , PM <sub>2.5</sub> and components Sulphate, Black Carbon, Organic Matter, Nitrate

The majority of primary air pollutants tend to be emitted from anthropogenic sources that involve fossil fuel combustion, for example the industry and power generation sectors (e.g. sulphur dioxide, SO<sub>2</sub>) or the transport sectors (e.g. nitrogen oxides, NO<sub>x</sub> or Black carbon, BC). Air pollutants can also be emitted from natural sources, for example volcanic SO<sub>2</sub> and mineral dust particles from soils.

Secondary air pollutants are formed from chemical reactions in the atmosphere. In urban environments a combination of meteorology (photolysis and low levels of boundary layer mixing) and high emissions of NO<sub>x</sub> and volatile organic compounds (VOCs) can lead to photochemical smog episodes due to high concentrations of Ozone (O<sub>3</sub>) forming. This type of air pollution incident is common in many major cities around the globe (e.g. Los Angeles). Secondary particulate matter e.g. sulphate (SO<sub>4</sub><sup>2-</sup>) and secondary organic aerosols (SOA), are formed by gas-to-particle

conversion. Under conditions of high atmospheric pressure (low amounts of dispersion) and low precipitation, high concentrations of air pollutants can occur, leading to poor air quality.

### **1.1.2 Impacts on Health**

A population exposed to high levels of air pollutants can experience detrimental impacts to their health. Epidemiological studies have identified an association between the concentration of air pollutants and observed effects on human health; concentration dose response relationships (Dockery et al., 1993; Pope et al., 1995; Seaton et al., 1995). This can be linked to short term morbidity health outcomes such as an increase in respiratory hospital admissions and cases of chronic bronchitis (World Health Organization, 2003; AEA Technology, 2005). Exposure to air pollutants has also been associated with long-term effects on human health over an individual's lifetime (e.g. excess premature mortality from lung cancer).

Particles with a diameter of less than 10  $\mu\text{m}$  cause the largest health effects as they are small enough to penetrate and lodge inside the lungs. This can lead to cardiovascular and respiratory diseases, as well as lung cancer (Brunekreef & Holgate, 2002; World Health Organization, 2003, 2014). Impacts on human health can occur even at low concentrations with no identifiable threshold for observable effects (Burnett et al., 2014).

Human exposure to elevated concentrations of  $\text{SO}_2$ , nitrogen dioxide ( $\text{NO}_2$ ) and  $\text{O}_3$  can also lead to morbidity and mortality from the exasperation of respiratory conditions (e.g. asthma, bronchitis, lung inflammation and lung disease) (World Health Organization, 2003). Exposure to high concentrations of  $\text{O}_3$  is currently the greatest concern of these gaseous pollutants.

Recent studies have attempted to quantify the impact on human health from exposure to air pollutants (Table 1.2). Human exposure to ambient concentrations of fine particulate matter has been attributed to an estimated 0.8 to 3.7 million premature deaths worldwide, mostly occurring in Asia (Cohen et al., 2005; World Health Organization, 2014). At a European level, present day concentrations of air pollutants are resulting in a substantial number of premature deaths and other health impacts, making exposure to air pollutants a significant health risk factor. Most of these global and regional estimates are provided at a relatively coarse resolution and are

anticipated to have neglected enhanced concentrations of air pollutants from urban areas.

A perceived economic impact on society can also result from the health effects of poor air quality. The World Health Organization (WHO) for Europe recently estimated the perceived economic costs to society across the countries of the WHO European region (53 in total) from premature deaths due to exposure to air pollution (both ambient and household) was US\$ 1.431 trillion in 2010 (WHO Regional Office for Europe & OECD, 2015). This highlights the very large economic costs of poor air quality.

**Table 1.2** Calculated long term health impacts from exposure to air pollutants in recent studies

Scale	Year	Premature mortality associated with exposure to ambient air pollutants (95% confidence intervals (C.I.))		Reference
		PM <sub>2.5</sub>	O <sub>3</sub>	
Global	2012	3.7 million	N/A	World Health Organization (2014)
Global	2010	3.15 (1.52 – 4.60) million	142,000 (90,000 - 208,000)	Lelieveld et al., (2015)
Global	2000	3.7 (2.6 - 4.4) million	0.7 (0.4 – 1.0) million	Anenberg et al., (2010)
Global	2000	0.8 million	N/A	Cohen et al., (2005)
European	2014	458,065 (301,304 – 602,092)	17,407 (8,413 – 25,782)	European Environment Agency (EEA), (2014)
UK	2008	29,000 (4,700 – 51,000, based changes in risk coefficient used)	N/A	COMEAP (2010)
USA	2005	200,000 (90,000 – 362,000, 90% C.I.)	5,000 (-900 – 11,000, 90% C.I.)	Caiazzo et al., (2013)

### 1.1.3 Air Quality Legislation

In response to episodes of poor air quality, legislation has been developed on both a national and international level to reduce air pollutants to concentrations that represent a minimum risk to human health and the environment. Some of the earliest modern legislation to control the emission of air pollutants was the implementation of Clean Air Acts in both the United Kingdom (1956) and United States (1963). These were enacted following large smog events in the 1940s and 50s across London (coal smoke) and Los Angeles (photochemical), which resulted in numerous deaths.

At an international level, the Convention on Long-Range Transboundary Air Pollution (CLRTAP) was set up by the United Nations Economic Commission for Europe (UNECE) in 1979. This was the first piece of legislation to deal with the problem of air pollution at a regional and transboundary level by requiring a reduction in emissions of air pollutants using abatement technologies (United Nations Economic Commission for Europe, 2004). CLRTAP has been extended by the adoption of additional protocols such as the UNECE Gothenburg Protocol of 1999 (subsequently revised in 2012), which sets limits on emissions of air pollutants from specific activities. Following on from this initial legislation, countries mainly in North America and Europe but also others around the world through the WHO, have now set air quality standards on the concentrations of air pollutants that would pose an unacceptable risk to human health (Table 1.3). With regards to particulate matter, legislation has tended to focus on regulating mass concentrations in the fine size fraction of particles less than 10 µm in diameter (PM<sub>10</sub>) and more recently on particles less than 2.5 µm in diameter (PM<sub>2.5</sub>).

**Table 1.3** Air quality standards set for major air pollutants by the European air quality directive, the WHO air quality guidelines (AQG) and the United States Environmental Protection Agency (US-EPA) National Ambient Air Quality Standards (NAAQS). Values in parenthesis show averaging period for which the standard is defined.

Pollutant	EU Limit Values <sup>1</sup>	WHO AQG <sup>2</sup>	USEPA NAAQS <sup>3</sup>
PM <sub>2.5</sub>	20 µg/m <sup>3</sup> (annual)	10 µg/m <sup>3</sup> (annual)	12 µg/m <sup>3</sup> (annual)
PM <sub>10</sub>	40 µg/m <sup>3</sup> (annual)	20 µg/m <sup>3</sup> (annual)	150 µg/m <sup>3</sup> (24 hours)
Ozone (O <sub>3</sub> )	120 µg/m <sup>3</sup> (max daily 8 hourly mean)	100 µg/m <sup>3</sup> (8 hour mean)	0.070 ppm (8 hour mean)
Nitrogen Dioxide (NO <sub>2</sub> )	40 µg/m <sup>3</sup> (annual)	40 µg/m <sup>3</sup> (annual)	53 ppb (annual)
Sulphur Dioxide (SO <sub>2</sub> )	125 µg/m <sup>3</sup> (24 hours)	125 µg/m <sup>3</sup> (24 hours)	75 ppb (1 hour)
Carbon Monoxide (CO)	10 mg/m <sup>3</sup> (max daily 8 hourly mean)	10 mg/m <sup>3</sup> (max daily 8 hourly mean)	9 ppm (8 hours)

<sup>1</sup> – Limit values from the 2008 ambient air quality directive (2008/50/EC)

<sup>2</sup> – WHO Air Quality Guideline values (WHO, 2006)

<sup>3</sup> – US-EPA National Ambient Air Quality Standards (<https://www.epa.gov/criteria-air-pollutants/naaqs-table>, accessed 05/05/16)

The European Union (EU) and other regional organisations such as the UNECE have introduced legislation since the 1970s across Europe in the form of “directives” to regulate air pollutant concentrations and set emission limits for specific activities. Directives covering standards for vehicle

emissions and fuel quality have also been implemented. The 2008 ambient air quality directive (2008/50/EC) is the most recent directive and sets legally binding limit values for ambient concentrations of major air pollutants (PM<sub>10</sub>, PM<sub>2.5</sub>, SO<sub>2</sub>, NO<sub>2</sub>, lead, benzene, carbon monoxide (CO)), which all member states must adhere to. These limit values (Table 1.3) have been set at levels for the protection of human health from both long and short term exposure to air pollutants. The 2008 ambient air quality directive updated and consolidated all historical EU air quality legislation which had previously set limit values and objectives since the 1970s. Limits on emissions of air pollutants (SO<sub>2</sub>, NO<sub>x</sub>, ammonia (NH<sub>3</sub>) and VOCs) are regulated under separate legislation of the UNECE Gothenburg Protocol, which has been translated into European law under the National Emission Ceilings Directive (2001/81/EC).

## 1.2 Aerosol Radiative Effects and Climate

Air pollutants can interact with the Earth's radiative balance and therefore influence climate. Tropospheric O<sub>3</sub> is also a greenhouse gas and directly interacts with the Earth's radiative balance by absorbing outgoing long wave radiation, resulting in a positive radiative effect. Aerosols or particulate matter can interact with climate directly, by either absorbing or reflecting incoming solar radiation and also by absorbing outgoing longwave radiation. They can also have an indirect effect on the radiative balance by modifying the microphysical properties of clouds. Aerosol particles of a certain size and composition can act as cloud condensation nuclei (CCN). CCN particles are able to influence the cloud droplet number (CDN) concentration, which modifies the properties of clouds and their interaction with radiation (Dusek et al., 2006).

This indirect modification can be traditionally separated into two main effects:

- 1 *The cloud albedo effect*, anthropogenic aerosols that are able to act as CCN cause the formation of more numerous smaller cloud droplets at a constant liquid water content increasing albedo and reflectivity of a cloud (Twomey, 1977); and
- 2 *The cloud lifetime effect*, a decrease in precipitation efficiency at a constant liquid water content due to the increased number of smaller cloud drops from aerosols acting as CCN, resulting in longer lived clouds (Albrecht, 1989).

Absorbing aerosols can change the local heating rate of the atmosphere, which can reduce cloud formation and affect the local energy budget; the semi-direct effect of aerosols on climate (Lohmann & Feichter, 2001). Figure 1.1 shows a summary of these interactions and also the new definitions within the 5<sup>th</sup> assessment report (AR5) of the Intergovernmental Panel on Climate Change (IPCC).

The direct and semi-direct effects have now been termed aerosol radiation interactions (ari) in the IPCC AR5 report whilst, the cloud albedo and lifetime effects are termed aerosol-cloud interactions (aci) (Boucher et al., 2013). Within these new definitions a distinction has now been made between the effects that have an instantaneous radiative forcing (the direct and cloud albedo effects) and those that induce a rapid adjustment of climate (the semi-direct and cloud lifetime effects). Combining the effects on the radiative balance from the instantaneous perturbation and rapid adjustments leads to an overall effective radiative forcing (ERF) from both ari and aci (Figure 1.1).

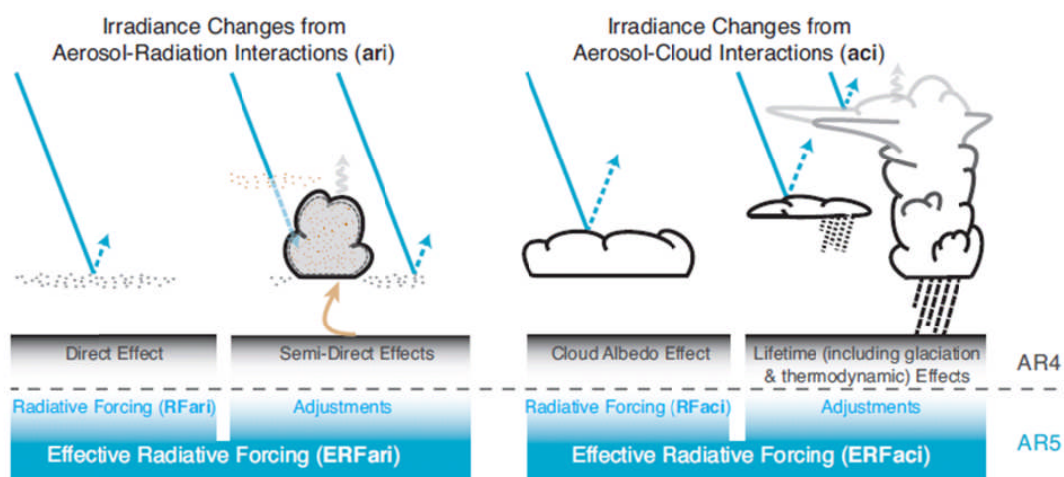


**Figure 1.1** Direct and indirect (via modification of cloud properties) interactions of aerosols with radiation; new definitions from the IPCC AR5 report and how they relate to other commonly used definitions (Boucher et al., 2013).

Figure 1.2 shows the anthropogenic atmospheric drivers of radiative forcing (RF) within the climate system (taken from the IPCC AR5 report). Radiative forcing (instantaneous) is defined by the IPCC AR5 report as;

*“the change in the net (down minus up) radiative flux (shortwave plus longwave) at the tropopause due to an imposed change after allowing stratospheric temperatures to readjust to radiative equilibrium, whilst holding surface and tropospheric temperatures and state variables such as water vapor and cloud cover fixed at unperturbed values”.*

RF is usually measured from the pre-industrial to present day and at the top of atmosphere (climatological tropopause).

The climate system can also respond to such changes in the radiative balance with rapid adjustments to clouds, surface temperature and precipitation. These responses are excluded from the above definition of radiative forcing but are included within the calculation of ERF (Figure 1.1). Rapid adjustments from aerosol induced cloud changes e.g. cloud lifetime and semi-direct effects are included within the ERF calculations. This is defined in the AR5 report as;

*“the change in net TOA downward radiative flux after allowing for atmospheric temperatures, water vapour and clouds to adjust, but with global mean surface temperature or a portion of surface conditions unchanged.”*

This includes simulations that use the method of fixing sea surface temperatures and sea ice fields.

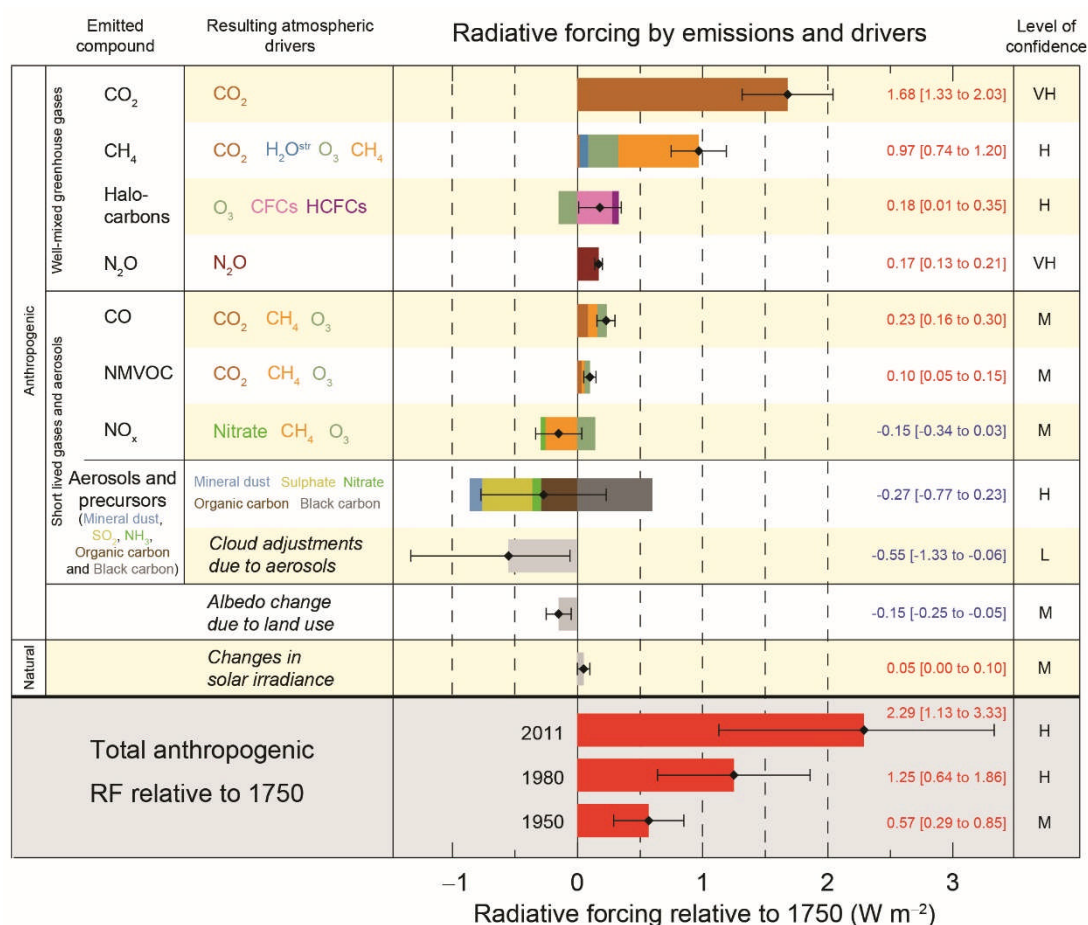


**Figure 1.2** Global effective radiative forcing (ERF) estimates of the main drivers of climate change relative to a 1750 baseline from AR5 (IPCC, 2013).

The confidence level in the net forcing (VH – very high, H – high, M – medium, L – low, VL – very low) is shown on the right.

Figure 1.2 shows the large positive radiative forcing from the well mixed greenhouse gases (e.g. global mean value for CO<sub>2</sub> of +1.68 W m<sup>-2</sup>) and the relatively small error bars, highlighting the high scientific certainty to which these effects are known. The radiative forcing due to aerosols is shown to be negative (global mean value of -0.27 W m<sup>-2</sup> for aerosols and -0.55 W m<sup>-2</sup> for cloud adjustments due to aerosols) but with large error bars, highlighting the large uncertainties that currently exist within these estimates. The radiative forcing from aerosols is influenced by the temporal and spatial distribution of the aerosol burden, optical properties and various chemistry climate processes (Haywood & Boucher 2000; Forster et al. 2007).

The individual components of aerosols can have different radiative effects (Figure 1.3). Sulphate particles have a cooling effect on climate by directly reflecting radiation (RF<sub>ari</sub> = -0.34 W m<sup>-2</sup>, Figure 1.3). BC is an aerosol component that has large human health effects, is a strong absorber of UV radiation (direct effects RF<sub>ari</sub> = +0.4 W m<sup>-2</sup>, Figure 1.3) and by coating with soluble components can act as an effective CCN to influence cloud properties (Menon et al. 2008; Bond et al. 2013; Andreae & Ramanathan 2013). Bond et al., (2013) provided another estimate of BC RF<sub>ari</sub> of +0.51 W m<sup>-2</sup> for fossil fuel and biofuel sources, which is larger as BC absorption is scaled to match observations. Estimates of RF<sub>ari</sub> for BC are uncertain due to model errors in reproducing the vertical profile and optical properties of BC across the globe (Bond et al., 2013). Organic aerosols of primary origin tend to be more reflective of radiation, as indicated by a RF<sub>ari</sub> of -0.09 W m<sup>-2</sup>. For SOA the median RF<sub>ari</sub> is -0.03 W m<sup>-2</sup> but with a large range reflecting the spread in the response of biogenic VOC emissions to land use change (Shindell et al., 2013).

An estimate of aerosol ERF (that takes into account both ari and aci) is provided from the IPCC AR5 report in Figure 1.4. This shows the large range, and hence uncertainty, in the different estimates of ERF that take into account the rapid adjustment of aerosols on cloud. A mean aerosol ERF value of -0.9 W m<sup>-2</sup> is obtained from the IPCC AR5 report (5 to 95% uncertainty range of -1.9 to -0.1 W m<sup>-2</sup>).

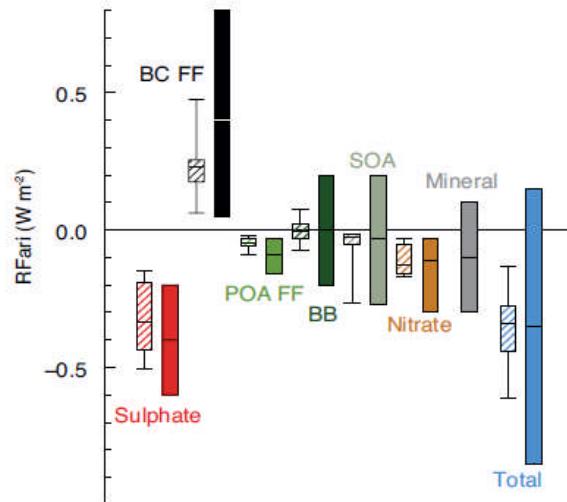


**Figure 1.3** Annual mean top of atmosphere radiative forcing due to aerosol radiation interactions from different aerosol components over the period 1750 to 2010, as presented in the IPCC AR5 (Boucher et al., 2013).

Hatched boxes show median(line), 5<sup>th</sup> to 95<sup>th</sup> percentile ranges (box) and min/max values (whiskers) from AeroCom II models (Myhre et al., 2013). Solid boxes show the AR5 estimates and 90% uncertainty ranges.

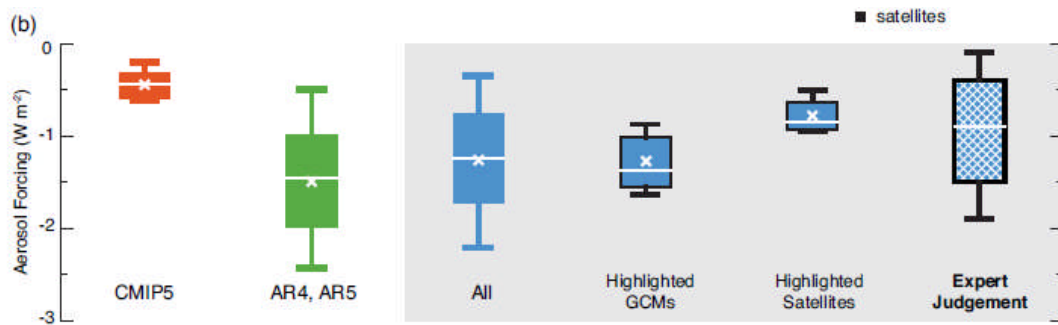


**Figure 1.4** Whisker plots showing estimates of the indirect effects of aerosol on radiation from Global Climate Model studies involving satellite data of RFari, ERFaci and ERFari+aci from the IPCC AR5 (Boucher et al., 2013).

CMIP5 (in red) shows RFari from CMIP5/ACCMIP models. ERFaci from GCMs (labelled AR4, AR5 in green), all estimates of ERFari+aci (labelled 'All' in blue), ERFari+aci from GCMs (labelled 'Highlighted GCMs' in blue), ERFari+aci from satellites (labelled 'Highlighted Satellites' in blue), and expert judgement based on estimates of ERFari+aci from these GCM and satellite studies (labelled 'Expert Judgement' in blue).

The large error bars in the predictions of the aerosol ERF arise mainly due to the large spatial and temporal variability in aerosols and the difficulties in modelling their complex interactions in the atmosphere, particularly with clouds. Also representing changes to the physical and chemical properties of aerosols is important as it can affect their interactions with clouds and climate. A reduction of this uncertainty is vital in order to improve the accuracy and precision of climate predictions, as future aerosol cloud effects are still anticipated to be important.

### 1.3 Anthropogenic Emission Trends

Global anthropogenic emissions of aerosol species (and their precursors) have increased throughout the industrial period (Figure 1.5) as a result of population increases and economic development. For example, global emissions of  $\text{SO}_2$  increased by a factor of 60 from 1850 to a peak in the 1980s (Lamarque et al., 2010; Granier et al., 2011; Smith et al., 2011). Other global emissions of anthropogenic species such as CO,  $\text{NO}_x$ , VOCs and  $\text{NH}_3$  have similar temporal trends to  $\text{SO}_2$  emissions (Lamarque et al. 2010). However, anthropogenic emissions of BC and Organic Carbon (OC) have continually increased from 1850 to 2000 (Figure 1.5).

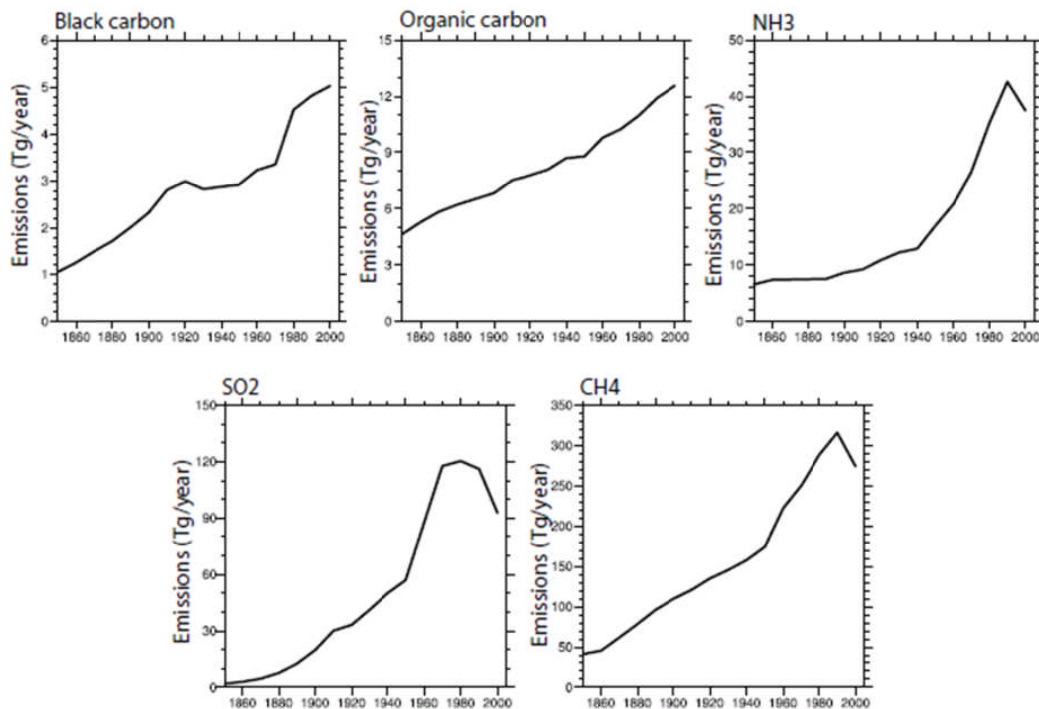


**Figure 1.5** Time series of the global total land emissions from all sectors for black carbon, organic carbon, ammonia ( $\text{NH}_3$ ), sulphur dioxide ( $\text{SO}_2$ ) and methane ( $\text{CH}_4$ ) from 1850 to present day (Lamarque et al. 2010).

Since the 1980s, anthropogenic emissions have reduced in certain regions, mainly North America and Europe, due to economic factors and from the implementation of air pollutant control measures (Figure 1.6). Over Europe, emissions of  $\text{SO}_2$  declined by 73% between 1980 and 2004 (Vestreng et al., 2007; Hand et al., 2012). In addition, European anthropogenic emissions of  $\text{NO}_x$ , CO and BC reduced by 30%, 58% and 55% respectively over the period 1980 to 2010 (Granier et al., 2011). However,  $\text{NH}_3$  emissions across Europe have continuously increased over the same time period, mainly due to uncontrolled emissions from the agricultural sector. The increase in  $\text{NH}_3$  could be particularly important in trying to improve future air quality over a

region such as Europe due to its influence on the formation of both sulphate and nitrate aerosols (Redington et al., 2009; Wang et al., 2013).

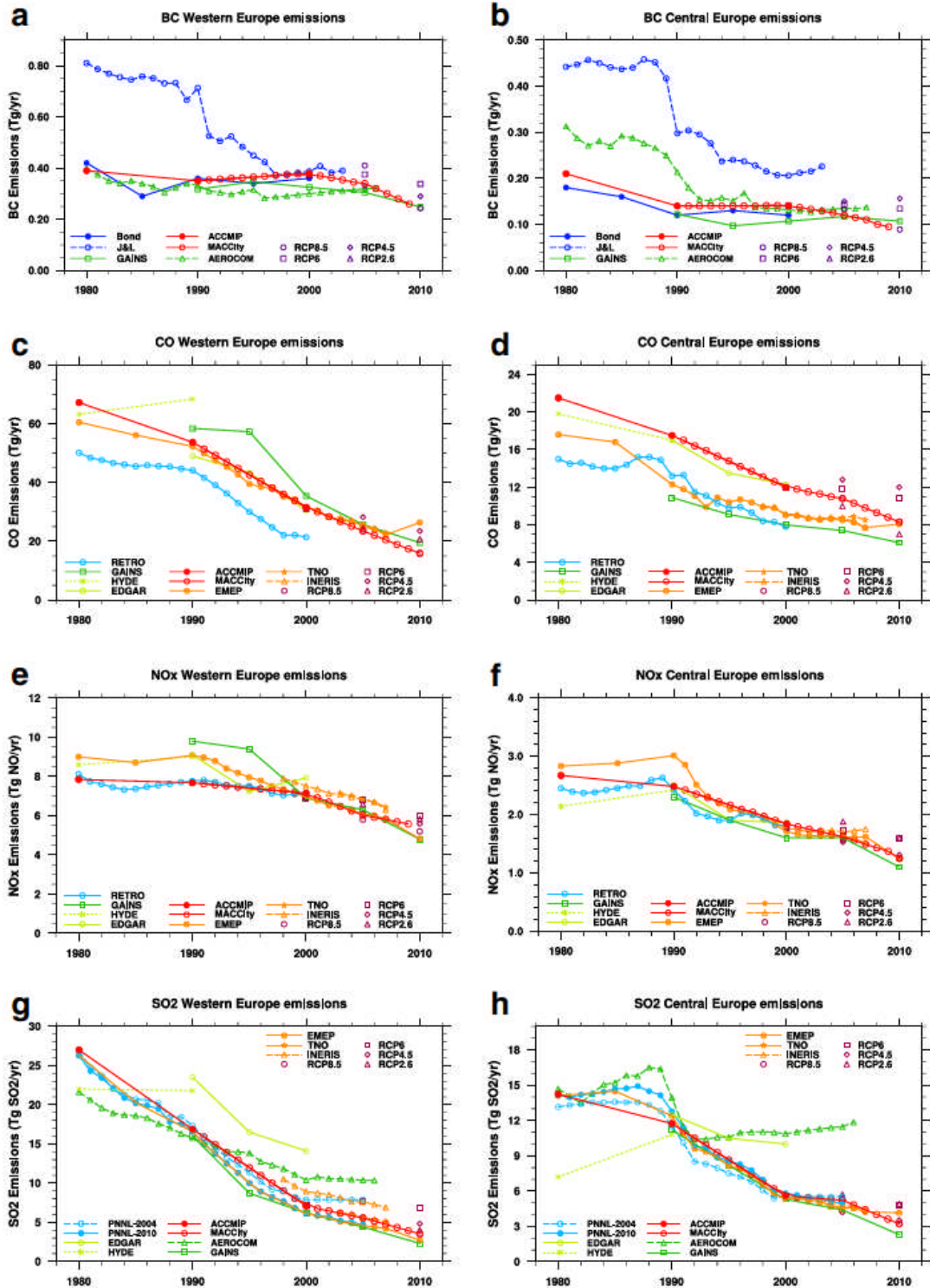


**Figure 1.6** Time series of the European emissions of BC, CO, NO<sub>x</sub> and SO<sub>2</sub> across Western and Central Europe from 1980 to 2010 in different emission inventories (Granier et al., 2011).

Whilst emissions have decreased across Europe, anthropogenic emissions have increased across other world regions due to population growth and

economic development (Forster et al. 2007; Manktelow et al. 2007; Leibensperger et al. 2012a). For example, SO<sub>2</sub> emissions in east Asia have increased by a factor of 7 from the 1960s to present day (Smith et al., 2011).

Natural emissions of aerosols and their precursor species are also important, with their emission flux strongly dependent on meteorological variables. They can contribute significantly to the background aerosol concentration, which makes them important to quantify, particularly as their pre-industrial and future state is uncertain (Andreae & Crutzen, 1997; Menon et al., 2002; Kloster et al., 2008; Carslaw et al., 2013).

Figure 1.6 highlights some of the discrepancies between different emission inventories in both the trend and magnitude of historical anthropogenic emissions. Emission inventories of aerosols and their precursor species represent a large uncertainty in modelling studies, although de Meij et al., (2006) showed that for model inter-comparisons structural differences in models were more important than the choice of inventory. Never-the-less it is important to have accurate inventories when predicting their impact on air quality and climate.

Changes in anthropogenic emissions affect aerosol concentrations and properties which can alter their impact on both air quality and the radiative balance (Arneth et al., 2009; Ramanathan & Feng, 2009; Fiore et al., 2012). The response of aerosol particles and their effect on climate to the substantial changes in anthropogenic emissions in both the past (Figures 1.5 and 1.6) and future is currently uncertain (Penner et al., 2010; Chalmers et al., 2012). Reductions in aerosol emissions have been attributed in part to the warming response in recent decades over the USA (Leibensperger et al., 2012a, 2012b; Mickley et al., 2012) and to an increase in extreme temperature and precipitation events in Europe (Sillmann et al., 2013). Simulating the effect on climate from the changes in emissions of aerosols (and their precursors) is particularly challenging due to their spatial and temporal variability in the atmosphere and the lack of knowledge regarding some processes (e.g. aerosol cloud interactions). It is important therefore to understand the response of aerosols (and their impacts) over the recent past when large changes in anthropogenic emissions have occurred to improve future predictions. In particular, it is important to understand the impact on air quality and climate from the implementation of historical legislation to reduce emissions of air pollutants, especially when designing future measures.

## 1.4 Long Term Aerosol Observations and Model Studies

Following the implementation of air pollution control legislation, ground-based monitoring networks were established to provide evidence of adherence to standards. The longest continuously operating networks monitoring aerosol concentrations and physiochemical properties exist in Europe (the European Monitoring and Evaluation Programme – EMEP, see Tørseth et al. (2012)) and North America (the Integrated Monitoring of Protected Visual Environments – IMPROVE, see <http://vista.cira.colostate.edu/improve/>). Observations of total aerosol mass and its constituent components are available from these networks since the 1970s. Aerosol Optical Depth (AOD) observations from the ground-based Aerosol Robotic Network (AERONET) (Holben et al., 1998) are available over the last 10 to 20 years across certain areas of the globe. Additionally long term observations of Surface Solar Radiation (SSR) are available since the 1950s over large parts of Europe from the ground-based Global Energy Balance Archive (GEBA). Whilst SSR is not a direct measurement of aerosols, changes in it can be used along with other observations and model simulations to infer the influence of aerosols on the surface radiation balance.

For model evaluation purposes there are limitations in both the spatial and temporal extent of such observational datasets. Additionally, the components and instrumental techniques used to provide measurements can be inconsistent throughout the entire operational time period at an individual measurement location. However, these observational datasets are a useful source of multi-decadal aerosol properties and concentrations with which to compare and evaluate model output.

Long term aerosol observations over Europe from the EMEP network show that both  $\text{SO}_2$  concentrations and  $\text{SO}_4^{2-}$  aerosol mass concentrations reduced by ~90% and 70% respectively over the period 1980 to 2009 (Figure 1.7 and in Tørseth et al. 2012). Large reductions in  $\text{SO}_2$  and  $\text{SO}_4^{2-}$  were also observed over the United States for a similar time period (Hand et al., 2012). These changes are primarily attributed to the reduction in anthropogenic emissions of  $\text{SO}_2$  due to economic factors and from the implementation of air quality legislation and abatement technologies. Smaller reductions have also occurred in concentrations of  $\text{NO}_2$ , ammonium and nitrate over the same time period (Fagerli & Aas, 2008).

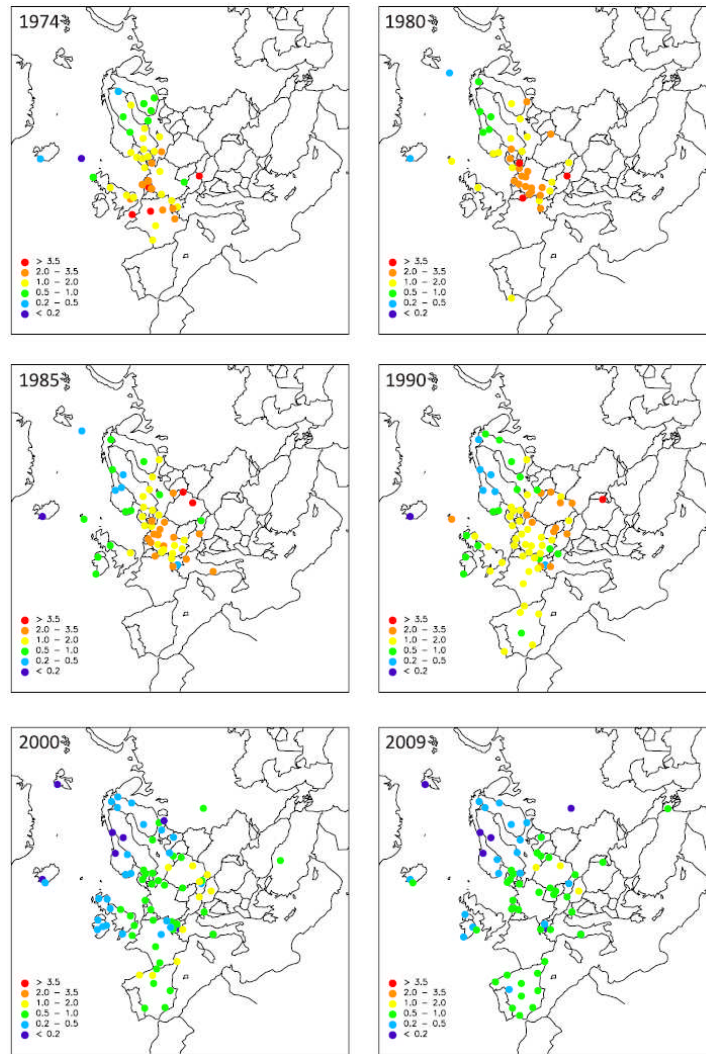


**Figure 1.7** Annual mean concentrations of  $\text{SO}_4^{2-}$  ( $\mu\text{g m}^{-3}$ ) in aerosols from 1974 to 2009 (Tørseth et al., 2012)

Reductions in both  $\text{PM}_{10}$  and  $\text{PM}_{2.5}$  were observed over Europe between 2000 and 2009 (Figure 1.8), although larger decreases were observed in smaller size particles (Barnpadimos et al., 2012; Tørseth et al., 2012). Aerosol number concentrations, a key parameter for aerosol climate interactions, were shown to decrease across Europe over the last 10 to 15 years with reductions in anthropogenic emissions identified as the strongest possible cause out of a number of options (Asmi et al., 2013). However, a similar study into temporal changes in aerosol optical properties (with potential climate implications) over Europe found no significant changes (Collaud Coen et al., 2013). Over the UK, Harrison et al., (2008) found that observations of  $\text{PM}_{10}$  have remained relatively stable between 1999 and 2006 even when reduction in anthropogenic emissions of precursor species are anticipated to have occurred.

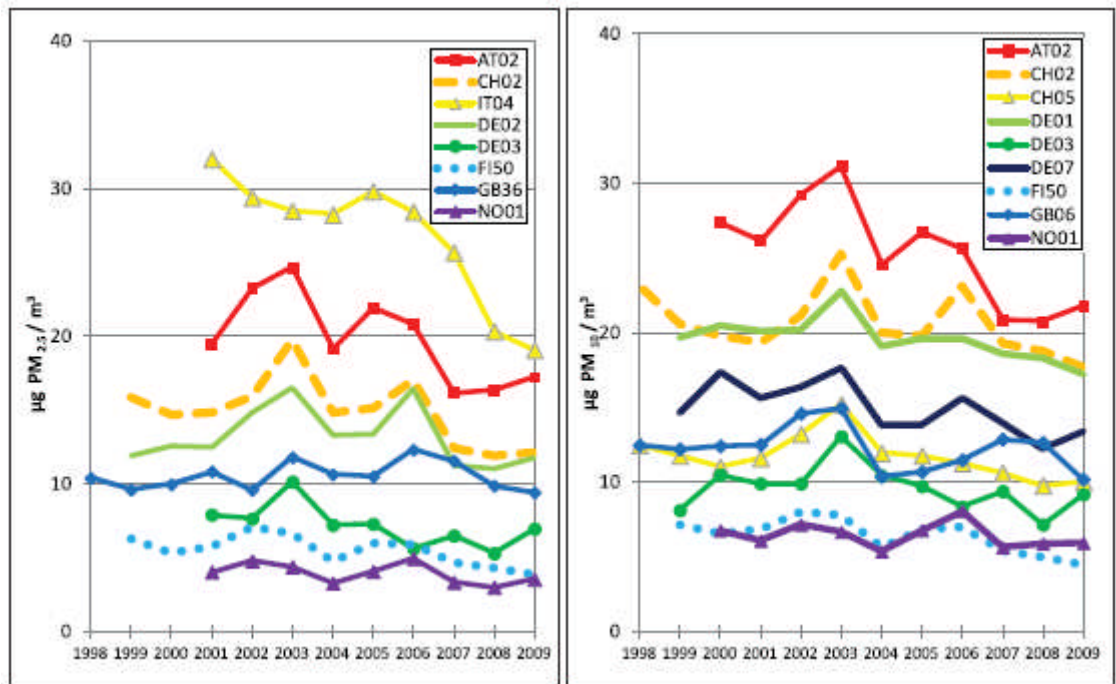


**Figure 1.8** Time series of PM<sub>2.5</sub> (left) and PM<sub>10</sub> (right) in  $\mu\text{g m}^{-3}$  at selected EMEP sites from 1998 to 2009 (Tørseth et al., 2012)

In contrast to the reduction in aerosol concentrations observed over Europe, measured AOD has increased over the last couple of decades in Asia (Krishna Moorthy et al., 2013). Increased anthropogenic aerosols due to industrialisation and population growth have been identified as major factors in this change and if it continues could have an important effect on climate over Asia.

Observed changes in SSR across Europe have shown a reduction or a “dimming” period in the 1980s and a subsequent increase in SSR or a “brightening” period from the 1990s onwards. Over Europe, these Observed changes in SSR have been in part attributed to changes in properties of clouds, aerosols and aerosol-cloud interactions (Wild, 2009).

Evaluating composition chemistry models against such observations is necessary to validate the simulated changes in aerosols and their radiative effects over multi-decadal timescales. Several studies have compared long-term aerosol observations to model simulations. Leibensperger et al., (2012a) used the Chemical Transport Model (CTM) GEOS-Chem to evaluate aerosol trends over the USA at decadal time slices and found that sulphate but not black carbon was well represented by the model. Berglen et al., (2007) compared European sulphate predicted by OsloCTM2 to observations and obtained a slight underprediction by the model when attempting to reproduce the reduction in observed concentrations.

Other studies have evaluated global models with a simplified aerosol scheme (mass only) for decadal time slices throughout the industrial period. Koch et al., (2011) found that their global simulations underestimated sulphate concentrations in the 1980s over Europe as well as the magnitude of the decreasing in concentrations. The inter-decadal variability of surface solar radiation was simulated well in this study but the magnitude was underestimated when compared to measurements. Skeie et al., (2011) achieved a good comparison between decadal mean concentrations of simulated and observed sulphate over Europe but under-predicted nitrate and organic aerosol concentrations over North America.

Other studies have evaluated aerosols in global models by using changes in AOD, a single property representative of the bulk aerosol. Lamarque et al., (2010) evaluated simulations of present day AOD against AERONET observations and reported a relatively good reproduction of inter-annual variability, apart from at high AOD values. Shindell et al., (2013) assessed AOD from the models involved in the Atmospheric Chemistry and Climate Model Inter comparison Project (ACCMIP) and showed that most captured the trends between 1980 to 2010 relatively well, although many under predicted present day AOD, particularly over East Asia.

A multi-model assessment of aerosol trends in Europe over the last decade was undertaken by Colette et al., (2011). Models were able to reproduce the decrease in  $PM_{10}$  observed at measurement sites but failed to reproduce the increase observed at certain locations. However, the modelled absolute  $PM_{10}$  mass concentrations were consistently lower than that measured. Chin et al., (2014) analysed changes in marine and continental aerosols from 1980 to 2009 using the GOCART model and numerous satellite and ground based observations of aerosol properties. The modelled multi-decadal changes in aerosol properties were comparable, but the overall simulated magnitudes were lower than that observed. This analysis highlighted the need for smaller spatial scale studies as important regional changes in aerosol properties can potentially be masked by compensatory changes observed at the global scale.

Model simulations set up to reproduce changes in SSR have been unable to reproduce both the timing and magnitude of the dimming period but are able to simulate the observed brightening trend (Folini & Wild, 2011; Allen et al., 2013). The failure to reproduce the dimming signal in observed SSR was attributed to an underestimation of the aerosol direct effect (Allen et al., 2013) whilst Chiacchio et al., (2015) found that the inclusion of aerosols

were necessary to replicate the observed brightening signal. These studies indicate that including a detailed treatment of aerosols is essential in being able to reproduce changes in surface radiative fluxes.

Multi-decadal observations of aerosols can provide direct evidence of the causes behind any spatial and temporal changes in them and also of the adherence to air quality limit values set for the protection of human health. In conjunction with model studies, observations can provide confidence in the results of simulations and also aid in the identification of the causes behind long term changes in aerosol properties and processes.

## **1.5 Aerosols Processes affected by Emission Changes**

Changes to the magnitude and location of anthropogenic emissions can induce significant non-linear responses in aerosol processes, properties and also their interactions with climate (Stier et al., 2006a). Understanding how aerosols interact with climate depends on a number of interrelated factors including; the distribution of emissions (both spatially and temporally), meteorological conditions (e.g. temperature, precipitation), transport processes within the overall model and the microphysical processes (secondary chemical production, water uptake, removal processes etc.) implemented within the aerosol model (Textor et al., 2007).

In order to identify appropriate future emission reduction policies it is essential to improve the understanding how these interactions of aerosol processes with climate have changed over the recent past (Stier et al., 2006b; Langmann et al., 2008).

### **1.5.1 Sources and Emissions**

Sources of aerosols and their precursor species are diverse and numerous, with both anthropogenic and natural origins. Aerosols can be either primary or secondary in nature. Primary aerosols are emitted directly into the atmosphere and can be from anthropogenic (from incomplete combustion) and natural sources (via mechanical formation mechanisms e.g. mineral dust, sea spray, biological debris). Secondary particles can be formed in-situ via gas-to-particle conversion (e.g. new particle formation of  $\text{SO}_4^{2-}$  from the emissions of  $\text{SO}_2$ ) or by the condensation of gas phase species onto existing aerosol particles. Table 1.4 shows global estimates of emission fluxes for primary and secondary aerosols from both natural and anthropogenic sources.

**Table 1.4** Global emission estimates for major aerosol classes (Seinfeld and Pandis, 2006, and references therein)

Source				Estimated Flux (Tg yr <sup>-1</sup> )		
Natural	Primary	Mineral Dust	0.1-1.0 µm	48		
			1.0-2.5 µm	260		
			2.5-5.0 µm	609		
			5.0-10.0 µm	573		
			0.1-10.0 µm	1490		
	Secondary	Seasalt			10,100	
			Volcanic Dust		30	
			Biological debris		50	
		Sulphate from DMS			12.4	
			Sulphates from volcanic SO <sub>2</sub>		20	
			Organic aerosol from biogenic VOC		11.2	
		Anthropogenic	Primary	Industrial dust (except BC)		100
				Black Carbon		12 <sup>a</sup>
				Organic aerosols		81 <sup>a</sup>
			Secondary	Sulphates from SO <sub>2</sub>		48.6 <sup>b</sup>
Nitrates from NO <sub>2</sub>				21.3 <sup>c</sup>		

<sup>a</sup>Tg C, <sup>b</sup>Tg S, <sup>c</sup>Tg NO<sub>3</sub>

Table 1.4 shows that emission fluxes of primary aerosols from natural sources are much larger than secondary anthropogenic sources. However, these tend to produce coarse particles that are larger in size and have shorter residence times in the atmosphere. Anthropogenic sources tend to produce particles in the accumulation size range (100 nm – 1 µm), which have longer residence times and are the size range of most importance for interaction with radiation. Whilst natural aerosol sources have tended to remain relatively constant, albeit with larger interannual variability, anthropogenic sources have increased over the industrial era thus having a strong influence on aerosol properties and effects.

Changes in anthropogenic emissions cannot be solely used to infer the change in aerosol radiative effects as it is important to consider aerosol lifetime, ageing, size, composition and mixing state (Stier et al., 2006b).

### 1.5.2 Chemical Composition

Aerosol particles are made up of a number of different chemical components that tend to be internally mixed. The extent of mixing is primarily determined by the nature and proximity of the source and the extent of processing (ageing) undergone. The chemical composition of aerosols is important in determining their interaction with radiation via optical properties and

influence on clouds (Lohmann & Feichter, 2005). Typical components include sulphate, ammonium, nitrate, seasalt, carbonaceous material and mineral dust; as summarised in Table 1.5.

Changes to anthropogenic emissions can affect aerosol formation rates by altering primary aerosol emissions as well as the availability of aerosol precursor species and the oxidative capacity of the atmosphere. It is important to consider how the oxidative capacity of the atmosphere has altered in response to emission changes over different regions when simulating aerosol concentrations (Unger et al., 2006; Berglen et al., 2007; Yu et al., 2012; Megaritis et al., 2013). In particular, a latitude dependent oxidation efficiency was shown as anthropogenic emissions have shifted southwards from Europe and North America towards east and south Asia over the last 30 years, which can affect aerosol formation (Manktelow et al., 2007; Pozzoli et al., 2011; Skeie et al., 2011).

Changes in anthropogenic emissions can also induce changes to other properties relevant to aerosol formation. Cloud water pH is an important property in aqueous phase formation of sulphate aerosols (Roelofs et al., 2001). The review by Ervens (2015) highlighted that the treatment of in-cloud aqueous phase sulphate formation and calculation of cloud water pH varies across different global composition climate models. The underrepresentation of this process has been identified in studies as a possible cause of the simulated underestimation of observed sulphate aerosol mass concentrations across regions such as Europe (Feichter et al., 1996; Kasibhatla et al., 1997; Roelofs et al., 2001; Berglen, 2004; Textor et al., 2006). Different representations of cloud water pH by the use of different cloud droplet schemes can also affect aerosol optical properties and interaction with radiation (Kreidenweis, 2003; Roelofs et al., 2006). Cloud water pH was identified as being the third most important processes controlling CCN uncertainty, particularly in winter across northern mid-latitudes (Lee et al., 2013). Understanding the sensitivity of sulphate aerosol formation to cloud water pH is therefore important to be able to accurately represent aerosol mass concentrations and aerosol interactions with climate. Reductions in the emissions of acidifying gases over the last 30 years across Europe and North America have resulted in an increase in cloud and rainwater pH (Vet et al., 2014; Schwab et al., 2016). The effect of such a temporal change in pH across different regions on sulphate aerosol formation and their radiative effects over recent decades is not currently quantified.

**Table 1.5** Summary of sources, formation and effects of aerosol components (Boucher et al., 2013)

Species	Formation	Main Sources	Effects
Sulphate (SO <sub>4</sub> <sup>2-</sup> ) or after reaction of H <sub>2</sub> SO <sub>4</sub> with NH <sub>3</sub> ammonium sulphate ((NH <sub>4</sub> ) <sub>2</sub> SO <sub>4</sub> )	Secondary particles formed from gas phase oxidation products of SO <sub>2</sub> and DMS. Also in-cloud aqueous phase oxidation to form secondary particles	Anthropogenic fossil fuel burning, volcanic and biomass burning emissions of SO <sub>2</sub> . Phytoplankton emissions of DMS	Strong scattering aerosol with RFari of -0.34 W m <sup>-2</sup> . CCN active.
Nitrate (NO <sub>3</sub> <sup>-</sup> ) or after reaction of HNO <sub>3</sub> with NH <sub>3</sub> ammonium nitrate (NH <sub>4</sub> NO <sub>3</sub> )	Secondary particles formed from reactions of NO <sub>x</sub> , nitric acid (HNO <sub>3</sub> ) and NH <sub>3</sub> . Requires low amounts of SO <sub>4</sub> <sup>2-</sup> and excess NH <sub>3</sub> .	NO <sub>x</sub> emissions from fossil fuel combustion, soils, lightning, biomass burning. NH <sub>3</sub> emissions from mainly agriculture.	Strong scattering aerosol with RFari of -0.11 W m <sup>-2</sup> . CCN active.
Black Carbon (BC)	Primary emissions	Incomplete combustion of fossil fuel, biofuel and biomass burning	Stronger absorber of shortwave radiation with RFari of +0.4 W m <sup>-2</sup> . CCN active when coated.
Particulate Organic Matter (POM)	Primary emissions. Also secondary formation from oxidation of biogenic or anthropogenic VOCs	Primary emissions from fossil fuel, biofuel and biomass burning. Also primary material from algae and pollen spores. Emissions of VOCs from both biogenic (vegetation) and anthropogenic (incomplete combustion) sources.	Light scattering and CCN active. Although some are also medium absorbers of UV and visible radiation. RFari of primary organic aerosol is -0.09 W m <sup>-2</sup> whilst form secondary it is -0.03 W m <sup>-2</sup> .
Sea salt (NaCl)	Primary emissions	White caps and bubble bursting induced by breaking of waves.	Light scattering in visible. CCN active. No individual RFari calculated.
Mineral Dust	Primary emissions	Mechanical attrition of wind on bare soil. Soil resuspension. Anthropogenic activities of agriculture and construction operations.	Light scattering of visible and absorber of infrared. RFari of -0.1 W m <sup>-2</sup> .

The chemical mixing state of aerosols will also alter in accordance with changes in precursor emissions. Changes to the chemical mixing state will alter the composition and ageing rate of particles within the climatically important internally mixed accumulation mode, affecting the aerosol optical properties and radiative effects (Stier et al., 2006b; Spracklen et al., 2010; Cappa et al., 2012).

It is uncertain how changes in emissions will affect aerosol burdens and lifetimes as they are predicted to both increase (Rae et al., 2007; Kloster et al., 2009) and decrease (Liao et al., 2006) under future emission scenarios. Geographical shifts in emissions can alter the atmospheric lifetime of aerosols due to the different chemical and meteorological conditions at the new location (Stier et al. 2006b; Textor et al. 2007; Kloster et al. 2008). Changes to aerosol burdens and lifetimes can affect the number of aerosols at climate relevant sizes and therefore also their radiative effect.

### 1.5.3 Microphysical Processes

The aerosol size distribution determines how aerosols interact with clouds and radiation and how efficiently they are removed from the atmosphere (i.e. lifetime). The aerosol size distribution can generally be split into four size modes based on particle diameter ( $D_p$ ): nucleation mode ( $D_p < 10$  nm), Aitken ( $D_p$  10-100 nm), accumulation ( $D_p$  100 nm – 1  $\mu$ m) and coarse ( $D_p > 1$   $\mu$ m). Nucleation and Aitken modes tend to be dominated by secondary aerosols (e.g.  $\text{SO}_4^{2-}$ ), which make up most of the number concentration. Whereas primary natural aerosols (e.g. mineral dust) tend to dominate the coarse mode and consequently the mass concentration. Aerosols in the accumulation mode have the longest residence time, provide the majority of CCN and are very efficient at scattering radiation, making this mode important for aerosol interactions with climate (Seinfeld & Pandis, 2006). Figure 1.9 and Table 1.6 summarise the various chemical and microphysical processes that influence the aerosol size distribution.

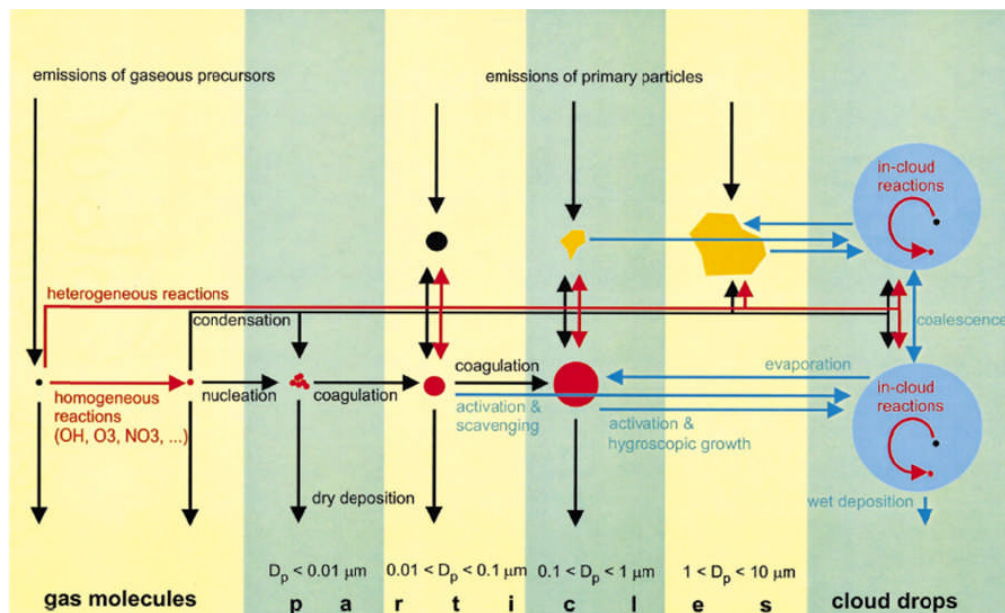


**Figure 1.9** Schematic of the microphysical and chemical processes that influence the evolution of the atmospheric aerosol (Raes et al., 2000).

The aerosol size distribution can be altered in response to changing sources of emissions and other chemical and microphysical processes in the atmosphere, which can ultimately affect the climate relevant properties of aerosols. Changes to the magnitude and location of anthropogenic emissions can alter the new particle formation rate at that location (Spracklen et al. 2010; Merikanto et al. 2010; Ahlm et al. 2013), which is important for producing particles of CCN relevant sizes. To reduce the uncertainty in aerosol radiative effects it is important to increase the understanding of how changes in emissions impact on the formation of climate relevant particles (CCN sizes) at different spatial and temporal scales.

**Table 1.6** Summary of the main microphysical processes influencing the aerosol size distribution

Process	Description	Example
New particle formation (nucleation)	When concentrations of volatile species exceed their equilibrium vapour pressure, particles can be nucleated to form new clusters, which quickly grow via condensation and coagulation	Sulphate formation from H <sub>2</sub> SO <sub>4</sub> vapour
Condensational growth	Conversion of gas-phase species to particles via heterogeneous nucleation (increases size and mass but conserves number). Important for smaller sized particles (<100 nm) and in regions of high particle number concentration (Raes et al., 2000).	H <sub>2</sub> SO <sub>4</sub> vapour and VOCs
Coagulation	Collision and adhesion of particles to form larger sizes (decreases number but conserves mass). Important in smaller sized particles and at high number concentrations.	Pre-existing particles of larger size
Activation	Activation of particles of a particular size and composition (subset behaving as CCN) into cloud droplets at a critical supersaturation	Hygroscopic particles e.g. SO <sub>4</sub> <sup>2-</sup> , NO <sub>3</sub> <sup>-</sup> , NaCl, organics

### 1.5.4 Removal

The main loss mechanism for aerosols in the atmosphere is wet removal via both in-cloud scavenging (removal of activated fraction) and rain out (below cloud impaction), which is strongly affected by their size and chemical composition. Dry deposition of particles onto surfaces is also important, especially for larger particles which are removed relatively quickly from the atmosphere by gravitational settling. Small particles can be removed from the atmosphere by diffusing to the Earth's surface. Particles between 0.1 and 1 µm in diameter tend to accumulate in the atmosphere as dry removal is slow but with the right hygroscopic properties they can be activated in clouds and removed by wet deposition. Aerosols within the accumulation mode tend to have lifetimes in the atmosphere of between a few days to

weeks (Seinfeld & Pandis, 2006). Changes to the geographical location of emissions can affect the aerosol burden and lifetime, as described in section 1.5.2. In addition, the representation of cloud and precipitation chemistry within global composition climate models is highly uncertain and can lead to large errors when reproducing wet deposition (Tost et al., 2007).

## 1.6 Summary and Motivation

Poor air quality from elevated levels of fine particulate matter are currently leading to a substantial number of premature mortalities around the world (World Health Organization, 2014). In addition, the radiative effects of aerosols on climate are relatively large and of opposite sign to the greenhouse gas effect, but their value is highly uncertain (Boucher et al., 2013). Aerosols have substantial impacts on air quality, human health and climate via modification of the Earth's radiative balance. Additionally, there are also important interactions and feedbacks between air quality and climate, as summarised in Figure 1.10. To improve our understanding and future predictions of aerosol impacts on air quality and climate, historical changes must first be investigated.

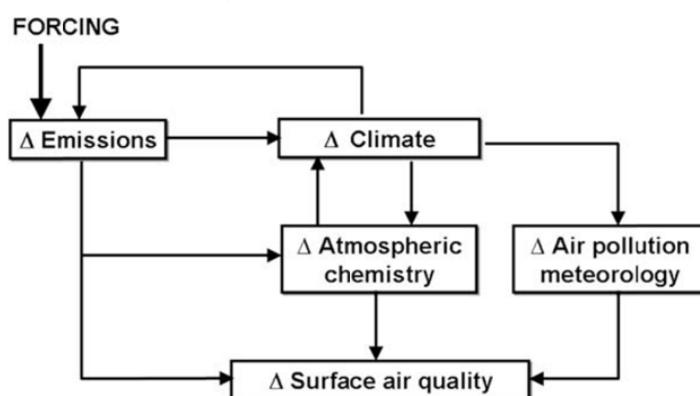


**Figure 1.10** Schematic showing the air quality chemistry climate interactions and feedbacks (Jacob & Winner, 2009).

The large change in anthropogenic emissions that has occurred over the industrial period has undoubtedly altered aerosol concentrations, properties and their effect on climate and air quality. To further the understanding of how changes in anthropogenic emissions have affected aerosols, air quality and climate, studies using detailed composition climate models along with long term aerosol observations are required over recent decades.

Previous model evaluation studies (see section 1.4) have tended to focus on a particular region of the world (e.g. USA; Leibensperger et al., (2012a)), used a simplified treatment (mass only) of aerosols (e.g. Koch et al., 2011)

or evaluated the model against a limited range of aerosol properties over a selected time period (e.g. AOD at time slices; Shindell et al., (2013)). This thesis will improve on such studies by using a larger number and type of long term observations of aerosol properties (sulphate, aerosol mass, number concentration, AOD and SSR) to evaluate a composition climate model, with an improved treatment of aerosols, across Europe; a region previously neglected for such long term model evaluation studies. The long term model evaluation across Europe is particularly important as it is a region that has experienced large changes in anthropogenic emissions over recent decades, and has the potential for additional future changes.

The reduction in anthropogenic emissions of air pollutants over the last 40 years across Europe has been in part due to the implementation of specific legislative measures and technology improvements. The impact on air quality and climate from historical or future changes in anthropogenic emissions has been assessed in studies by Unger et al., (2008), Colette et al., (2011) and Koch et al., (2011). However, such studies have not attributed the impact on air quality, human health and climate to the specific legislation and policy measures that were implemented to reduce air pollutant emissions. It is important to assess the impact of past air pollutant legislative and policy measures when designing future measures to make sure the desired improvements in air quality and human health are achieved, as well as avoiding any inadvertent impacts on climate.

Changes in anthropogenic emissions can also affect properties relevant to aerosol formation and aerosol radiative effects, like cloud water pH. The complexity with which global composition climate models represent cloud water pH varies (Ervens, 2015) and has been identified as causing some of the simulated underestimation in sulphate aerosol mass over Europe (Roelofs et al., 2001; Berglen, 2004). In addition, aerosol optical properties and their interaction with radiation can also be affected by the use of different cloud droplet schemes, and hence cloud water pH (Kreidenweis, 2003; Roelofs et al., 2006). In an uncertainty analysis of aerosol properties and processes, Lee et al., (2013) found that cloud droplet pH was the third most important factor controlling uncertainty in CCN concentrations. Therefore understanding the sensitivity of sulphate aerosol formation to variations in cloud water pH induced by emission changes is important in accurately determining how aerosols and their interaction with climate has changed over time. There are currently no studies into the effect of temporal changes in cloud water pH on sulphate aerosol formation and aerosol

radiative effects over recent decades. This could be particularly important as changes in anthropogenic emissions are different regionally and could induce important but different responses in cloud water pH and aerosols.

Understanding the response of aerosols to anthropogenic emissions is complicated by the interaction of air quality with climate (Figure 1.10), and the potentially large but uncertain feedback response of air quality to changes in climate (Jacob & Winner, 2009; von Schneidemesser et al., 2015).

It is important therefore to understand the effect that changes in anthropogenic emissions have on aerosol properties and processes and how this alters their interaction with the radiative balance. This is particularly important over the latter half of the 20<sup>th</sup> Century when significant changes in anthropogenic emissions have occurred across different regions. In particular, it is important to understand the impact on emissions and aerosols from the implementation of air pollutant control legislation when designing any future legislation. Comparing long term observations to output from a global composition climate model will aid in determining the response of aerosol processes and properties to applied perturbations, which are important to ensure that future mitigation measures deliver the anticipated benefits.

## **1.7 Thesis Aims and Objectives**

The overall aim of this thesis is to investigate how changes in anthropogenic emissions of aerosol precursor species have impacted aerosols and their radiative effect. The work will focus on the European regional domain over the period 1960 to 2009 when large changes in anthropogenic emissions have occurred. The work has been carried out using the global composition climate model HadGEM3-UKCA and observations of aerosol properties from monitoring networks over Europe.

The individual aims of each chapter are set out below:

1. How have aerosols and their radiative effects varied across Europe over the period 1960 to 2009 in response to changes in anthropogenic emissions?
  - a. What are the observed trends in aerosol properties over Europe?
  - b. Can a global composition climate model reproduce such long term trends?

- c. What processes or understanding are we missing within our model that is limiting our ability to reproduce such long term trends?
  - d. How has the aerosol radiative effect changed across Europe over the period 1960 to 2009 in response to changes in anthropogenic emissions?
  - e. Given the model evaluation of aerosol properties can we have confidence in the simulated changes in the aerosol radiative effects?
2. How important is a spatially and temporally varying value of cloud water pH for the accurate prediction of sulphate aerosol formation and its radiative effects?
- a. What is the global and regional impact of a change in pH on sulphate aerosol formation?
  - b. Does a changes in pH improve the long term model evaluation of sulphate aerosols over Europe?
  - c. How does a change in cloud water pH affect the aerosol size distribution and number of particles available at climate relevant sizes?
  - d. What is the impact on the aerosol radiative effect of the change in cloud water pH over the period 1960 to 2009?
  - e. Is a fixed global value of cloud water pH sufficient to represent sulphate formation and its radiative impact over the period 1960 to 2009?
3. What is the impact of historical European air quality policy measures and technology changes on air quality, human health and climate?
- a. How much have historical European policy measures to reduce air pollutants impacted on anthropogenic emissions?
  - b. How much has particulate air quality been improved by the implementation of air pollution mitigation measures and technology improvements?
  - c. What has been the impact on human health from the implementation of these measures?
  - d. What are the unintended impacts on climate from the implementation of historical European measures to reduce air pollutants?

## 1.8 References

- AEA Technology (2005). Methodology for the Cost-Benefit analysis for CAFE: Volume 2: Health Impact Assessment.
- Ahlm, L., Julin, J., Fountoukis, C., Pandis, S.N. & Riipinen, I. (2013). Particle number concentrations over Europe in 2030: the role of emissions and new particle formation. *Atmospheric Chemistry and Physics*. 13 (4). p.pp. 10271–10283.
- Albrecht, B.A. (1989). Aerosols, Cloud Microphysics and Fractional Cloudiness. *Science*. 245 (4923). p.pp. 1227–1230.
- Allen, R.J., Norris, J.R. & Wild, M. (2013). Evaluation of multidecadal variability in CMIP5 surface solar radiation and inferred underestimation of aerosol direct effects over Europe, China, Japan, and India. *Journal of Geophysical Research: Atmospheres*. 118 (12). p.pp. 6311–6336.
- Andreae, M.O. & Crutzen, P.J. (1997). Atmospheric Aerosols : Biogeochemical Sources and in Atmospheric Chemistry Role. *Science*. 276 (5315). p.pp. 1052–1058.
- Andreae, M.O. & Ramanathan, V. (2013). Climate's Dark Forcings. *Science*. 340 (6130). p.pp. 280–281.
- Anenberg, S.C., Horowitz, L.W., Tong, D.Q. & West, J.J. (2010). An estimate of the global burden of anthropogenic ozone and fine particulate matter on premature human mortality using atmospheric modeling. *Environmental Health Perspectives*. 118 (9). p.pp. 1189–1195.
- Arnth, A., Unger, N., Kulmala, M. & Andreae, M.O. (2009). Clean the Air, Heat the Planet? *Science*. 326 (5953). p.pp. 672–673.
- Asmi, A., Collaud Coen, M., Ogren, J. A., Andrews, E., Sheridan, P., Jefferson, A., Weingartner, E., Baltensperger, U., Bukowiecki, N., Lihavainen, H., Kivekäs, N., Asmi, E., Aalto, P.P., Kulmala, M., Wiedensohler, a., Birmili, W., Hamed, A., O'Dowd, C., G Jennings, S., Weller, R., Flentje, H., Fjaeraa, A. M., Fiebig, M., Myhre, C.L., Hallar, A. G., Swietlicki, E., Kristensson, A. & Laj, P. (2013). Aerosol decadal trends – Part 2: In-situ aerosol particle number concentrations at GAW and ACTRIS stations. *Atmospheric Chemistry and Physics*. 13 (2). p.pp. 895–916.
- Baltensperger, U. & Nyeki, S. (1998). Atmospheric Aerosols. In: I. Colbeck (ed.). *Physical and Chemical Properties of Aerosols*. Blackie Academics and Professional.

- Barmpadimos, I., Keller, J., Oderbolz, D., Hueglin, C. & Prévôt, A.S.H. (2012). One decade of parallel fine (PM<sub>2.5</sub>) and coarse (PM<sub>10</sub>–PM<sub>2.5</sub>) particulate matter measurements in Europe: trends and variability. *Atmospheric Chemistry and Physics*. 12. p.pp. 3189–3203.
- Berglen, T.F. (2004). A global model of the coupled sulfur/oxidant chemistry in the troposphere: The sulfur cycle. *Journal of Geophysical Research*. 109 (D19). p.p. D19310.
- Berglen, T.F., Myhre, G., Isaksen, I.S.A., Vestreng, V. & Smith, S.J. (2007). Sulphate trends in Europe: are we able to model the recent observed decrease? *Tellus B*. 59 (4). p.pp. 773–786.
- Bond, T.C., Doherty, S.J., Fahey, D.W., Forster, P.M., Berntsen, T., DeAngelo, B.J., Flanner, M.G., Ghan, S., Karcher, B., Koch, D., Kinne, S., Kondo, Y., Quinn, P.K., Sarofim, M.C., Schultz, M.G., Schulz, M., Venkataraman, C., Zhang, H., Zhang, S., Bellouin, N., Guttikunda, S.K., Hopke, P.K., Jacobson, M.Z., Kaiser, J.W., Klimont, Z., Lohmann, U., Schwarz, J.P., Shindell, D.T., Storelvmo, T., Warren, S.G. & Zender, C.S. (2013). Bounding the role of black carbon in the climate system: A scientific assessment. *Journal of Geophysical Research: Atmospheres*. 118 (11). p.pp. 5380–5552.
- Boucher, O., Randall, P., Artaxo, P., Bretherton, C., Feingold, G., Forster, P., Kerminen, V.-M., Kondo, Y., Liao, H., Lohmann, U., Rasch, P., Satheesh, S.K., Sherwood, S., Stevens, B. & Zhang, X.Y. (2013). Clouds and Aerosols. In: *Climate Change 2013: The Physical Science Basis. Contribution of Working Group I to the Fifth Assessment Report of the Intergovernmental Panel on Climate Change*. Cambridge University Press.
- Brunekreef, B. & Holgate, S.T. (2002). Air pollution and health. *Lancet*. 360 (9341). p.pp. 1233–42.
- Burnett, R.T., Arden Pope, C., Ezzati, M., Olives, C., Lim, S.S., Mehta, S., Shin, H.H., Singh, G., Hubbell, B., Brauer, M., Ross Anderson, H., Smith, K.R., Balme, J.R., Bruce, N.G., Kan, H., Laden, F., Prüss-Ustün, A., Turner, M.C., Gapstur, S.M., Diver, W.R. & Cohen, A. (2014). An integrated risk function for estimating the global burden of disease attributable to ambient fine particulate matter exposure. *Environmental Health Perspectives*. 122. p.pp. 397–403.
- Caiazzo, F., Ashok, A., Waitz, I.A., Yim, S.H.L. & Barrett, S.R.H. (2013). Air pollution and early deaths in the United States. Part I: Quantifying the impact of major sectors in 2005. *Atmospheric Environment*. 79. p.pp. 198–208.

- Cappa, C.D., Onasch, T.B., Massoli, P., Worsnop, D.R., Bates, T.S., Cross, E.S., Davidovits, P., Hakala, J., Hayden, K.L., Jobson, B.T., Kolesar, K.R., Lack, D. a, Lerner, B.M., Li, S.-M., Mellon, D., Nuaaman, I., Olfert, J.S., Petäjä, T., Quinn, P.K., Song, C., Subramanian, R., Williams, E.J. & Zaveri, R. a (2012). Radiative absorption enhancements due to the mixing state of atmospheric black carbon. *Science (New York, N.Y.)*. 337 (6098). p.pp. 1078–81.
- Carslaw, K.S., Lee, L. A., Reddington, C.L., Pringle, K.J., Rap, A., Forster, P.M., Mann, G.W., Spracklen, D. V., Woodhouse, M.T., Regayre, L. a. & Pierce, J.R. (2013). Large contribution of natural aerosols to uncertainty in indirect forcing. *Nature*. 503 (7474). p.pp. 67–71.
- Chalmers, N., Highwood, E.J., Hawkins, E., Sutton, R. & Wilcox, L.J. (2012). Aerosol contribution to the rapid warming of near-term climate under RCP 2.6. *Geophysical Research Letters*. 39 (18). p.pp. 2–7.
- Chiacchio, M., Solmon, F., Giorgi, F., Stackhouse, P. & Wild, M. (2015). Evaluation of the radiation budget with a regional climate model over Europe and inspection of dimming and brightening. *Journal of Geophysical Research: Atmospheres*. 120 (5). p.pp. 1951–1971.
- Chin, M., Diehl, T., Tan, Q., Prospero, J.M., Kahn, R.A., Remer, L.A., Yu, H., Sayer, A.M., Bian, H., Geogdzhayev, I. V., Holben, B.N., Howell, S.G., Huebert, B.J., Hsu, N.C., Kim, D., Kucsera, T.L., Levy, R.C., Mishchenko, M.I., Pan, X., Quinn, P.K., Schuster, G.L., Streets, D.G., Strode, S.A., Torres, O. & Zhao, X.-P. (2014). Multi-decadal aerosol variations from 1980 to 2009: a perspective from observations and a global model. *Atmospheric Chemistry and Physics*. 14 (7). p.pp. 3657–3690.
- Cohen, A.J., Ross Anderson, H., Ostro, B., Pandey, K.D., Krzyzanowski, M., Künzli, N., Gutschmidt, K., Pope, A., Romieu, I., Samet, J.M. & Smith, K. (2005). The Global Burden of Disease Due to Outdoor Air Pollution. *Journal of Toxicology and Environmental Health, Part A*. 68 (January 2016). p.pp. 1301–1307.
- Colette, A., Granier, C., Hodnebrog, Ø., Jakobs, H., Maurizi, A., Nyiri, A., Bessagnet, B., D’Angiola, A., D’Isidoro, M., Gauss, M., Meleux, F., Memmesheimer, M., Mieville, A., Rouïl, L., Russo, F., Solberg, S., Stordal, F. & Tampieri, F. (2011). Air quality trends in Europe over the past decade: a first multi-model assessment. *Atmospheric Chemistry and Physics*. 11 (22). p.pp. 11657–11678.
- Collaud Coen, M., Andrews, E., Asmi, A., Baltensperger, U., Bukowiecki, N., Day, D., Fiebig, M., Fjaeraa, A. M., Flentje, H., Hyvärinen, A., Jefferson, A., Jennings, S.G., Kouvarakis, G., Lihavainen, H., Lund Myhre, C., Malm, W.C., Mihapopoulos,

- N., Molenaar, J. V., O'Dowd, C., Ogren, J. A., Schichtel, B. A., Sheridan, P., Virkkula, A., Weingartner, E., Weller, R. & Laj, P. (2013). Aerosol decadal trends – Part 1: In-situ optical measurements at GAW and IMPROVE stations. *Atmospheric Chemistry and Physics*. 13 (2). p.pp. 869–894.
- COMEAP (2010). The Mortality Effects of Long-term Exposure to Particulate Air Pollution in the United Kingdom.
- Dockery, D.W., Pope III, C.A., Xu, X., Spengler, J.D., Ware, J.H., Fay, M.E., Ferris, B.G. & Speizer, F.E. (1993). An Association between Mortality and Air Pollution in Six U.S. Cities. *N Engl J Med*. 329 (24). p.pp. 1753–1759.
- Dusek, U., Frank, G.P., Hildebrandt, L., Curtius, J., Schneider, J., Walter, S., Chand, D., Drewnick, F., Hings, S., Jung, D., Borrmann, S. & Andreae, M.O. (2006). Size matters more than chemistry for cloud-nucleating ability of aerosol particles. *Science (New York, N.Y.)*. 312 (5778). p.pp. 1375–8.
- Ervens, B. (2015). Modeling the Processing of Aerosol and Trace Gases in Clouds and Fogs. *Chemical Reviews*. 115. p.pp. 4157–4198.
- European Environment Agency (EEA) (2014). Air quality in Europe - 2014 report.
- Fagerli, H. & Aas, W. (2008). Trends of nitrogen in air and precipitation: Model results and observations at EMEP sites in Europe, 1980–2003. *Environmental Pollution*. 154 (3). p.pp. 448–461.
- Feichter, J., Kjellström, E., Rodhe, H., Dentener, F., Lelieveld, J. & Roelofs, G.-J. (1996). Simulation of the tropospheric sulfur cycle in a global climate model. *Atmospheric Environment*. 30 (10-11). p.pp. 1693–1707.
- Fiore, A.M., Naik, V., Spracklen, D. V, Steiner, A., Unger, N., Prather, M., Bergmann, D., Cameron-Smith, P.J., Cionni, I., Collins, W.J., Dalsøren, S., Eyring, V., Folberth, G. A, Ginoux, P., Horowitz, L.W., Josse, B., Lamarque, J.-F., MacKenzie, I. a, Nagashima, T., O'Connor, F.M., Righi, M., Rumbold, S.T., Shindell, D.T., Skeie, R.B., Sudo, K., Szopa, S., Takemura, T. & Zeng, G. (2012). Global air quality and climate. *Chemical Society reviews*. 41 (19). p.pp. 6663–83.
- Folini, D. & Wild, M. (2011). Aerosol emissions and dimming/brightening in Europe: Sensitivity studies with ECHAM5-HAM. *Journal of Geophysical Research*. 116 (D21). p.p. D21104.
- Forster, P.M., Ramaswamy, V., Artaxo, P., Bernsten, T., Betts, R., Fahey, D.W., Haywood, J., Lean, J., Lowe, D.C., Myhre, G., Nganga, J., Prinn, R., Raga, G., Schulz, M. & Van Dorland, R. (2007). Changes in Atmospheric Constituents and in Radiative Forcing. In: *Climate Change 2007: The Physical Science Basis. Contribution of Working Group 1 to the Fourth Assessment Report of the*

Intergovernmental Panel on Climate Change. S. Solomon, D. Quin, M. Manning, Z. Chen, M. Marquis, K. B. Averyt, M. Tignor, & H. L. Miller (eds.). Cambridge University Press.

Fowler, D., Pilegaard, K., Sutton, M.A., Ambus, P., Raivonen, M., Duyzer, J., Simpson, D., Fagerli, H., Fuzzi, S., Schjoerring, J.K., Granier, C., Neftel, A., Isaksen, I.S.A., Laj, P., Maione, M., Monks, P.S., Burkhardt, J., Daemmgen, U., Neiryneck, J., Personne, E., Wichink-Kruit, R., Butterbach-Bahl, K., Flechard, C., Tuovinen, J.P., Coyle, M., Gerosa, G., Loubet, B., Altimir, N., Gruenhage, L., Ammann, C., Cieslik, S., Paoletti, E., Mikkelsen, T.N., Ro-Poulsen, H., Cellier, P., Cape, J.N., Horváth, L., Loreto, F., Niinemets, Ü., Palmer, P.I., Rinne, J., Misztal, P., Nemitz, E., Nilsson, D., Pryor, S., Gallagher, M.W., Vesala, T., Skiba, U., Brüggemann, N., Zechmeister-Boltenstern, S., Williams, J., O'Dowd, C., Facchini, M.C., de Leeuw, G., Flossman, A., Chaumerliac, N. & Erisman, J.W. (2009). Atmospheric composition change: Ecosystems–Atmosphere interactions. *Atmospheric Environment*. 43 (33). p.pp. 5193–5267.

Granier, C., Bessagnet, B., Bond, T.C., D'Angiola, A., Denier van der Gon, H., Frost, G.J., Heil, A., Kaiser, J.W., Kinne, S., Klimont, Z., Kloster, S., Lamarque, J.-F., Liousse, C., Masui, T., Meleux, F., Mieville, A., Ohara, T., Raut, J.-C., Riahi, K., Schultz, M.G., Smith, S.J., Thompson, A., Aardenne, J., Werf, G.R. & Vuuren, D.P. (2011). Evolution of anthropogenic and biomass burning emissions of air pollutants at global and regional scales during the 1980–2010 period. *Climatic Change*. 109 (1-2). p.pp. 163–190.

Hand, J.L., Schichtel, B. A., Malm, W.C. & Pitchford, M.L. (2012). Particulate sulfate ion concentration and SO<sub>2</sub> emission trends in the United States from the early 1990s through 2010. *Atmospheric Chemistry and Physics*. 12 (21). p.pp. 10353–10365.

Harrison, R.M., Stedman, J. & Derwent, D. (2008). New Directions: Why are PM<sub>10</sub> concentrations in Europe not falling? *Atmospheric Environment*. 42 (3). p.pp. 603–606.

Haywood, J. & Boucher, O. (2000). Estimates of the direct and indirect radiative forcing due to tropospheric aerosols: A review. *Review of Geophysics*. 38 (4). p.pp. 513–543.

Holben, B.N., Eck, T.F., Slutsker, I., Tanré, D., Buis, J.P., Setzer, A., Vermote, E., Reagan, J.A., Kaufman, Y.J., Nakajima, T., Lavenu, F., Jankowiak, I. & Smirnov, A. (1998). AERONET—A Federated Instrument Network and Data Archive for Aerosol Characterization. *Remote Sensing of Environment*. 66 (1). p.pp. 1–16.

- IPCC (2013). Summary for Policymakers. In: *Climate Change 2013: The Physical Science Bases. Contribution of Working Group 1 to the Fifth Assessment Report of the Intergovernmental Panel on Climate Change*. T. F. Stocker, D. Qin, G.-K. Plattner, M. Tignor, S. K. Allen, J. Boschung, A. Nauels, Y. Xia, Y. Bex, & P. M. Midgley (eds.). Cambridge University Press, Cambridge, United Kingdom and New York, NY, USA.
- Jacob, D.J. & Winner, D. A. (2009). Effect of climate change on air quality. *Atmospheric Environment*. 43 (1). p.pp. 51–63.
- Jacobson, M.Z. (2002). *Atmospheric Pollution: History, Science and Regulation*. Cambridge University Press, Cambridge, United Kingdom and New York, NY, USA.
- Kasibhatla, P., Chameides, W.L. & John, J. St. (1997). A three-dimensional global model investigation of seasonal variations in the atmospheric burden of anthropogenic sulfate aerosols. *Journal of Geophysical Research*. 102 (D3). p.pp. 3737–3759.
- Kloster, S., Dentener, F., Feichter, J., Raes, F., van Aardenne, J., Roeckner, E., Lohmann, U., Stier, P. & Swart, R. (2008). Influence of future air pollution mitigation strategies on total aerosol radiative forcing. *Atmospheric Chemistry and Physics*. 8 (21). p.pp. 6405–6437.
- Kloster, S., Dentener, F., Feichter, J., Raes, F., Lohmann, U., Roeckner, E. & Fischer-Bruns, I. (2009). A GCM study of future climate response to aerosol pollution reductions. *Climate Dynamics*. 34 (7-8). p.pp. 1177–1194.
- Koch, D., Bauer, S.E., Del Genio, A., Faluvegi, G., McConnell, J.R., Menon, S., Miller, R.L., Rind, D., Ruedy, R., Schmidt, G. a. & Shindell, D.T. (2011). Coupled Aerosol-Chemistry–Climate Twentieth-Century Transient Model Investigation: Trends in Short-Lived Species and Climate Responses. *Journal of Climate*. 24 (11). p.pp. 2693–2714.
- Kreidenweis, S.M. (2003). Modification of aerosol mass and size distribution due to aqueous-phase SO<sub>2</sub> oxidation in clouds: Comparisons of several models. *Journal of Geophysical Research*. 108 (D7). p.p. 4213.
- Krishna Moorthy, K., Suresh Babu, S., Manoj, M.R. & Satheesh, S.K. (2013). Buildup of aerosols over the Indian Region. *Geophysical Research Letters*. 40. p.pp. 1–4.
- Lamarque, J.-F., Bond, T.C., Eyring, V., Granier, C., Heil, a., Klimont, Z., Lee, D., Liousse, C., Mieville, a., Owen, B., Schultz, M.G., Shindell, D.T., Smith, S.J., Stehfest, E., Van Aardenne, J., Cooper, O.R., Kainuma, M., Mahowald, N.,

- McConnell, J.R., Naik, V., Riahi, K. & van Vuuren, D.P. (2010). Historical (1850–2000) gridded anthropogenic and biomass burning emissions of reactive gases and aerosols: methodology and application. *Atmospheric Chemistry and Physics*. 10 (15). p.pp. 7017–7039.
- Langmann, B., Varghese, S., Marmer, E., Vignati, E., Wilson, J., Stier, P. & O’Dowd, C. (2008). Aerosol distribution over Europe: a model evaluation study with detailed aerosol microphysics. *Atmospheric Chemistry and Physics*. 8 (6). p.pp. 1591–1607.
- Lee, L.A., Pringle, K.J., Reddington, C.L., Mann, G.W., Stier, P., Spracklen, D. V., Pierce, J.R. & Carslaw, K.S. (2013). The magnitude and causes of uncertainty in global model simulations of cloud condensation nuclei. *Atmospheric Chemistry and Physics*. 13 (17). p.pp. 8879–8914.
- Leibensperger, E.M., Mickley, L.J., Jacob, D.J., Chen, W.-T., Seinfeld, J.H., Nenes, A., Adams, P.J., Streets, D.G., Kumar, N. & Rind, D. (2012a). Climatic effects of 1950–2050 changes in US anthropogenic aerosols – Part 1: Aerosol trends and radiative forcing. *Atmospheric Chemistry and Physics*. 12 (7). p.pp. 3333–3348.
- Leibensperger, E.M., Mickley, L.J., Jacob, D.J., Chen, W.-T., Seinfeld, J.H., Nenes, A., Adams, P.J., Streets, D.G., Kumar, N. & Rind, D. (2012b). Climatic effects of 1950–2050 changes in US anthropogenic aerosols – Part 2: Climate response. *Atmospheric Chemistry and Physics*. 12 (7). p.pp. 3349–3362.
- Lelieveld, J., Evans, J.S., Fnais, M., Giannadaki, D. & Pozzer, a (2015). The contribution of outdoor air pollution sources to premature mortality on a global scale. *Nature*. 525 (7569). p.pp. 367–71.
- Liao, H., Chen, W.-T. & Seinfeld, J.H. (2006). Role of climate change in global predictions of future tropospheric ozone and aerosols. *Journal of Geophysical Research*. 111 (D12). p.p. D12304.
- Lohmann, U. & Feichter, J. (2001). Can the direct and semi-direct aerosol effect compete with the indirect effect on a global scale? *Geophysical Research Letters*. 28 (1). p.pp. 159–161.
- Lohmann, U. & Feichter, J. (2005). Global indirect aerosol effects: a review. *Atmospheric Chemistry and Physics*. 5. p.pp. 715–737.
- Manktelow, P.T., Mann, G.W., Carslaw, K.S., Spracklen, D. V. & Chipperfield, M.P. (2007). Regional and global trends in sulfate aerosol since the 1980s. *Geophysical Research Letters*. 34 (14). p.p. L14803.
- Megaritis, A.G., Fountoukis, C., Charalampidis, P.E., Pilinis, C. & Pandis, S.N. (2013). Response of fine particulate matter concentrations to changes of

- emissions and temperature in Europe. *Atmospheric Chemistry and Physics*. 13 (6). p.pp. 3423–3443.
- de Meij, A., Krol, M., Dentener, F., Vignati, E., Cuvelier, C. & Thunis, P. (2006). The sensitivity of aerosol in Europe to two different emission inventories and temporal distribution of emissions. *Atmospheric Chemistry and Physics*. 6 (2). p.pp. 4287–4309.
- Menon, S., Genio, A.D.D., Koch, D. & Tselioudis, G. (2002). GCM Simulations of the Aerosol Indirect Effect: Sensitivity to Cloud Parameterization and Aerosol Burden. *Journal of the Atmospheric Sciences*. 59 (3). p.pp. 692–713.
- Menon, S., Unger, N., Koch, D., Francis, J., Garrett, T., Sednev, I., Shindell, D.T. & Streets, D. (2008). Aerosol climate effects and air quality impacts from 1980 to 2030. *Environmental Research Letters*. 3 (2). p.p. 024004.
- Merikanto, J., Spracklen, D. V., Pringle, K.J. & Carslaw, K.S. (2010). Effects of boundary layer particle formation on cloud droplet number and changes in cloud albedo from 1850 to 2000. *Atmospheric Chemistry and Physics*. 10 (2). p.pp. 695–705.
- Mickley, L.J., Leibensperger, E.M., Jacob, D.J. & Rind, D. (2012). Regional warming from aerosol removal over the United States: Results from a transient 2010–2050 climate simulation. *Atmospheric Environment*. 46. p.pp. 545–553.
- Myhre, G., Shindell, D., Breon, F.-M., Collins, W., Fuglestedt, J., Huang, J., Koch, D., Lamarque, J.-F., Lee, D., Mendoza, B., Nakajima, T., Robock, A., Stephens, G., Takemura, T. & Zhang, H. (2013). Anthropogenic and Natural Radiative Forcing. In: *Climate Change 2013: The Physical Science Basis. Contribution of Working Group I to the Fifth Assessment Report of the Intergovernmental Panel on Climate Change*. T. F. Stocker, D. Qin, G.-K. Plattner, M. Tignor, S. K. Allen, J. Boschung, A. Nauels, Y. Xia, V. Bex, & P. M. Midgley (eds.). Cambridge University Press, Cambridge, United Kingdom and New York, NY, USA.
- Penner, J.E., Prather, M.J., Isaksen, I.S. A., Fuglestedt, J.S., Klimont, Z. & Stevenson, D.S. (2010). Short-lived uncertainty? *Nature Geoscience*. 3 (9). p.pp. 587–588.
- Pope, C. A., Bates, D. V. & Raizenne, M.E. (1995). Health effects of particulate air pollution: Time for reassessment? *Environmental Health Perspectives*. 103 (3237). p.pp. 472–480.
- Pozzoli, L., Janssens-Maenhout, G., Diehl, T., Bey, I., Schultz, M.G., Feichter, J., Vignati, E. & Dentener, F. (2011). Re-analysis of tropospheric sulfate aerosol and ozone for the period 1980–2005 using the aerosol-chemistry-climate model

- ECHAM5-HAMMOZ. *Atmospheric Chemistry and Physics*. 11 (18). p.pp. 9563–9594.
- Rae, J.G.L., Johnson, C.E., Bellouin, N., Boucher, O., Haywood, J.M. & Jones, A. (2007). Sensitivity of global sulphate aerosol production to changes in oxidant concentrations and climate. *Journal of Geophysical Research*. 112 (D10). p.p. D10312.
- Raes, F., Dingenen, R. Van, Vignati, E., Wilson, J., Putaud, J.-P., Seinfeld, J.H. & Adams, P.J. (2000). Formation and cycling of aerosols in the global troposphere. *Atmospheric Environment*. 34 (25). p.pp. 4215–4240.
- Ramanathan, V. & Feng, Y. (2009). Air pollution, greenhouse gases and climate change: Global and regional perspectives. *Atmospheric Environment*. 43 (1). p.pp. 37–50.
- Redington, A.L., Derwent, R.G., Witham, C.S. & Manning, A.J. (2009). Sensitivity of modelled sulphate and nitrate aerosol to cloud, pH and ammonia emissions. *Atmospheric Environment*. 43 (20). p.pp. 3227–3234.
- Roelofs, G.J., Kasibhatla, P., Barrie, L., Bergmann, D., Bridgeman, C., Chin, M., Christensen, J., Easter, R., Feichter, J., Jeuken, a, Kjellstrom, E., Koch, D., Land, C., Lohmann, U. & Rasch, P. (2001). Analysis of regional budgets of sulfur species modeled for the COSAM exercise. *Tellus Series B-Chemical and Physical Meteorology*. 53 (5). p.pp. 673–694.
- von Schneidemesser, E., Monks, P.S., Allan, J.D., Bruhwiler, L., Forster, P., Fowler, D., Lauer, A., Morgan, W.T., Paasonen, P., Righi, M., Sindelarova, K. & Sutton, M. a. (2015). Chemistry and the Linkages between Air Quality and Climate Change. *Chemical Reviews*. 115 (10). p.pp. 3856–3897.
- Schwab, J.J., Wolfe, D., Casson, P., Brandt, R., Demerjian, K.L., Husain, L., Dutkiewicz, V.A., Civerolo, K.L. & Rattigan, O. V. (2016). Atmospheric Chemistry Measurements at Whiteface Mountain, NY: Cloud Water Chemistry, Precipitation Chemistry, and Particulate Matter. *Aerosol and Air Quality Research*. 16. p.pp. 827–840.
- Seaton, A., Godden, D., MacNee, W. & Donaldson, K. (1995). Particulate air pollution and acute health effects. *The Lancet*. 345 (8943). p.pp. 176–178.
- Seinfeld, J.H. & Pandis, S.N. (2006). *Atmospheric Chemistry and Physics From Air Pollution to Climate Change*. Second. Wiley-Interscience.
- Shindell, D.T., Lamarque, J.-F., Schulz, M., Flanner, M., Jiao, C., Chin, M., Young, P.J., Lee, Y.H., Rotstayn, D., Mahowald, N., Milly, G., Faluvegi, G., Collins, W.J., Conley, A.J., Dalsoren, S., Easter, R., Ghan, S., Horowitz, L., Liu, X., Myhre, G.,

- Nagashima, T., Naik, V., Rumbold, S.T., Skeie, R., Sudo, K., Szopa, S., Takemura, T., Voulgarakis, A., Yoon, J.-H. & Lo, F. (2013). Radiative forcing in the ACCMIP historical and future climate simulations. *Atmospheric Chemistry and Physics*. 13. p.pp. 2939–2974.
- Sillmann, J., Pozzoli, L., Vignati, E., Kloster, S. & Feichter, J. (2013). Aerosol effect on climate extremes in Europe under different future scenarios. *Geophysical Research Letters*. 40. p.pp. 1–6.
- Skeie, R.B., Berntsen, T.K., Myhre, G., Tanaka, K., Kvalevåg, M.M. & Hoyle, C.R. (2011). Anthropogenic radiative forcing time series from pre-industrial times until 2010. *Atmospheric Chemistry and Physics*. 11 (22). p.pp. 11827–11857.
- Smith, S.J., van Aardenne, J., Klimont, Z., Andres, R.J., Volke, A. & Delgado Arias, S. (2011). Anthropogenic sulfur dioxide emissions: 1850–2005. *Atmospheric Chemistry and Physics*. 11 (3). p.pp. 1101–1116.
- Spracklen, D. V., Carslaw, K.S., Merikanto, J., Mann, G.W., Reddington, C.L., Pickering, S., Ogren, J. A., Andrews, E., Baltensperger, U., Weingartner, E., Boy, M., Kulmala, M., Laakso, L., Lihavainen, H., Kivekäs, N., Komppula, M., Mihalopoulos, N., Kouvarakis, G., Jennings, S.G., O'Dowd, C., Birmili, W., Wiedensohler, A., Weller, R., Gras, J., Laj, P., Sellegri, K., Bonn, B., Krejci, R., Laaksonen, A., Hamed, A., Minikin, A., Harrison, R.M., Talbot, R. & Sun, J. (2010). Explaining global surface aerosol number concentrations in terms of primary emissions and particle formation. *Atmospheric Chemistry and Physics*. 10 (10). p.pp. 4775–4793.
- Stier, P., Feichter, J. & Kloster, S. (2006a). Emission-Induced Nonlinearities in the Global Aerosol System: Results from the ECHAM5-HAM Aerosol-Climate Model. *Journal of Climate*. 19 (16). p.pp. 3845–3862.
- Stier, P., Feichter, J., Roeckner, E., Kloster, S. & Esch, M. (2006b). The evolution of the global aerosol system in a transient climate simulation from 1860 to 2100. *Atmospheric Chemistry and Physics*. 6 (10). p.pp. 3059–3076.
- Textor, C., Schulz, M., Guibert, S., Kinne, S., Balkanski, Y., Bauer, S., Berntsen, T., Berglen, T., Boucher, O., Chin, M., Dentener, F., Diehl, T., Easter, R., Feichter, H., Fillmore, D., Ghan, S., Ginoux, P., Gong, S., Grini, a., Hendricks, J., Horowitz, L., Huang, P., Isaksen, I., Iversen, T., Kloster, S., Koch, D., Kirkevåg, a., Kristjansson, J.E., Krol, M., Lauer, a., Lamarque, J.F., Liu, X., Montanaro, V., Myhre, G., Penner, J., Pitari, G., Lamarque, J.F., Liu, X., Montanaro, V., Myhre, G., Penner, J., Pitari, G., Reddy, S., Seland, Ø., Stier, P., Takemura, T. & Tie, X. (2006). Analysis and quantification of the diversities of aerosol life cycles within AeroCom. *Atmospheric Chemistry and Physics*. 6. p.pp. 1777–1813.

- Textor, C., Schulz, M., Guibert, S., Kinne, S., Balkanski, Y., Bauer, S., Bernsten, T., Berglen, T., Boucher, O., Chin, M., Dentener, F., Diehl, T., Feichter, J., Fillmore, D., Ginoux, P., Gong, S., Grini, A., Hendricks, J., Horowitz, L., Huang, P., Isaksen, I.S.A., Iversen, T., Kloster, S., Koch, D., Kirkevåg, A., Kristjansson, J.E., Krol, M., Lauer, A., Lamarque, J.F., Liu, X., Montanaro, V., Myhre, G., Penner, J.E., Pitari, G., Reddy, M.S., Seland, Ø., Stier, P., Takemura, T. & Tie, X. (2007). The effect of harmonized emissions on aerosol properties in global models – an AeroCom experiment. *Atmospheric Chemistry and Physics*. 7 (17). p.pp. 4489–4501.
- Tørseth, K., Aas, W., Breivik, K., Fjæraa, A. M., Fiebig, M., Hjellbrekke, A. G., Lund Myhre, C., Solberg, S. & Yttri, K.E. (2012). Introduction to the European Monitoring and Evaluation Programme (EMEP) and observed atmospheric composition change during 1972–2009. *Atmospheric Chemistry and Physics*. 12 (12). p.pp. 5447–5481.
- Tost, H., Jöckel, P., Kerkweg, A., Pozzer, A., Sander, R. & Lelieveld, J. (2007). Global cloud and precipitation chemistry and wet deposition: tropospheric model simulations with ECHAM5/MESSy1. *Atmospheric Chemistry and Physics*. 7. p.pp. 2733–2757.
- Twomey, S. (1977). The Influence of Pollution on the Shortwave Albedo of Clouds. *Journal of the Atmospheric Science*. 34. p.pp. 1149–1152.
- Unger, N., Shindell, D.T., Koch, D. & Streets, D.G. (2008). Air pollution radiative forcing from specific emissions sectors at 2030. *Journal of Geophysical Research*. 113 (D2). p.p. D02306.
- Unger, N., Shindell, D.T., Koch, D. & Streets, D.G. (2006). Cross influences of ozone and sulfate precursor emissions changes on air quality and climate. *Proceedings of the National Academy of Sciences of the United States of America*. 103 (12). p.pp. 4377–80.
- United Nations Economic Commission for Europe (2004). *Clearing the Air: 25 years of the Convention on Long-Range Transboundary Air Pollution*. J. Sliggers & W. Kakebeeke (eds.).
- Vautard, R., Yiou, P. & van Oldenborgh, G.J. (2009). Decline of fog, mist and haze in Europe over the past 30 years. *Nature Geoscience*. 2 (2). p.pp. 115–119.
- Vestreng, V., Myhre, G., Fagerli, H., Reis, S. & Tarrasón, L. (2007). Twenty-five years of continuous sulphur dioxide emission reduction in Europe. *Atmospheric Chemistry and Physics*. 7 (13). p.pp. 3663–3681.
- Vet, R., Artz, R.S., Carou, S., Shaw, M., Ro, C.U., Aas, W., Baker, A., Bowersox, V.C., Dentener, F., Galy-Lacaux, C., Hou, A., Pienaar, J.J., Gillett, R., Forti, M.C.,

Gromov, S., Hara, H., Khodzher, T., Mahowald, N.M., Nickovic, S., Rao, P.S.P. & Reid, N.W. (2014). A global assessment of precipitation chemistry and deposition of sulfur, nitrogen, sea salt, base cations, organic acids, acidity and pH, and phosphorus. *Atmospheric Environment*. 93. p.pp. 3–100.

Wang, Y., Zhang, Q. Q., He, K., Zhang, Q. and Chai, L.: Sulfate-nitrate-ammonium aerosols over China: response to 2000–2015 emission changes of sulfur dioxide, nitrogen oxides, and ammonia, *Atmos. Chem. Phys.*, 13(5), 2635–2652, doi:10.5194/acp-13-2635-2013, 2013.

WHO (2006). Air quality guidelines. Global update 2005. Particulate matter, ozone, nitrogen dioxide and sulfur dioxide.

WHO Regional Office for Europe & OECD (2015). Economic cost of the health impact of air pollution in Europe: Clean air, health and wealth. Copenhagen: WHO Regional Office for Europe.

Wild, M. (2009). Global dimming and brightening: A review. *Journal of Geophysical Research*. 114. p.p. D00D16.

World Health Organization (2014). Burden of disease from Ambient Air Pollution for 2012. [Online]. 2014. Available from: [http://www.who.int/phe/health\\_topics/outdoorair/databases/AAP\\_BoD\\_results\\_March2014.pdf](http://www.who.int/phe/health_topics/outdoorair/databases/AAP_BoD_results_March2014.pdf). [Accessed: 3 May 2015].

World Health Organization (2003). Health Aspects of Air Pollution with Particulate Matter, Ozone and Nitrogen Dioxide. Bonn.

Yu, H., Folberth, G., Hess, P.G., Schulz, M., Shindell, D.T., Takemura, T., Tan, Q., Chin, M., West, J.J., Atherton, C., Bellouin, N., Bergmann, D.J., Bey, I., Bian, H. & Diehl, T. (2012). An HTAP multi-model assessment of the influence of regional anthropogenic emission reductions on aerosol direct radiative forcing and the role of intercontinental transport. *Journal of Geophysical Research*. 118 (2). p.pp. 700–720.

## Chapter 2 Methods

### 2.1 Introduction

Atmospheric chemistry and aerosols have been incorporated into the third generation of the Met Office's Hadley Centre Global Environment Model (HadGEM) through the United Kingdom Chemistry and Aerosols (UKCA) programme. The version used here is HadGEM3-UKCA; a coupled composition climate model able to simulate the interaction between chemistry, aerosols and their impacts on the radiative balance of the climate system.

The dynamical core of HadGEM3-UKCA is based upon the dynamics scheme implemented by Davies et al., (2005) in the Met Office's Unified Model (UM). This simulates the processes of large scale advection of tracers, convective uplift and boundary layer mixing. Chemistry is calculated "online" in HadGEM3-UKCA using the scheme described in O'Connor et al., (2014). The modal aerosol scheme of the Global Model of Aerosol Process (GLOMAP-mode) is used within this version of HadGEM3-UKCA to simulate the interaction of aerosols with chemistry and climate (Mann et al. 2010). GLOMAP-mode is used in preference to the sectional GLOMAP-bin scheme because of the computational requirements in coupling an aerosol scheme to a climate model, but the two schemes do produce comparative results (Mann et al., 2012). Descriptions of the chemistry and aerosol scheme as well as features of importance in the climate model are described in the next sections.

### 2.2 The Chemistry Scheme

Chemistry is calculated 'online' (i.e. oxidants are interactively regenerated) in HadGEM3-UKCA within the Troplisop scheme; the standard tropospheric chemistry scheme with additional reactions for isoprene to treat 55 chemical species, as described in O'Connor et al., (2014). The mechanism involves chemistry for tropospheric  $O_3$ ,  $HO_x$ ,  $NO_x$  and VOC species with reactions (uni-, bi- and ter-molecular) of odd oxygen ( $O_x$ ), nitrogen ( $NO_y$ ), hydrogen ( $HO_x = OH + HO_2$ ) and CO, as well as methane ( $CH_4$ ) and other short chain non-methane VOCs. A photolysis scheme (Fast-J) is implemented within UKCA which calculates online photolysis rates based on the current

distribution of clouds, ozone and aerosols (Wild et al., 2000), allowing for the inclusion of aerosol and climate feedbacks on the chemistry.

To allow for coupling to the aerosol model, the chemistry scheme has been extended to include additional reactions for sulphur and monoterpene oxidation (Spracklen et al., 2006; Mann et al., 2010; Scott et al., 2014). These include reactions for the following additional species that are important for aerosol formation: SO<sub>2</sub>, sulphuric acid (H<sub>2</sub>SO<sub>4</sub>), dimethyl sulphide (DMS), methane sulphonic acid (MSA), carbon disulphide (CS<sub>2</sub>), carbonyl sulphide (COS) and monoterpenes. In the gas phase sulphate aerosol mass can be formed by the oxidation of SO<sub>2</sub> with the hydroxyl radical (OH).

If low level clouds are present then the oxidation of sulphur species (S(IV) to S(VI)) to form sulphate aerosols can occur in the aqueous phase via reactions with hydrogen peroxide (H<sub>2</sub>O<sub>2</sub>) and O<sub>3</sub>; traditionally the dominant and most well understood in-cloud oxidants (Ervens, 2015).

A simple scheme is included to account for the oxidation of biogenic VOCs and subsequent SOA formation. SOA is formed from the products (SEC-ORG; Table 2.1) of monoterpene (equivalent to  $\alpha$ -pinene, MONOTERP in Table 2.1) oxidation at a yield of 13%, which are assumed to be involatile and condense onto existing aerosols (Spracklen et al., 2006).

The TropIsop scheme and modifications described above contains enough detailed chemistry to cover reactions leading to and affecting aerosol formation, processing and loss within the troposphere. Chemical reactions within the stratosphere were not considered as it was outside the scope of this thesis. Table 2.1 shows a summary of the gas-phase chemistry reactions that directly influence aerosol formation and used within GLOMAP-mode.

Schemes for dry and wet deposition of gas phase chemical species are included within the model (O'Connor et al., 2014), which allows for components to be removed from the atmosphere.

**Table 2.1** Summary of the gas and aqueous phase chemistry used within GLOMAP-mode (Mann et al., 2010).

Chemical Reaction
$DMS + OH \rightarrow SO_2^{(a)}$
$DMS + OH \rightarrow 0.6 SO_2 + 0.4 DMSO^{(b)}$
$DMSO + OH \rightarrow 0.6 SO_2 + 0.4 MSA^{(b)}$
$DMS + NO_3 \rightarrow SO_2^{(a)}$
$CS_2 + OH \rightarrow SO_2 + COS^{(b)}$
$COS + OH \rightarrow SO_2^{(b)}$
$SO_2 + OH + M \rightarrow H_2SO_4^{(b)}$
$MONOTERP + OH \rightarrow 0.13 SEC-ORG^{(a)}$
$MONOTERP + NO_3 \rightarrow 0.13 SEC-ORG^{(a)}$
$MONOTERP + O_3 \rightarrow 0.13 SEC-ORG^{(a)}$
$HO_2 + HO_2 \rightarrow H_2O_2^{(c)}$
$HSO_3^- + H_2O_2 \rightarrow SO_4^{2-} + 2H^+ + H_2O (aq)^{(d)}$
$HSO_3^- + O_3 \rightarrow SO_4^{2-} + H^+ + O_2 (aq)^{(d)}$
$SO_3^{2-} + O_3 \rightarrow SO_4^{2-} + O_2 (aq)^{(d)}$

<sup>(a)</sup> Atkinson et al., (1989), <sup>(b)</sup> Pham et al., (1995), <sup>(c)</sup> Jones et al., (2001), <sup>(d)</sup> Seinfeld & Pandis, (2006)

## 2.3 The Aerosol Model

The Global Model of Aerosol Processes (GLOMAP) is a global aerosol microphysical model that simulates the evolution of size resolved number and mass of aerosol particles with different compositions. The modal version of GLOMAP uses log-normal modes to represent the aerosol size distribution and simulates the interaction of various aerosol processes including size resolved primary emissions, cloud processing, new particle formation, hygroscopic growth, coagulation, condensation, deposition and scavenging processes (Mann et al., 2010). The coupling of GLOMAP-mode to the climate model has resulted in modifications to the wet and dry aerosol deposition processes from that in the standard offline version of GLOMAP-mode.

### 2.3.1 Gas Phase and Primary Aerosol Emissions

Monthly mean emissions (to include seasonal variations) of SO<sub>2</sub> are included within the model from both anthropogenic (energy, transport, industry, shipping, agriculture, residential and waste sectors) and natural (volcanoes and biomass burning) sources. Low level sources from the agricultural, residential, shipping, transportation and waste sectors are assumed to emit SO<sub>2</sub> into the lowest level of the model. Whilst higher level sources from the

energy and industrial sectors are assumed to emit SO<sub>2</sub> at altitudes between 100 - 300m above the surface, representative of chimney stack emissions.

An additional source of new sulphate particles can be nucleated within the SO<sub>2</sub> plumes emitted from power plants and volcanoes (Brock et al., 2002; Stevens et al., 2012). To represent this process that occurs on the sub-grid scale of the model, a 2.5% fraction of SO<sub>2</sub> emissions is assumed to occur directly as primary sulphate particles, based on AEROCOM recommendations (Dentener et al., 2006). The effective log-normal emitted size distribution of sub-grid sulphate used within GLOMAP is based on that used by Stier et al., (2005).

Natural emissions of SO<sub>2</sub> from volcanoes (both continuous and explosively erupting types) are included from Andres & Kasgnoc, (1998) and Halmer et al., (2002), using injection heights based on the recommendations in Dentener et al., (2006) for both types of volcanoes. SO<sub>2</sub> emissions from wildfire (biomass burning) are included within the model from the MACCity (MACC and CityZen project) inventory (Granier et al., 2011) and are distributed uniformly over the lowest 3 km of the atmosphere.

Emissions of DMS in the model are based on monthly seawater concentration fields from Kettle & Andreae, (2000) and a wind speed dependent air–sea exchange parameterisation (Liss & Merlivat, 1986). Emission fluxes of sea salt are calculated using the surface wind speed parameterisation of Gong, (2003) and are emitted into the accumulation and coarse modes. Monthly mean emissions of monoterpenes from vegetation are prescribed from the values in Guenther et al., (1995). These emission fluxes are constant throughout the monthly and daily cycle and do not account for any adjustments due to the local environmental meteorological variables e.g. temperature (Spracklen et al., 2006).

The simulation of mineral dust aerosols is undertaken using the six-bin mass scheme developed by Woodward, (2001), which is separately incorporated within the host UM. Dust emissions depend on the surface soil type (bare soil fraction) and particle size distribution of the soil, as well as the wind speed and soil moisture exceeding threshold values. This scheme simulates the evolution of the mass of dust particles with dry size radii between 0.03 to 30 µm.

Primary emissions of BC and OC are included as monthly mean fluxes from anthropogenic fossil fuel (energy, transport, industry, shipping, and agriculture), anthropogenic biofuel (residential, waste and agricultural waste

sectors) and natural (volcanoes and biomass burning) sources. Particles are emitted using an initial log-normal size distribution based on the size settings recommended by AEROCOM (Dentener et al., 2006), with modifications as in Stier et al., (2005). Biomass and biofuel emissions have a geometric mean diameter of 150 nm, whilst for fossil fuel emissions it is set at 60 nm. Both biomass and biofuel emissions have a geometric standard deviation of 1.59. Biofuel and fossil fuel emissions occur within the lowest model level whilst; biomass burning emissions are distributed uniformly over the lowest 3 km of the atmosphere.

See section 2.6 for details of the anthropogenic emission inventories used for each of the simulations within this thesis.

### **2.3.2 Aerosol Microphysics**

GLOMAP-mode uses log-normal modes to represent aerosol number and mass concentrations within the nucleation (dry diameter ( $D_p$ ) <10 nm), Aitken ( $D_p$  10 – 100 nm), accumulation ( $D_p$  100 nm to 1  $\mu$ m) and coarse ( $D_p$  >1  $\mu$ m) modes of the size distribution. Each mode has a constant geometric standard deviation but a varying geometric mean diameter. When the geometric mean diameter exceeds the upper size range of the mode (defined above) particle number and mass are transferred between modes through aerosol microphysical processes included within GLOMAP (coagulation, condensational growth and in-cloud processing). The insoluble species can be transferred into their respective soluble modes following the process of condensational ageing. New particles are formed via binary homogeneous nucleation in both the boundary layer and free troposphere within the model. Particles can be completely removed via the processes of wet and dry deposition. Aerosols within the log-normal modes can be a combination of internal and external mixtures of components. HadGEM3-UKCA is set up here to simulate sulphate, BC, particulate organic matter (POM) and sea salt within four soluble modes and one insoluble Aitken mode; the standard component setup of aerosols available within the model. There is no representation of ammonium nitrate aerosols within this version of the model. For a more detailed description of the aerosol microphysical processes see Spracklen et al., (2005) and Mann et al., (2010).

#### **2.3.2.1 New Particle Formation**

Nucleation is the formation of small new clusters of particles (primarily from the vapour to liquid droplet phase), which can then grow via the coalescence and condensation of gaseous precursors (Seinfeld & Pandis 2006).  $H_2SO_4$  is

assumed to be the principal gas-phase species involved in nucleation (Raes et al. 2000; Andreae 2013). Throughout the boundary layer, activation or kinetic mechanisms can be used within GLOMAP-mode to simulate new particle formation (Spracklen et al. 2010). Boundary layer nucleation has not been implemented within this version of the model and is not a mechanism to new particle formation used within this thesis. New particle formation in the free troposphere is represented by the binary homogeneous ( $\text{H}_2\text{SO}_4\text{-H}_2\text{O}$ ) mechanism within GLOMAP-Mode (Kulmala et al., 1998), which dominates new particle formation in the free troposphere (Spracklen et al. 2010). Other mechanisms involving organic oxidation products (of both biogenic and anthropogenic origin), ammonia and amines also contribute to the nucleation rate of new particles (Metzger et al., 2010; Almeida et al., 2013). These additional nucleation schemes are not currently available for use within the version of HadGEM3-UKCA used within this thesis, although an organically mediated nucleation scheme has been implemented and tested in a version of GLOMAP-mode (Scott et al., 2014).

### **2.3.2.2 Coagulation**

Coagulation occurs in GLOMAP-mode via collisions of particles both within and between modes. Coagulation is the adhesion of particles together to form larger but less numerous particles (i.e. reducing particle number but conserving mass). The parameterisation within GLOMAP-mode only considers coagulation from Brownian diffusion, the dominant coagulation process for submicron aerosol. Coagulation between Aitken and nucleation sized particles is an important growth mechanism but if larger sized particles already exist then they can act as a sink of secondary particles. For further details see Mann et al., (2010).

### **2.3.2.3 Condensation**

Condensation of  $\text{H}_2\text{SO}_4$  and VOC oxidation products (SEC-ORG) occur onto existing primary particles (acting as a condensational sink), with the size and composition of these particles determining the specific growth rates. This acts to increase the size and mass of particles but does not change the overall number concentration, shifting the size distribution to larger sizes. Both the processes of nucleation and condensational growth compete for the available condensable vapours, determined by a number of “competition sub-steps” (Mann et al., 2010). The existence of larger sized particles at any location in the atmosphere can suppress new particle formation by providing a condensational sink for growth (Spracklen et al. 2010).

Condensation of both  $\text{H}_2\text{SO}_4$  and SEC-ORG within GLOMAP-mode can also 'age' insoluble particles to become partially soluble. The 'ageing' of insoluble particles can also occur via inter-modal coagulation of smaller water soluble particles. In GLOMAP-mode an insoluble particle is required to be coated by 10 monolayers to make it soluble, which also partially determines the timescale for wet removal of the insoluble BC and POM aerosol (Mann et al., 2010).

#### **2.3.2.4 In-cloud Oxidation/Cloud Processing**

When low level clouds are present in the model (defined by the cloud fraction of the model grid box), aqueous phase oxidation of sulphur dioxide can occur through reaction with  $\text{H}_2\text{O}_2$  and  $\text{O}_3$ , accounting for the majority of sulphate aerosol formed in the troposphere (Chin et al., 1996; Barth et al., 2000; Roelofs et al., 2001; Faloon, 2009). Oxidation by  $\text{H}_2\text{O}_2$  is the preferential pathway under most conditions and is pH independent (Seinfeld & Pandis, 2006). Whereas, oxidation by  $\text{O}_3$  is highly sensitive to pH and is preferential only under certain conditions.

In HadGEM3-UKCA  $\text{SO}_2$  first dissolves in cloud droplets using a Henry's law equilibrium approach. A grid box is defined as having low level clouds present if the cloud liquid water content exceeds  $0.2 \text{ g m}^{-3}$ ; that of typical stratocumulus clouds.  $\text{SO}_2$  dissolves in cloud water to form the  $\text{HSO}_3^-$  species, which can also further dissociate to  $\text{SO}_3^{2-}$ . Both these species can lead to sulphate aerosol formation via the oxidation reactions with  $\text{H}_2\text{O}_2$  and  $\text{O}_3$ , as in Table 2.1. Cloud water pH depends on the kinetic and thermodynamic processes of an evolving cloud droplet size distribution and is complicated to calculate in models (Fahey, 2003). Within the standard setup of HadGEM3-UKCA a fixed cloud water pH of 5.0 is chosen for aqueous phase reactions, which is considered to be representative of the 'effective' pH of the bulk cloud droplets based on the observed variability in pH (Collett et al., 1993; Benedict et al., 2012; Murray et al., 2013).

The processing of aerosols in low-level clouds involves the uptake and chemical reaction of gases to grow particles that exist in non-precipitating clouds. This creates a minimum in the size distribution between the Aitken and accumulation modes due to differing growth rates between activated and non-activated particles (Hoppel et al., 1994). To enable cloud processing within the model a minimum activation dry radius is defined, representing the smallest sized hygroscopic particles that are activated to cloud droplets. The activation radius is controlled by cloud updraught velocities which are difficult to obtain in a global model at the sub-grid scale.

Variations in the values of the activation radius lead to uncertainties in the prediction of aerosol number concentrations (Spracklen et al., 2005b). Within HadGEM3-UKCA the activation dry radius is assumed to be a globally representative bulk value of 37.5 nm, that of typical marine stratocumulus clouds with supersaturation values of 0.2% (Spracklen et al., 2005a; Mann et al., 2010).

Cloud processing takes place by firstly defining the fraction of particle mass and number larger than the activation diameter in the Aitken mode and transferring it to the soluble accumulation mode. The sulphate aerosol mass produced from the in-cloud oxidation routes is then partitioned between the soluble accumulation and coarse modes of the modal aerosol size distribution according to the ratio of their respective number concentrations to their sum. This allows larger particles within the Aitken mode to become activated and cloud processed as well as producing the minimum in the size distribution between the soluble Aitken and accumulation modes (Mann et al., 2010).

### **2.3.3 Removal Processes**

#### **2.3.3.1 Dry Deposition**

Small particles can be removed from the atmosphere by diffusing to the Earth's surface and large particles can settle out by gravity based on Slinn, (1982) and (Zhang et al., 2001). The particle size, land surface type and wind speed determine the rate of deposition. Dry deposition is fastest for larger sized particles and over certain land surface types.

Particles between 0.1 and 1  $\mu\text{m}$  in diameter tend to accumulate in the atmosphere as dry removal is slow and with the right hygroscopic properties can become activated in clouds and removed by wet deposition.

Dry deposition of aerosols follows the approach in Spracklen et al., (2005) and Mann et al., (2010) by calculating deposition velocities for Brownian diffusion over different surface types.

#### **2.3.3.2 Wet Deposition**

Wet removal of particles from the atmosphere can occur via in-cloud nucleation scavenging (rainout) or below cloud impact scavenging (washout). All of the activated particles within the soluble accumulation and coarse modes (i.e.  $>100$  nm) are assumed to be scavenged by cloud droplets in the cloudy fraction of each grid box by large scale precipitation. Convective rainfall is treated in a similar way but assumes a cloud fraction of

30% and a 99% rain conversion rate over 6 hours in grid boxes where convective rain is produced (Kipling et al., 2013). Aerosols are removed in both large scale and convective precipitation at a rate proportional to the amount of condensate converted to rain. Aerosol is not returned to the atmosphere when rain water evaporates but is removed immediately. The soluble nucleation and Aitken modes as well as the insoluble Aitken mode are not subject to nucleation scavenging.

Below cloud impaction of rain drops onto aerosols follows the method of Slinn, (1984) and is calculated using a lookup table of raindrop-aerosol collection efficiencies Beard & Grover, (1973) based on the geometric mean dry radius of mode and a size distribution of raindrops (Sekhon & Srivastava, 1971). The terminal velocity of rain drops is from Easter & Hales, (1983).

## **2.4 The Climate Model**

The coupling of chemistry and aerosols to a climate model allows the interaction and feedback of composition changes on climate to be simulated. In particular, the effect of aerosols on climate requires the simulation of how changes in aerosols affect clouds and the radiative balance.

The impact of radiatively active chemical and aerosol species on the Earth's radiation balance is calculated 'online' within the HadGEM model using the Edwards-Slingo radiation code (Edwards & Slingo, 1996). To enable the interaction of the GLOMAP-Mode aerosol scheme to the UM radiation scheme, a sub-routine within the HadGEM model, UKCA\_RADAER, was developed by Bellouin (2010).

### **2.4.1 Aerosol Radiation Interactions**

Aerosol optical properties are first obtained from pre-computed look-up tables of monochromatic optical properties for all modal radii and refractive indices. Based on the chemical composition of the aerosols within each mode, waveband averaged optical properties can be obtained (Bellouin, 2010). Waveband-averaged scattering and absorption coefficients can then be obtained across the entire modelled size distribution along with a volume-weighted average of component refractive indices within each mode (Bellouin et al. 2013). The aerosol optical properties are then used within the radiation scheme to calculate the perturbation of the radiative fluxes at both long and short wavelengths from including atmospheric aerosols; the direct aerosol effect or ari.

## 2.4.2 Aerosol Cloud Interactions

GLOMAP-mode calculates CCN as the number concentration of soluble particles larger than the dry activation radius of 37.5 nm. The CCN number concentrations are used to calculate the aerosol interaction with clouds (ACI) or aerosol indirect effects. The effect of changes in CCN number concentrations on the CDN concentrations is calculated by using the empirical relationship derived by Jones et al., (2001), which was based on an external mixture of sulphate and sea salt particles:

$$CDN = 3.75 \times 10^8 (1 - \exp(-2.5 \times 10^{-9} CCN)) \quad (1)$$

Where CDN and CCN are given in  $\text{m}^{-3}$  and a minimum CDN value of  $5.0 \times 10^6 \text{ m}^{-3}$  is used in the model (to take account of naturally occurring continental sources of CCN (Jones et al., 2001)). This relationship was used within this version of HadGEM3-UKCA and throughout this thesis to calculate the impact on CDN concentrations from changes in CCN concentrations, as derived from the aerosol scheme.

The CDN concentrations are then used to calculate the cloud effective radius (using the formula within Jones et al., (2001)) and subsequently the cloud albedo. The aerosol cloud albedo effect is determined from changes in the cloud albedo (and its influence on the radiative balance) due to aerosol induced changes in CCN concentrations, CDN concentrations and the cloud effective radius.

By coupling UKCA to the precipitation scheme in the climate model, the rapid adjustment of clouds due to aerosol effects (cloud lifetime) can be calculated by using the effect of aerosols on CDN, cloud effective radius and eventually the auto-conversion of cloud droplets to rain, as described in Jones et al., (2001).

In more recent versions of HadGEM3-UKCA (not used in this thesis), the aerosol activation scheme to calculate CCN concentrations has been improved by coupling the aerosol output to the Köhler-theory based activation scheme of Abdul-Razzak & Ghan, (2000). This scheme takes into account the aerosols properties (size, number and composition) in addition to important meteorological parameters at the sub-grid scale (updraft velocity, temperature and pressure). This allows for a more representative calculation of the number of activated aerosols that can influence the CDN concentrations and thus affect the radiation balance.

### **2.4.3 Set up of radiation scheme**

Within all the simulations used for this thesis, the radiation scheme has been set up in a 'double-call' configuration. At each time step, the radiation scheme is called twice; the first call uses the modelled aerosol concentration fields, and the second uses an aerosol free atmosphere for clear sky radiative calculations and a prescribed default CDN field (based on an aerosol climatology of  $300 \text{ cm}^{-3}$  over land and  $100 \text{ cm}^{-3}$  over oceans) for all sky radiative calculations. The double-call configuration effectively eliminates any radiative feedbacks from aerosol effects onto the climate system by prohibiting the rapid adjustment of clouds. It is therefore able to diagnose and quantify aerosol radiative effects for both ari and aci at each time step within each model grid box.

## **2.5 Health Impacts**

The calculation of health effects from pollutant concentrations is based on the concept of a concentration dose-response function (CRF) for both short and long term effects. The calculations in this thesis will only consider the long term health effects from exposure to fine particulate matter ( $\text{PM}_{2.5}$ ). The CRF provide a relationship between changes in exposure of a population to long-term concentrations of  $\text{PM}_{2.5}$  and the relative risk (RR) of disease. CRFs have been traditionally based upon epidemiological studies in North America over the last 30 years by the American Cancer Society (Pope III, 2002). These CRFs were derived based on  $\text{PM}_{2.5}$  concentrations that were below  $30 \mu\text{g m}^{-3}$  and did not take into account exposure to elevated concentrations of  $>30 \mu\text{g m}^{-3}$ , that regularly occur in densely populated urban environments. To account for population exposure across the full range of  $\text{PM}_{2.5}$  concentrations CRFs were extrapolated by linear and log-linear models to capture a full range of RRs (Cohen et al., 2004; Ostro, 2004).

The upper range of RRs derived using linear and log-linear models were found to be outside the range that could be constrained by observations. To constrain the CRF at high values of  $\text{PM}_{2.5}$ , Burnett et al., (2014) used observed epidemiological meta-data of exposure from different combustion sources (e.g., ambient air pollution, household air pollution, second hand smoking and active smoking) to develop integrated exposure response functions (IERs). In addition, the concept of a threshold concentration was introduced; a concentration below which there is no evidence of detrimental health effects. The RR curves from the IERs for five different diseases (for

adults over 25 years of age: stroke, ischemic heart disease (IHD), chronic obstructive pulmonary disease (COPD) and lung cancer (LC); for infants less than 5 years of age: acute lower respiratory infection (ALRI)) are calculated as follows:

$$RR(C) = 1 + \alpha [1 - \exp(-\gamma(C - C_0)^\delta)] \quad (2)$$

*for*  $C \leq C_0 \quad RR = 1$

Where  $RR(C)$  is the relative risk of disease based on the  $PM_{2.5}$  concentrations  $C$ ,  $C_0$  is the minimum risk  $PM_{2.5}$  concentration above which there is evidence of a health effect (typical range of  $5.8 - 8.0 \text{ g } \mu\text{m}^{-3}$ ) and parameters  $\alpha$ ,  $\gamma$  and  $\delta$  determine the shape of the CRF for each disease.

The health impacts from exposure to  $PM_{2.5}$  for a particular disease are calculated by using the change in annual mean concentrations of  $PM_{2.5}$ , the baseline rate of disease for a particular country and the spatial distribution of the total exposed population. The relationship defined by Apte et al., (2015) is used to calculate the change in mortality ( $\Delta M$ ) for a particular disease within a model grid box  $i$  and within a specific country  $k$  due to a change in annual mean  $PM_{2.5}$  concentration from  $C_i$  to  $C_i^*$ :

$$\Delta M_{i,j} = P_i \times \hat{I}_{j,k} \times (RR_j(C_i^*) - RR_j(C_i)), \text{ where } \hat{I}_{j,k} = \frac{I_{j,k}}{\overline{RR}_{j,k}} \quad (3)$$

Where  $M$  is premature mortality in a particular age stratum ( $z$ ) for disease  $j$  due to  $PM_{2.5}$  in grid box  $i$  within country  $k$ .  $P_i$  represents the population within each grid box  $i$ ,  $I_{j,k}$  is the baseline mortality rate for a particular disease  $j$  in country  $k$ , and  $RR_j(C_i)$  is the RR at concentration  $C_i$ . The underlying baseline mortality rate for disease  $j$  is not altered in this calculation.  $\overline{RR}_{i,k}$  represents the average population-weighted RR for disease  $j$  within country  $k$ , as defined by Apte et al., (2015). The grouping of  $\hat{I}_{j,k} = I_{j,k}/\overline{RR}_{j,k}$  indicates the hypothetical underlying baseline mortality rate for country  $k$  if  $PM_{2.5}$  concentrations are reduced to that of the minimum risk within country  $k$ .

The change in mortality calculated in (3) represents that for an individual disease within an individual grid box. Summing over all the diseases for each grid box within a particular region yields the total change in mortality for the change in exposure to  $PM_{2.5}$  concentrations.

Health effects from air pollutants can also have a perceived economic effect on society. A monetary value is assigned to particular health impacts associated with air pollution, which are then used to calculate the economic value from a change in the risk of mortality across a population (Hutton & Menne, 2014; WHO Regional Office for Europe & OECD, 2015). The

concept used in this thesis is the “value of a statistical life” (VSL), which is derived from surveys of an individual’s willingness to pay (WTP) to maintain the current standard of life in the event of an increased level of mortality (OECD, 2012). A baseline VSL figure of US\$3 million is provided by OECD, (2012), which can then be adjusted to obtain values for individual countries. This allows the economic value of air pollution to be quantified in addition to the impact on human health. These values can be used in the cost-benefit assessment of emission mitigation measures.

## **2.6 The Experiments**

HadGEM3-UKCA was used in this thesis in atmosphere only mode to output monthly 3D fields at a horizontal resolution of  $1.875^\circ \times 1.25^\circ$  (approximately 140 km at mid latitudes) and with 63 vertical levels up to 40 km (based on  $\sigma$ -hybrid pressure levels). Meteorological fields within the model experiments have all been ‘nudged’ at 6 hour intervals to the European Centre for Medium-range Weather Forecast (ECMWF) reanalysis products (Uppala et al., 2005; Dee et al., 2011). In HadGEM the potential temperature and horizontal wind fields are relaxed towards the values within the reanalysis fields (Telford et al., 2008, 2013). Using nudging attempts to constrain the meteorology produced within the climate model to that observed in the reanalysis product over a given time period. This enables a realistic representation of the observed meteorology to be produced by the model, which is necessary when comparing model values to observations or when attempting to reproduce the atmospheric composition that occurred under particular meteorological conditions.

Sea surface temperatures and sea ice extent were prescribed with the monthly values used within CMIP5 to provide a realistic representation of the historical ocean state within the model (Hurrell et al., 2008). The atmosphere and land surface exchange of  $\text{CO}_2$ , heat and moisture are coupled using the Met Office Surface Exchange Scheme (MOSES; Essery et al., 2002).

Concentrations of greenhouse gases from 1960 to 2010 are obtained from data used in the development of the CMIP5 historical scenarios as well as the Reference Concentration Pathways (RCPs). Monthly zonal aerosol optical depth fields are provided for the stratosphere to take account of volcanic emissions that reach this height. Monthly fields of stratospheric  $\text{O}_3$  concentrations are also used within this setup. Greenhouse gas concentrations, stratospheric aerosol and ozone fields are provided to

produce a realistic radiative balance so that any changes due to variations in aerosols can be accurately diagnosed.

Using this standard configuration, a number of different experiments have been undertaken as part of this thesis (using slight modifications to the standard setup) to investigate the interaction of aerosols and climate.

### **2.6.1 Time varying emissions 1960-2009**

To study how atmospheric aerosols and their radiative impact have changed across Europe over the recent past, HadGEM3-UKCA was setup to output monthly 3D aerosol fields over the period 1960 to 2009. The model has been nudged to the ECMWF meteorological fields ERA-40 (Uppala et al., 2005) from 1960 to 2000 and ERA-Interim (Dee et al., 2011) for the period 2000-2009. Nudging to meteorological fields attempts to provide a realistic representation of meteorology and allows for the model evaluation against available measurement data to be conducted using consistent meteorology. The computational expense of conducting the historical simulations meant that it was not possible to re-run them with ERA-interim re-analysis fields from 1979 to ascertain the impact of different re-analysis products on the results.

As part of these simulations, anthropogenic emissions from the MACCity inventory are used, as described in Granier et al. (2011) and available from the Emissions of atmospheric Compounds & Compilation of Ancillary Data (ECCAD; [http://eccad.sedoo.fr/eccad\\_extract\\_interface/JSF/page\\_login.jsf](http://eccad.sedoo.fr/eccad_extract_interface/JSF/page_login.jsf)). This emission dataset is based on that used in the ACCMIP, derived from Lamarque et al. (2010), for 1960 to 2000, and RCP 8.5 for emissions since the year 2000. None of these previous datasets provided detailed monthly emissions of the principal tropospheric gases over recent decades. The MACCity dataset improved on the existing inventories by providing sector based monthly emissions of the main tropospheric species of interest over the period 1960 to 2010, allowing the impact from temporal changes in anthropogenic emissions on aerosols to be studied.

To generate the MACCity inventory yearly emissions for each species and within each sector are calculated by linearly interpolating between the start and end year of each decade. A seasonal cycle is then applied to the yearly emissions to generate monthly emissions at  $0.5^\circ$  by  $0.5^\circ$  horizontal resolution, which account for seasonal variation over the years 1960 to 2010. Emissions from sectors such as agricultural activities, energy production, and transportation (both land and ship) are included within the

MACCity inventory. Emissions are provided for SO<sub>2</sub>, BC, OC, NO<sub>x</sub>, NH<sub>3</sub> and also for speciated VOCs. Most emissions are applied at the surface apart from SO<sub>2</sub>, which is injected at a higher level based on chimney stack height, and aircraft NO<sub>x</sub> which is supplied as a 3D field in the atmosphere.

Biomass burning emissions are included as the wildfire (forest, grassland and savanna fires) emissions from the MACCity dataset based upon a similar methodology as described above. Emissions of BC, OC and SO<sub>2</sub> from fires are distributed uniformly over the lowest 3 km of the model to represent the vertical extent of biomass burning fires.

For these experiments and the results presented in Chapter 3, the aerosol radiative forcing is defined as the difference in the shortwave aerosol radiative effect in a single year to that of the 1980-2000 mean.

### **2.6.2 Alternative pH**

To study the effect of changes in cloud water pH (a parameter related to aerosol formation), along with changes in anthropogenic emissions, on sulphate aerosol formation and aerosol radiative effects, a similar experimental set up as described in section 2.6.1 has been used. The only difference for these simulations occurred through changes to the in-cloud SO<sub>2</sub> oxidation scheme. In HadGEM3-UKCA the standard cloud water pH value of 5.0, considered to be representative of the effective pH of bulk cloud droplets, was increased to a value of 6.5. The value of pH 6.5 was chosen based on the upper range of values used within the analysis by Lee et al., (2013), obtained by an expert elicitation and literature search. Lee et al., (2013) found that cloud water pH was the third most important parameter controlling uncertainty in CCN, particularly in the northern hemisphere winter.

3D monthly aerosol fields were outputted over the period 1960 to 2009 using this new cloud water pH value. The output from these simulations can then be compared to those produced in 2.6.1 to ascertain the sensitivity of sulphate aerosol formation and its radiative effects to spatial and temporal changes in cloud water pH. The aerosol forcing used in this part of the thesis (Chapter 4) is defined as the difference between shortwave aerosol radiative effects in 2009 and 1970 using different values of cloud water pH.

### **2.6.3 European Air Quality Measures**

The same initial set up of HadGEM3-UKCA was used in these experiments to quantify the impact of European air quality policy measures and

technology improvements on air quality, human health and climate. The main difference in these experiments is the use of monthly mean anthropogenic emissions of CO, SO<sub>2</sub>, NO<sub>x</sub>, VOCs, OC and BC from version 4.3 of the Emission Database for Global Atmospheric Research (EDGAR) (EC-JRC/PBL, 2015). Monthly emissions are provided at a 0.5° by 0.5° horizontal resolution across similar sectors to those in the MACCity inventory of energy, industry, transport, agriculture, residential, waste and others (<http://edgar.jrc.ec.europa.eu/pegasos>). The anthropogenic emissions used in these experiments was switched from MACCity to EDGAR as this inventory was used to develop the emission scenario to consider the non-implementation of specific European air quality legislation and technology measures. This presented some inconsistencies between the two inventories which are mentioned below and discussed in Crippa et al., (2016a).

Two sets of simulations using HadGEM3-UKCA were conducted with different anthropogenic emissions, whilst all other emissions were kept the same. Actual 2010 anthropogenic emissions were used within the reference (REF) simulations. The NO-AQ simulations used anthropogenic emissions that would have occurred in 2010 if air quality policy measures and technology improvements to reduce air pollutants between 1970 and 2010 did not occur. The anthropogenic emissions for the NO-AQ simulations used 1970 emission factors with 2010 economic activity data to simulate a stagnation of technology improvements. Changes in the makeup of the energy supply that are not due to specific legislation e.g. the switch from coal to gas are still accounted for within the NO-AQ scenario. Additionally it was assumed that emissions were not reduced in the NO-AQ scenario due to the non-implementation of end-of-pipe treatment technologies such as particle filter traps and flue gas desulphurisation (Crippa et al., 2016a). These emission changes were applied only within the energy, industry and transportation sectors as they were the sectors historically targeted by air pollution control legislation.

A full description of the anthropogenic emission scenarios used in these experiments are provided in Crippa et al., (2016a). The stagnation of technology improvements are applied globally within the NO-AQ emissions scenario and some of the European emissions standards (e.g. vehicle emission standards) are also applied outside of Europe (Crippa et al., 2016b). This means that there are the potential for global implications of these emission changes however, in this thesis the focus is on the impact of

these measures over Europe (defined as the domain of 10°W – 36°E and 36°N – 61°N).

Figure 2.1 shows the total European (Domain area of 10°W – 36°E, 36°N – 61°N) emissions across all sectors of SO<sub>2</sub>, BC and OC in 2010 from the MACCity (used in Chapter 3 and 4) and EDGAR inventory (used in Chapter 5). Small differences in emissions occur in 2010 between the inventories used within this thesis, which can be considered as acceptable when taken in the context of the uncertainties inherent within individual emission inventories (Janssens-Maenhout et al., 2015; Crippa et al., 2016a).

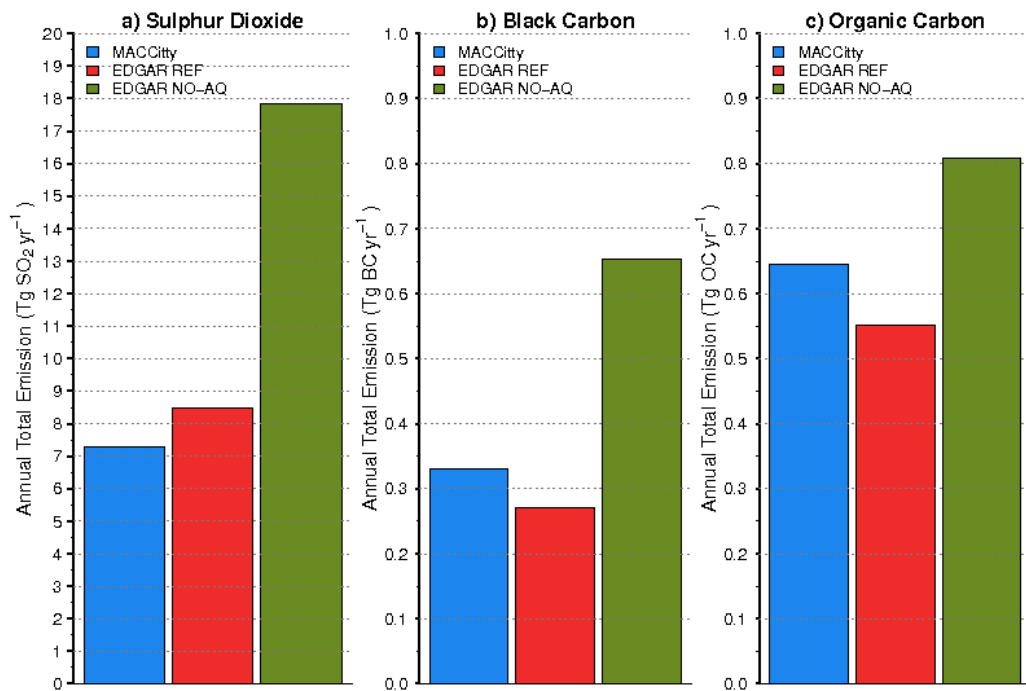


**Figure 2.1** Total annual European emissions of sulphur dioxide (SO<sub>2</sub>), black carbon (BC) and organic carbon (OC) in 2010 from the MACCity and EDGAR (both the reference and NO-AQ scenarios) emissions inventory.

## 2.7 Long Term Aerosol Observations over Europe

Long term observations of aerosol properties across Europe from 1978 to 2010 were collected and analysed to enable a multi-decadal evaluation of HadGEM3-UKCA on a monthly and annual basis. The details of the ground based observations that have been collected, processed and analysed for use in this thesis are shown in Table 2.2.

The number of observation sites in Table 2.2 is the maximum number available for use over the entire time period, with only a subset of sites actually conducting observations for a particular time period. For each

dataset a different amount of processing and analysis was required, which is summarised below.

**Table 2.2** Details of the ground based observations and where used within this thesis

Monitoring Network	Measurements	Time period	Number of Sites used	Chapter used
EMEP	Total sulphate aerosol mass concentrations	1978-2010	97	3,4
EMEP	Total suspended particle mass concentrations	1978-2005	42	3
EMEP	PM <sub>10</sub> mass concentrations	1996-2010	55	3
EMEP	Sulphur dioxide mass concentrations	1978-2010	161	3,4
EMEP	Rainwater pH	1972-2010	39	4
EUSAAR and GUAN	Aerosol size distributions providing number concentrations of particles greater than 30, 50 and 100 nm dry diameter	2008-2009	17	3
AERONET	Aerosol optical depth (AOD) at 440 nm wavelength	1994-2010	20	3
GEBA	Incident surface solar radiation	1922-2010	56	3

EUSAAR – European Supersite for Atmospheric Aerosol Research, GUAN - German Ultrafine Network

### 2.7.1 EMEP Observations

Measurements of sulphur dioxide concentrations (1978 to 2009), sulphate mass concentrations (1978 to 2009), SPM (total aerosol mass with no size cut –off; 1978 to 2005), PM<sub>10</sub> (1996 to 2009) and rainwater pH (1972 to 2009) were obtained from the EMEP network. Measurements of SPM up to 1998 were only used due to a reduction in availability and quality of observations post 1998. Measurement data from all the monitoring locations in Table 2.2 are shown in Figure 2.2.

Sites were only selected for use in the analysis if they have been continuously operating for more than 5 years. Individual site data files containing a single year of observations were downloaded for all the years that data was available from the EBAS database (<http://ebase.nilu.no>). EBAS brings together in one place and in standard format, observations (mainly ground based) from a number of different projects, including CREATE, EUSAAR and EUCARRI. For individual monitoring locations data files exist for multiple different instruments, measuring aerosol properties at different time resolutions (hourly, daily, weekly, monthly). Measurement data can overlap when two different instruments are used over the same time period for the same property at the same location. When this overlap was

detected observation data was compared from the two different instruments to check for systematic biases and whether the different datasets could be used. If they were found to be incompatible then the instrument with the longer time series of observations was solely used.

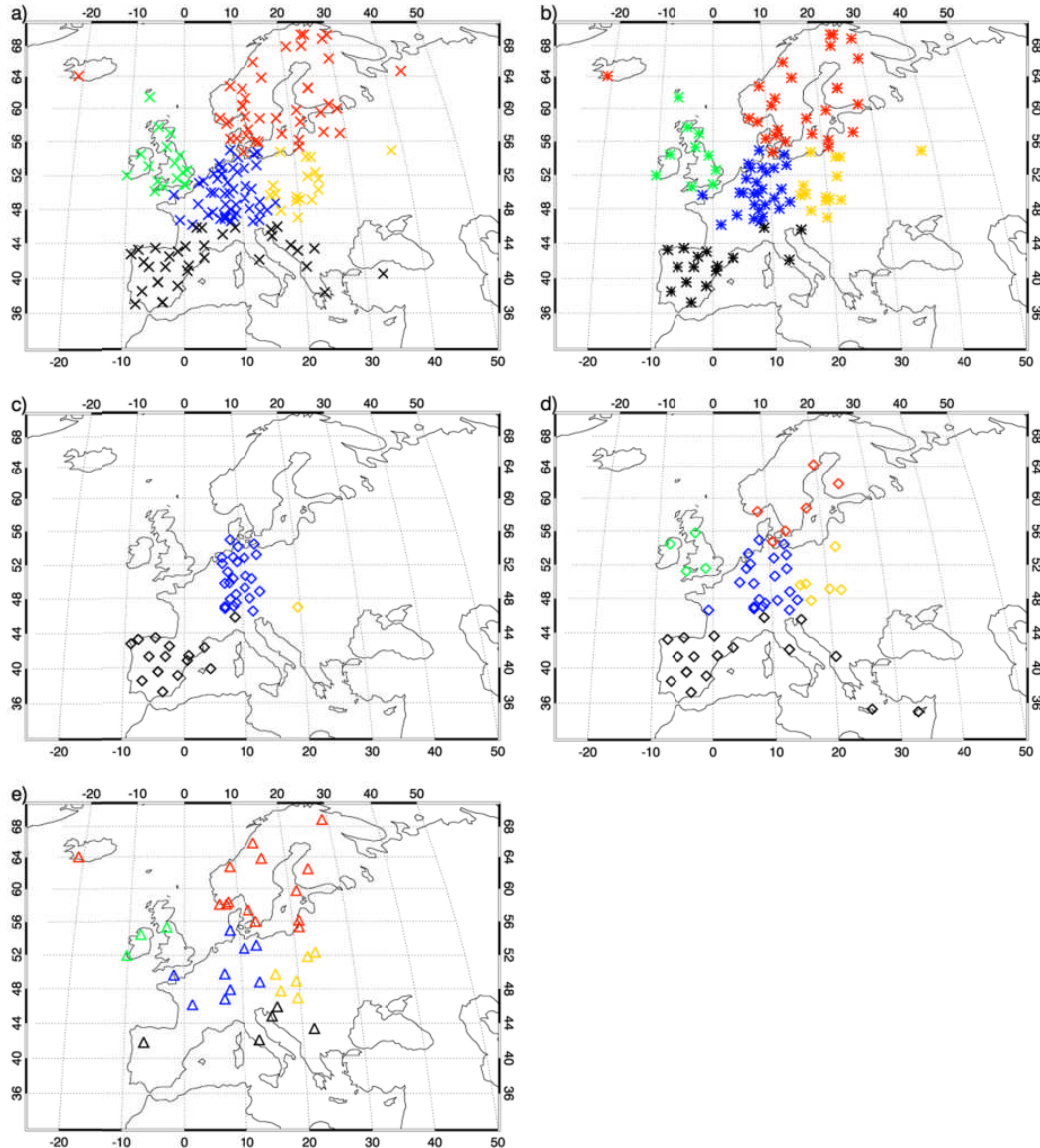


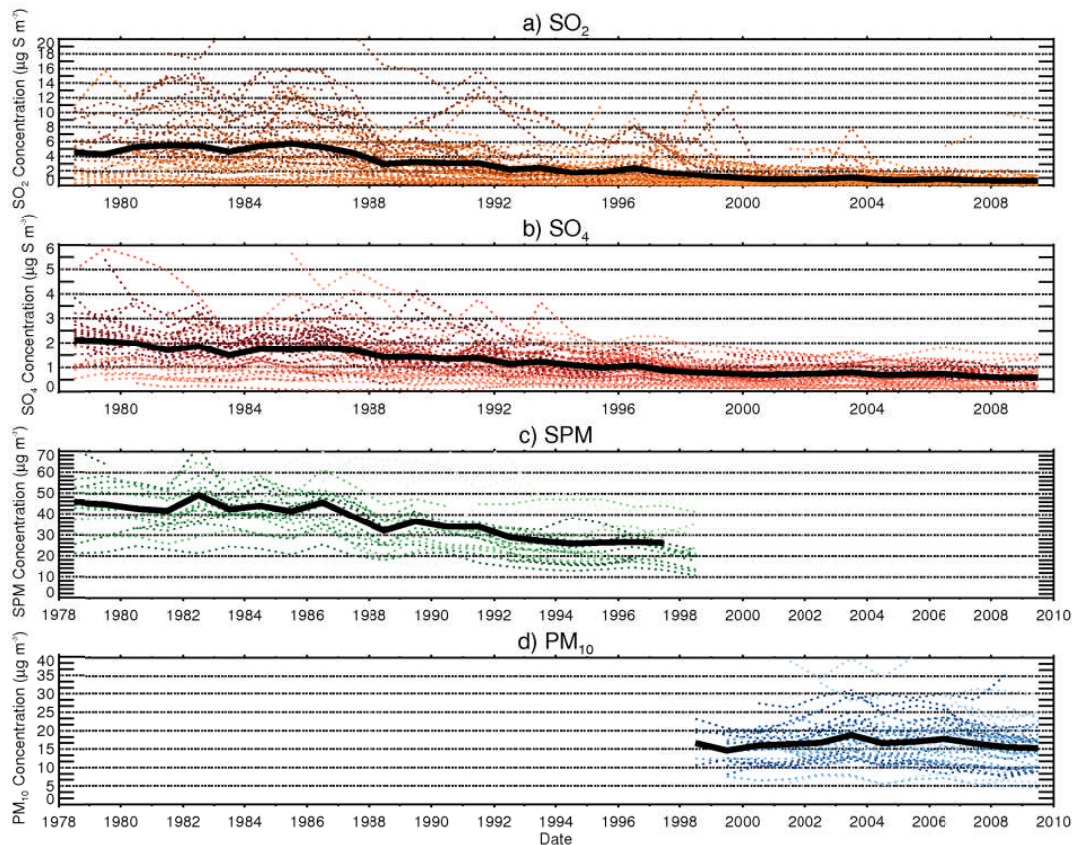
**Figure 2.2** Spatial location of all the measurement sites used within this thesis from the EMEP network for a) SO<sub>2</sub>, b) sulphate, c) SPM, d) PM<sub>10</sub> and e) rainwater pH. Locations have been colour coded by the sub-regional definition used in Chapter 3: Northern Europe (red), North West Europe (green), Central Europe (blue), Southern Europe (black) and Eastern Europe (yellow).

Initially, observations were collated together into a single file for a particular location based upon the instrument type and time resolution of measurement data used. This file was then processed to produce monthly and annual mean values, providing that the data capture rate for the averaging period was above 75%. As part of the averaging procedure the raw data was

quality assured by screening for anomalous values and checking if the data flag in the original measurement record was acceptable.

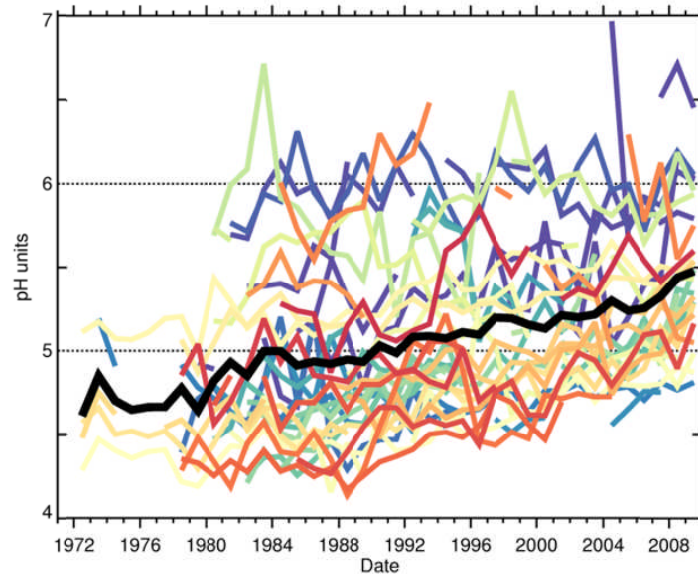
Annual and monthly mean values for each site and each instrument type could then be combined together to produce European mean values across the entire measurement period, providing that no bias and/or errors were detected between sites and instruments.

Figure 2.3 shows a time series of observational data used in thesis for SO<sub>2</sub>, sulphate, SPM and PM<sub>10</sub> at each individual monitoring location, along with a multi-site mean value. Long term aerosol observations over Europe from the EMEP network show that both SO<sub>2</sub> concentrations and SO<sub>4</sub><sup>2-</sup> aerosol mass concentrations reduced by ~90% and 70% respectively over the period 1980 to 2009 (Figure 2.3a and b). Total suspended particulate matter (SPM), which covers particles of all sizes, reduced by ~40% across Europe over the period 1978 to 1998 (Figure 2.3c). Smaller reductions in PM<sub>10</sub> (Figure 2.3d) was observed over Europe between 2000 and 2009.



**Figure 2.3** Time series of the European observations of a) Sulphur dioxide (SO<sub>2</sub>), b) sulphate aerosol (SO<sub>4</sub>), c) total suspended particulate matter (SPM) and d) particulate matter with a diameter of less than 10 µm (PM<sub>10</sub>) from the EMEP network over the period 1978 to 2010. Coloured lines are observations at each individual measurement location with the solid black lines showing the mean value of all observations for each year.

Figure 2.4 shows a similar time series for all the rainwater pH observations, available from each individual monitoring location in the EMEP network. An increase in rainwater pH is observed across the majority of sites in Europe since the 1980s.



**Figure 2.4** Time series of European observations of rainwater pH from the EMEP network over the period 1972 to 2010. Coloured lines represent observations at each individual monitoring location with the solid black line showing the mean value of all observations for each year.

### 2.7.2 Aerosol Size distributions

Observations of the aerosol size distribution at sites operated by the EUSAAR and GUAN network were collected and processed by Asmi et al., (2011) for 2008 and 2009. A model evaluation of aerosol number concentrations was conducted on the year 2008 measurements, as no long term aerosol size distribution data was available. Monthly and annual mean values of total number concentrations above dry diameters of 30 nm (N30), 50 nm (N50), and 100 nm (N100) were calculated from the size distribution data and used in the comparison with the HadGEM3-UKCA output (Figure 2.5). The same 17 low altitude measurement locations were used in the comparison, as in (Mann et al., 2014).

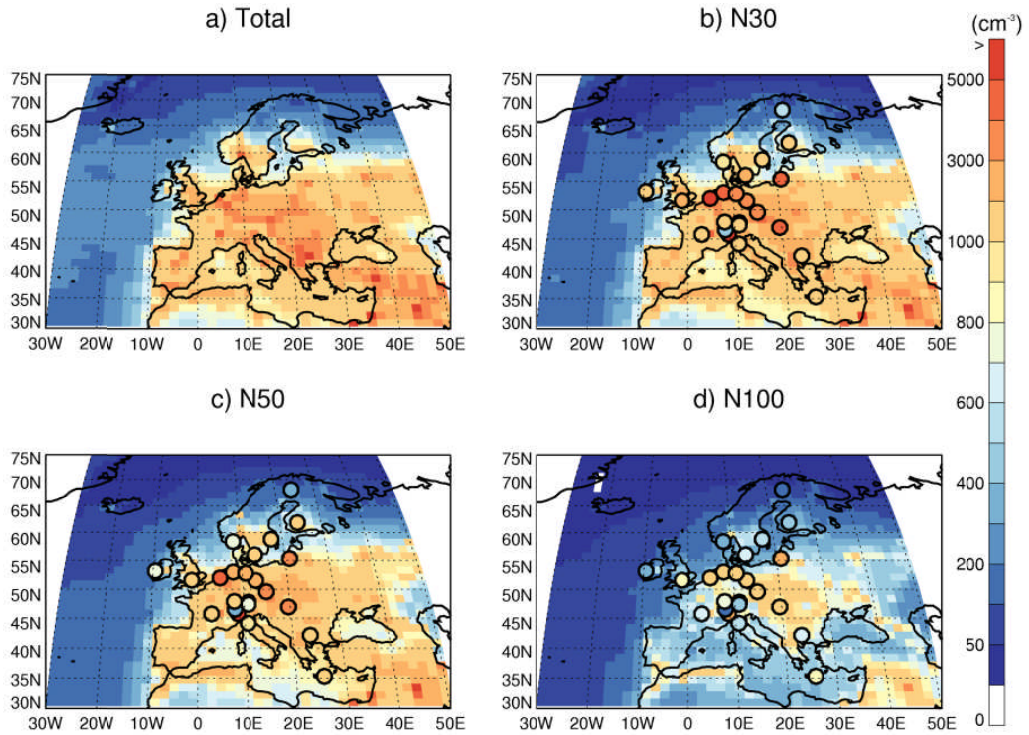


**Figure 2.5** Annual mean aerosol number concentrations from HadGEM3-UKCA with observations from EUSAAR and GUAN overplotted in 2008 for a) total aerosol number concentrations, b) N30 (particles greater than 30 nm in diameter), c) N50 (>50 nm) and d) N100 (>100 nm)

### 2.7.3 AOD

AOD observations were collected from AERONET for sites across Europe from 1994, although most sites have only started to measure since 2000. Due to the lack of available data it was decided not to use any data prior to 2000. The Level 2.0 data product (cloud screened and quality assured) was obtained from the AERONET website for 20 sites that have been operating for longer than 5 years over the period 2000 to 2010 (Figure 2.6).

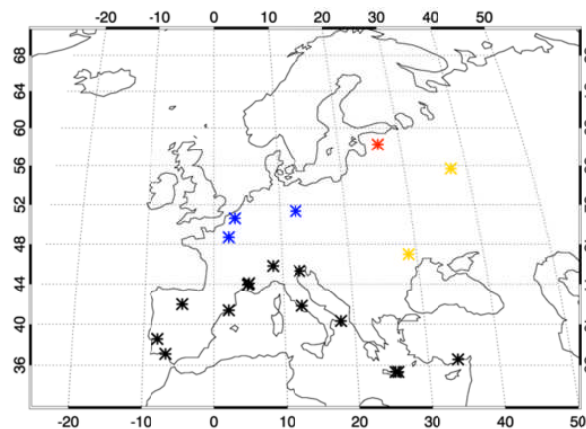


**Figure 2.6** Location of the AOD monitoring sites from AERONET (colour coded by the sub-regional definition used in Chapter 3: Northern Europe (red), North West Europe (green), Central Europe (blue), Southern Europe (black) and Eastern Europe (yellow)).

The best spatial and temporal coverage in AOD data was provided at the 440 nm wavelength and this was selected for use in the model evaluation. Figure 2.7 shows a time series for monthly values of AOD at 440 nm at all long term monitoring sites across Europe from AERONET.

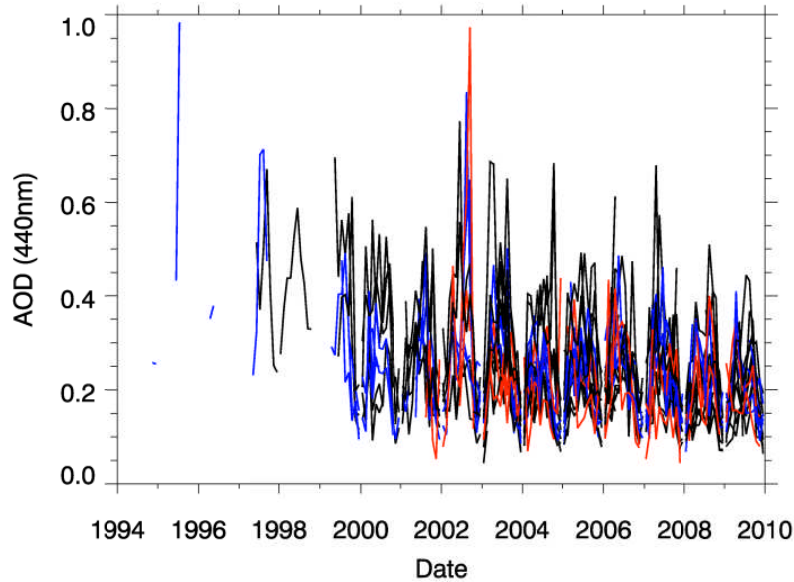


**Figure 2.7** Time series of aerosol optical depth observations from AERONET at 440 nm wavelength over the period 1994 to 2010. Coloured lines represent observations at each individual monitoring location for the months of each year.

### 2.7.4 Surface Solar Radiation

The dataset of surface solar radiation observations over Europe was obtained from the GEBA network and that used in Sanchez-Lorenzo et al., (2013). Files of monthly mean values of incident SSR under all-sky conditions (expressed as mean irradiance in  $W m^{-2}$ ) were provided for 56 sites across Europe that have been operating prior to 1971 (Figure 2.8).

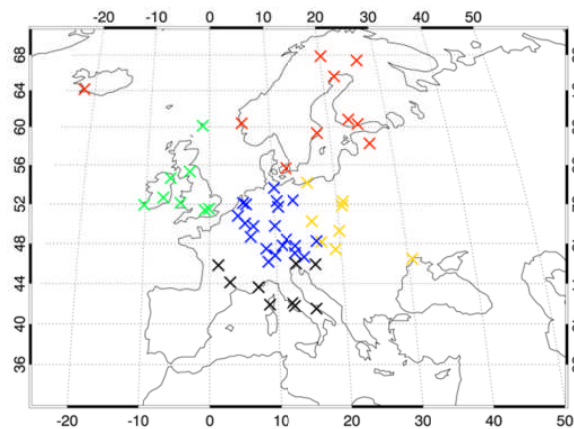


**Figure 2.8** Location of the surface solar radiation monitoring sites from GEBA (colour coded by the sub-regional definition used in Chapter 3: Northern Europe (red), North West Europe (green), Central Europe (blue), Southern Europe (black) and Eastern Europe (yellow)).

Observations are available prior to the 1960-2010 time period considered in this thesis, as shown by the long time series of SSR at four selected sites in Figure 2.9.

Measurement sites are mainly located in central Europe and the Mediterranean area. The SSR dataset used in this thesis has been previously quality controlled to remove any outliers or gross errors in the data and also checked for temporal consistency using a standard normal homogeneity test (Sanchez-Lorenzo et al., 2013).

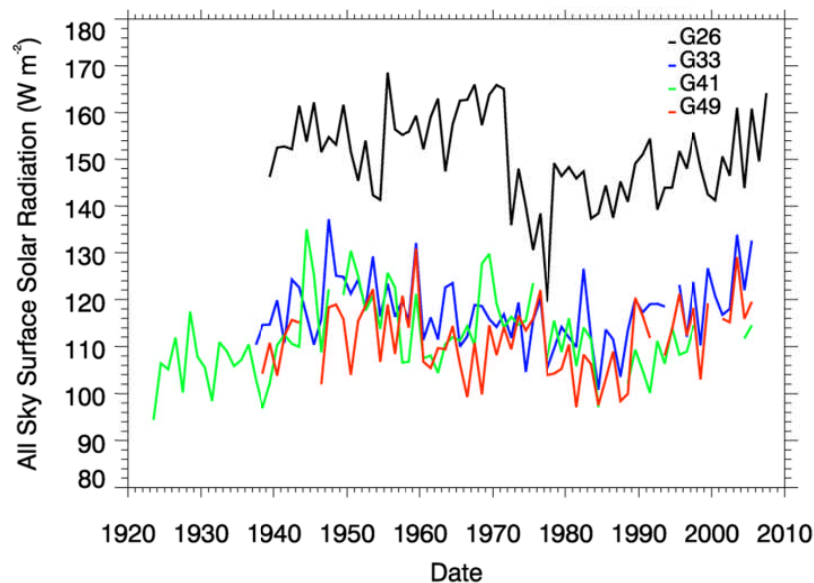


**Figure 2.9** Observations of all-sky incident surface solar radiation since 1920 at four individual European measurement locations: G26 – Locarno-Monti (Switzerland), G33 – Potsdam (Germany), G41 – Stockholm (Sweden) and G49 – Wageningen (Netherlands).

The dataset was used as either monthly or annual values (calculated only if 75% of data for a site was available for a year) and collated together to provide a European mean of individual sites (Figure 2.10a). SSR data tends to be presented as anomaly values relative to a mean period. The mean period here was chosen as 1980-2000 as it was considered to have the greatest concentration of most reliable observations (A. Sanchez-Lorenzo, 2014, personal communication). SSR anomaly values were calculated at each individual measurement location before calculating a European mean anomaly value to avoid any spatial sampling bias. Figure 2.10b shows the individual SSR anomaly values across all monitoring locations used within this thesis, in addition to the multi-site mean value.

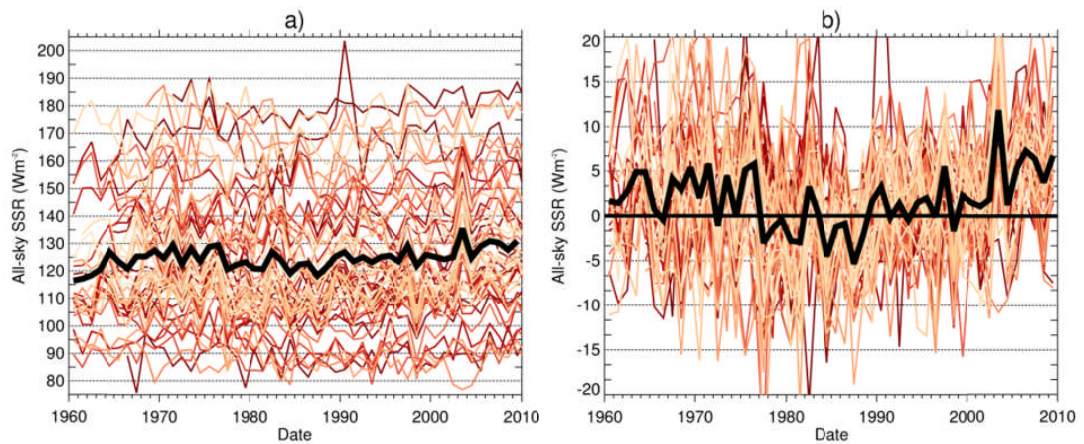


**Figure 2.10** Observations of a) all-sky incident surface solar radiation across all monitoring sites used within this thesis. b) incident surface solar radiation at each monitoring relative to the 1980-2000 mean value at each site. Thick black line represents mean value across all monitoring locations.

## 2.8 References

- Abdul-Razzak, H. & Ghan, S.J. (2000). A parameterization of aerosol activation: 2. Multiple aerosol types. *Journal of Geophysical Research*. 105 (D5). p.p. 6837.
- Almeida, J., Schobesberger, S., Kürten, A., Ortega, I.K., Kupiainen-Määttä, O., Praplan, A.P., Adamov, A., Amorim, A., Bianchi, F., Breitenlechner, M., David, A., Dommen, J., Donahue, N.M., Downard, A., Dunne, E., Duplissy, J., Ehrhart, S., Flagan, R.C., Franchin, A., Guida, R., Hakala, J., Hansel, A., Heinritzi, M., Henschel, H., Jokinen, T., Junninen, H., Kajos, M., Kangasluoma, J., Keskinen, H., Kupc, A., Kurtén, T., Kvashin, A.N., Laaksonen, A., Lehtipalo, K., Leiminger, M., Leppä, J., Loukonen, V., Makhmutov, V., Mathot, S., McGrath, M.J., Nieminen, T., Olenius, T., Onnela, A., Petäjä, T., Riccobono, F., Riipinen, I., Rissanen, M., Rondo, L., Ruuskanen, T., Santos, F.D., Sarnela, N., Schallhart, S., Schnitzhofer, R., Seinfeld, J.H., Simon, M., Sipilä, M., Stozhkov, Y., Stratmann, F., Tomé, A., Tröstl, J., Tsagkogeorgas, G., Vaattovaara, P., Viisanen, Y., Virtanen, A., Vrtala, A., Wagner, P.E., Weingartner, E., Wex, H., Williamson, C., Wimmer, D., Ye, P., Yli-Juuti, T., Carslaw, K.S., Kulmala, M., Curtius, J., Baltensperger, U., Worsnop, D.R., Vehkamäki, H. & Kirkby, J. (2013). Molecular understanding of sulphuric acid-amine particle nucleation in the atmosphere. *Nature*. 502. p.pp. 359–363.
- Andreae, M.O. (2013). The Aerosol Nucleation Puzzle. *Science*. 339 (6122). p.p. 911.
- Andres, R.J. & Kasgnoc, A.D. (1998). A time-averaged inventory of subaerial volcanic sulfur emissions. *Journal of Geophysical Research*. 103 (D19). p.p. 25251.

- Apte, J.S., Marshall, J.D., Cohen, A.J. & Brauer, M. (2015). Addressing Global Mortality from Ambient PM 2.5. *Environmental Science & Technology*. 49. p.pp. 8057–8066.
- Asmi, A., Wiedensohler, A., Laj, P., Fjaeraa, A.-M., Sellegri, K., Birmili, W., Weingartner, E., Baltensperger, U., Zdimal, V., Zikova, N., Putaud, J.-P., Marinoni, A., Tunved, P., Hansson, H.-C., Fiebig, M., Kivekäs, N., Lihavainen, H., Asmi, E., Ulevicius, V., Aalto, P.P., Swietlicki, E., Kristensson, A., Mihalopoulos, N., Kalivitis, N., Kalapov, I., Kiss, G., de Leeuw, G., Henzing, B., Harrison, R.M., Beddows, D., O'Dowd, C., Jennings, S.G., Flentje, H., Weinhold, K., Meinhardt, F., Ries, L. & Kulmala, M. (2011). Number size distributions and seasonality of submicron particles in Europe 2008–2009. *Atmospheric Chemistry and Physics*. 11 (11). p.pp. 5505–5538.
- Atkinson, R., Baulch, D.L., Cox, R.A., Hampson JR, R.F., Kerr, J.A. & Troe, J. (1989). Evaluated Kinetic and Photochemical Data for Atmospheric Chemistry: Supplement III. *Journal Physical Chemical Reference Data*. 18 (2). p.pp. 881–1097.
- Barth, M.C., Rasch, P.J., Kiehl, J.T., Benkovitz, C.M. & Schwartz, S.E. (2000). Sulfur chemistry in the National Center for Atmospheric Research Community Climate Model: Description, evaluation, features, and sensitivity to aqueous chemistry. *Journal of Geophysical Research*. 105 (D1). p.p. 1387.
- Beard, K. V. & Grover, S.N. (1973). Numerical Collision Efficiencies for Small Raindrops Colliding with Micron Size Particles. *Journal of the Atmospheric Sciences*. 31 (2) p.pp. 543–550.
- Bellouin, N. (2010). Interaction of UKCA aerosols with radiation: UKCA\_RADAER.
- Bellouin, N., Mann, G.W., Woodhouse, M.T., Johnson, C., Carslaw, K.S. & Dalvi, M. (2013). Impact of the modal aerosol scheme GLOMAP-mode on aerosol forcing in the Hadley Centre Global Environmental Model. *Atmospheric Chemistry and Physics*. 13 (6). p.pp. 3027–3044.
- Benedict, K.B., Lee, T. & Collett, J.L. (2012). Cloud water composition over the southeastern Pacific Ocean during the VOCALS regional experiment. *Atmospheric Environment*. 46. p.pp. 104–114.
- Brock, C. A, Washenfelder, R.A., Trainer, M., Ryerson, T.B., Wilson, J.C., Reeves, J.M., Huey, L.G., Holloway, J.S., Parrish, D.D., Hübler, G. & Fehsenfeld, F.C. (2002). Particle growth in the plumes of coal-fired power plants. *Journal of Geophysical Research*. 107 (D12). p.pp. AAC 9–1–AAC 9–14.

- Burnett, R.T., Arden Pope, C., Ezzati, M., Olives, C., Lim, S.S., Mehta, S., Shin, H.H., Singh, G., Hubbell, B., Brauer, M., Ross Anderson, H., Smith, K.R., Balme, J.R., Bruce, N.G., Kan, H., Laden, F., Prüss-Ustün, A., Turner, M.C., Gapstur, S.M., Diver, W.R. & Cohen, A. (2014). An integrated risk function for estimating the global burden of disease attributable to ambient fine particulate matter exposure. *Environmental Health Perspectives*. 122. p.pp. 397–403.
- Chin, M., Jacob, D.J., Gardner, G.M., Foreman-Fowler, M.S., Spiro, P.A. & Savoie, D.L. (1996). A global three-dimensional model of tropospheric sulfate. *Journal of Geophysical Research*. 101 (D13). p.p. 18667.
- Cohen, A.J., Anderson, H.R., Ostro, B., Pandey, K.D., Krzyzanowski, M., Künzli, N., Gutschmidt, K., Iij, C.A.P., Romieu, I., Samet, J.M. & Smith, K.R. (2004). Mortality Impacts of Urban Air Pollution. In: *Comparative Quantification of Health Risks*. pp. 1353–1434.
- Collett, J., Oberholzer, B. & Staehelin, J. (1993). Cloud chemistry at Mt Rigi, Switzerland: Dependence on drop size and relationship to precipitation chemistry. *Atmospheric Environment. Part A. General Topics*. 27 (1). p.pp. 33–42.
- Crippa, M., Janssens-Maenhout, G., Dentener, F., Guizzardi, D., Sindelarova, K., Muntean, M., Van Dingenen, R. & Granier, C. (2016a). Forty years of improvements in European air quality: regional policy-industry interactions with global impacts. *Atmospheric Chemistry and Physics*. 16 (6). p.pp. 3825–3841.
- Crippa, M., Janssens-Maenhout, G., Guizzardi, D. & Galmarini, S. (2016b). EU effect: exporting emission regulations through global market economy. *Journal of Environmental Management*. submitted.
- Davies, T., Cullen, M.J.P., Malcolm, A.J., Mawson, M.H., Staniforth, A., White, A.A. & Wood, N. (2005). A new dynamical core for the Met Office's global and regional modelling of the atmosphere. *Quarterly Journal of the Royal Meteorological Society*. 131 (608). p.pp. 1759–1782.
- Dee, D.P., Uppala, S.M., Simmons, A.J., Berrisford, P., Poli, P., Kobayashi, S., Andrae, U., Balmaseda, M.A., Balsamo, G., Bauer, P., Bechtold, P., Beljaars, A.C.M., van de Berg, L., Bidlot, J., Bormann, N., Delsol, C., Dragani, R., Fuentes, M., Geer, A.J., Haimberger, L., Healy, S.B., Hersbach, H., Hólm, E. V., Isaksen, L., Kållberg, P., Köhler, M., Matricardi, M., McNally, A.P., Monge-Sanz, B.M., Morcrette, J.-J., Park, B.-K., Peubey, C., de Rosnay, P., Tavolato, C., Thépaut, J.-N. & Vitart, F. (2011). The ERA-Interim reanalysis: configuration and performance of the data assimilation system. *Quarterly Journal of the Royal Meteorological Society*. 137 (656). p.pp. 553–597.

- Dentener, F., Kinne, S., Bond, T.C., Boucher, O., Cofala, J., Generoso, S., Ginoux, P., Gong, S., Hoelzemann, J.J., Ito, A., Marelli, L., Penner, J.E., Putaud, J.-P., Textor, C., Schulz, M., van der Werf, G.R. & Wilson, J. (2006). Emissions of primary aerosol and precursor gases in the years 2000 and 1750 prescribed datasets for AeroCom. *Atmospheric Chemistry and Physics*. 6 (12). p.pp. 4321–4344.
- Easter, R.C. & Hales, J.M. (1983). Interpretation of the OSCAR data for reactive gas scavenging. In: *Precipitation Scavenging, Dry Deposition, and Resuspension*. New York, USA: Elsevier Ltd, pp. 649–662.
- EC-JRC/PBL (2015). EDGAR version 4.3. [Online]. 2015. Available from: <http://edgar.jrc.ec.europa.eu/>.
- Edwards, J.M. & Slingo, A. (1996). Studies with a flexible new radiation code. I: Choosing a configuration for a large-scale model. *Quarterly Journal of the Royal Meteorological Society*. 122 (531). p.pp. 689–719.
- Ervens, B. (2015). Modeling the Processing of Aerosol and Trace Gases in Clouds and Fogs. *Chemical Reviews*. 115. p.pp. 4157–4198.
- Essery, R. L.H., Best, M.J., Betts, R. & Cox, P.M. (2002). Explicit Representation of Subgrid Heterogeneity in a GCM Land Surface Scheme. *Journal of Hydrometeorology*. 4. p.pp. 530–543.
- Fahey, K.M. (2003). Size-resolved aqueous-phase atmospheric chemistry in a three-dimensional chemical transport model. *Journal of Geophysical Research*. 108 (D22). p.p. 4690.
- Faloona, I. (2009). Sulfur processing in the marine atmospheric boundary layer: A review and critical assessment of modeling uncertainties. *Atmospheric Environment*. 43 (18). p.pp. 2841–2854.
- Gong, S.L. (2003). A parameterization of sea-salt aerosol source function for sub- and super-micron particles. *Global Biogeochemical Cycles*. 17 (4). p.p. 1097.
- Granier, C., Bessagnet, B., Bond, T.C., D'Angiola, A., Denier van der Gon, H., Frost, G.J., Heil, A., Kaiser, J.W., Kinne, S., Klimont, Z., Kloster, S., Lamarque, J.-F., Liousse, C., Masui, T., Meleux, F., Mieville, A., Ohara, T., Raut, J.-C., Riahi, K., Schultz, M.G., Smith, S.J., Thompson, A., Aardenne, J., Werf, G.R. & Vuuren, D.P. (2011). Evolution of anthropogenic and biomass burning emissions of air pollutants at global and regional scales during the 1980–2010 period. *Climatic Change*. 109 (1-2). p.pp. 163–190.
- Guenther, A., Hewitt, C.N., Erickson, D., Fall, R., Geron, C., Graedel, T., Harley, P., Klinger, L., Lerdau, M., McKay, W.A., Pierce, T., Scholes, B., Steinbrecher, R., Tallamraju, R., Taylor, J. & Zimmerman, P. (1995). A global model of natural

- volatile organic compound emissions. *Journal of Geophysical Research*. 100 (D5). p.p. 8873.
- Halmer, M.M., Schmincke, H.-U. & Graf, H.-F. (2002). The annual volcanic gas input into the atmosphere, in particular into the stratosphere: a global data set for the past 100 years. *Journal of Volcanology and Geothermal Research*. 115 (3-4). p.pp. 511–528.
- Hoppel, W. a., Frick, G.M., Fitzgerald, J.W. & Larson, R.E. (1994). Marine boundary layer measurements of new particle formation and the effects nonprecipitating clouds have. *Journal of Geophysical Research*. 99 (D7). p.pp. 14443–14459.
- Hurrell, J.W., Hack, J.J., Shea, D., Caron, J.M. & Rosinski, J. (2008). A New Sea Surface Temperature and Sea Ice Boundary Dataset for the Community Atmosphere Model. *Journal of Climate*. 21 (19). p.pp. 5145–5153.
- Hutton, G. & Menne, B. (2014). Economic Evidence on the Health Impacts of Climate Change in Europe. *Environmental Health Insights*. 8. p.pp. 43–52.
- Janssens-Maenhout, G., Crippa, M., Guizzardi, D., Dentener, F., Muntean, M., Pouliot, G., Keating, T., Zhang, Q., Kurokawa, J., Wankmüller, R., Denier van der Gon, H., Kuenen, J.J.P., Klimont, Z., Frost, G., Darras, S., Koffi, B. & Li, M. (2015). HTAP\_v2.2: a mosaic of regional and global emission grid maps for 2008 and 2010 to study hemispheric transport of air pollution. *Atmospheric Chemistry and Physics*. 15 (19). p.pp. 11411–11432.
- Jones, A., Roberts, D.L., Woodage, M.J. & Johnson, C.E. (2001). Indirect sulphate aerosol forcing in a climate model with an interactive sulphur cycle. *Journal of Geophysical Research*. 106 (D17). p.p. 20293.
- Kettle, A.J. & Andreae, M.O. (2000). Flux of dimethylsulfide from the oceans: A comparison of updated data sets and flux models. *Journal of Geophysical Research*. 105 (D22). p.p. 26793.
- Kipling, Z., Stier, P., Schwarz, J.P., Perring, A.E., Spackman, J.R., Mann, G.W., Johnson, C.E. & Telford, P.J. (2013). Constraints on aerosol processes in climate models from vertically-resolved aircraft observations of black carbon. *Atmospheric Chemistry and Physics*. 13 (12). p.pp. 5969–5986.
- Kulmala, M., Laaksonen, A. & Pirjola, L. (1998). Parameterizations for sulfuric acid/water nucleation rates. *Journal of Geophysical Research*. 103 (D7). p.pp. 8301–8307.
- Lamarque, J.-F., Bond, T.C., Eyring, V., Granier, C., Heil, a., Klimont, Z., Lee, D., Liousse, C., Mieville, a., Owen, B., Schultz, M.G., Shindell, D.T., Smith, S.J., Stehfest, E., Van Aardenne, J., Cooper, O.R., Kainuma, M., Mahowald, N.,

- McConnell, J.R., Naik, V., Riahi, K. & van Vuuren, D.P. (2010). Historical (1850–2000) gridded anthropogenic and biomass burning emissions of reactive gases and aerosols: methodology and application. *Atmospheric Chemistry and Physics*. 10 (15). p.pp. 7017–7039.
- Lee, L.A., Pringle, K.J., Reddington, C.L., Mann, G.W., Stier, P., Spracklen, D. V., Pierce, J.R. & Carslaw, K.S. (2013). The magnitude and causes of uncertainty in global model simulations of cloud condensation nuclei. *Atmospheric Chemistry and Physics*. 13 (17). p.pp. 8879–8914.
- Liss, P. & Merlivat, L. (1986). Air-Sea Gas Exchange Rates: Introduction and Synthesis. In: *The Role of Air-Sea Exchange in Geochemical Cycling*. D. Reidel, pp. 113–127.
- Mann, G.W., Carslaw, K.S., Spracklen, D. V., Ridley, D. a., Manktelow, P.T., Chipperfield, M.P., Pickering, S.J. & Johnson, C.E. (2010). Description and evaluation of GLOMAP-mode: a modal global aerosol microphysics model for the UKCA composition-climate model. *Geoscientific Model Development*. 3 (2). p.pp. 519–551.
- Mann, G.W., Carslaw, K.S., Ridley, D. a., Spracklen, D. V., Pringle, K.J., Merikanto, J., Korhonen, H., Schwarz, J.P., Lee, L. a., Manktelow, P.T., Woodhouse, M.T., Schmidt, a., Breider, T.J., Emmerson, K.M., Reddington, C.L., Chipperfield, M.P. & Pickering, S.J. (2012). Intercomparison of modal and sectional aerosol microphysics representations within the same 3-D global chemical transport model. *Atmospheric Chemistry and Physics*. 12 (10). p.pp. 4449–4476.
- Mann, G.W., Carslaw, K.S., Reddington, C.L., Pringle, K.J., Schulz, M., Asmi, A., Spracklen, D. V., Ridley, D.A., Woodhouse, M.T., Lee, L.A., Zhang, K., Ghan, S.J., Easter, R.C., Liu, X., Stier, P., Lee, Y.H., Adams, P.J., Tost, H., Lelieveld, J., Bauer, S.E., Tsigaridis, K., van Noije, T.P.C., Strunk, A., Vignati, E., Bellouin, N., Dalvi, M., Johnson, C.E., Bergman, T., Kokkola, H., von Salzen, K., Yu, F., Luo, G., Petzold, A., Heintzenberg, J., Clarke, A., Ogren, J.A., Gras, J., Baltensperger, U., Kaminski, U., Jennings, S.G., O'Dowd, C.D., Harrison, R.M., Beddows, D.C.S., Kulmala, M., Viisanen, Y., Ulevicius, V., Mihalopoulos, N., Zdimal, V., Fiebig, M., Hansson, H.-C., Swietlicki, E. & Henzing, J.S. (2014). Intercomparison and evaluation of global aerosol microphysical properties among AeroCom models of a range of complexity. *Atmospheric Chemistry and Physics*. 14 (9). p.pp. 4679–4713.
- Metzger, A., Verheggen, B., Dommen, J., Duplissy, J., Prevot, A.S.H., Weingartner, E., Riipinen, I., Kulmala, M., Spracklen, D. V, Carslaw, K.S. & Baltensperger, U. (2010). Evidence for the role of organics in aerosol particle formation under

atmospheric conditions. *Proceedings of the National Academy of Sciences of the United States of America*. 107 (15). p.pp. 6646–51.

Murray, G.L.D., Kimball, K.D., Hill, L.B., Hislop, J.E. & Weathers, K.C. (2013). Long-Term Trends in Cloud and Rain Chemistry on Mount Washington, New Hampshire. *Water, Air, & Soil Pollution*. 224 (9). p.p. 1653.

O'Connor, F.M., Johnson, C.E., Morgenstern, O., Abraham, N.L., Braesicke, P., Dalvi, M., Folberth, G.A., Sanderson, M.G., Telford, P.J., Voulgarakis, A., Young, P.J., Zeng, G., Collins, W.J. & Pyle, J.A. (2014). Evaluation of the new UKCA climate-composition model – Part 2: The Troposphere. *Geoscientific Model Development*. 7 (1). p.pp. 41–91.

OECD (2012). *Mortality risk evaluation in environment, health and transport policies*. Paris: Organisation for Economic Co-operation and Development.

Ostro, B. (2004). *Outdoor air pollution Assessing the environmental burden of disease at national and local levels*. 2nd Ed. A. Prüss-Üstün, D. Campbell-Lendrum, C. Corvalán, & A. Woodward (eds.). Geneva: World Health Organization (WHO Environmental Burden of Disease Series, No. 5).

Pham, M., Müller, J.-F., Brasseur, G.P., Granier, C. & Megie, G. (1995). A three-dimensional study of the tropospheric sulfur cycle. *Journal of Geophysical Research*. 100 (D12). p.pp. 26061–26092.

Pope III, C.A. (2002). Lung Cancer, Cardiopulmonary Mortality, and Long-term Exposure to Fine Particulate Air Pollution. *JAMA*. 287 (9). p.pp. 1132–1141.

Raes, F., Dingenen, R. Van, Vignati, E., Wilson, J., Putaud, J.-P., Seinfeld, J.H. & Adams, P.J. (2000). Formation and cycling of aerosols in the global troposphere. *Atmospheric Environment*. 34 (25). p.pp. 4215–4240.

Roelofs, G.J., Kasibhatla, P., Barrie, L., Bergmann, D., Bridgeman, C., Chin, M., Christensen, J., Easter, R., Feichter, J., Jeuken, a, Kjellstrom, E., Koch, D., Land, C., Lohmann, U. & Rasch, P. (2001). Analysis of regional budgets of sulfur species modeled for the COSAM exercise. *Tellus Series B-Chemical and Physical Meteorology*. 53 (5). p.pp. 673–694.

Sanchez-Lorenzo, A., Wild, M. & Trentmann, J. (2013). Validation and stability assessment of the monthly mean CM SAF surface solar radiation dataset over Europe against a homogenized surface dataset (1983–2005). *Remote Sensing of Environment*. 134. p.pp. 355–366.

Scott, C.E., Rap, A., Spracklen, D. V., Forster, P.M., Carslaw, K.S., Mann, G.W., Pringle, K.J., Kivekäs, N., Kulmala, M., Lihavainen, H. & Tunved, P. (2014). The

direct and indirect radiative effects of biogenic secondary organic aerosol. *Atmospheric Chemistry and Physics*. 14. p.pp. 447–470.

Seinfeld, J.H. & Pandis, S.N. (2006). *Atmospheric Chemistry and Physics From Air Pollution to Climate Change*. Second. Wiley-Interscience.

Sekhon, R.S. & Srivastava, R.C. (1971). Doppler Radar Observations of Drop-Size Distributions in a Thunderstorm. *Journal of the Atmospheric Sciences*. 28 (6) p.pp. 983–994.

Slinn, W.G.N. (1982). Predictions for particle deposition to vegetative canopies. *Atmospheric Environment*. 16 (7). p.pp. 1785–1794.

Slinn, W.G.N. (1984). Precipitation Scavenging. In: D. Randerson (ed.). *Atmospheric Science and Power Production*. US Department of Energy.

Spracklen, D. V., Pringle, K.J., Carslaw, K.S., Chipperfield, M.P. & Mann, G.W. (2005a). A global off-line model of size-resolved aerosol microphysics: I. Model development and prediction of aerosol properties. *Atmospheric Chemistry and Physics*. 5 (1). p.pp. 2227–2252.

Spracklen, D. V., Pringle, K.J., Carslaw, K.S., Chipperfield, M.P. & Mann, G.W. (2005b). A global off-line model of size-resolved aerosol microphysics: II. Identification of key uncertainties. *Atmospheric Chemistry and Physics*. 5 (3). p.pp. 3233–3250.

Spracklen, D. V., Carslaw, K.S., Kulmala, M., Kerminen, V.-M., Mann, G.W. & Sihto, S.-L. (2006). The contribution of boundary layer nucleation events to total particle concentrations on regional and global scales. *Atmospheric Chemistry and Physics*. 6 (12). p.pp. 5631–5648.

Spracklen, D. V., Carslaw, K.S., Merikanto, J., Mann, G.W., Reddington, C.L., Pickering, S., Ogren, J. A., Andrews, E., Baltensperger, U., Weingartner, E., Boy, M., Kulmala, M., Laakso, L., Lihavainen, H., Kivekäs, N., Komppula, M., Mihalopoulos, N., Kouvarakis, G., Jennings, S.G., O'Dowd, C., Birmili, W., Wiedensohler, A., Weller, R., Gras, J., Laj, P., Sellegri, K., Bonn, B., Krejci, R., Laaksonen, A., Hamed, A., Minikin, A., Harrison, R.M., Talbot, R. & Sun, J. (2010). Explaining global surface aerosol number concentrations in terms of primary emissions and particle formation. *Atmospheric Chemistry and Physics*. 10 (10). p.pp. 4775–4793.

Stevens, R.G., Pierce, J.R., Brock, C.A., Reed, M.K., Crawford, J.H., Holloway, J.S., Ryerson, T.B., Huey, L.G. & Nowak, J.B. (2012). Nucleation and growth of sulfate aerosol in coal-fired power plant plumes: Sensitivity to background aerosol and meteorology. *Atmospheric Chemistry and Physics*. 12 (1). p.pp. 189–206.

- Stier, P., Feichter, J., Kinne, S., Kloster, S., Vignati, E., Wilson, J., Ganzeveld, L., Tegen, I., Werner, M., Balkanski, Y., Schulz, M., Boucher, O., Minikin, A. & Petzold, A. (2005). The aerosol-climate model ECHAM5-HAM. *Atmospheric Chemistry and Physics*. 5 (4). p.pp. 1125–1156.
- Telford, P.J., Abraham, N.L., Archibald, A. T., Braesicke, P., Dalvi, M., Morgenstern, O., O'Connor, F.M., Richards, N. A. D. & Pyle, J. A. (2013). Implementation of the Fast-JX Photolysis scheme into the UKCA component of the MetUM chemistry climate model. *Geoscientific Model Development*. 6 (1). p.pp. 161–177.
- Telford, P.J., Braesicke, P., Morgenstern, O. & Pyle, J. A. (2008). Technical Note: Description and assessment of a nudged version of the new dynamics Unified Model. *Atmospheric Chemistry and Physics*. 8 (6). p.pp. 1701–1712.
- Uppala, S.M., Kållberg, P.W., Simmons, A.J., Andrae, U., Bechtold, V.D.C., Fiorino, M., Gibson, J.K., Haseler, J., Hernandez, A., Kelly, G.A., Li, X., Onogi, K., Saarinen, S., Sokka, N., Allan, R.P., Andersson, E., Arpe, K., Balmaseda, M.A., Beljaars, A.C.M., Berg, L. Van De, Bidlot, J., Bormann, N., Caires, S., Chevallier, F., Dethof, A., Dragosavac, M., Fisher, M., Fuentes, M., Hagemann, S., Hólm, E., Hoskins, B.J., Isaksen, L., Janssen, P.A.E.M., Jenne, R., McNally, A.P., Mahfouf, J.-F., Morcrette, J.-J., Rayner, N.A., Saunders, R.W., Simon, P., Sterl, A., Trenberth, K.E., Untch, A., Vasiljevic, D., Viterbo, P. & Woollen, J. (2005). The ERA-40 re-analysis. *Quarterly Journal of the Royal Meteorological Society*. 131 (612). p.pp. 2961–3012.
- WHO Regional Office for Europe & OECD (2015). Economic cost of the health impact of air pollution in Europe: Clean air, health and wealth. Copenhagen: WHO Regional Office for Europe.
- Wild, O., Zhu, X. & Prather, M.J. (2000). Fast-J: Accurate Simulation of In- and Below-Cloud Photolysis in Tropospheric Chemical Models. *Journal of Atmospheric Chemistry*. 37 (3). p.pp. 245–282.
- Woodward, S. (2001). Modeling the atmospheric life cycle and radiative impact of mineral dust in the Hadley Centre climate model. *Journal of Geophysical Research*. 106 (D16). p.pp. 18155–18166.
- Zhang, L., Gong, S., Padro, J. & Barrie, L. (2001). A size-segregated particle dry deposition scheme for an atmospheric aerosol module. *Atmospheric Environment*. 35 (3). p.pp. 549–560.

**Chapter 3**  
**Modelled and Observed Changes in aerosols and surface  
solar radiation over Europe between 1960 and 2009**



# Modelled and observed changes in aerosols and surface solar radiation over Europe between 1960 and 2009

S. T. Turnock<sup>1</sup>, D. V. Spracklen<sup>1</sup>, K. S. Carslaw<sup>1</sup>, G. W. Mann<sup>1,2</sup>, M. T. Woodhouse<sup>1,a</sup>, P. M. Forster<sup>1</sup>, J. Haywood<sup>3</sup>, C. E. Johnson<sup>3</sup>, M. Dalvi<sup>3</sup>, N. Bellouin<sup>4</sup>, and A. Sanchez-Lorenzo<sup>5</sup>

<sup>1</sup>Institute of Climate and Atmospheric Science, School of Earth and Environment, University of Leeds, Leeds, UK

<sup>2</sup>National Centre for Atmospheric Science, University of Leeds, Leeds, UK

<sup>3</sup>Met Office, Fitzroy Road, Exeter, Devon, UK

<sup>4</sup>Department of Meteorology, University of Reading, Reading, UK

<sup>5</sup>Pyrenean Institute of Ecology, Spanish National Research Council, Zaragoza, Spain

<sup>a</sup>now at: CSIRO Ocean and Atmosphere, Aspendale, Victoria, Australia

Correspondence to: S. T. Turnock (s.t.turnock12@leeds.ac.uk)

Received: 2 April 2015 – Published in Atmos. Chem. Phys. Discuss.: 8 May 2015

Revised: 31 July 2015 – Accepted: 4 August 2015 – Published: 25 August 2015

**Abstract.** Substantial changes in anthropogenic aerosols and precursor gas emissions have occurred over recent decades due to the implementation of air pollution control legislation and economic growth. The response of atmospheric aerosols to these changes and the impact on climate are poorly constrained, particularly in studies using detailed aerosol chemistry–climate models. Here we compare the HadGEM3-UKCA (Hadley Centre Global Environment Model–United Kingdom Chemistry and Aerosols) coupled chemistry–climate model for the period 1960–2009 against extensive ground-based observations of sulfate aerosol mass (1978–2009), total suspended particle matter (SPM, 1978–1998), PM<sub>10</sub> (1997–2009), aerosol optical depth (AOD, 2000–2009), aerosol size distributions (2008–2009) and surface solar radiation (SSR, 1960–2009) over Europe. The model underestimates observed sulfate aerosol mass (normalised mean bias factor (NMBF) = −0.4), SPM (NMBF = −0.9), PM<sub>10</sub> (NMBF = −0.2), aerosol number concentrations (N30 NMBF = −0.85; N50 NMBF = −0.65; and N100 NMBF = −0.96) and AOD (NMBF = −0.01) but slightly overpredicts SSR (NMBF = 0.02). Trends in aerosol over the observational period are well simulated by the model, with observed (simulated) changes in sulfate of −68 % (−78 %), SPM of −42 % (−20 %), PM<sub>10</sub> of −9 % (−8 %) and AOD of −11 % (−14 %). Discrepancies in the magnitude of simulated aerosol mass do not affect the ability of the model to reproduce the observed SSR trends. The positive change in

observed European SSR (5 %) during 1990–2009 (“brightening”) is better reproduced by the model when aerosol radiative effects (ARE) are included (3 %), compared to simulations where ARE are excluded (0.2 %). The simulated top-of-the-atmosphere aerosol radiative forcing over Europe under all-sky conditions increased by > 3.0 W m<sup>−2</sup> during the period 1970–2009 in response to changes in anthropogenic emissions and aerosol concentrations.

## 1 Introduction

Aerosols can cause acid deposition, degradation of atmospheric visibility, changes to Earth’s radiative balance, and are also a major source of air pollution, which affects human health. Aerosols interact with climate by absorbing and reflecting incoming solar radiation and by modifying the microphysical properties of clouds. These effects have been defined in the latest Intergovernmental Panel on Climate Change (IPCC) report (Boucher et al., 2013) as aerosol–radiation interactions (ARI) and aerosol–cloud interactions (ACI). Aerosols (also referred to as particulate matter (PM)) are detrimental to air quality and human health, as particles below a certain size can penetrate into the lungs causing respiratory and cardiovascular problems (COMEAP, 2010). Strategies that attempt to mitigate climate change and poor air quality are inherently connected and have the potential to

induce both benefits and penalties for either depending on the particular species targeted (Arneth et al., 2009; Ramanathan and Feng, 2009; Fiore et al., 2012).

Here we use a global coupled chemistry–climate model to improve our understanding of changes in aerosols over Europe from 1960 to 2009. The climate impact of aerosols over this period, in response to emission changes, was calculated as an aerosol radiative forcing. An assessment of the confidence in this effect was obtained from the ability of the model to reproduce observed long-term changes in a number of aerosol properties including mass concentrations and aerosol optical depth (AOD).

Anthropogenic emissions of aerosol particles and their precursors have increased significantly since pre-industrial times. For example, global SO<sub>2</sub> emissions have increased by a factor of 60 from the pre-industrial to a peak in the 1970s (Lamarque et al., 2010; Granier et al., 2011; Smith et al., 2011). However, from the 1980s onwards, regional reductions in anthropogenic emissions (mainly North America and Europe) have occurred due to air quality mitigation strategies, which has led to a decline in European SO<sub>2</sub> emissions of 73 % between 1980 and 2004 (Vestreng et al., 2007; Hand et al., 2012). Anthropogenic emissions of oxides of nitrogen (NO<sub>x</sub>), carbon monoxide (CO) and black carbon (BC) have also decreased over Europe between 1980 and 2010 by 30, 58 and 55 % respectively (Granier et al., 2011). Conversely, anthropogenic emissions from eastern Asia have increased due to population growth and economic development, leading to an increase in SO<sub>2</sub> emissions of a factor of 7 from the 1960s to the present day (Smith et al., 2011).

Changes in anthropogenic emissions and aerosol concentrations affect Earth's climate (Arneth et al., 2009; Ramanathan and Feng, 2009; Fiore et al., 2012). The effect of past and future changes in emissions on aerosols and their associated climate impacts is uncertain (Penner et al., 2010; Chalmers et al., 2012). In addition, emission inventories of aerosols and their precursor species account for large uncertainty in models (de Meij et al., 2006). It is therefore important to understand and evaluate the changes to aerosol processes and properties that have occurred over recent decades where we have aerosol measurements.

Ground-based monitoring networks providing observations of aerosol concentrations and physiochemical properties were established following air pollution control legislation. The longest continuous measurements of aerosols are available in North America and Europe from the 1970s to present day. In Europe, observations of aerosol mass concentrations (both sulfate and total) are available from the European Monitoring and Evaluation Programme (EMEP) network (Tørseth et al., 2012) and similar data for North America are available from the Integrated Monitoring of Protected Visual Environments (IMPROVE) network (<http://vista.cira.colostate.edu/improve/>). In addition, AOD has been monitored in Europe over the last decade by the ground-based Aerosol Robotic Network (AERONET) (Holben et al.,

1998). There are limitations in the spatial and temporal extent of the data from these networks, as well as in the consistency of the instrumental techniques used and components measured throughout the monitoring period. However, they do provide a useful source of multidecadal aerosol data with which to evaluate model predictions.

Several studies have analysed long-term trends in observed aerosols. Tørseth et al. (2012) used observations from the EMEP network to show a decline in sulfate aerosol mass from the 1970s to present day and a decline in PM<sub>10</sub> (mass of particles with diameter < 10 μm) from 2000 to 2009. Asmi et al. (2013) and Barmapadimos et al. (2012) reported a reduction in the aerosol number and mass concentration over the last 10–15 years across Europe. However, Collaud Coen et al. (2013) found no significant changes in aerosol optical properties over Europe for a similar period. Similarly, Harrison et al. (2008) analysed changes in aerosol mass concentrations over the UK and reported relatively stable concentrations over 2000–2010, even when emission reductions are anticipated to have occurred.

Evaluating the ability of chemistry–climate models to reproduce observed trends is necessary in order to reliably predict the climate effects of aerosols over this period. Many studies qualitatively match the direction of observed trends in aerosol but underestimate both absolute concentrations and the magnitude of observed trends (Berglen et al., 2007; Colette et al., 2011; Koch et al., 2011; Chin et al., 2014). Leibensperger et al. (2012) used the chemical transport model (CTM) GEOS-Chem to evaluate aerosol trends over the USA at decadal time slices and found that sulfate but not BC was represented well by the model. A multimodel assessment of aerosol trends in Europe over the last decade showed models successfully simulate observed negative trends in PM<sub>10</sub> but fail to reproduce the positive trends observed at some locations and typically underestimate absolute concentrations (Colette et al., 2011). Observed reductions in sulfate over Europe have also been underestimated by other studies (Berglen et al., 2007; Koch et al., 2011). Over Europe, Skeie et al. (2011) reproduced the observed change in decadal average sulfate concentrations but overestimated nitrate aerosol concentrations.

Several studies (Lamarque et al., 2010; Shindell et al., 2013) have also assessed long-term changes in AOD. Lamarque et al. (2010) evaluated simulations of present day AOD against AERONET observations and reported a relatively good reproduction of interannual variability, except in regions of high AOD. Shindell et al. (2013) assessed AOD from the models involved in the Atmospheric Chemistry and Climate Model Intercomparison Project (ACCMIP) and showed that most captured the observed trends between 1980 and 2010 relatively well, although many were underpredicted in the present day, particularly over eastern Asia.

Changes in surface solar radiation (SSR) do not provide a direct measurement of aerosols but they can be used to infer their influence on the surface radiation balance. The Global

Energy Balance Archive (GEBA) provides long-term observations of SSR from the 1950s until present day over a large part of Europe (Sanchez-Lorenzo et al., 2013). These measurements can also be used as a general measure to validate radiation balance predictions from global climate models against the observed surface variations. Such observations have shown that the European “dimming” period of the 1980s and the subsequent “brightening” period of the 1990s–2000s can be attributed partly to changes in clouds, concentrations of aerosols and aerosol–cloud effects (Wild, 2009). Model simulations have been evaluated against SSR observations and demonstrated issues in simulating the timing and magnitude of observed SSR trends. In an assessment of the models contributing to the 5th Coupled Model Intercomparison Project (CMIP5), Allen et al. (2013) showed that the dimming trend over Europe was underestimated in all models, potentially due to an under-represented aerosol direct effect. However, the CMIP5 models were able to reproduce the observed brightening trend. Folini and Wild (2011) performed transient simulations with ECHAM5-HAM over Europe (with interactive aerosols) and found that simulated reductions in SSR occurred too early in the model, whereas the increase in SSR was correctly timed. Using a regional climate model over Europe driven by reanalysis data, Chiacchio et al. (2015) overestimated SSR, simulated a premature onset of dimming and demonstrated that only simulations including aerosols were able to reproduce the observed brightening trend. In addition, Koch et al. (2011) simulated the correct interdecadal variability in SSR but underestimated the magnitude of observed SSR.

These previous studies have either simplified their treatment of aerosols or the model was evaluated against a limited range of aerosol properties over a relatively coarse spatial and temporal scale. The importance of studies at regional spatial scales was also highlighted as changes in aerosols at this level can potentially be masked by compensatory changes observed on the global scale. Here we simulate monthly-mean aerosol concentrations from 1960 to 2009 using the HadGEM3-UKCA (Hadley Centre Global Environment Model-United Kingdom Chemistry and Aerosols) global chemistry–climate model, which includes aerosol microphysics (aerosol number and mass size distributions). We evaluate the ability of the model to consistently capture observed changes in bulk in situ aerosol properties (PM, aerosol size distributions and chemical components) as well as radiative properties (AOD, SSR) over Europe. We also calculate the regional top of atmosphere radiative perturbations due to simulated changes in aerosols. This has enabled a detailed regional analysis and evaluation of the changing radiative impact of aerosols due to variations in emissions.

Section 2 describes the HadGEM3-UKCA model, the simulations performed and the long-term observations used. Section 3 discusses and evaluates the simulated changes to European aerosols and surface solar radiation. Section 4 presents

aerosol radiative forcing over Europe. Conclusions are presented in Sect. 5.

## 2 Methods

### 2.1 Model description and simulations

#### 2.1.1 General

We used the coupled chemistry–climate model HadGEM3-UKCA to study the interaction between chemistry, aerosols and the impacts on the radiation balance of the climate system. HadGEM3-UKCA is part of the third generation of the Met Office’s Hadley Centre Global Environment Model (HadGEM) family, which incorporates an online treatment of chemistry and aerosols through the United Kingdom Chemistry and Aerosols (UKCA) programme. The Met Office Unified Model (UM) acts as the dynamical core and provides the components for atmospheric transport and tracer mixing. This is based on the dynamics implemented by Davies et al. (2005) and includes processes such as large-scale advection, convective uplift and boundary layer mixing. A description of the atmosphere-only version of HadGEM3 is provided in Hewitt et al. (2011). Morgenstern et al. (2009) and O’Connor et al. (2014) describe the incorporation and evaluation of UKCA into HadGEM.

HadGEM3-UKCA is used here in atmosphere-only mode. We output monthly 3-D aerosol and radiation fields for the years 1960–2009 at a resolution of  $1.875^\circ \times 1.25^\circ$  (approximately 140 km at mid latitudes) with 63 vertical levels up to 40 km. The 3-D meteorological fields were nudged at 6 h intervals to the European Centre for Medium-Range Weather Forecasts (ECMWF) Reanalysis (ERA-40) (Uppala et al., 2005) for the years 1960–2000 and ERA-Interim (Dee et al., 2011) for 2000–2009. Sea surface temperatures and sea ice fields were prescribed in accordance with those used in CMIP5 (Hurrell et al., 2008). Coupling between the land surface and atmosphere was simulated using the Met Office Surface Exchange Scheme (MOSES; Essery et al., 2002). By nudging to reanalysis data, we ensure that the model produces a realistic representation of the meteorological conditions under which aerosol observations were taken.

Tropospheric ozone,  $\text{HO}_X$ ,  $\text{NO}_X$  and VOC (volatile organic compounds) chemistry was calculated using the mechanism described by O’Connor et al. (2014), which includes reactions of odd oxygen ( $\text{O}_X$ ), nitrogen ( $\text{NO}_Y$ ), hydrogen ( $\text{HO}_X = \text{OH} + \text{HO}_2$ ) and CO, as well as methane and other short chain non-methane VOCs. The scheme has been extended to include additional sulfur (Mann et al., 2010), monoterpene (Spracklen et al., 2006) and isoprene (Scott et al., 2014) chemistry.

The Fast-J photolysis scheme is implemented within UKCA to calculate online photolysis rates based on the distribution of clouds, ozone and aerosols (Wild et al., 2000).

Dry and wet deposition of gas-phase species is described in O'Connor et al. (2014).

HadGEM3-UKCA uses the modal aerosol scheme of the Global Model of Aerosol Processes (GLOMAP mode) (Mann et al., 2010). GLOMAP mode uses log-normal modes to represent the aerosol size distribution and simulates the evolution of the size-resolved number and mass of aerosol particles with different compositions. GLOMAP simulates the interaction of various aerosol processes including size-resolved primary emissions, cloud processing, new particle formation, hygroscopic growth, coagulation, condensation, deposition and scavenging. Log-normal modes are used to represent aerosols in the nucleation (diameter ( $D$ ) < 10 nm), Aitken ( $D$  10–100 nm), accumulation ( $D$  100 nm–1  $\mu$ m) and coarse ( $D$  > 1  $\mu$ m) modes. In this study the model is set up to simulate sulfate, BC, organic carbon (OC) and sea salt aerosol in five different modes (four soluble and one insoluble Aitken modes). Secondary organic aerosol (SOA) is formed from products of monoterpene oxidation, which are generated at 13 % yield and assumed to be involatile (Spracklen et al., 2006). There is no representation of ammonium nitrate in this version of the model. Mineral dust is simulated using a separate six-bin scheme developed by Woodward (2001) and covers particle sizes from 0.03 to 30  $\mu$ m in radius.

### 2.1.2 Aerosol radiative effects

The Edwards–Slingo radiation code (Edwards and Slingo, 1996) calculates changes in Earth's radiation balance from chemical and aerosol species. ARI (aerosol direct effects) are calculated according to Bellouin et al. (2013) from waveband-averaged scattering and absorption coefficients obtained from modelled size distributions and a volume-weighted average of component refractive indices within each mode. GLOMAP-mode provides the aerosol fields for the calculation of ACI online within the model, in accordance with that described in Bellouin et al. (2013). Simulated cloud condensation nuclei (CCN) concentrations are used to calculate cloud droplet number (CDN) concentrations based on the empirical relationship derived by Jones et al. (2001). The cloud albedo effect is calculated using simulated CDN. The coupling of UKCA to the precipitation scheme potentially allows for the effect of aerosols on cloud lifetime (rapid adjustments for ACI) to be diagnosed. This can be done by calculating the influence they have on CDN concentrations, cloud effective radius and ultimately the auto-conversion of cloud drops to precipitation, as described in Jones et al. (2001). However, in this study, because we nudge to reanalysis fields, the changes in the radiative balance due to aerosols are not allowed to feedback on to the meteorology.

The radiation scheme was called twice for each time step (every 30 m) in a double-call radiation configuration (Bellouin et al., 2013). The first call uses the modelled aerosol fields and the second call uses an aerosol-free atmosphere

for the clear-sky radiative calculation and a prescribed default CDN field (based on an aerosol climatology) for the cloud radiation calculation. This approach therefore eliminates the model's radiatively-driven response to changes in aerosols, enabling the radiative forcing from ARI and ACI to be calculated with no rapid adjustments to clouds permitted from either effect. Here we calculate an aerosol radiative forcing (only from the direct and first indirect effects) as the difference between monthly values in each year of the simulation and the monthly mean aerosol radiative state in the period 1980–2000. An estimate of the cloud albedo effect (first aerosol indirect) can be obtained by subtracting the radiative effect obtained under all-sky conditions from those under clear skies.

### 2.1.3 Aerosol emissions

Sea salt emissions are calculated using the surface wind speed and the parameterisation of Gong (2003). Emissions from tropospheric volcanoes (both continuous and explosively erupting) are included from Andres and Kasgnoc (1998) and Halmer et al. (2002) using the AEROCOM recommendations. Dimethyl sulfide (DMS) emissions are calculated from monthly seawater concentration fields (Kettle and Andreae, 2000) and a wind speed dependent air–sea exchange parameterisation (Liss and Merlivat, 1986). Wildfire (biomass burning) emissions are from the MACC-city (MACC/CityZEN EU projects) inventory (Granier et al., 2011) for 1980–2009 and from the RETRO inventory from 1960 to 1980 (Schultz et al., 2008). Monoterpene emissions from vegetation are prescribed as monthly mean fields from Guenther et al. (1995). Dust emissions from the surface are calculated online using a six-bin scheme (Woodward, 2001) and depend on the particle size distribution of the soil, surface soil type (represented by a bare soil fraction), soil moisture and wind speed. Dust is emitted when the wind speed exceeds a threshold value and if the soil moisture is below a certain level.

Monthly mean anthropogenic emissions of CO, SO<sub>2</sub>, NO<sub>x</sub>, OC and BC from 1960 to 2009 are taken from the MACC-city inventory (Granier et al., 2011). Emissions are provided at a 0.5° by 0.5° resolution and are based on those from ACCMIP and the IPCC Reference Concentration Pathway (RCP) scenario 8.5 for energy, transportation, industry, shipping, agriculture, residential and waste sectors.

Figure 1 shows the European and regional domains used throughout this study. Figure 2 shows the emissions of SO<sub>2</sub>, OC, BC, NH<sub>3</sub> and NO<sub>x</sub> across Europe from the MACC-city inventory between 1960 and 2009. Anthropogenic emissions of SO<sub>2</sub> over the European domain have increased from 33 Tg yr<sup>-1</sup> in 1960 to a peak of 46 Tg yr<sup>-1</sup> in 1980 before decreasing at a relatively constant rate to 11 Tg yr<sup>-1</sup> in 2009 (Fig. 2a). Between 1980 and 2009, European anthropogenic SO<sub>2</sub> emissions in this data set declined by 70 %, in agreement with previous assessments (Vestreng et al., 2007; Tørseth

et al., 2012). The emissions of  $\text{NO}_x$  have decreased by 20 % and followed a similar temporal trend to  $\text{SO}_2$ . A continuous decline in BC and OC emissions occurred from the 1960s to present day, due to reductions in the residential sector, partially offset by recent increases from the transportation sector. The emissions of  $\text{NH}_3$  across Europe (not used as part of the aerosol scheme in this study due to the absence of ammonium nitrate) increased continuously over the period 1960–2009, driven largely by the agriculture sector.

Figure 2b–f show the annual emissions of each species from the MACCity inventory across the individual European regions. Emissions of OC (Fig. 2f) and  $\text{SO}_2$  (Fig. 2b) have decreased across all the different European regions. Emissions of  $\text{NO}_x$  and BC (Fig. 2c, e) increase until the 1980s–1990s before declining across all regions, except in southern Europe. Anthropogenic emissions from northern and central Europe have declined from the 1980s onwards, whereas emissions from southern Europe have either increased or remained unchanged.

## 2.2 Observations

Ground-based measurements of aerosols used in this study are listed in Table 1 and include aerosol mass concentrations (sulfate and total mass) from the EMEP network (<http://www.emep.int>), AOD from AERONET (<http://aeronet.gsfc.nasa.gov/>), aerosol size distributions from EUSAAR (European Supersites for Atmospheric Aerosol Research) and GUAN (German Ultrafine Aerosol Network) (Asmi et al., 2011) and SSR from the GEBA database (<http://www.geba.ethz.ch/history/index>). All data used in this study are presented as either monthly or annual averages. Figure 1 shows the location of all the measurement sites along with the five regions of Europe. Figure 3 shows the temporal evolution in the number of measurement sites used in this analysis for each observation. We note that the number of locations reporting sulfate and SSR has declined since 2000.

### 2.2.1 EMEP observations

The EMEP network has reported the concentrations of sulfate and total aerosol mass at locations across Europe from 1978 until present day (Tørseth et al., 2012). Measurements of total suspended particle matter (SPM) are an early measure of particulate matter and available from 1978 to 2005, with most measurements from Germany, Switzerland and Spain. However, only measurements up to and including 1998 are used due to the reduced availability of data in the period 1999–2005 (Fig. 3). The SPM measurements cover all particle sizes and may be influenced by local sources of very large particles (diameter  $> 10 \mu\text{m}$ ). Measurements of  $\text{PM}_{10}$  are available from EMEP from 1996 until present day. Sulfate aerosol mass measurements are available from 1978 until present day.

We used sulfate aerosol mass,  $\text{PM}_{10}$  and total SPM from the sites that have been continuously operating for more than 5 years (Fig. 1a). The measurements were made using different measurement techniques and time frequencies (hourly and daily). The raw data were screened to remove any anomalous data points according to the flag in the original data records. Monthly and annual mean values were then calculated from the screened data for sites that had more than 75 % of measurements in the averaging period.

### 2.2.2 Aerosol size distribution

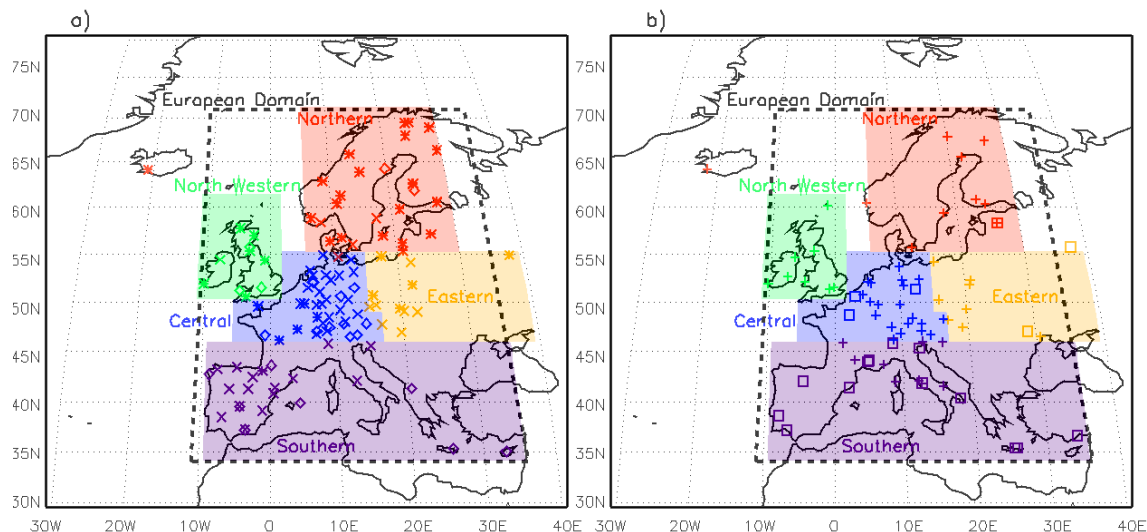
Aerosol size distribution data over Europe from the EUSAAR and GUAN ground-based monitoring sites have previously been collected and processed by Asmi et al. (2011) over the period 2008–2009. Here we use the same 17 low altitude sites as in the multimodel comparison by Mann et al. (2014) to compare modelled and observed aerosol number concentrations at three different size fractions ( $> 30 \text{ nm}$  (N30),  $> 50 \text{ nm}$  (N50) and  $> 100 \text{ nm}$  (N100) dry diameter) over the period 2008–2009.

### 2.2.3 AOD

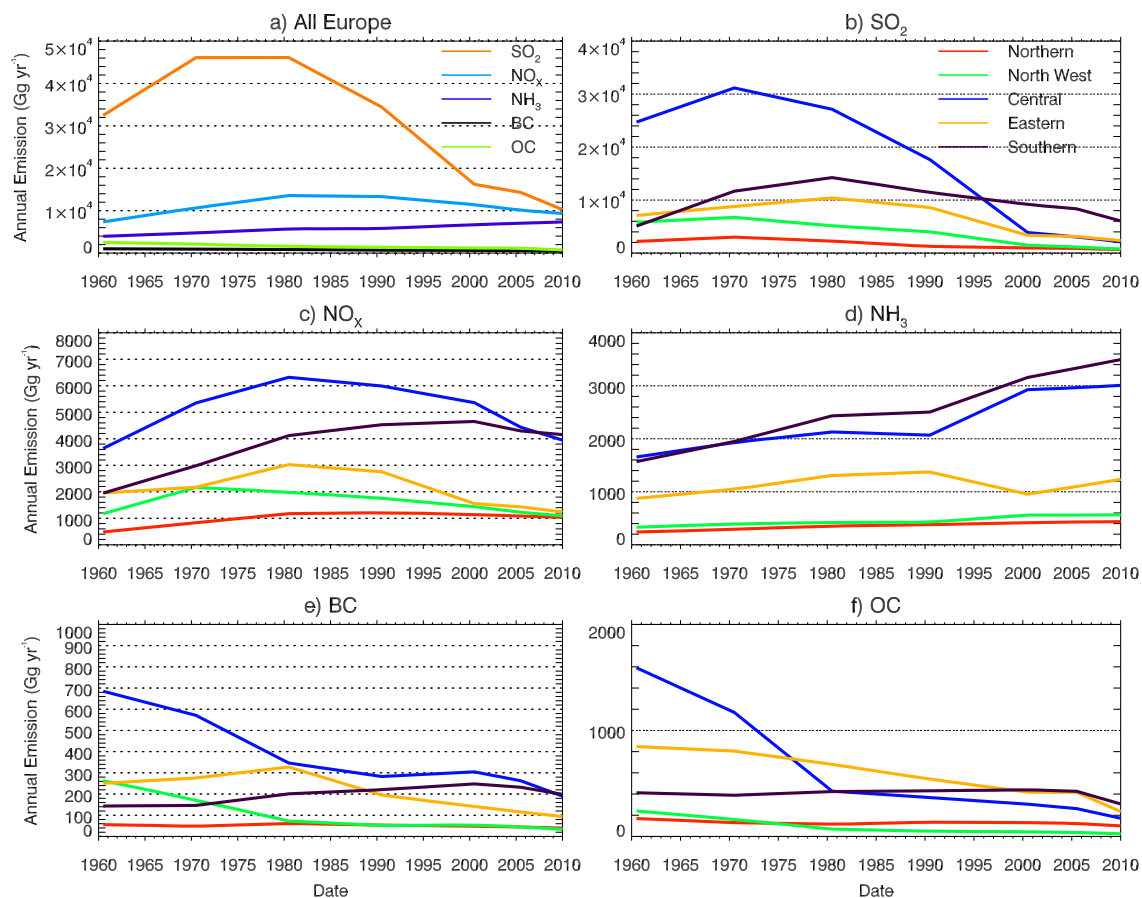
The AERONET program is a ground-based network of sun photometers, currently with more than 200 sites providing aerosol optical, microphysical and radiative properties (Holben et al., 1998). Observed AOD values are available over Europe from the mid-1990s but most sites only started operating within the last 10 years (Fig. 3) and there are relatively few consistent long-term data sets available before 2000. We used the Level 2.0 data product (cloud-screened and quality assured) from 20 sites that have been operating for longer than 5 years over Europe between 2000 and 2009. AOD measurements have the best record for wavelengths of 440, 500 and 675 nm. We used the 440 nm wavelength as it has the best spatial and temporal coverage.

### 2.2.4 Surface solar radiation

GEBA contains worldwide measurements of energy fluxes at the surface from more than 2000 sites, with the highest density over Europe. Monthly mean values of incident SSR (expressed as mean irradiance, in  $\text{W m}^{-2}$ ) have been obtained from 56 sites across Europe starting before the 1970s, provided by Sanchez-Lorenzo et al. (2013), and include more than 20 sites that have data in the 1960s. The length of this observational record enabled the model evaluation to be extended prior to the availability of sulfate data. These measurements therefore enable an indirect evaluation of aerosol changes in the model across the entire time period of the simulations and also the validation of how changes in aerosols can affect Earth's radiation balance.



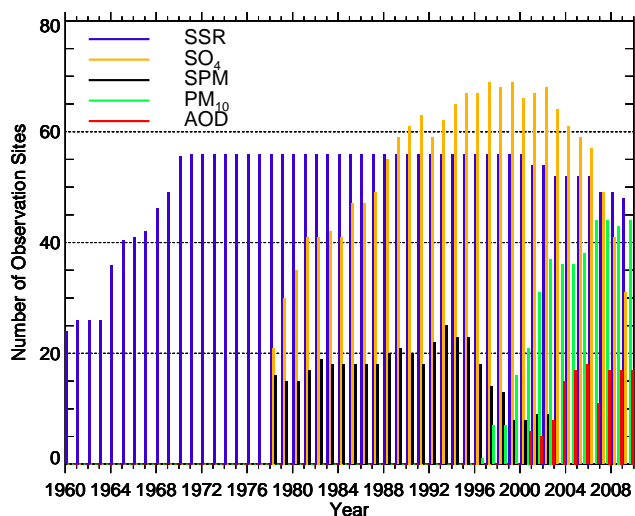
**Figure 1.** Location of measurements used in this study for (a) sulfate aerosol mass (\*), total aerosol mass (◇) and sites that have measured both (\*), (b) AOD (□) and surface solar radiation (+). Regional European definitions are north-western Europe (green), northern Europe (red), central Europe (blue), eastern Europe (orange) and southern Europe (purple).



**Figure 2.** Annual European emissions ( $\text{Gg yr}^{-1}$ ) of aerosols and aerosol precursors from the MACCity inventory over the period 1960–2009. (a) Total European emissions of sulfur dioxide ( $\text{SO}_2$ , orange), organic carbon (OC, light green), black carbon (BC, black), ammonia ( $\text{NH}_3$ , light purple) and oxides of nitrogen ( $\text{NO}_x$ , blue). (b)–(f) show European regional emissions for (b)  $\text{SO}_2$ , (c)  $\text{NO}_x$ , (d)  $\text{NH}_3$ , (e) BC and (f) OC. Regions are as defined in Fig. 1: northern (red), north-western (green), central (blue), eastern (orange), southern (purple).

**Table 1.** Details of the ground-based observations used in this study.

Data source	Measurements	Period	Total number of sites available
EMEP	total sulfate aerosol mass concentrations	1978–2009	97
EMEP	total suspended particle mass concentrations	1978–2005	42
EMEP	PM <sub>10</sub> mass concentrations	1996–2009	52
EUSAAR and GUAN	aerosol number concentrations greater than 30 nm (N30), 50 nm (N50) and 100 nm (N100) in dry diameter	2008–2009	24
AERONET	aerosol optical depth (AOD)	1994–2009	21
GEBA	surface solar radiation (SSR)	1928–2009	50

**Figure 3.** Temporal variation in the number of locations measuring surface solar radiation (SSR), sulfate aerosol mass (SO<sub>4</sub>), total suspended particle mass (SPM), PM<sub>10</sub> mass and aerosol optical depth (AOD).

### 2.3 Model evaluation metrics

Comparisons were made using monthly and annual mean values at individual monitoring locations and also across Europe as a whole. Model values were linearly interpolated to each measurement site using the relative contribution from the four closest surrounding model grid squares. The absolute and percentage change in the simulated and observed values of sulfate, SPM, PM<sub>10</sub>, AOD and SSR were calculated as the difference between the mean of the initial 5 years and the most recent 5 years of data.

The temporal trend in simulated and observed data was calculated by fitting an ordinary least squares linear model to the data using the function

$$Y_i = a + bX_i (i = 1, \dots, n). \quad (1)$$

The standard error (SE) of the trend line was used to provide an assessment of the error. For each simulated and observed trend,  $\pm$  two SE in the gradient was applied to provide an

uncertainty range. Firstly, the standard deviation of the residuals ( $\sigma$ ) was determined and then used to calculate the SE.

The simulated temporal trends were evaluated by comparing against observed trends; if the gradient of the simulated and observed trends are within  $\pm$  two SE of each other we considered them to be similar.

An assessment of model accuracy is provided here by calculating the normalised mean bias factor (NMBF) of the model when compared to the observations (Yu et al., 2006). This metric is symmetric (i.e. not biased towards underprediction or overprediction) and is not biased when a low number of observed values are used. It is defined as

$$\text{NMBF} = S [\exp(|\ln(\bar{M}/\bar{O})|) - 1], \quad (2)$$

where

$$S = (\bar{M} - \bar{O}) / |\bar{M} - \bar{O}|. \quad (3)$$

where  $M$  represents the model values and  $O$  represents the observed values. The sign of the NMBF indicates whether the model underestimates (negative) or overestimates (positive) the observed values. For a negative NMBF, the model values are a factor of  $1 - \text{NMBF}$  below the observed values and for a positive NMBF the model values are a factor of  $1 + \text{NMBF}$  above the observations (Yu et al., 2006). That is, NMBF =  $-0.5$  means the model is a factor 1.5 low biased and NMBF =  $0.5$  means the model is a factor 1.5 high biased.

The goodness of fit between the model and observations is obtained by calculating the square of the linear Pearson correlation coefficient. A measure of the difference between model and observational values is provided by calculating the root mean square error (RMSE).

## 3 Results

### 3.1 Simulated european aerosols and surface solar radiation from 1960 to 2009

Figure 4a shows the simulated European (land only) mass concentrations of the different aerosol components over the

period 1960–2009. Simulated  $\text{PM}_{10}$  declines from the early 1980s until 2009, coinciding with the reduction in anthropogenic emissions (Fig. 2). Continually decreasing mass concentrations of BC and OC are simulated between 1960 and 2009. Simulated sulfate mass concentrations increase from 1960 to a peak around 1980 and decrease thereafter.

Figure 4b shows the change in simulated European surface aerosol number concentrations over the total, N30, N50 and N100 size fractions between 1960 and 2009. Aerosol number concentrations across all size fractions increase from 1960 to a peak in 1970 before declining to concentrations that are 50 % lower in 2009.

Simulated European AOD (Fig. 4c) increases from 1960 to a peak in 1973 before decreasing till 2009 to an AOD that is lower than that simulated 1960. Figure 4d shows that simulated European SSR decreases from 1960 to 1980 (dimming) and then increases until 2009 (brightening).

## 3.2 Model evaluation

### 3.2.1 Sulfate aerosol mass

Figure 5a–d compare simulated single year annual mean sulfate concentrations over Europe for 1980, 1990, 2000 and 2009 against observations. Observed and simulated annual mean European sulfate aerosol concentrations declined by 68 and 78 % respectively over the period 1978–2009 (Table 2). In 1980 (Fig. 5a) simulated and observed sulfate concentrations were largest in central Europe. In 2000 and 2009 (Fig. 5c, d) both simulated and observed sulfate concentrations in central Europe declined substantially, with the largest simulated concentrations over south-eastern Europe.

The model underestimates European annual mean sulfate aerosol mass concentrations in the period 1978–2009 (NMBF =  $-0.384$ , Table 2), with summertime concentrations overestimated (NMBF =  $0.694$ ) and wintertime concentrations underestimated (NMBF =  $-2.19$ ). Figure 6 shows the range of model bias in seasonal sulfate across European regions for the period 1978–2009. In summer, observed sulfate is underestimated by the model at the start of the period before coming into closer agreement towards the end of the period (Figs. 5e, 6). The model underestimates observed summertime sulfate across northern and southern Europe (NMBF between 0 and  $-1$ ), and overestimates sulfate in central and eastern Europe (NMBF  $< 1$ ). The model consistently underestimates wintertime sulfate (NMBF of  $-1$  to  $-6$ ) across all the European regions, with the largest discrepancy occurring in northern Europe.

An underprediction of wintertime European sulfate concentrations has been previously reported and may be due to an underestimation of oxidants in the model (Berglen et al., 2007; Manktelow et al., 2007; Langmann et al., 2008). In wintertime over northern Europe, the region with largest model bias, low concentrations of  $\text{H}_2\text{O}_2$  limit in-cloud aqueous-phase oxidation of  $\text{SO}_2$ . Under these condi-

tions, oxidation by ozone is the dominant sulfate formation mechanism (Kreidenweis, 2003). We hypothesise that oxidation by ozone could be under-represented in the model, resulting in an underestimation of wintertime sulfate. This will be explored further in a future publication. Model underestimation could also be due to an artificially high wet deposition rate of sulfate, caused by an enhanced occurrence of drizzle precipitation within this version of the model (Walters et al., 2011).

Although the model underestimates absolute sulfate concentrations, the simulated trend over the period 1978–2009 ( $-0.04 \pm 0.002 \mu\text{g S m}^{-3} \text{yr}^{-1}$ ) is in good agreement with the observed trend ( $-0.05 \pm 0.002 \mu\text{g S m}^{-3} \text{yr}^{-1}$ ), at least on a European-wide annual mean basis (Fig. 5e). These trends can be considered similar as they are within two standard errors of each other. The largest decline in both simulated and observed sulfate concentrations occurred during 1980–2000, when average concentrations changed by  $-0.05 \mu\text{g S m}^{-3} \text{yr}^{-1}$ . Between 1980 and 2000, average simulated and observed concentrations declined by 50–60 %, corresponding to a 60–70 % decrease in anthropogenic emissions of  $\text{SO}_2$  (Fig. 2). A smaller reduction in sulfate aerosol mass of 13–18 % was simulated and observed in the period 2000–2009, when average concentrations changed by  $-0.015 \mu\text{g S m}^{-3} \text{yr}^{-1}$ . Figure 7 compares the simulated and observed linear trends in sulfate concentrations at all measurement locations. The model reproduces the observed linear trends in the annual mean concentrations. However, linear trends in wintertime sulfate aerosol mass are underestimated (by a factor of 3) but overestimated in summertime (by a factor of 1.3). This corresponds with the calculated NMBFs for winter and summertime mass concentrations, which showed an under- and overprediction respectively.

### 3.2.2 Total aerosol mass

Figure 8a and b compare simulated and observed annual mean total SPM concentrations over Europe in 1980 and 1990. The spatial changes in SPM over this period are less distinct than for sulfate. Simulated and observed SPM decreases over central Europe and increases over eastern Europe between 1980 and 1990. In contrast to sulfate aerosol mass, the simulated 20 % decrease in SPM mass concentrations in the period 1978–1998 is considerably lower than the 50 % observed decrease.

The model underpredicts the observed European annual mean SPM mass concentrations, with a NMBF of  $-0.88$  in the period 1978–1998 (Table 3). A consistent underprediction of observed SPM concentrations was modelled across all European regions in both summer and winter (Fig. 9a). The model substantially underpredicts SPM concentrations in wintertime for southern and eastern Europe (NMBF of  $-8$  to  $-0.5$ ). In summertime and across all European regions the model underpredicts observations by a smaller amount (NMBF of 0 to  $-2$ ). The large underprediction of

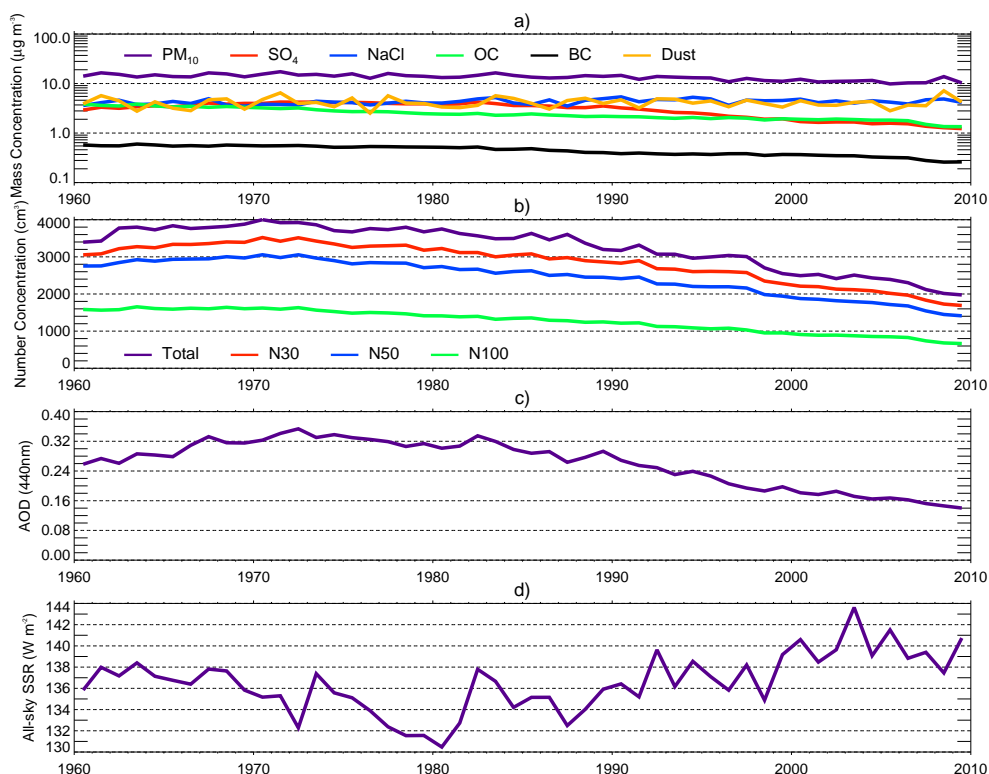


**Figure 4.** Simulated European annual mean (a)  $\text{PM}_{10}$  and composition-resolved surface mass concentration; (b) aerosol number concentration for particles with dry diameter  $> 3$  (total),  $> 30$  (N30),  $> 50$  (N50) and  $> 100$  nm (N100); (c) AOD at 440 nm; and (d) SSR between 1960 and 2009. Mean values are calculated over the European land domain shown in Fig. 1.

**Table 2.** Statistical summary of modelled and observed annual and seasonal (DJF and JJA) mean sulfate at all long-term ( $> 20$  years data) measurement sites (34 sites) between 1978 and 2009. Absolute and relative (%) changes in concentrations are calculated as the difference between the mean of the initial 5 years of data minus the mean of the last 5 years of data. Trends that are above or below the value of twice of the standard error of the trend (95 % confidence) are highlighted in bold.

Component	Type	Absolute change in concentration ( $\mu\text{g S m}^{-3}$ )	Standard deviation of mean value	% Change in concentration	Calculated linear trend ( $\mu\text{g S m}^{-3} \text{ yr}^{-1}$ )	$-2^* \text{ SE of trend}$	$+2^* \text{ SE of trend}$	$r^2$	NMBF	RMSE
Sulfate annual	observed	-1.23	0.466	-68 %	-0.048	-0.053	-0.043	0.434	-0.384	0.334
	model	-1.15	0.424	-78 %	-0.044	-0.048	-0.040			
Sulfate DJF	observed	-1.67	0.65	-73 %	<b>-0.064</b>	-0.073	-0.055	0.385	-2.19	0.978
	model	-0.53	0.20	-75 %	<b>-0.020</b>	-0.023	-0.017			
Sulfate JJA	observed	-1.39	0.57	-70 %	<b>-0.056</b>	-0.064	-0.048	0.434	0.694	1.17
	model	-3.35	1.34	-86 %	<b>-0.138</b>	-0.152	-0.124			

observed SPM mass concentrations could indicate that an additional emission source or process for generating supermicron aerosol mass is missing from the model, particularly in the 1980s and early 1990s when the model bias is largest.

Figure 8c shows that the larger observed trend in European annual mean SPM mass over the period 1978–1998 of  $-1.19 \pm 0.22 \mu\text{g m}^{-3} \text{ yr}^{-1}$  is substantially different to the simulated trend of  $-0.26 \pm 0.12 \mu\text{g m}^{-3} \text{ yr}^{-1}$  (Table 3). Figure 10a shows that the observed trends in SPM mass concentrations are underpredicted at all the measurement locations,

with little seasonal differences. The calculated trends in simulated and observed SPM values are considered to be different as they are outside the range of  $\pm$  two standard errors of each trend line (Table 3).

Figure 8d and e compare simulated and observed annual mean  $\text{PM}_{10}$  mass concentrations over Europe in 2000 and 2009. A slight reduction in  $\text{PM}_{10}$  mass concentrations of 8–9 % was both observed and simulated over this period (Table 3), with the largest reductions occurring over central and north-eastern continental Europe.

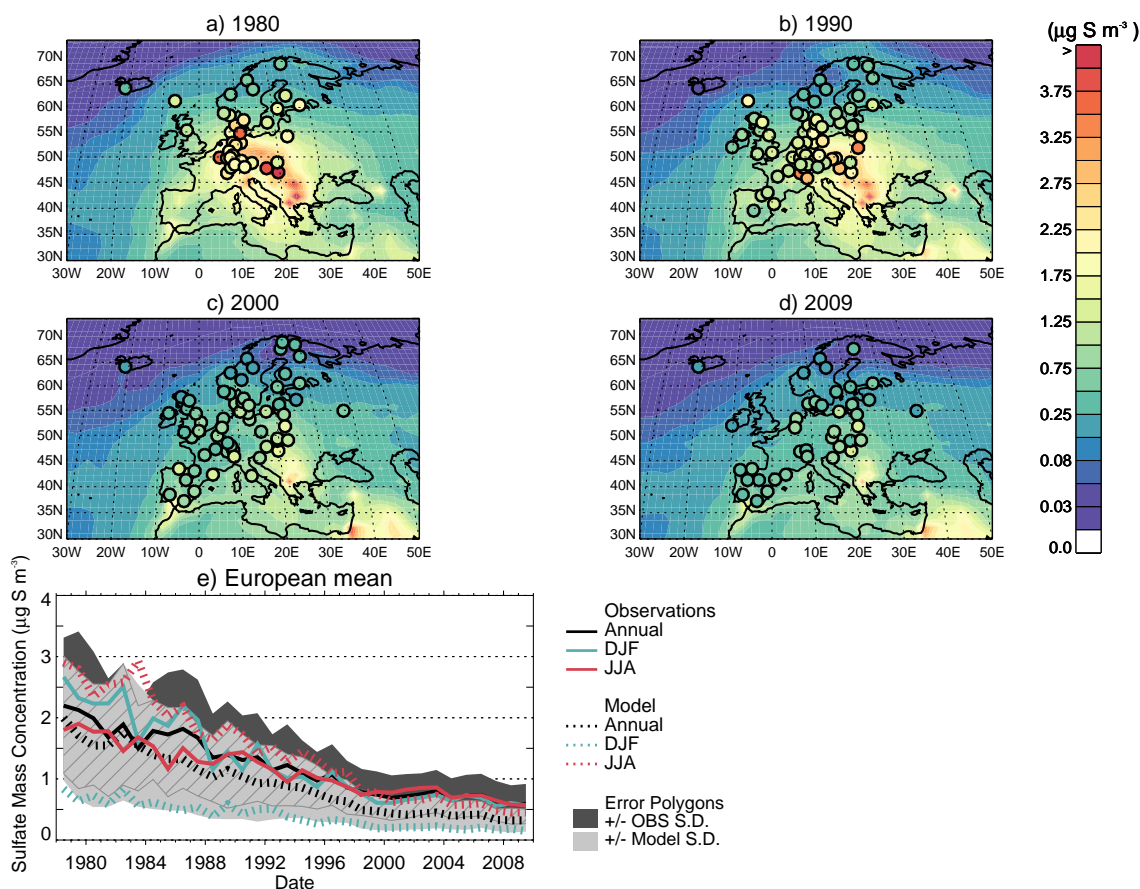


**Figure 5.** Annual mean sulfate aerosol mass concentrations ( $\mu\text{g S m}^{-3}$ ) from the lowest model level with observations overplotted in circles for (a) 1980, (b) 1990, (c) 2000 and (d) 2009. (e) Time series of annual and seasonal mean observed (solid lines) and modelled (dashed lines) sulfate concentrations averaged across all measurement locations for each particular year. Shaded areas show  $\pm 1$  standard deviation of the modelled (light grey) and observed (dark grey) annual mean values, with the hatching identifying areas of overlap.

The model generally underestimates observed  $\text{PM}_{10}$  mass concentrations (NMBF of 0 to  $-1$ ) for the majority of European regions and across most of the evaluated years (Fig. 9b). An exception occurs across northern and north-western Europe in wintertime where the model overpredicts concentrations (NMBF of 0–2). This is potentially caused by an overestimation of sea salt aerosol (as also seen in studies by Mann et al., 2010, 2012), so it mostly affects coastal locations. Overall, the model simulates European  $\text{PM}_{10}$  mass concentrations between 1997 and 2009 within a factor of 2 and is much improved when compared to the simulation of total SPM between 1978 and 1998.

The temporal changes in  $\text{PM}_{10}$  mass concentrations (Fig. 8f) highlight the smaller difference between simulated and observed  $\text{PM}_{10}$  across Europe compared to SPM. The linear trends for observed ( $-0.27 \pm 0.24 \mu\text{g m}^{-3} \text{ yr}^{-1}$ ) and simulated ( $-0.14 \pm 0.16 \mu\text{g m}^{-3} \text{ yr}^{-1}$ )  $\text{PM}_{10}$  mass concentrations over the period 1997–2009 are similar (gradients within twice the standard error of each other) (Table 3). However, Fig. 10b shows that the magnitude of the observed

downward trends is slightly underpredicted at the majority of measurement locations, with little difference between summer and winter.

The model underpredicts SPM mass concentrations by up to  $20 \mu\text{g m}^{-3}$  in the 1980s and  $\text{PM}_{10}$  by less than  $5 \mu\text{g m}^{-3}$  in the 2000s. This larger underprediction in the 1990s could be due to errors in the measurement of SPM, as most of these observations are not well documented (Tørseth et al., 2012) and may have substantial uncertainty. We compared SPM and  $\text{PM}_{10}$  observations during a period when both variables were observed at six monitoring sites in Spain, and found SPM was greater than  $\text{PM}_{10}$  by  $6\text{--}17 \mu\text{g m}^{-3}$ . Taking this into account, along with the better model agreement for  $\text{PM}_{10}$  mass, indicates that coarse-sized particles ( $D > 10 \mu\text{m}$ ) are under-represented by the model. Potential anthropogenic sources of coarse particles that are not represented in the model include road traffic dust and construction sources.

Underprediction of aerosol mass could be due to underestimation of aerosol processes, as well as missing aerosol sources from the model. The model does not include nitrate

**Table 3.** Statistical summary of modelled and observed annual and seasonal (DJF and JJA) mean SPM concentrations at all long-term (> 20 years of data) measurement sites (34 sites) between 1978 and 1998. A similar comparison is presented for PM<sub>10</sub> mass concentrations at all long-term (> 10 years of data) measurement sites (16 sites) between 1997 and 2009. Absolute and relative (%) changes in concentrations are calculated as the difference between the mean of the initial 5 years of data minus the mean of the last 5 years of data. Trends that are above or below the value of twice of the standard error of the trend (95 % confidence) are highlighted in bold.

Component	Type	Absolute change in concentration ( $\mu\text{g m}^{-3}$ )	Standard deviation of mean value	% Change in concentration	calculated linear trend ( $\mu\text{g m}^{-3} \text{ yr}^{-1}$ )	-2* SE of trend	+2* SE of trend	$r^2$	NMBF	RMSE
SPM Annual	observed	-18.32	7.96	-42 %	<b>-1.19</b>	-1.41	-0.97	0.104	-0.88	18.04
	model	-4.11	2.36	-20 %	<b>-0.26</b>	-0.39	-0.14			
SPM DJF	observed	-24.50	10.81	-51 %	<b>-1.52</b>	-1.91	-1.13	0.044	-0.852	19.39
	model	-3.95	3.82	-19 %	<b>-0.27</b>	-0.52	-0.02			
SPM JJA	observed	-14.80	7.74	-35 %	<b>-1.04</b>	-1.36	-0.72	0.354	-0.796	16.41
	model	-5.06	2.94	-23 %	<b>-0.38</b>	-0.51	-0.25			
PM <sub>10</sub> Annual	observed	-1.50	1.84	-9 %	-0.27	-0.50	-0.03	0.037	-0.221	3.35
	model	-1.08	1.16	-8 %	-0.14	-0.30	0.02			
PM <sub>10</sub> DJF	observed	-1.53	2.35	-9 %	-0.29	-0.61	0.03	0.023	-0.12	4.01
	model	-2.40	3.04	-15 %	-0.29	-0.73	0.14			
PM <sub>10</sub> JJA	observed	0.19	1.87	1 %	-0.02	-0.31	0.27	0.295	-0.339	4.66
	model	3.12	2.75	30 %	0.32	-0.06	0.70			

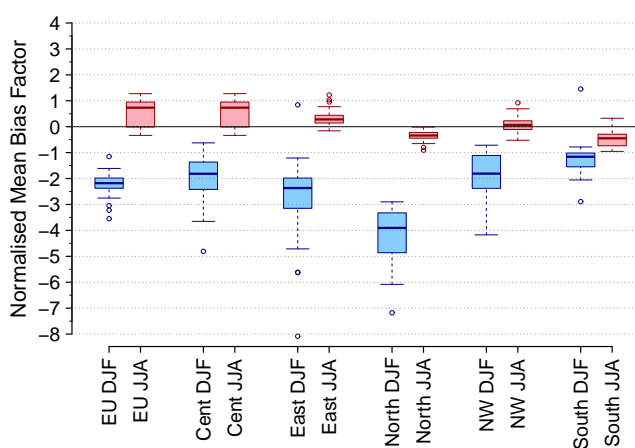


**Figure 6.** European and sub-regional normalised mean bias factors for summertime (red) and wintertime (blue) sulfate aerosol mass concentrations across all the years that data were available. The solid line shows the median value, the boxes show the 25th and 75th percentile values with the error bars showing the maximum and minimum values and the circles representing outliers (values > 1.5 × interquartile range).

aerosol which could account for  $1\text{--}3 \mu\text{g m}^{-3}$  of aerosol mass over Europe (Fagerli and Aas, 2008; Bellouin et al., 2011; Pozzer et al., 2012). This could be particularly important in reducing the model bias in winter and over northern and north-western Europe where nitrate concentrations are anticipated to be largest. The reductions in  $\text{SO}_2$  emissions and increase in  $\text{NH}_3$  emissions across Europe over the last 30 years (Fig. 2) could have important impacts on aerosol composi-

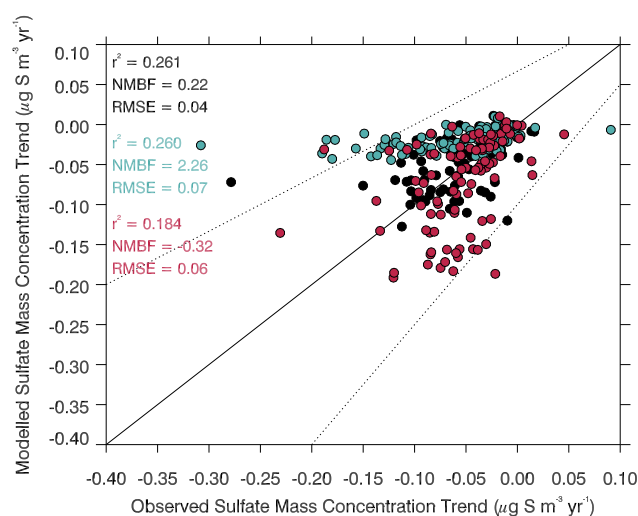


**Figure 7.** Annual (black), summertime (red) and wintertime (blue) trends in modelled and observed sulfate aerosol mass concentrations ( $\mu\text{g S m}^{-3} \text{ yr}^{-1}$ ) at each individual monitoring location over their operational period between 1978 and 2009.

tion (Fagerli and Aas, 2008). In historical periods with high  $\text{SO}_2$  emissions, sulfate aerosol dominates and nitrate concentrations are likely to be small. In the recent past and in the future, declines in  $\text{SO}_2$  and sulfate aerosol mass, coupled with an increase in  $\text{NH}_3$  emissions, may lead to increased nitrate aerosol concentrations. Inclusion of nitrate aerosol would reduce the model bias in PM<sub>10</sub> concentrations over more recent years but would have a smaller fractional impact in the 1980s–1990s due to the dominance of sulfate concentrations.

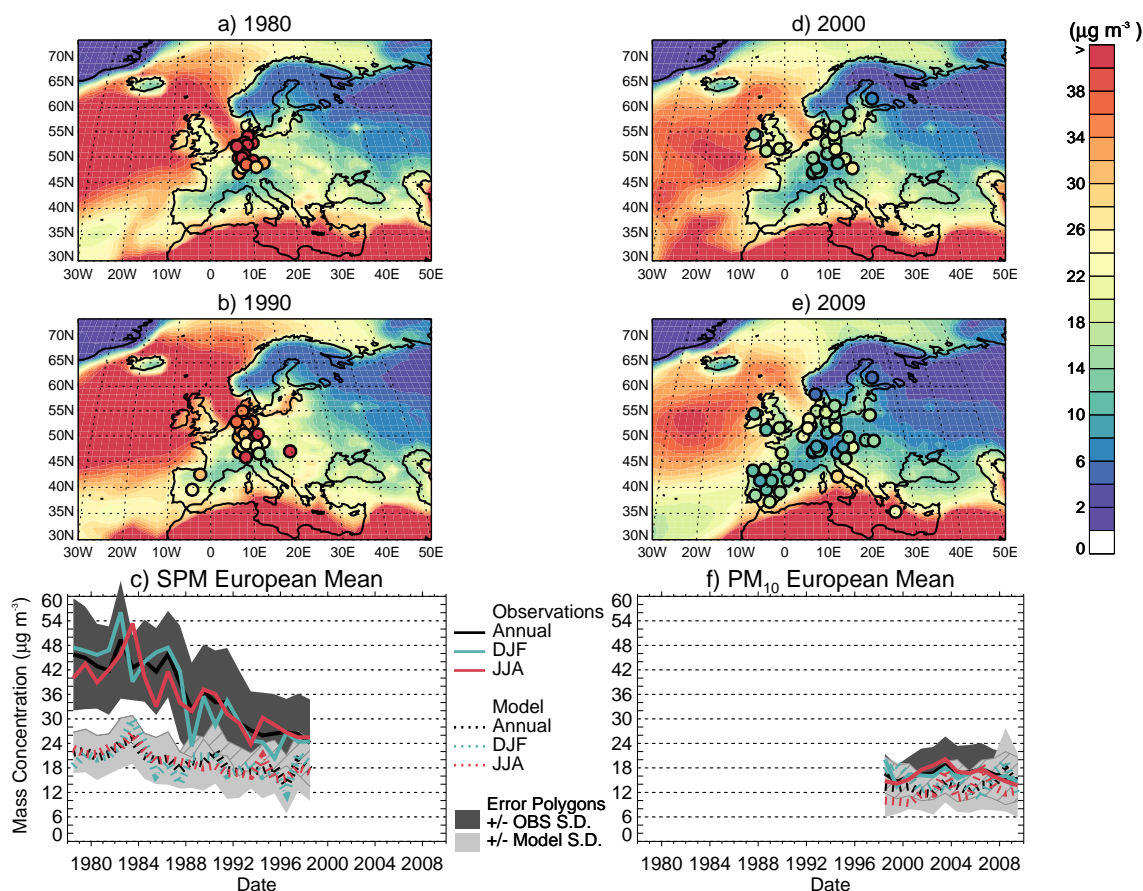


**Figure 8.** Annual mean SPM mass concentrations ( $\mu\text{g m}^{-3}$ ) from the lowest model level with observations overplotted in circles for (a) 1980 and (b) 1990. (d) and (e) are the same as (a) and (b) but for  $\text{PM}_{10}$  mass concentrations in 2000 and 2009. A time series of annual and seasonal mean observed (solid lines) and modelled (dashed lines) (c) SPM and (f)  $\text{PM}_{10}$  concentrations averaged across all measurement locations for each particular year. Shaded areas show  $\pm 1$  standard deviation of the modelled (light grey) and observed (dark grey) annual mean values, with the hatching identifying areas of overlap.

The model also does not include primary biological aerosol sources, which may contribute  $1\text{--}2\ \mu\text{g m}^{-3}$  to  $\text{PM}_{10}$  mass over Europe (Heald and Spracklen, 2009); the contribution to  $D > 10\ \mu\text{m}$  is not known.

Uncertainty in aerosol precursor emissions will also contribute to the model–observation discrepancy. In particular, domestic wood burning and wildfires could contribute up to 50 % of OC locally over Europe and may be underestimated in emission data sets (Hodzic et al., 2007; Langmann et al., 2008; Manders et al., 2012). The calculation of SOA is also a large uncertainty, particularly the proportions from anthropogenic and biogenic sources. Global aerosol models typically underpredict the amount of organic aerosols in the atmosphere (Tsigaridis et al., 2014), particularly from anthropogenic sources (Volkamer et al., 2006; Farina et al., 2010; Spracklen et al., 2011). Anthropogenic sources (or anthropogenically modified biogenic sources) that are not accounted for here may contribute up to  $3\ \mu\text{g m}^{-3}$  of SOA over Europe (Spracklen et al., 2011).

Nevertheless, even using the upper estimates of some of these potential missing sources, there still appears to be a model underprediction of total aerosol mass particularly during the early period (1980–1990), suggesting that additional sources or processes are missing within the model or that removal processes are overestimated.

### 3.2.3 Aerosol size distribution

Figure 11a–c compare simulated and observed annual mean surface aerosol number concentrations averaged over the period 2008–2009 for particles with dry diameter greater than 30, 50 and 100 nm. The model underestimates the observed aerosol number concentrations for all size fractions, with a slightly larger model bias for larger size particles ( $N_{100}$  NMBF =  $-0.96$ ;  $N_{50}$  NMBF =  $-0.65$ ; and  $N_{30}$  NMBF =  $-0.85$ ). The model substantially underestimates aerosol number concentrations over all size fractions at the high latitude Arctic monitoring locations of Pallas and Zeppelin. In addition, simulated aerosol number concentrations are under-

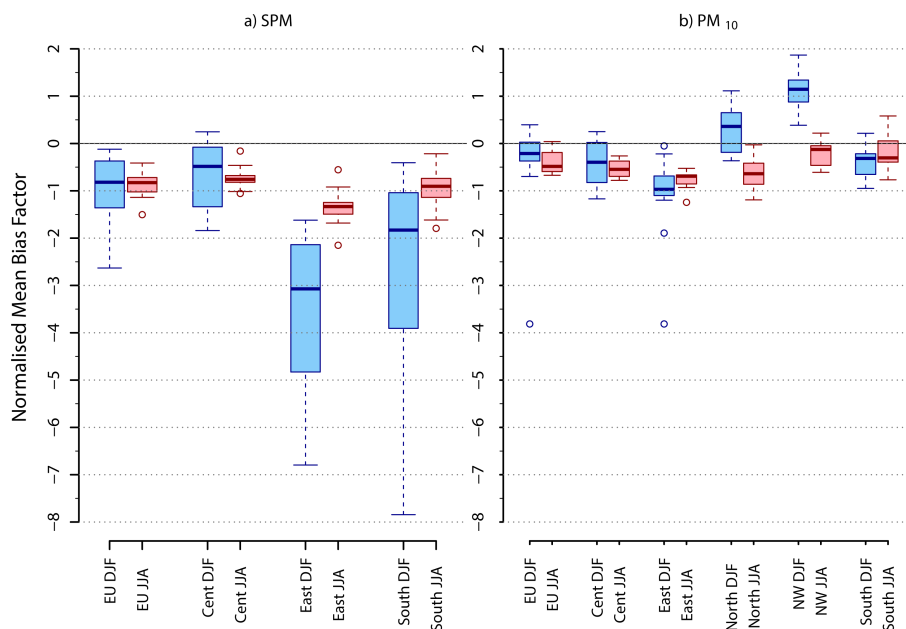


**Figure 9.** European and sub-regional normalised mean bias factors for summertime (red) and wintertime (blue) (a) SPM and (b) PM<sub>10</sub> mass concentrations across all the years that data were available. The solid line shows the median value, the boxes show the 25th and 75th percentile values with the error bars showing the maximum and minimum values and the circles representing outliers (values > 1.5 × interquartile range).

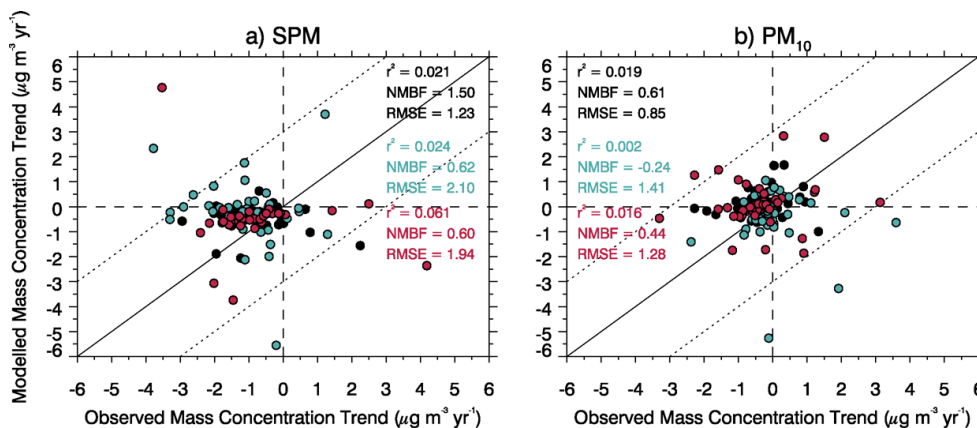


**Figure 10.** Calculated annual (black), summertime (red) and wintertime (blue) linear trends in modelled and observed (a) SPM and (b) PM<sub>10</sub> mass concentrations ( $\mu\text{g S m}^{-3} \text{ yr}^{-1}$ ) at each individual monitoring location over their operational period between 1978 and 2002 for SPM and between 1996 and 2009 for PM<sub>10</sub>.

estimated to a larger extent at the more polluted, central European monitoring sites of Ispra, Preila, Bösel and K-Pusztá.

The model is able to reproduce the observed aerosol number concentrations within a factor of 2 at the majority of European monitoring locations, which is in agreement with the recent intercomparison and evaluation of global aerosol microphysical models (Mann et al., 2014). In addition, Mann et al. (2014) also found that all of the evaluated models underestimated aerosol number concentrations in the Arctic.

This suggests that N50 concentrations (a proxy for CCN concentrations) are slightly underpredicted by the model in the present day but have declined across Europe (Fig. 4b) by 50 % since the 1970s, with a large potential impact on the European radiative balance. However, over the more recent period of 2001–2010 no discernible trend was found in aerosol number concentration by Asmi et al. (2013) across three central European monitoring sites.

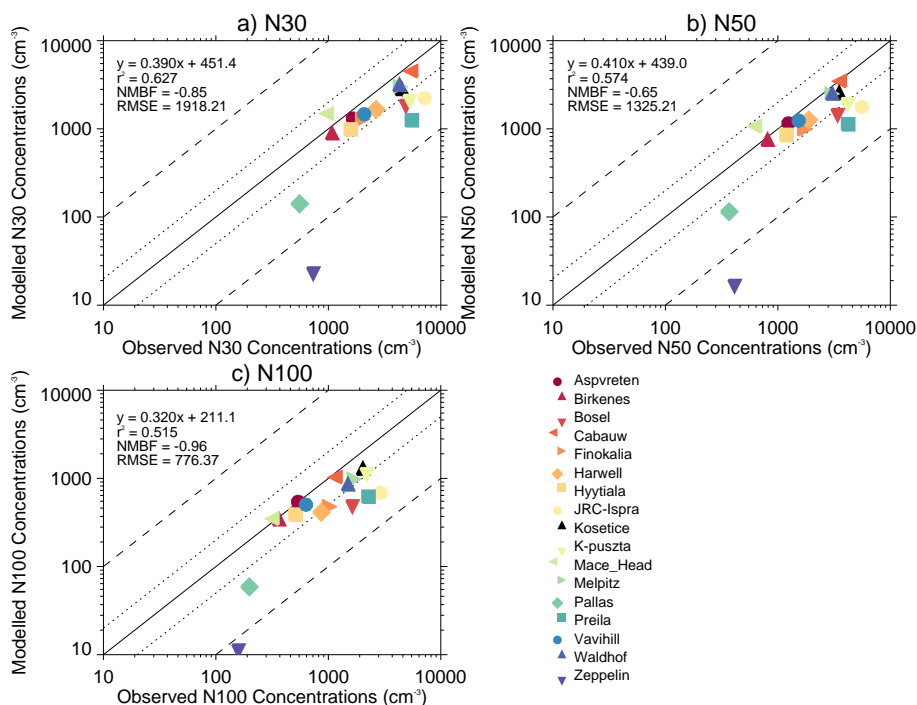


**Figure 11.** Annual mean observed vs. simulated aerosol number concentrations for (a) N30 (particles greater than 30 nm diameter), (b) N50 (> 50 nm) and (c) N100 (> 100 nm) at monitoring sites across Europe.

### 3.2.4 Aerosol optical depth

Figure 12a, b compare simulated and observed annual mean AOD at 440 nm in 2000 and 2009. The largest simulated and observed AOD occurs over eastern and south-eastern Europe. The model is relatively unbiased against annual mean AOD (NMBF = -0.013). The model captures the observed seasonal cycle in European AOD with the highest AOD in the summer and lowest in the winter but overestimates wintertime AOD (NMBF = 0.258) and underestimates summertime AOD (NMBF = -0.167) (Table 4). These seasonal biases are of opposite sign to those for sulfate and PM<sub>10</sub>. However, we note that simulation of AOD requires information on aerosol optics, aerosol size distribution and atmospheric humidity, meaning it is difficult to relate to comparisons of surface aerosol mass.

Observed and simulated AOD has declined over the period 2000–2009 (Fig. 12c). Table 4 shows that at the three monitoring locations with the longest data records (9–10 years), simulated and observed AOD has declined by a similar magnitude (11–14 %) but AOD is underestimated by the model (NMBF = -0.296). The observed AOD trend at the three long-term sites in the period 2000–2009 is  $-0.007 \pm 0.004 \text{ yr}^{-1}$  and is similar to that modelled of  $-0.006 \pm 0.0008 \text{ yr}^{-1}$  (Table 4). The trend in observed wintertime AOD ( $-0.006 \pm 0.002 \text{ yr}^{-1}$ ) is well captured by the model ( $-0.007 \pm 0.002 \text{ yr}^{-1}$ ). The larger observed summertime trend of  $-0.014 \pm 0.003 \text{ yr}^{-1}$  is under-

estimated ( $-0.005 \pm 0.002 \text{ yr}^{-1}$ ). The ability of the model to reproduce the decline in AOD is similar for sulfate and PM<sub>10</sub>.

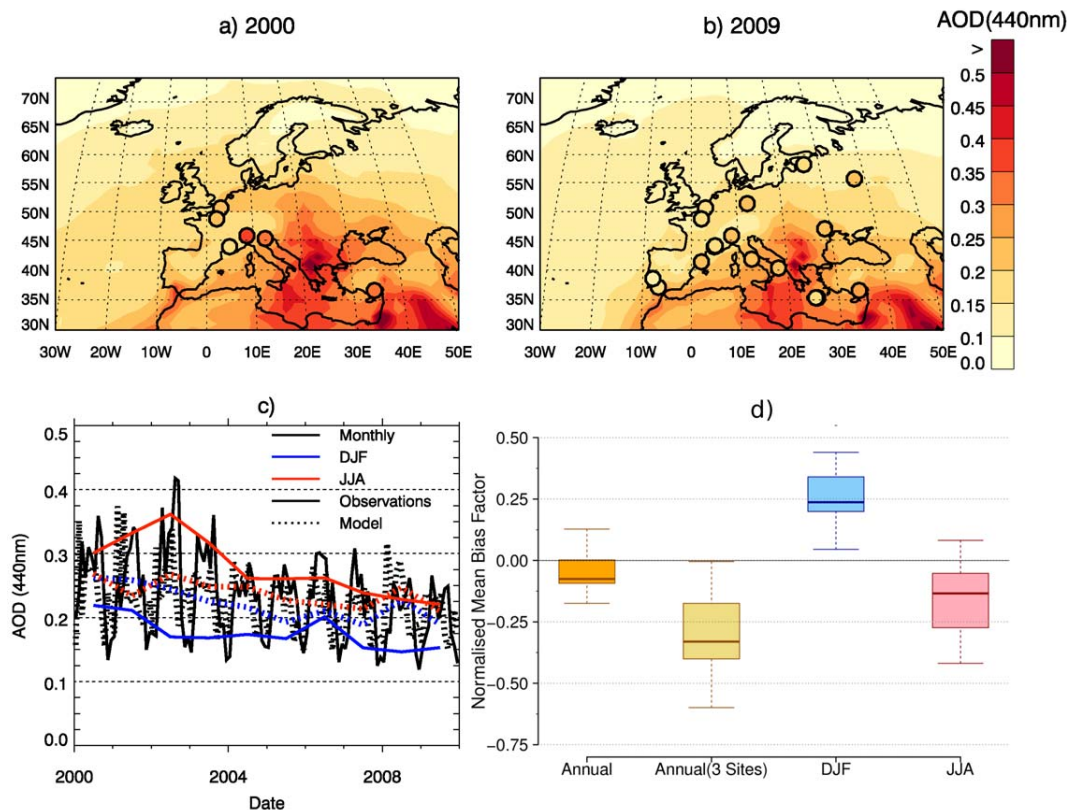
### 3.2.5 Surface solar radiation

Figure 13 shows simulated and observed annual mean all-sky SSR anomalies across Europe between 1960 and 2009, relative to a 1980–2000 mean. The long-term mean was based on the period 1980–2000, considered to be the period with the most reliable observations. Evaluation of SSR has been split into three distinct time periods (1960–1974, 1975–1989 and 1990–2009) based on the changes in the observed all-sky SSR values (Table 5). The observed SSR anomaly is generally positive and relatively constant in the period 1960–1974. There is a decrease in observed SSR from 1975 until the late 1980s, after which a strong increase in SSR is observed from 1990 to 2009.

Between 1990 and 2009 both the observed and simulated European SSR increases by 5.8 and 4.0 W m<sup>-2</sup> respectively with similar positive linear trends ( $0.37\text{--}0.32 \text{ W m}^{-2} \text{ yr}^{-1}$ ; Table 5). The highest spatial correlation ( $r^2 = 0.90$ ) between modelled and observed SSR values occurs in the period 1990–2009, whereas the bias (NMBF = 0.04) and error (RMSE = 8.0) in SSR are similar to that in 1975–1989. An evaluation of seasonal mean modelled and observed SSR also showed small differences in the NMBF over each season for all time periods, although RMSE is larger and the spatial correlation is smaller in summer. The positive SSR trend

**Table 4.** Statistical summary of modelled and observed annual and seasonal (DJF and JJA) mean AOD at all long-term (> 7 years of data) measurement sites (13 sites) between 2000 and 2009. A similar comparison is presented at the three measurement locations that contain annual mean observations throughout every year between 2000 and 2009 (AOD, three sites). Absolute and relative (%) changes in concentrations are calculated as the difference between the mean of the initial 5 years of data minus the mean of the last 5 years of data. Trends that are above or below the value of twice of the standard error of the trend (95 % confidence) are highlighted in bold.

Component	Type	Absolute change in AOD	Standard deviation of mean value	% Change in AOD	Calculated linear trend (AOD yr <sup>-1</sup> )	-2* SE of trend	+2* SE of trend	r <sup>2</sup>	NMBF	RMSE
AOD	observed	-0.03	0.022	-12 %	-0.0061	-0.009	-0.003	0.031	-0.013	0.026
	model	-0.006	0.014	-2 %	0.00005	-0.003	0.003			
AOD 3 Sites	observed	-0.03	0.037	-11 %	-0.007	-0.014	-0.001	0.011	-0.296	0.066
	model	-0.03	0.019	-14 %	-0.006	-0.007	-0.004			
AOD DJF	observed	-0.024	0.026	-13 %	-0.0063	-0.010	-0.002	0.024	0.258	0.050
	model	-0.040	0.027	-16 %	-0.0074	-0.011	-0.004			
AOD JJA	observed	-0.072	0.047	-23 %	-0.014	-0.019	-0.008	0.039	-0.167	0.053
	model	-0.030	0.021	-12 %	-0.005	-0.008	-0.002			



**Figure 12.** Annual mean AOD at 440 nm with observations from the AERONET sites overplotted for (a) 2000 and (b) 2009. (c) Time series of monthly and seasonal mean observed (solid lines) and modelled (dashed lines) AOD at 440 nm averaged across all measurement locations. (d) European NMBFs of AOD for annual (orange), summertime (red) and wintertime (blue) across all the years and sites that data were available. The annual NMBF for the three sites with the longest continuous record (> 9 years) is shown in yellow.

**Table 5.** Statistical summary of simulated and observed annual mean SSR for three different time periods (1960–1974, 1975–1989 and 1990–2009) at the 20 measurement sites across Europe which have a continuous 50-year data record. Absolute and relative (%) changes in SSR are calculated as the difference between the mean of the initial 5 years of data minus the mean of the last 5 years of data for the time period considered. Trends that are above or below the value of twice of the standard error of the trend (95 % confidence) are highlighted in bold.

Type	Time period	Absolute change in SSR ( $\text{W m}^{-2}$ )	Standard deviation of mean value	% Change in SSR	Calculated linear trend ( $\text{W m}^{-2} \text{yr}^{-1}$ )	$-2^* \text{ SE}$ of trend	$+2^* \text{ SE}$ of trend	$r^2$	NMBF	RMSE
observed	1960–1974	−0.79	2.40	−1	−0.011	−0.309	0.286	0.838	0.002	7.72
model + ARE		−1.67	1.89	−1	−0.088	−0.317	0.141			
model − ARE		−0.20	2.12	−0.2	0.069	−0.237	0.376	0.748	0.045	11.04
observed	1975–1989	−2.24	3.42	−2	−0.259	−0.658	0.140	0.803	0.029	8.43
model + ARE		3.12	3.06	3	0.304	−0.036	0.643			
model − ARE		1.89	3.50	1.6	0.187	−0.191	0.564	0.757	0.063	11.84
observed	1990–2009	5.78	3.47	5	0.369	0.153	0.584	0.896	0.043	8.00
model + ARE		3.98	3.04	3	0.316	0.125	0.507			
model − ARE		0.27	2.92	0.2	0.09	−0.185	0.366	0.828	0.053	10.23

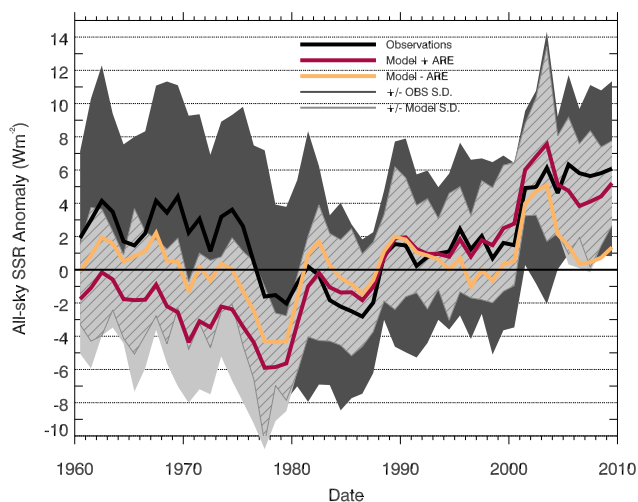


**Figure 13.** Observed (black line) and simulated (red line) European annual mean all-sky SSR anomalies ( $\text{W m}^{-2}$ ) relative to a 1980–2000 average. Simulated all-sky SSR not including aerosol radiative effects (ARE) is also shown (orange line). Values are calculated as the average across all measurement locations within Europe (see Fig. 1). The standard deviation of the annual mean for each year is shown by the shaded areas of dark grey for the observations and light grey for the model with the hatching representing where the areas overlap.

(brightening) observed between the late 1980s and 2009 is reproduced by the model, but simulated brightening begins several years earlier than observed. The positive trend in SSR anomaly across Europe from the mid-1980s to present day corresponds with the observed and simulated decrease in aerosol concentrations. Figure 13 also shows the modelled all-sky SSR anomalies without aerosol radiative effects (ARE). Without ARE the simulated trend in SSR is underestimated ( $0.09 \pm 0.14 \text{ W m}^{-2} \text{ yr}^{-1}$ ), suggesting that changes

in aerosol concentrations are a dominant driver of SSR trends during this period. The simulated positive trend in SSR including ARE presented here is in agreement with other studies over this period (Wild, 2009; Allen et al., 2013; Sanchez-Lorenzo et al., 2013; Chiacchio et al., 2015).

In the period 1975–1989, both the modelled and observed SSR anomalies are generally negative, which coincides with the maximum anthropogenic emissions and atmospheric aerosol loading. Over this period the observed SSR decreases by an average of  $2.2 \text{ W m}^{-2}$ , whilst simulated SSR increases by  $3.1 \text{ W m}^{-2}$  (Table 5). A similar discrepancy in sign and magnitude is also apparent in the linear trends of the model ( $0.30 \pm 0.17 \text{ W m}^{-2} \text{ yr}^{-1}$ ) and observations ( $-0.26 \pm 0.20 \text{ W m}^{-2} \text{ yr}^{-1}$ ). This reflects the model's inability to simulate the timing and magnitude of the observed dimming trend in SSR values between 1975 and 1989 (Fig. 13). Over this period the simulated and observed SSR values have a lower correlation ( $r^2 = 0.80$ ) and larger error (RMSE = 8.43) than the 1990–2009 period, indicating a slightly poorer representation by the model. The model without ARE also shows similar disagreements (Table 5), potentially indicating that errors in the simulation of aerosol are not causing simulated discrepancy in SSR during this period.

Over the period 1960–1974, simulated European annual mean SSR remained relatively constant (Fig. 13) and is of a similar magnitude (Table 5) to that observed. Over this period the observed SSR anomalies are positive (compared to a 1980–2000 mean), whilst the modelled SSR anomalies are negative. The small observed trend of  $-0.01 \pm 0.15 \text{ W m}^{-2} \text{ yr}^{-1}$  over the period 1960–1974 is overestimated by the model ( $-0.09 \pm 0.11 \text{ W m}^{-2} \text{ yr}^{-1}$ ). The stronger simulated negative trend in SSR between 1960 and 1974 indicates that the dimming observed in the period 1974–1989 occurs too early in the model. The model without ARE does not show a dimming trend over this period (but does have a large uncertainty; Table 5), which implies that the

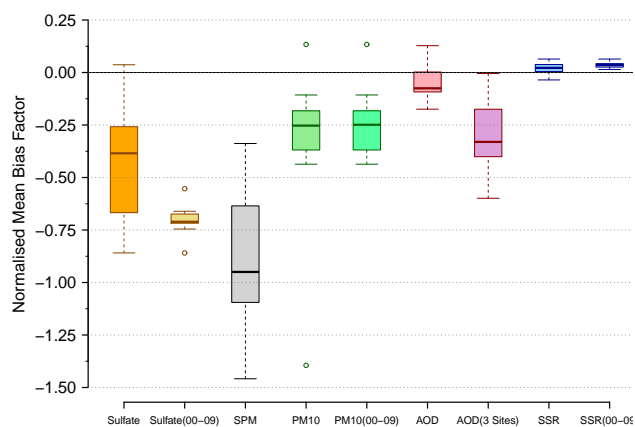


**Figure 14.** European normalised mean bias factors for sulfate aerosol mass, SPM mass, PM<sub>10</sub> mass, AOD and SSR across all the years where data were available (see Tables 2–5) and separately for the period 2000–2009. The solid line shows the median value, the boxes show the 25th and 75th percentile values with the error bars showing the maximum and minimum values and the circles representing outliers (values > 1.5 × interquartile range).

discrepancy in the SSR trend could be due to uncertainties in simulated aerosols.

Understanding the discrepancy in simulated SSR prior to 1980 is difficult because aerosol observations are not available. Possible causes of model discrepancy include errors in simulated aerosol, problems with the observations, or the ECMWF reanalysis product. With regards to observational uncertainties, there were fewer observations of SSR before 1970 (Fig. 3) and there is also a larger correction factor associated with data from the available sites (Sanchez-Lorenzo et al., 2013). This suggests that observational error may be larger in the early period. Prior to 2000, the model is forced by the ERA-40 reanalysis. ERA-40 was improved in the 1970s by the inclusion of additional measurements, most notably from satellites (Uppala et al., 2005). Larger errors in the reanalyses prior to 1980 (Uppala et al., 2005) could cause errors in the generation of clouds by the host GCM (global circulation model), which would affect simulated SSR.

### 3.2.6 Evaluation summary

Figure 14 summarises the comparison between simulated and observed sulfate, SPM, PM<sub>10</sub>, AOD and SSR across Europe separately for their entire operational period and also for the period 2000–2009 (when PM<sub>10</sub> and AOD observations are available). The model underpredicts SPM, PM<sub>10</sub> and sulfate aerosol mass over both periods. The largest underprediction occurs for SPM (1978–1998, NMBF = −0.88), with smaller underpredictions for sulfate (1978–2009, NMBF = −0.38) and PM<sub>10</sub> (1997–2009, NMBF = −0.22). Simulated European annual mean SSR has a smaller model bias (1960–2009, NMBF = 0.02). Over the period 2000–2009, the model has comparatively small biases in AOD (NMBF

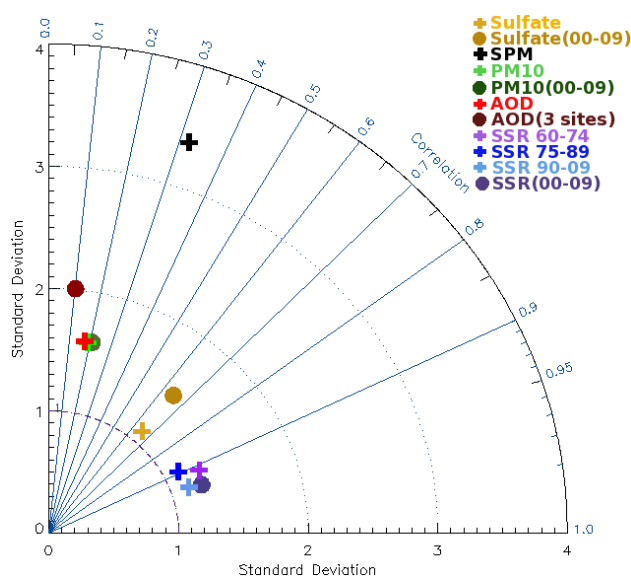


**Figure 15.** Taylor diagram comparing simulated and observed European sulfate mass concentrations, SPM, PM<sub>10</sub>, AOD and SSR. Comparisons are made across all the years where observations are available. We additionally show results for the period 2000–2009, where sulfate, PM<sub>10</sub>, AOD and SSR are consistently available. For AOD, we separately plot the three locations with the longest observational record. For SSR we also plot the three different time periods (1960–1974, 1975–1989, 1990–2009). Correlation coefficients are plotted against the observed standard deviations normalised relative to the simulated standard deviation.

= −0.013) and SSR (NMBF = 0.036) but larger biases for sulfate (NMBF = −0.71) and PM<sub>10</sub> (NMBF = −0.22). The model also underestimates aerosol number concentrations across the N30 (NMBF = −0.85), N50 (NMBF = −0.65) and N100 (NMBF = −0.96) size fractions in 2008–2009. Underestimation of annual and seasonal mean surface sulfate, PM<sub>10</sub> and aerosol number concentration is therefore not manifested in the simulation of the annual and seasonal cycle of AOD or SSR. Calculation of AOD requires information on the aerosol vertical profile, aerosol optics, aerosol size distribution and atmospheric humidity. Simulation of SSR strongly depends on model representation of clouds. A direct comparison of model performance in simulating surface aerosol mass with AOD or SSR is therefore complicated. Figure 15 shows the spatial correlation and variability (represented by the standard deviation in observed values normalised to the modelled values,  $SD_{\text{obs}}/SD_{\text{mod}}$ ) in sulfate, SPM, PM<sub>10</sub>, AOD and SSR. In general, SSR and sulfate are better simulated in terms of spatial correlation and variability, with poorer model simulation of SPM, PM<sub>10</sub> and AOD.

The observed negative trends in sulfate, PM<sub>10</sub> and AOD ( $-0.05 \mu\text{g S m}^{-3} \text{ yr}^{-1}$ ,  $-0.27 \mu\text{g m}^{-3} \text{ yr}^{-1}$  and  $-0.007 \text{ yr}^{-1}$ ) are all well reproduced by the model ( $-0.04 \mu\text{g S m}^{-3} \text{ yr}^{-1}$ ,  $-0.14 \mu\text{g m}^{-3} \text{ yr}^{-1}$  and  $-0.006 \text{ yr}^{-1}$ ). Over the period 1990–2009, observed trends in SSR ( $0.37 \text{ W m}^{-2} \text{ yr}^{-1}$ ) are also

**Table 6.** Global and European shortwave top of atmosphere all-sky and clear-sky aerosol RF, relative to a 1980–2000 mean. Values for 1972 are included as this is when the simulated minimum aerosol RF occurs over Europe. For comparison we include global carbon dioxide RF (relative to 1750) from the IPCC fifth assessment report (Myhre et al., 2013).

Year	All-sky aerosol RF ( $\text{W m}^{-2}$ )		Clear-sky aerosol RF ( $\text{W m}^{-2}$ )		Estimates of $\text{CO}_2$ RF (Myhre et al., 2013)
	Global	Europe	Global	Europe	
1960	+0.9	+0.8	+0.4	+0.2	+0.7
1970	-0.1	-1.0	+0.01	-0.1	+0.9
1972	-0.1	-1.4	+0.2	-1.6	NA
1980	-0.4	-0.6	+0.01	-0.5	+1.1
1990	+0.01	+0.1	+0.04	-0.1	+1.3
2000	+0.4	+1.7	-0.1	+1.1	+1.5
2009	+0.3	+2.1	+0.1	+1.9	+1.8

well simulated by the model when ARE are included ( $0.32 \text{ W m}^{-2} \text{ yr}^{-1}$ ), but poorly simulated when ARE are excluded ( $0.09 \text{ W m}^{-2} \text{ yr}^{-1}$ ). This confirms that being able to simulate the decline in aerosol concentrations over Europe is important for reproducing the observed brightening trend in SSR between 1990 and 2009. Prior to 1990, the model does not simulate trends in SSR as well but few aerosol observations are available to determine the reason for model failure, which could be caused by issues with simulated aerosol, clouds or with the observations.

#### 4 European aerosol radiative forcing trends

Figure 16 shows the changes in simulated European mean top of atmosphere (TOA) outgoing radiation, relative to a 1980–2000 mean, under all-sky (Fig. 16a) and clear-sky conditions (Fig. 16b) with the numbers presented in Table 6. Here we define this difference in TOA radiation as a radiative forcing (RF) between the current year and the long-term mean state. European mean all-sky RF (Fig. 16a) decreases by  $> 2.0 \text{ W m}^{-2}$  (cooling trend) over the period 1960–1972, corresponding to the increase in simulated aerosol loading. From 1973 to 2009, European mean all-sky radiation increases by  $> 3.0 \text{ W m}^{-2}$  (warming trend), corresponding to the simulated reduction of aerosols. All-sky RF showed the largest increase of  $6.0 \text{ W m}^{-2}$  over central Europe between 1973 and 2009, which is consistent with this region having experienced the largest change in anthropogenic emissions (Fig. 2) and aerosol concentrations (Fig. 8). Other regions of Europe have a similar temporal change but with a smaller magnitude.

The simulated clear-sky aerosol TOA RF (Fig. 16b) is similar to that simulated under all-sky conditions. European mean clear-sky RF decreased by  $> 1.5 \text{ W m}^{-2}$  between 1960 and 1972 (cooling) and from 1973 to 2009 it increased by  $> 3.0 \text{ W m}^{-2}$  (warming). Marmer et al. (2007) reported a similar change of  $+2.0 \text{ W m}^{-2}$  in the direct shortwave

RF from sulfate aerosols over Europe between 1980 and 2000. This indicates the strong influence directly exerted by aerosols on the European radiative balance in response to changes in anthropogenic emissions. An estimate of the cloud albedo effect is obtained as the difference between the all-sky and clear-sky RF. Over the period 1973–2009, the cloud albedo effect is estimated to have increased by  $0.44 \text{ W m}^{-2}$  (warming), indicating that it is a relatively small change when compared to that from the direct effect.

The changes in aerosol RF we simulate over Europe are slightly larger than those calculated for the USA by Leibensperger et al. (2012) of approximately  $+1 \text{ W m}^{-2}$  for the direct effect and  $+1 \text{ W m}^{-2}$  for the indirect (first and second) effects. The smaller changes in aerosol RF reported by Leibensperger et al. (2012) are possibly related to the smaller reductions in sulfate aerosol mass concentrations observed over the USA of  $\sim 0.8 \mu\text{g S m}^{-3}$  (40%) when compared to those observed over Europe of  $1.2 \mu\text{g S m}^{-3}$  (70%).

The calculated changes in all-sky TOA RF indicate the extent to which changes in anthropogenic emissions over the last 50 years have affected the European radiative balance. Reductions in anthropogenic aerosols have resulted in a positive response in the European radiative balance. We estimate that the magnitude of these emission reductions has caused European mean all-sky RF to increase by  $> 3.0 \text{ W m}^{-2}$  between the mid-1970s and 2009, mainly due to the direct aerosol effect (as shown by similar changes in the clear-sky RF). Table 6 shows that the change in European mean aerosol RF is much larger than the change in global mean aerosol RF of  $+0.4 \text{ W m}^{-2}$ . Shindell et al. (2013) reported a multimodel evaluation of aerosol RF over the period 1850–2100, with six of the nine models reporting a positive increase in global mean aerosol RF between 1980 and 2000, qualitatively similar to the results presented here. At the global scale, our simulated change in all-sky aerosol RF between 1970 and 2009 is  $\sim 40\%$  of the magnitude of change in global  $\text{CO}_2$  radiative forcing over the same period. At the European scale, the simulated change in all-sky aerosol RF is more than 3 times the change in global mean  $\text{CO}_2$  RF. This indicates the large regional impact that decreasing aerosol concentrations have had on the radiative balance and climate over Europe compared to other forcing agents.

The agreement between the model and observations in the changes in aerosols and in the brightening period of the surface radiation balance between the 1990 and 2009 improve our confidence in the magnitude and temporal change of the simulated TOA RF over this period when most of the change occurs ( $2.0 \text{ W m}^{-2}$ ). Future work needs to explore the potential climate implications from these changes to the radiative balance. It will be important to understand the role of European air quality legislation in observed emission reductions as this may have important implications when considering the impact of future air quality mitigation measures on climate.

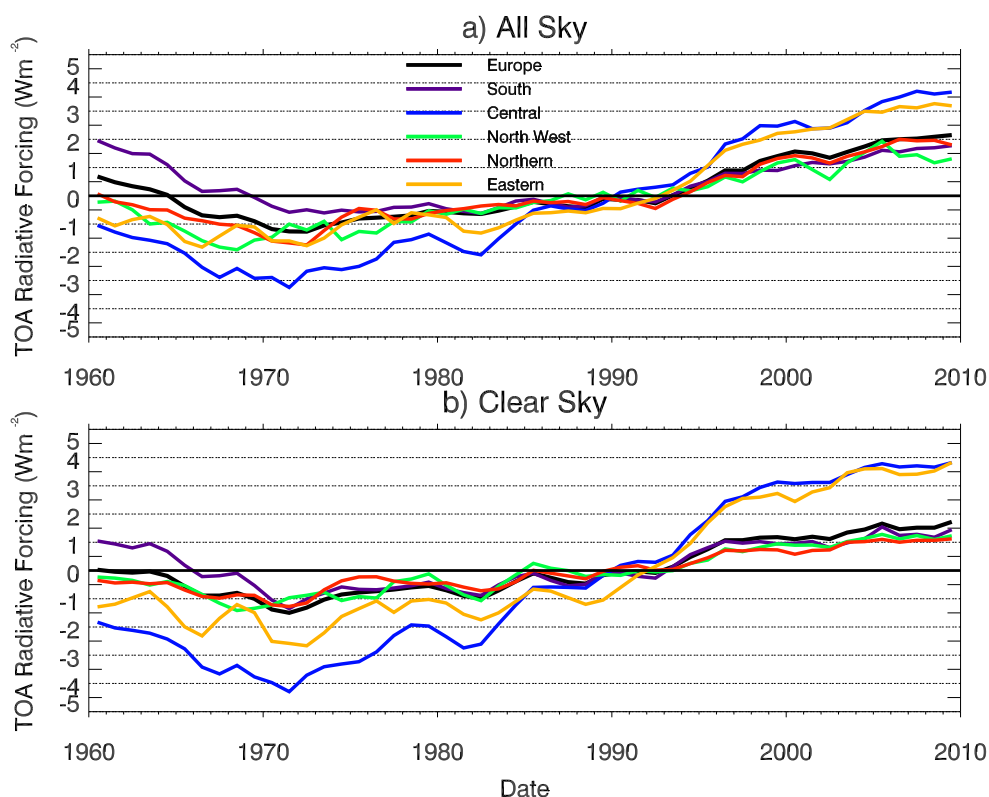


**Figure 16.** European and sub-regional top of atmosphere aerosol radiative forcing ( $\text{Wm}^{-2}$ ), relative to a 1980–2009 average, under (a) all-sky and (b) clear-sky conditions. European regions are as defined in Fig. 1

## 5 Conclusions

We used the HadGEM3-UKCA coupled chemistry–climate model to simulate changes in aerosols between 1960 and 2009, a period over which anthropogenic sources of aerosol changed substantially. We evaluated the model against European observations of sulfate aerosol mass, total SPM,  $\text{PM}_{10}$  mass concentrations, aerosol number concentrations, AOD and surface SSR. We also calculated the impact of changes in atmospheric aerosols on European aerosol radiative forcing.

The model underpredicts sulfate aerosol mass concentrations (NMBF =  $-0.4$ ), SPM (1978–1998, NMBF =  $-0.9$ ) and  $\text{PM}_{10}$  (1997–2009, NMBF =  $-0.2$ ). In addition, the model underpredicts present-day aerosol number concentrations over the size fractions of N30 (NMBF =  $-0.85$ ), N50 (NMBF =  $-0.65$ ) and N100 (NMBF =  $-0.96$ ). Underestimation of aerosol number and mass could be due to uncertainties in the observations (Tørseth et al., 2012), an overestimation of deposition processes or underestimated sources of PM including nitrate, anthropogenic SOA, domestic biomass combustion, dust and primary biological aerosol particles. The larger underestimation of particles with diameters  $> 10 \mu\text{m}$  suggests that the sources of such particles may be more uncertain and are not well treated by the model. The

model particularly underestimates sulfate in winter and over northern Europe potentially due to an under-representation of the in-cloud oxidation of sulfur species to sulfate via reaction with ozone or an enhanced wet deposition rate, caused by artificial high drizzle precipitation. Biases in simulated AOD (2000–2009, NMBF =  $-0.01$ ) are smaller than for surface aerosol concentrations. Calculation of AOD requires information on the aerosol vertical profile, aerosol optics, aerosol size distribution and atmospheric humidity and complicates any direct comparison between surface aerosol mass and AOD.

Observed trends in surface aerosol mass and AOD were generally well represented by the model. Sulfate aerosol mass declines by 68 % in the observations and by 78 % in the model between 1978 and 2009, consistent with the decrease in  $\text{SO}_2$  emissions over Europe. The observed European annual mean SPM decreased by 42 % between 1978 and 1998, compared to a simulated decrease of 20 %. Between 1997 and 2009  $\text{PM}_{10}$  mass concentrations decreased by 9 % in the observations and by 8 % in the model. Between 2000 and 2009 AOD decreased by 11 % in the observations and by 14 % in the model at observation sites with more than 9 years of data.

The all-sky European SSR was shown to increase between 1990 and 2009 in both the model ( $4.0 \text{ W m}^{-2}$ ) and

observations ( $5.8 \text{ W m}^{-2}$ ) (brightening). In the model simulation where aerosol radiative effects were excluded, European all-sky SSR increased by only  $0.3 \text{ W m}^{-2}$ . This comparison suggests that observed brightening post-1990 is driven by changes in aerosol that are well captured by the model. Accounting for changes to aerosols is therefore important to reproduce the European brightening trend from 1990 to 2009.

Prior to 1990, there are discrepancies between observed and simulated all-sky SSR anomalies. Specifically, the model is unable to reproduce the magnitude and timing of the observed reduction in SSR values (dimming). These errors in SSR coincide with the largest model bias in observed SPM concentrations between 1978 and 1980 (Fig. 8c), but the lack of extensive aerosol observations prior to 1980 prevents isolation of the cause of this model observational discrepancy in SSR. Possible reasons include errors in simulated aerosols, errors associated with the meteorological reanalysis fields, and issues with the measurement data (less SSR observations were available before 1970).

From the peak in aerosol loading in the early 1970s, European all-sky aerosol TOA radiative forcing has increased by  $> 3.0 \text{ W m}^{-2}$ , due to a reduction in the aerosol cooling effect. Changes in European mean RF are mainly due to changes in the direct aerosol effect, as shown by the similarity between clear-sky and all-sky RF. The largest RF is over central Europe ( $+6.0 \text{ W m}^{-2}$ ), which has seen the largest change in anthropogenic emissions and aerosol concentrations. The change in European mean aerosol RF is much larger than that globally and also 3 times as large as the change in global mean  $\text{CO}_2$  RF over the period 1970–2009. Our evaluation showed that the model is able to reproduce the observed changes in SSR over the period 1990–2009, during which two-thirds of the simulated change in RF occurred ( $2.0 \text{ W m}^{-2}$ ). Our evaluation therefore provides confidence in the simulated changes of TOA RF. The reductions in anthropogenic aerosol emissions over this period have resulted in a positive response in the radiative balance over Europe, which may have contributed to increasing temperatures across Europe (Philipona et al., 2009). The RFs simulated in this work are similar in magnitude to those reported by Marmer et al. (2007) over Europe and by Leibensperger et al. (2012) over the USA. The change in anthropogenic aerosol emissions over the period 1970–2009, in part due to measures to improve air quality, has led to a considerable reduction in the concentrations of aerosols over Europe. This decrease in aerosols has reduced the aerosol radiative cooling effect over Europe. Attempts to improve European air quality over the last 30–40 years have potentially had non-negligible impacts on European climate (Arneth et al., 2009; Philipona et al., 2009; Ramanathan and Feng, 2009; Fiore et al., 2012) and should be the subject of future study. These air quality–climate interactions should be considered when designing any future measures to improve air quality and mitigate climate change.

*Acknowledgements.* Steven Turnock would like to acknowledge the funding for his PhD studentship from the Natural Environment Research Council (NERC) and Met Office. For making their data available to be used in this study we would like to acknowledge the EMEP, GEBA and AERONET measurement networks along with any data managers involved in data collection. We would also like to acknowledge Ari Asmi for providing the aerosol size distribution data from the EUSAAR and GUAN networks and Carly Reddington for pre-processing this data set for use in the model evaluation. Anthropogenic and biomass-burning emissions from the MACCity data set were retrieved from the ECCAD emissions server. This work was also made possible by participation in the EU Framework 7 PEGASOS project (no. 265148). We acknowledge use of the MONSooN system, a collaborative facility supplied under the Joint Weather and Climate Research Programme, a strategic partnership between the Met Office and the Natural Environment Research Council. Matthew Woodhouse would like to thank the Royal Society for support via the International Exchange Scheme. Arturo Sanchez-Lorenzo was supported by a postdoctoral fellowship JCI-2012-12508 and projects CGL2014-55976-R, CGL2014-52135-C3-1-R financed by the Spanish Ministry of Economy and Competitiveness.

Edited by: A. Hofzumahaus

## References

- Allen, R. J., Norris, J. R., and Wild, M.: Evaluation of multi-decadal variability in CMIP5 surface solar radiation and inferred underestimation of aerosol direct effects over Europe, China, Japan, and India, *J. Geophys. Res.-Atmos.*, 118, 6311–6336, doi:10.1002/jgrd.50426, 2013.
- Arneth, A., Unger, N., Kulmala, M., and Andreae, M. O.: Clean the Air, Heat the Planet?, *Science*, 326, 672–673, doi:10.1126/science.1181568, 2009.
- Asmi, A., Wiedensohler, A., Laj, P., Fjaeraa, A.-M., Sellegri, K., Birmili, W., Weingartner, E., Baltensperger, U., Zdimal, V., Zikova, N., Putaud, J.-P., Marinoni, A., Tunved, P., Hansson, H.-C., Fiebig, M., Kivekäs, N., Lihavainen, H., Asmi, E., Ulevicius, V., Aalto, P. P., Swietlicki, E., Kristensson, A., Mihalopoulos, N., Kalivitis, N., Kalapov, I., Kiss, G., de Leeuw, G., Henzing, B., Harrison, R. M., Beddows, D., O'Dowd, C., Jennings, S. G., Flentje, H., Weinhold, K., Meinhardt, F., Ries, L., and Kulmala, M.: Number size distributions and seasonality of submicron particles in Europe 2008–2009, *Atmos. Chem. Phys.*, 11, 5505–5538, doi:10.5194/acp-11-5505-2011, 2011.
- Asmi, A., Collaud Coen, M., Ogren, J. A., Andrews, E., Sheridan, P., Jefferson, A., Weingartner, E., Baltensperger, U., Bukowiecki, N., Lihavainen, H., Kivekäs, N., Asmi, E., Aalto, P. P., Kulmala, M., Wiedensohler, A., Birmili, W., Hamed, A., O'Dowd, C., G Jennings, S., Weller, R., Flentje, H., Fjaeraa, A. M., Fiebig, M., Myhre, C. L., Hallar, A. G., Swietlicki, E., Kristensson, A., and Laj, P.: Aerosol decadal trends – Part 2: In-situ aerosol particle number concentrations at GAW and ACTRIS stations, *Atmos. Chem. Phys.*, 13, 895–916, doi:10.5194/acp-13-895-2013, 2013.
- Barnpadimos, I., Keller, J., Oderbolz, D., Hueglin, C., and Prévôt, A. S. H.: One decade of parallel fine ( $\text{PM}_{2.5}$ ) and coarse ( $\text{PM}_{10}$ – $\text{PM}_{2.5}$ ) particulate matter measurements in Europe:

- trends and variability, *Atmos. Chem. Phys.*, 12, 3189–3203, doi:10.5194/acp-12-3189-2012, 2012.
- Bellouin, N., Rae, J., Jones, A., Johnson, C., Haywood, J., and Boucher, O.: Aerosol forcing in the Climate Model Intercomparison Project (CMIP5) simulations by HadGEM2-ES and the role of ammonium nitrate, *J. Geophys. Res.*, 116, D20206, doi:10.1029/2011JD016074, 2011.
- Bellouin, N., Mann, G. W., Woodhouse, M. T., Johnson, C., Carslaw, K. S., and Dalvi, M.: Impact of the modal aerosol scheme GLOMAP-mode on aerosol forcing in the Hadley Centre Global Environmental Model, *Atmos. Chem. Phys.*, 13, 3027–3044, doi:10.5194/acp-13-3027-2013, 2013.
- Berglen, T. F., Myhre, G., Isaksen, I. S., Vestreng, V., and Smith, S. J.: Sulphate trends in Europe: are we able to model the recent observed decrease?, *Tellus B*, 59, 773–786, doi:10.3402/tellusb.v59i4.17056, 2007.
- Boucher, O., Randall, P., Artaxo, P., Bretherton, C., Feingold, G., Forster, P., Kerminen, V.-M., Kondo, Y., Liao, H., Lohmann, U., Rasch, P., Satheesh, S. K., Sherwood, S., Stevens, B., and Zhang, X. Y.: Clouds and Aerosols, in: *Climate Change 2013: The Physical Science Basis. Contribution of Working Group I to the Fifth Assessment Report of the Intergovernmental Panel on Climate Change*, Cambridge University Press, Cambridge, 2013.
- Chalmers, N., Highwood, E. J., Hawkins, E., Sutton, R., and Wilcox, L. J.: Aerosol contribution to the rapid warming of near-term climate under RCP 2.6, *Geophys. Res. Lett.*, 39, 2–7, doi:10.1029/2012GL052848, 2012.
- Chiacchio, M., Solmon, F., Giorgi, F., Stackhouse, P., and Wild, M.: Evaluation of the radiation budget with a regional climate model over Europe and inspection of dimming and brightening, *J. Geophys. Res.-Atmos.*, 120, 1951–1971, doi:10.1002/2014JD022497, 2015.
- Chin, M., Diehl, T., Tan, Q., Prospero, J. M., Kahn, R. A., Remer, L. A., Yu, H., Sayer, A. M., Bian, H., Geogdzhayev, I. V., Holben, B. N., Howell, S. G., Huebert, B. J., Hsu, N. C., Kim, D., Kucsera, T. L., Levy, R. C., Mishchenko, M. I., Pan, X., Quinn, P. K., Schuster, G. L., Streets, D. G., Strode, S. A., Torres, O., and Zhao, X.-P.: Multi-decadal aerosol variations from 1980 to 2009: a perspective from observations and a global model, *Atmos. Chem. Phys.*, 14, 3657–3690, doi:10.5194/acp-14-3657-2014, 2014.
- Colette, A., Granier, C., Hodnebrog, Ø., Jakobs, H., Maurizi, A., Nyiri, A., Bessagnet, B., D'Angiola, A., D'Isidoro, M., Gauss, M., Meleux, F., Memmesheimer, M., Mieville, A., Rouil, L., Russo, F., Solberg, S., Stordal, F., and Tampieri, F.: Air quality trends in Europe over the past decade: a first multi-model assessment, *Atmos. Chem. Phys.*, 11, 11657–11678, doi:10.5194/acp-11-11657-2011, 2011.
- Collaud Coen, M., Andrews, E., Asmi, A., Baltensperger, U., Bukowiecki, N., Day, D., Fiebig, M., Fjaeraa, A. M., Flentje, H., Hyvärinen, A., Jefferson, A., Jennings, S. G., Kouvarakis, G., Lihavainen, H., Lund Myhre, C., Malm, W. C., Mihapopoulos, N., Molnar, J. V., O'Dowd, C., Ogren, J. A., Schichtel, B. A., Sheridan, P., Virkkula, A., Weingartner, E., Weller, R., and Laj, P.: Aerosol decadal trends – Part I: In-situ optical measurements at GAW and IMPROVE stations, *Atmos. Chem. Phys.*, 13, 869–894, doi:10.5194/acp-13-869-2013, 2013.
- COMEAP: The Mortality Effects of Long-term Exposure to Particulate Air Pollution in the United Kingdom, Tech. rep., Health Protection Agency for the Committee on the Medical Effects of Air Pollutants, 2010.
- Davies, T., Cullen, M. J. P., Malcolm, A. J., Mawson, M. H., Staniforth, A., White, A. A., and Wood, N.: A new dynamical core for the Met Office's global and regional modelling of the atmosphere, *Q. J. Roy. Meteor. Soc.*, 131, 1759–1782, doi:10.1256/qj.04.101, 2005.
- de Meij, A., Krol, M., Dentener, F., Vignati, E., Cuvelier, C., and Thunis, P.: The sensitivity of aerosol in Europe to two different emission inventories and temporal distribution of emissions, *Atmos. Chem. Phys.*, 6, 4287–4309, doi:10.5194/acp-6-4287-2006, 2006.
- Dee, D. P., Uppala, S. M., Simmons, A. J., Berrisford, P., Poli, P., Kobayashi, S., Andrae, U., Balmaseda, M. A., Balsamo, G., Bauer, P., Bechtold, P., Beljaars, A. C. M., van de Berg, L., Bidlot, J., Bormann, N., Delsol, C., Dragani, R., Fuentes, M., Geer, A. J., Haimberger, L., Healy, S. B., Hersbach, H., Hólm, E. V., Isaksen, L., Kållberg, P., Köhler, M., Matricardi, M., McNally, A. P., Monge-Sanz, B. M., Morcrette, J.-J., Park, B.-K., Peubey, C., de Rosnay, P., Tavolato, C., Thépaut, J.-N., and Vitart, F.: The ERA-Interim reanalysis: configuration and performance of the data assimilation system, *Q. J. Roy. Meteor. Soc.*, 137, 553–597, doi:10.1002/qj.828, 2011.
- Edwards, J. M. and Slingo, A.: Studies with a flexible new radiation code. I: Choosing a configuration for a large-scale model, *Q. J. Roy. Meteorol. Soc.*, 122, 689–719, doi:10.1002/qj.49712253107, 1996.
- Essery, R. L. H., Best, M. J., Betts, R., and Cox, P. M.: Explicit Representation of Subgrid Heterogeneity in a GCM Land Surface Scheme, *J. Hydrometeorol.*, 4, 530–543, 2002.
- Fagerli, H. and Aas, W.: Trends of nitrogen in air and precipitation: Model results and observations at EMEP sites in Europe, 1980–2003, *Environ. Pollut.*, 154, 448–461, 2008.
- Farina, S. C., Adams, P. J., and Pandis, S. N.: Modeling global secondary organic aerosol formation and processing with the volatility basis set: Implications for anthropogenic secondary organic aerosol, *J. Geophys. Res.*, 115, D09202, doi:10.1029/2009JD013046, 2010.
- Fiore, A. M., Naik, V., Spracklen, D. V., Steiner, A., Unger, N., Prather, M., Bergmann, D., Cameron-Smith, P. J., Cionni, I., Collins, W. J., Dalsøren, S., Eyring, V., Folberth, G. a., Ginoux, P., Horowitz, L. W., Josse, B., Lamarque, J.-F., MacKenzie, I. a., Nagashima, T., O'Connor, F. M., Righi, M., Rumbold, S. T., Shindell, D. T., Skeie, R. B., Sudo, K., Szopa, S., Takemura, T., and Zeng, G.: Global air quality and climate., *Chem. Soc. Rev.*, 41, 6663–83, doi:10.1039/c2cs35095e, 2012.
- Folini, D. and Wild, M.: Aerosol emissions and dimming/brightening in Europe: Sensitivity studies with ECHAM5-HAM, *J. Geophys. Res.*, 116, D21104, doi:10.1029/2011JD016227, 2011.
- Gong, S. L.: A parameterization of sea-salt aerosol source function for sub- and super-micron particles, *Global Biogeochem. Cy.*, 17, 1097, doi:10.1029/2003GB002079, 2003.
- Granier, C., Bessagnet, B., Bond, T. C., D'Angiola, A., Denier van der Gon, H., Frost, G. J., Heil, A., Kaiser, J. W., Kinne, S., Klimont, Z., Kloster, S., Lamarque, J.-F., Lioussé, C., Masui, T., Meleux, F., Mieville, A., Ohara, T., Raut, J.-C., Riahi, K., Schultz, M. G., Smith, S. J., Thompson, A., Aardenne, J., Werf, G. R., and Vuuren, D. P.: Evolution of anthropogenic and

- biomass burning emissions of air pollutants at global and regional scales during the 1980–2010 period, *Clim. Change*, 109, 163–190, doi:10.1007/s10584-011-0154-1, 2011.
- Guenther, A., Hewitt, C. N., Erickson, D., Fall, R., Geron, C., Graedel, T., Harley, P., Klinger, L., Lerdau, M., McKay, W. A., Pierce, T., Scholes, B., Steinbrecher, R., Tallamraju, R., Taylor, J., and Zimmerman, P.: A global model of natural volatile organic compound emissions, *J. Geophys. Res.*, 100, 8873, doi:10.1029/94JD02950, 1995.
- Hand, J. L., Schichtel, B. A., Malm, W. C., and Pitchford, M. L.: Particulate sulfate ion concentration and SO<sub>2</sub> emission trends in the United States from the early 1990s through 2010, *Atmos. Chem. Phys.*, 12, 10353–10365, doi:10.5194/acp-12-10353-2012, 2012.
- Harrison, R. M., Stedman, J., and Derwent, D.: New Directions: Why are PM<sub>10</sub> concentrations in Europe not falling?, *Atmos. Environ.*, 42, 603–606, doi:10.1016/j.atmosenv.2007.11.023, 2008.
- Heald, C. L. and Spracklen, D. V.: Atmospheric budget of primary biological aerosol particles from fungal spores, *Geophys. Res. Lett.*, 36, 1–5, doi:10.1029/2009GL037493, 2009.
- Hewitt, H. T., Copley, D., Culverwell, I. D., Harris, C. M., Hill, R. S. R., Keen, A. B., McLaren, A. J., and Hunke, E. C.: Design and implementation of the infrastructure of HadGEM3: the next-generation Met Office climate modelling system, *Geosci. Model Dev.*, 4, 223–253, doi:10.5194/gmd-4-223-2011, 2011.
- Hodzic, A., Madronich, S., Bohn, B., Massie, S., Menut, L., and Wiedinmyer, C.: Wildfire particulate matter in Europe during summer 2003: meso-scale modeling of smoke emissions, transport and radiative effects, *Atmos. Chem. Phys.*, 7, 4043–4064, doi:10.5194/acp-7-4043-2007, 2007.
- Holben, B., Eck, T., Slutsker, I., Tanré, D., Buis, J., Setzer, A., Vermote, E., Reagan, J., Kaufman, Y., Nakajima, T., Lavenue, F., Jankowiak, I., and Smirnov, A.: AERONET—A Federated Instrument Network and Data Archive for Aerosol Characterization, *Remote Sens. Environ.*, 66, 1–16, doi:10.1016/S0034-4257(98)00031-5, 1998.
- Hurrell, J. W., Hack, J. J., Shea, D., Caron, J. M., and Rosinski, J.: A New Sea Surface Temperature and Sea Ice Boundary Dataset for the Community Atmosphere Model, *J. Climate*, 21, 5145–5153, doi:10.1175/2008JCLI2292.1, 2008.
- Jones, A., Roberts, D. L., Woodage, M. J., and Johnson, C. E.: Indirect sulphate aerosol forcing in a climate model with an interactive sulphur cycle, *J. Geophys. Res.*, 106, 20293, doi:10.1029/2000JD000089, 2001.
- Kettle, A. J. and Andreae, M. O.: Flux of dimethylsulfide from the oceans: A comparison of updated data sets and flux models, *J. Geophys. Res.*, 105, 26793, doi:10.1029/2000JD900252, 2000.
- Koch, D., Bauer, S. E., Del Genio, A., Faluvegi, G., McConnell, J. R., Menon, S., Miller, R. L., Rind, D., Ruedy, R., Schmidt, G. a., and Shindell, D. T.: Coupled Aerosol-Chemistry–Climate Twentieth-Century Transient Model Investigation: Trends in Short-Lived Species and Climate Responses, *J. Climate*, 24, 2693–2714, doi:10.1175/2011JCLI3582.1, 2011.
- Kreidenweis, S. M.: Modification of aerosol mass and size distribution due to aqueous-phase SO<sub>2</sub> oxidation in clouds: Comparisons of several models, *J. Geophys. Res.*, 108, 4213, doi:10.1029/2002JD002697, 2003.
- Lamarque, J.-F., Bond, T. C., Eyring, V., Granier, C., Heil, A., Klimont, Z., Lee, D., Liousse, C., Mieville, A., Owen, B., Schultz, M. G., Shindell, D., Smith, S. J., Stehfest, E., Van Aardenne, J., Cooper, O. R., Kainuma, M., Mahowald, N., McConnell, J. R., Naik, V., Riahi, K., and van Vuuren, D. P.: Historical (1850–2000) gridded anthropogenic and biomass burning emissions of reactive gases and aerosols: methodology and application, *Atmos. Chem. Phys.*, 10, 7017–7039, doi:10.5194/acp-10-7017-2010, 2010.
- Langmann, B., Varghese, S., Marmer, E., Vignati, E., Wilson, J., Stier, P., and O’Dowd, C.: Aerosol distribution over Europe: a model evaluation study with detailed aerosol microphysics, *Atmos. Chem. Phys.*, 8, 1591–1607, doi:10.5194/acp-8-1591-2008, 2008.
- Leibensperger, E. M., Mickley, L. J., Jacob, D. J., Chen, W.-T., Seinfeld, J. H., Nenes, A., Adams, P. J., Streets, D. G., Kumar, N., and Rind, D.: Climatic effects of 1950–2050 changes in US anthropogenic aerosols – Part I: Aerosol trends and radiative forcing, *Atmos. Chem. Phys.*, 12, 3333–3348, doi:10.5194/acp-12-3333-2012, 2012.
- Liss, P. and Merlivat, L.: Air-Sea Gas Exchange Rates: Introduction and Synthesis, in: *The Role of Air-Sea Exchange in Geochemical Cycling*, 113–127, D. Reidel, 1986.
- Manders, A. M. M., van Meijgaard, E., Mues, A. C., Kranenburg, R., van Ulft, L. H., and Schaap, M.: The impact of differences in large-scale circulation output from climate models on the regional modeling of ozone and PM, *Atmos. Chem. Phys.*, 12, 9441–9458, doi:10.5194/acp-12-9441-2012, 2012.
- Manktelow, P. T., Mann, G. W., Carslaw, K. S., Spracklen, D. V., and Chipperfield, M. P.: Regional and global trends in sulfate aerosol since the 1980s, *Geophys. Res. Lett.*, 34, L14803, doi:10.1029/2006GL028668, 2007.
- Mann, G. W., Carslaw, K. S., Spracklen, D. V., Ridley, D. A., Manktelow, P. T., Chipperfield, M. P., Pickering, S. J., and Johnson, C. E.: Description and evaluation of GLOMAP-mode: a modal global aerosol microphysics model for the UKCA composition-climate model, *Geosci. Model Dev.*, 3, 519–551, doi:10.5194/gmd-3-519-2010, 2010.
- Mann, G. W., Carslaw, K. S., Ridley, D. A., Spracklen, D. V., Pringle, K. J., Merikanto, J., Korhonen, H., Schwarz, J. P., Lee, L. A., Manktelow, P. T., Woodhouse, M. T., Schmidt, A., Breider, T. J., Emmerson, K. M., Reddington, C. L., Chipperfield, M. P., and Pickering, S. J.: Intercomparison of modal and sectional aerosol microphysics representations within the same 3-D global chemical transport model, *Atmos. Chem. Phys.*, 12, 4449–4476, doi:10.5194/acp-12-4449-2012, 2012.
- Mann, G. W., Carslaw, K. S., Reddington, C. L., Pringle, K. J., Schulz, M., Asmi, A., Spracklen, D. V., Ridley, D. A., Woodhouse, M. T., Lee, L. A., Zhang, K., Ghan, S. J., Easter, R. C., Liu, X., Stier, P., Lee, Y. H., Adams, P. J., Tost, H., Lelieveld, J., Bauer, S. E., Tsigaridis, K., van Noije, T. P. C., Strunk, A., Vignati, E., Bellouin, N., Dalvi, M., Johnson, C. E., Bergman, T., Kokkola, H., von Salzen, K., Yu, F., Luo, G., Peltold, A., Heintzenberg, J., Clarke, A., Ogren, J. A., Gras, J., Baltensperger, U., Kaminski, U., Jennings, S. G., O’Dowd, C. D., Harrison, R. M., Beddows, D. C. S., Kulmala, M., Viisanen, Y., Ulevicius, V., Mihalopoulos, N., Zdimal, V., Fiebig, M., Hansson, H.-C., Swietlicki, E., and Henzing, J. S.: Intercomparison and evaluation of global aerosol microphysical properties among AeroCom models of a range of complexity, *Atmos. Chem. Phys.*, 14, 4679–4713, doi:10.5194/acp-14-4679-2014, 2014.

- Marmer, E., Langmann, B., Fagerli, H., and Vestreng, V.: Direct shortwave radiative forcing of sulfate aerosol over Europe from 1900 to 2000, *J. Geophys. Res.*, 112, D23S17, doi:10.1029/2006JD008037, 2007.
- Morgenstern, O., Braesicke, P., O'Connor, F. M., Bushell, A. C., Johnson, C. E., Osprey, S. M., and Pyle, J. A.: Evaluation of the new UKCA climate-composition model – Part 1: The stratosphere, *Geosci. Model Dev.*, 2, 43–57, doi:10.5194/gmd-2-43-2009, 2009.
- Myhre, G., Shindell, D., Breon, F.-M., Collins, W., Fuglestvedt, J., Huang, J., Koch, D., Lamarque, J.-F., Lee, D., Mendoza, B., Nakajima, T., Robock, A., Stephens, G., Takemura, T., and Zhang, H.: Anthropogenic and Natural Radiative Forcing, in: *Climate Change 2013: The Physical Science Basis. Contribution of Working Group I to the Fifth Assessment Report of the Intergovernmental Panel on Climate Change*, Cambridge University Press, Cambridge, United Kingdom and New York, NY, USA, 2013.
- O'Connor, F. M., Johnson, C. E., Morgenstern, O., Abraham, N. L., Braesicke, P., Dalvi, M., Folberth, G. A., Sanderson, M. G., Telford, P. J., Voulgarakis, A., Young, P. J., Zeng, G., Collins, W. J., and Pyle, J. A.: Evaluation of the new UKCA climate-composition model – Part 2: The Troposphere, *Geosci. Model Dev.*, 7, 41–91, doi:10.5194/gmd-7-41-2014, 2014.
- Penner, J. E., Prather, M. J., Isaksen, I. S. a., Fuglestvedt, J. S., Klimont, Z., and Stevenson, D. S.: Short-lived uncertainty?, *Nat. Geosci.*, 3, 587–588, doi:10.1038/ngeo932, 2010.
- Philipona, R., Behrens, K., and Ruckstuhl, C.: How declining aerosols and rising greenhouse gases forced rapid warming in Europe since the 1980s, *Geophys. Res. Lett.*, 36, L02806, doi:10.1029/2008GL036350, 2009.
- Pozzer, A., de Meij, A., Pringle, K. J., Tost, H., Doering, U. M., van Aardenne, J., and Lelieveld, J.: Distributions and regional budgets of aerosols and their precursors simulated with the EMAC chemistry-climate model, *Atmos. Chem. Phys.*, 12, 961–987, doi:10.5194/acp-12-961-2012, 2012.
- Ramanathan, V. and Feng, Y.: Air pollution, greenhouse gases and climate change: Global and regional perspectives, *Atmos. Environ.*, 43, 37–50, doi:10.1016/j.atmosenv.2008.09.063, 2009.
- Sanchez-Lorenzo, A., Wild, M., and Trentmann, J.: Validation and stability assessment of the monthly mean CM SAF surface solar radiation dataset over Europe against a homogenized surface dataset (1983–2005), *Remote Sens. Environ.*, 134, 355–366, doi:10.1016/j.rse.2013.03.012, 2013.
- Schultz, M. G., Heil, A., Hoelzemann, J. J., Spessa, A., Thonicke, K., Goldammer, J. G., Held, A. C., Pereira, J. M. C., and van het Bolscher, M.: Global wildland fire emissions from 1960 to 2000, *Global Biogeochem. Cy.*, 22, GB2002, doi:10.1029/2007GB003031, 2008.
- Scott, C. E., Rap, A., Spracklen, D. V., Forster, P. M., Carslaw, K. S., Mann, G. W., Pringle, K. J., Kivekäs, N., Kulmala, M., Lihavainen, H., and Tunved, P.: The direct and indirect radiative effects of biogenic secondary organic aerosol, *Atmos. Chem. Phys.*, 14, 447–470, doi:10.5194/acp-14-447-2014, 2014.
- Shindell, D. T., Lamarque, J.-F., Schulz, M., Flanner, M., Jiao, C., Chin, M., Young, P. J., Lee, Y. H., Rotstayn, L., Mahowald, N., Milly, G., Faluvegi, G., Balkanski, Y., Collins, W. J., Conley, A. J., Dalsoren, S., Easter, R., Ghan, S., Horowitz, L., Liu, X., Myhre, G., Nagashima, T., Naik, V., Rumbold, S. T., Skeie, R., Sudo, K., Szopa, S., Takemura, T., Voulgarakis, A., Yoon, J.-H., and Lo, F.: Radiative forcing in the ACCMIP historical and future climate simulations, *Atmos. Chem. Phys.*, 13, 2939–2974, doi:10.5194/acp-13-2939-2013, 2013.
- Skeie, R. B., Berntsen, T. K., Myhre, G., Tanaka, K., Kvalevåg, M. M., and Hoyle, C. R.: Anthropogenic radiative forcing time series from pre-industrial times until 2010, *Atmos. Chem. Phys.*, 11, 11827–11857, doi:10.5194/acp-11-11827-2011, 2011.
- Smith, S. J., van Aardenne, J., Klimont, Z., Andres, R. J., Volke, A., and Delgado Arias, S.: Anthropogenic sulfur dioxide emissions: 1850–2005, *Atmos. Chem. Phys.*, 11, 1101–1116, doi:10.5194/acp-11-1101-2011, 2011.
- Spracklen, D. V., Carslaw, K. S., Kulmala, M., Kerminen, V.-M., Mann, G. W., and Sihto, S.-L.: The contribution of boundary layer nucleation events to total particle concentrations on regional and global scales, *Atmos. Chem. Phys.*, 6, 5631–5648, doi:10.5194/acp-6-5631-2006, 2006.
- Spracklen, D. V., Jimenez, J. L., Carslaw, K. S., Worsnop, D. R., Evans, M. J., Mann, G. W., Zhang, Q., Canagaratna, M. R., Allan, J., Coe, H., McFiggans, G., Rap, A., and Forster, P.: Aerosol mass spectrometer constraint on the global secondary organic aerosol budget, *Atmos. Chem. Phys.*, 11, 12109–12136, doi:10.5194/acp-11-12109-2011, 2011.
- Tørseth, K., Aas, W., Breivik, K., Fjæraa, A. M., Fiebig, M., Hjellbrekke, A. G., Lund Myhre, C., Solberg, S., and Yttri, K. E.: Introduction to the European Monitoring and Evaluation Programme (EMEP) and observed atmospheric composition change during 1972–2009, *Atmos. Chem. Phys.*, 12, 5447–5481, doi:10.5194/acp-12-5447-2012, 2012.
- Tsigaridis, K., Daskalakis, N., Kanakidou, M., Adams, P. J., Artaxo, P., Bahadur, R., Balkanski, Y., Bauer, S. E., Bellouin, N., Benedetti, A., Bergman, T., Berntsen, T. K., Beukes, J. P., Bian, H., Carslaw, K. S., Chin, M., Curci, G., Diehl, T., Easter, R. C., Ghan, S. J., Gong, S. L., Hodzic, A., Hoyle, C. R., Iversen, T., Jathar, S., Jimenez, J. L., Kaiser, J. W., Kirkevåg, A., Koch, D., Kokkola, H., Lee, Y. H., Lin, G., Liu, X., Luo, G., Ma, X., Mann, G. W., Mihalopoulos, N., Morcrette, J.-J., Müller, J.-F., Myhre, G., Myriokefalitakis, S., Ng, N. L., O'Donnell, D., Penner, J. E., Pozzoli, L., Pringle, K. J., Russell, L. M., Schulz, M., Sciare, J., Seland, Ø., Shindell, D. T., Sillman, S., Skeie, R. B., Spracklen, D., Stavroukou, T., Steenrod, S. D., Takemura, T., Tittia, P., Tilmes, S., Tost, H., van Noije, T., van Zyl, P. G., von Salzen, K., Yu, F., Wang, Z., Wang, Z., Zaveri, R. A., Zhang, H., Zhang, K., Zhang, Q., and Zhang, X.: The AeroCom evaluation and intercomparison of organic aerosol in global models, *Atmos. Chem. Phys.*, 14, 10845–10895, doi:10.5194/acp-14-10845-2014, 2014.
- Uppala, S. M., Kållberg, P. W., Simmons, A. J., Andrae, U., Bechtold, V. D. C., Fiorino, M., Gibson, J. K., Haseler, J., Hernandez, A., Kelly, G. A., Li, X., Onogi, K., Saarinen, S., Sokka, N., Allan, R. P., Andersson, E., Arpe, K., Balmaseda, M. A., Beljaars, A. C. M., Berg, L. V. D., Bidlot, J., Bormann, N., Caires, S., Chevallier, F., Dethof, A., Dragosavac, M., Fisher, M., Fuentes, M., Hagemann, S., Hólm, E., Hoskins, B. J., Isaksen, I., Janssen, P. A. E. M., Jenne, R., McNally, A. P., Mahfouf, J.-F., Morcrette, J.-J., Rayner, N. A., Saunders, R. W., Simon, P., Sterl, A., Trenberth, K. E., Untch, A., Vasiljevic, D., Viterbo, P., and Woollen, J.: The ERA-40 re-analysis, *Q. J. Roy. Meteor. Soc.*, 131, 2961–3012, doi:10.1256/qj.04.176, 2005.

- Vestreng, V., Myhre, G., Fagerli, H., Reis, S., and Tarrasón, L.: Twenty-five years of continuous sulphur dioxide emission reduction in Europe, *Atmos. Chem. Phys.*, 7, 3663–3681, doi:10.5194/acp-7-3663-2007, 2007.
- Volkamer, R., Jimenez, J. L., San Martini, F., Dzepina, K., Zhang, Q., Salcedo, D., Molina, L. T., Worsnop, D. R., and Molina, M. J.: Secondary organic aerosol formation from anthropogenic air pollution: Rapid and higher than expected, *Geophys. Res. Lett.*, 33, L17811, doi:10.1029/2006GL026899, 2006.
- Walters, D. N., Best, M. J., Bushell, A. C., Copsey, D., Edwards, J. M., Falloon, P. D., Harris, C. M., Lock, A. P., Manners, J. C., Morcrette, C. J., Roberts, M. J., Stratton, R. A., Webster, S., Wilkinson, J. M., Willett, M. R., Boutle, I. A., Earnshaw, P. D., Hill, P. G., MacLachlan, C., Martin, G. M., Moufouma-Okia, W., Palmer, M. D., Petch, J. C., Rooney, G. G., Scaife, A. A., and Williams, K. D.: The Met Office Unified Model Global Atmosphere 3.0/3.1 and JULES Global Land 3.0/3.1 configurations, *Geosci. Model Dev.*, 4, 919–941, doi:10.5194/gmd-4-919-2011, 2011.
- Wild, M.: Global dimming and brightening: A review, *J. Geophys. Res.*, 114, D00D16, doi:10.1029/2008JD011470, 2009.
- Wild, O., Zhu, X., and Prather, M. J.: Fast-J: Accurate Simulation of In- and Below-Cloud Photolysis in Tropospheric Chemical Models, *J. Atmos. Chem.*, 37, 245–282, doi:10.1023/A:1006415919030, 2000.
- Woodward, S.: Modeling the atmospheric life cycle and radiative impact of mineral dust in the Hadley Centre climate model, *J. Geophys. Res.*, 106, 18155, doi:10.1029/2000JD900795, 2001.
- Yu, H., Kaufman, Y. J., Chin, M., Feingold, G., Remer, L. A., Anderson, T. L., Balkanski, Y., Bellouin, N., Boucher, O., Christopher, S., DeCola, P., Kahn, R., Koch, D., Loeb, N., Reddy, M. S., Schulz, M., Takemura, T., and Zhou, M.: A review of measurement-based assessments of the aerosol direct radiative effect and forcing, *Atmos. Chem. Phys.*, 6, 613–666, doi:10.5194/acp-6-613-2006, 2006.

## **Chapter 4**

### **The spatial and temporal importance of pH to sulphate aerosols and radiative forcing over the period 1960 to 2009**

## **The Spatial and Temporal Importance of cloud water pH to Global Sulphate Aerosols and their Radiative Effect over the Period 1960 to 2009**

**S. T. Turnock<sup>1†</sup>, G. W. Mann<sup>1,2</sup>, M. T. Woodhouse<sup>3</sup>, K. S. Carslaw<sup>1</sup> and D. V. Spracklen<sup>1</sup>**

<sup>1</sup>Institute of Climate and Atmospheric Science, School of Earth and Environment, University of Leeds, Leeds, UK.

<sup>2</sup>National Centre for Atmospheric Science, University of Leeds, Leeds, UK.

<sup>3</sup>CSIRO Ocean and Atmosphere, Aspendale, Victoria, Australia.

Corresponding author: Steven Turnock (steven.turnock@metoffice.gov.uk)

† Now at Met Office Hadley Centre, Fitzroy Road, Exeter, UK.

### **Key Points:**

- Cloud water pH can affect the ability to reproduce both changes in sulphate aerosol mass and its aerosol radiative effects over different spatial and temporal scales
- The comparison of simulated and observed sulphate and sulphur dioxide mass concentrations over Europe is improved by increasing cloud water pH
- Aerosol radiative forcing between 1970 and 2009 can vary over regions by up to a factor of 5 depending on the choice of pH at the start and end points

## **Abstract**

Sulphate is a major component of fine particulate matter. In-cloud aqueous phase oxidation with ozone is one of the principal routes to sulphate aerosol formation, which is strongly dependent on cloud water pH. Here the sensitivity of sulphate formation to cloud water pH and its implications for aerosol radiative effects are explored over the period 1970 to 2009. The mass of sulphate aerosol reduces at a global scale, but increases by 20% over regions with large SO<sub>2</sub> emissions. Global cloud condensation nuclei concentrations reduce by ~50%. The aerosol radiative forcing between 1970 and 2009 varies by a factor of 5 and changes from +6.9 to -4.6 Wm<sup>-2</sup> over the North Atlantic depending on whether an increase or decrease in pH is assumed. Global composition climate models should calculate a spatially and temporally varying cloud water pH to improve the representation of aerosol radiative effects over recent decades.

## **4.1 Introduction**

Sulphate is a major component of the fine aerosol mass, comprising 32% of the submicron particle mass over much of the world (Zhang et al., 2007). It contributes to problems such as reduced visibility, acidic deposition, poor air quality and impacts on human health. Sulphate is largely present in the fine size fraction of aerosols (less than 2.5 microns) where it can interact both directly and indirectly (via the modification of cloud microphysical properties) with the Earth's radiative balance, leading to a large, but uncertain, cooling effect on climate (IPCC, 2013). Accurate quantification of sulphate formation over different spatial and temporal scales is therefore important to be able to quantify impacts on both air quality and climate.

Sulphate aerosol is produced from the oxidation of sulphur dioxide (SO<sub>2</sub>) via gas-phase reactions with the hydroxyl radical (OH) or by aqueous phase reactions in cloud droplets with hydrogen peroxide (H<sub>2</sub>O<sub>2</sub>), ozone (O<sub>3</sub>), O<sub>2</sub> plus transition metal ion catalysts and other oxidants (Seinfeld & Pandis, 2006; Harris et al., 2013; Ervens, 2015 and references within). Globally aqueous phase oxidation is the dominant pathway to sulphate formation with 60-80% of tropospheric sulphate formed through this way compared to 15 – 35% from gas phase oxidation (Chin et al., 1996; Barth et al., 2000; Roelofs et al., 2001; Faloon, 2009). The largest uncertainties in modelling in-cloud sulphate formation tend not to come from the chemical mechanism but depend on the predicted cloud properties such as the liquid water content,

cloud processing time and precipitation rates (wet deposition), which also impact on the aerosol size distribution/composition and availability of oxidants (Pandis & Seinfeld, 1989; Rasch et al., 2000).

The rate of in-cloud dissolution and subsequent aqueous phase reactions of  $\text{SO}_2$  are dependent on the pH of the cloud water, which is determined by the balance of dissolved acids (sulfuric, nitric and carbonic) and bases (ammonia and base cations from sea salt aerosol or mineral dust). The oxidation rate of S(IV) by  $\text{H}_2\text{O}_2$  is approximately independent of pH and is the preferential pathway at a pH <5.5. Conversely, the oxidation rate of S(IV) by  $\text{O}_3$  is highly sensitive to pH and is the preferential pathway for pH >5.5 (Seinfeld & Pandis, 2006). Increasing the pH by 1 unit can increase the oxidation reaction rate of S(IV) with  $\text{O}_3$  by a factor of 100 (Kreidenweis, 2003).

Cloud water pH is highly variable in space and time. Low cloud water pH tends to be associated with smaller particles that are mainly acidic in nature (e.g. sulphate), whereas larger particles tend to have higher pH due to the presence of carbonates from mineral dust or sea salt (Gurciullo & Pandis, 1997). Consistent observations of cloud water pH are restricted to a few locations with limited temporal trends. The observed values of cloud water pH vary from 3 to 7 across coastal marine environments and continental areas of USA, Europe, China and India (Collett et al., 1993; Plessow et al., 2001; Aleksic et al., 2009; Sun et al., 2010; Benedict et al., 2012; Murray et al., 2013; Budhavant et al., 2014). Since the mid-1980s observed cloud water pH increased from 4 to ~5 in the north eastern United States due to reductions in emissions of acidifying gases, as a result of the Clean Air Act (Aleksic et al., 2009; Murray et al., 2013; Schwab et al., 2016).

There are substantially more measurements of rainwater pH. The trend in observed rainwater pH is anticipated to correlate with that of cloud water but rainwater tends to be more dilute and therefore less acidic due to different cloud scavenging efficiencies and the rate of chemical reactions (Collett et al., 1993; Aleksic et al., 2009). Rodhe et al., (2002) used a global chemical transport model to show the spatial variability of pH in precipitation, with lowest values (pH 4-5) occurring in the polluted continental regions of the world and higher values (pH >6) over dust source regions and marine locations. A review by Vet et al., (2014) summarised rainwater pH observations from around the globe and reported that over Europe and North America values have increased by >0.5 pH units since the 1980s due to reductions in anthropogenic emissions of  $\text{SO}_2$ . It is reasonable to assume

that a similar change in cloud water pH would also have occurred over these regions, which could have important consequences for the formation of sulphate aerosols.

The treatment of in-cloud aqueous phase sulphate formation varies between global models from those using a fixed pH to those explicitly calculating the pH of different sized cloud droplets (Fahey, 2003; Ervens, 2015; Table A1). The results from the multi-model Comparison of large-scale atmospheric sulphate aerosol models (COSAM) project highlighted the importance of accurately representing the value of cloud water pH for aqueous phase formation of sulphate aerosols in global models (Barrie et al., 2001; Lohmann et al., 2001; Roelofs et al., 2001). Over the UK and Germany, increasing the fixed value of pH from 5 to 5.5-5.8 in two models was shown to improve the comparison of simulated sulphate mass with observations (Redington et al., 2009; Banzhaf et al., 2012). The underrepresentation of in-cloud aqueous phase sulphate formation has been previously identified as a possible reason for some of the modelled underestimation of observed sulphate mass and overestimation of SO<sub>2</sub> concentrations across regions like Europe, which are important in simulating particulate air quality (Feichter et al., 1996; Kasibhatla et al., 1997; Roelofs et al., 2001; Berglen, 2004; Textor et al., 2006).

The optical properties of aerosols and the cloud droplet number concentrations can be affected by the different cloud droplet schemes used within models, which can lead to uncertainties in the aerosol radiative effects (Kreidenweis, 2003; Roelofs et al., 2006). Cloud droplet pH was found to be the third most important parameter controlling CCN uncertainty in winter, especially across the northern mid-latitudes (Lee et al., 2013). It is important to understand how processes such as cloud water pH have varied over the industrial period to properly quantify the effect of this on cloud albedo radiative forcing, as the uncertainty could be larger if their pre-industrial baseline state and changes occurring from it are not properly accounted for (Carslaw et al., 2013; Regayre et al., 2014).

It is therefore important to consider the spatial and temporal effect of changes in cloud water pH on sulphate aerosol formation and ultimately their radiative effects over recent decades, especially for regions such as Europe and Asia where large changes in SO<sub>2</sub> emissions, and consequently acidity, have occurred. Here we test the sensitivity of aqueous phase sulphate formation to changes in pH over a 50 year time period in a global composition climate model. The analysis shows that changes to sulphate

and the aerosol size distribution from an increase in pH can lead to large differences in aerosol radiative effects between 1970 and 2009.

## **4.2 Materials and Methods**

### **4.2.1 HadGEM3-UKCA composition-climate model**

The global composition-climate model HadGM3-UKCA, as described in Turnock et al. (2015), is used to simulate aerosol processes and their impact on the radiative balance. The model was used in atmosphere-only mode and nudged to the European Centre for Medium-Range Weather Forecasts (ECMWF) reanalysis. Monthly 3D aerosol, gas-phase and radiation fields were output at a horizontal resolution of 1.875 x 1.25 (~140 km at mid latitudes) with 63 levels in the vertical (~40 km). The model includes a comprehensive tropospheric chemistry scheme with additional reactions involving sulphur, monoterpenes and isoprene (Spracklen et al., 2006; Mann et al., 2010; O'Connor et al., 2014; Scott et al., 2014).

The modal aerosol scheme of the Global Model of Aerosol Processes (GLOMAP-mode) is used within this version of HadGEM3-UKCA (Mann et al., 2010). GLOMAP-mode simulates the evolution of size-resolved number and mass of sulphate, black carbon, particulate organic matter and sea salt aerosol components across the nucleation, Aitken, accumulation and coarse modes. Ammonium nitrate is not represented in this version of the model. Dust aerosol mass concentrations are calculated using a 6-bin scheme (Woodward, 2001).

Natural aerosol emissions are calculated using interactive parameterizations or monthly mean emission fields of sea-salt, volcanoes and dimethyl sulphide. Anthropogenic emissions of CO, SO<sub>2</sub>, NO<sub>x</sub>, Organic Carbon and Black Carbon are provided at a 0.5 by 0.5 horizontal resolution from the MACCity inventory (Granier et al., 2011).

The Edwards & Slingo (1996) radiation code within HadGEM3-UKCA has been used to calculate the changes to the Earth's radiative balance from the differences in aerosols. A 'double-call' radiation configuration has been used to diagnose the aerosol radiative effect (ARE) from aerosol radiation interactions (ari, direct effect) and aerosol cloud interactions (aci, 1<sup>st</sup> indirect effect); that is the difference between a radiation call with aerosol fields included and an aerosol free atmosphere (Bellouin et al., 2013; Turnock et al., 2015). The change in ARE is the difference between calculated ARE in two different simulations. Aerosol radiative forcings (ARF) are defined here

as the difference between ARE in 1970 and 2009. Feedbacks onto the meteorology are not permitted in the 'double-call' set up and therefore rapid adjustments to clouds and the atmosphere from changes in aerosols are not accounted for.

This model version has been previously evaluated against long term European observations of aerosols (see Turnock et al. 2015). Turnock et al. (2015) showed that the model was able to reproduce the observed trends in sulphate aerosol mass over the period 1978 to 2009. However, the model consistently underestimated winter time sulphate mass, particularly over northern Europe, which could be potentially due to enhanced removal processes (e.g. wet deposition) or an under-prediction in formation mechanisms. As the model bias was particularly strong over northern Europe in wintertime when oxidants (especially  $H_2O_2$ ) are limited, it was hypothesized that sulphate aerosol formation through in-cloud oxidation of  $SO_2$  with  $O_3$  was under-represented. The model evaluation will be further explored in this study by comparing additional simulations using different pH against observations of sulphate aerosol mass and sulphur dioxide concentrations (in accordance with Turnock et al., 2015).

#### 4.2.2 Sulphate aerosol formation in HadGEM3-UKCA

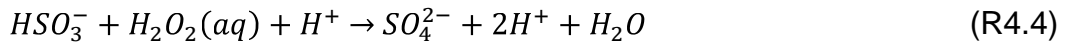
Sulphate aerosols can be formed in the gas phase by  $SO_2$  reacting with the hydroxyl radical to form sulfuric acid vapour:



The aerosol processes of condensation and nucleation compete for the available sulfuric acid vapour to form secondary aerosol particles (via reaction with ammonia), increasing the aerosol number concentration. Globally nucleation tends to account for a lower amount of sulphate aerosol but is preferential in the free troposphere, leading to the formation of more numerous smaller sized particles.

When low level clouds are present, aqueous phase oxidation of sulphur dioxide can occur through reaction with  $H_2O_2$  and  $O_3$ , accounting for the majority of sulphate aerosol mass formed in the troposphere. In HadGEM3-UKCA sulphur dioxide first dissolves in cloud droplets using a Henry's law equilibrium approach. A grid box is defined as having low level clouds present if the cloud liquid water content exceeds  $0.2 \text{ g m}^{-3}$ , that of typical

stratocumulus clouds.  $\text{SO}_2$  dissolves in cloud water to form the  $\text{HSO}_3^-$  species, which can also further dissociate to  $\text{SO}_3^{2-}$ . Both these species can lead to sulphate aerosol formation via the following oxidation reactions:



The sulphate aerosol mass produced from the in-cloud oxidation pathways is partitioned into the soluble accumulation and coarse modes of the modal aerosol size distribution according to the ratio of their respective number concentrations to their sum. This produces sulphate particles of larger sizes and with more mass.

### 4.2.3 Simulations

We completed two simulations over the period 1960 to 2009. A baseline simulation (identified here as pH 5.0) used a cloud water pH of 5.0. This is the standard cloud water pH used within HadGEM3-UKCA and uses a fixed value similar to other global climate models to represent the pH of bulk cloud droplets (see Table S1). An additional simulation (identified here as pH 6.5) was conducted where the cloud water pH was changed to pH 6.5 to explore the sensitivity of in-cloud sulphate formation to pH and its impact on aerosol radiative effects over recent decades. The value of pH 6.5 was chosen based on the upper range of values (obtained by an expert elicitation and literature search) used within the analysis by Lee et al., (2013), which found that droplet pH is the third most important parameter controlling CCN uncertainty, particularly in the northern hemisphere winter.

## 4.3 Results and Discussions

### 4.3.1 Sulphate Formation

The calculated global burdens of  $\text{SO}_2$ , sulphate and gas phase  $\text{H}_2\text{SO}_4$  are shown in Table A2 and are within the range of those calculated for other model studies (Spracklen et al., 2005a; Berglen, 2004; Textor et al., 2006; Mann et al., 2010). Figure 4.1 shows the impact of increasing cloud water pH on column burdens of  $\text{SO}_2$  and sulphate aerosol mass concentrations. An increase in cloud water pH causes a ~66% reduction in the global  $\text{SO}_2$  burden (Fig. 4.1a and Table A2) as more  $\text{SO}_2$  is oxidized through reactions R4.4 and R4.5. The largest absolute reductions occur over regions that have

the largest anthropogenic emissions of  $\text{SO}_2$  e.g. Europe, North America and East Asia.

The sulphate aerosol mass burden increases by ~20% over Europe, North America and East Asia with increased cloud water pH. Over these regions oxidants tend to be limited, particularly  $\text{H}_2\text{O}_2$  in winter (Berglen, 2004). Increasing cloud water pH favours sulphate formation via in-cloud oxidation by  $\text{O}_3$  and leads to the large increase in sulphate aerosol mass (Fig. 1b), especially in winter (Fig. A1) when  $\text{O}_3$  is not as limited as  $\text{H}_2\text{O}_2$ .

However, in other areas of the world the sulphate aerosol mass burden reduces with an increase in cloud water pH. The global sulphate aerosol mass burden reduces by ~30% (Table A2). An increase in sulphate aerosol mass occurs within the lowest few kilometres of the atmosphere (Fig. A2) due to the presence of low clouds that facilitate aqueous phase oxidation reactions.  $\text{SO}_2$  is depleted at these altitudes by reactions R4.5 and R4.6 and less is available to form sulphate via gas-phase oxidation (R4.1), as indicated by the reductions in gas phase  $\text{H}_2\text{SO}_4$  (Fig. A3) and the fluxes of nucleation and condensation within the global sulphur budget (Table A3). Additionally, the global atmospheric lifetime of sulphate reduces from an increase in cloud water pH. Enhanced sulphate deposition rates result from the increased in-cloud formation of larger sulphate particles within the accumulation and coarse modes that are more efficiently removed from the atmosphere by wet deposition. The increase in cloud water pH reduces the global sulphate mass burden but increases it over regions where  $\text{SO}_2$  concentrations are high enough that enhanced production outweighs loss.

A time series of the difference in  $\text{SO}_2$  and sulphate mass burdens between the two pH simulations across four regions is shown in Figure 4.1c and 4.1d. The increase in cloud water pH causes the largest increase in sulphate mass burden to occur in the 1970s-80s over Europe and north eastern United States. Whereas, over China the increase in cloud water pH results in the largest increase in sulphate mass burden in the 2000s. These regional differences reflect the relative changes in anthropogenic emissions of  $\text{SO}_2$  (decreases in emissions over Europe and north eastern United States and an increase over China) and the regional impact on sulphate formation when pH is increased.

The value of cloud water pH used is important when simulating the  $\text{SO}_2$  and sulphate mass concentrations and their impacts on air quality and climate across different regions and time periods. Aqueous phase sulphate formation across industrialized regions such as Europe is particularly

sensitive to changes in cloud water pH due to the elevated  $\text{SO}_2$  concentrations and seasonal limitation in oxidants.

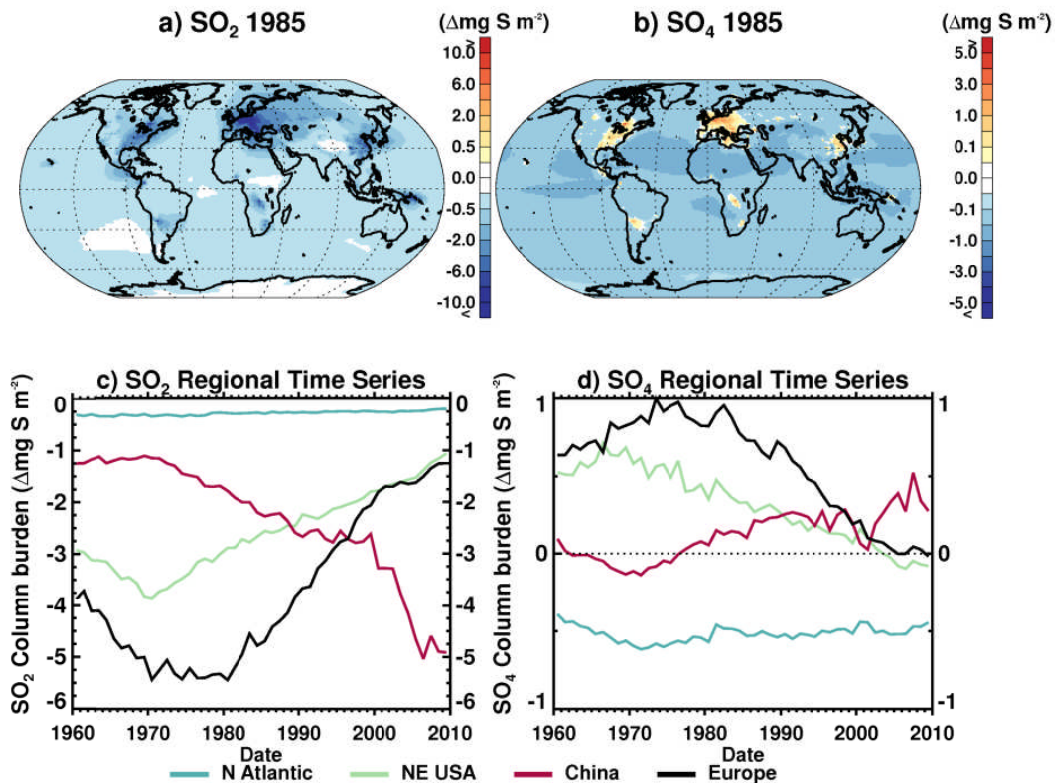


**Figure 4.1** Differences between the pH 6.5 and pH 5.0 simulations in column mass burdens of a) sulphur dioxide ( $\text{SO}_2$ ) and b) sulphate aerosol ( $\text{SO}_4^{2-}$ ) for the mid-year of the period, 1985. The temporal evolution of the difference in regional column burdens for c)  $\text{SO}_2$  and d)  $\text{SO}_4$  over the North Atlantic, NE USA, China and European regions, as defined in Figure A4.

### 4.3.2 Model Evaluation

Here we use long term observations across Europe from the EMEP network over the period 1978 - 2009 to evaluate ground level sulphate aerosol and sulphur dioxide mass concentrations from both the pH 5.0 and pH 6.5 simulations. Figure 4.2 compares the simulated and observed sulphate aerosol mass concentrations over the period 1978 to 2009. The increase in cloud water pH from 5.0 to 6.5 improves the simulated sulphate trends in winter but slightly overestimates the annual mean and summer trends at the majority of EMEP measurement locations (Fig. 4.2a and 4.2b). Similarly an increase in cloud water pH improves the comparison of simulated sulphate aerosol mass against observations in winter (lower model bias), although simulated values in summer are slightly overestimated (Fig. 4.2c and 4.2d).

A similar comparison has been undertaken for simulated and observed values of sulphur dioxide in Figure A5. An increase in cloud water pH from 5.0 to 6.5 reduces the overestimation of simulated  $\text{SO}_2$  concentrations when

compared to observations at sites across Europe for all years in both winter and summer.

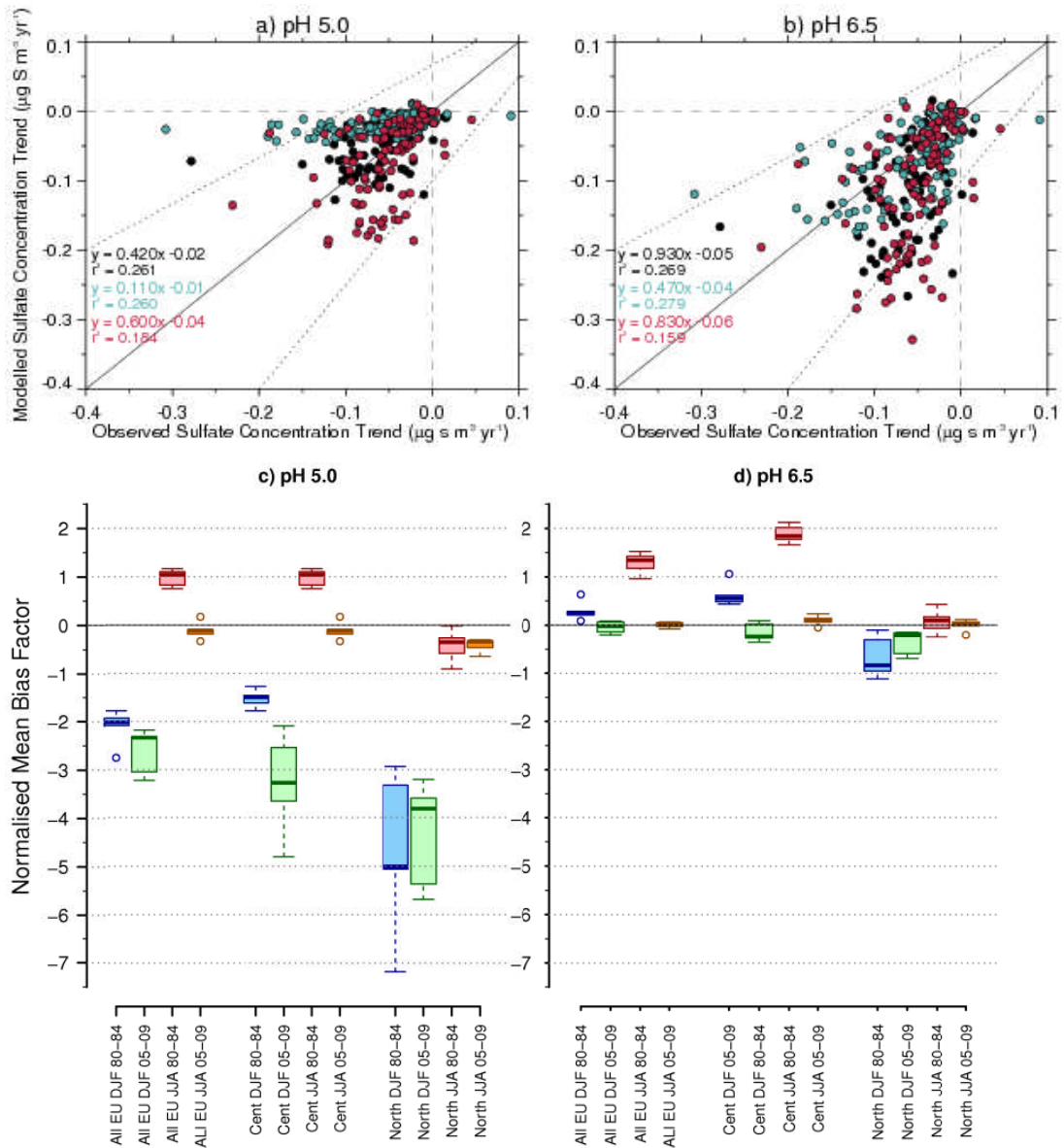


**Figure 4.2** Model evaluation of sulphate aerosol mass concentrations across Europe over the period 1978 to 2009. Annual (black), summertime (JJA, red) and wintertime (DJF, blue) trends in modelled and observed sulphate mass concentrations at each EMEP station for a) pH 5.0 and b) pH 6.5 simulations. European normalized mean bias factors for sulphate aerosol concentrations over the period 1980-1984 and 2005-2009 in summertime (JJA, red (80-84) and orange (05-09)) and wintertime (DJF, blue (80-84) and green (05-09)) in c) pH 5.0 and d) pH 6.5 simulations. Central and north regions of Europe are as defined in Turnock et al. (2015).

The potential impact of a time varying cloud water pH is investigated by comparing simulated sulphate mass concentrations using pH 5.0 and pH 6.5 against observed values at different monitoring sites for two time periods of 1980-84 and 2005-09 (Fig. 4.2c – d and Fig. A6). In the 1980s simulated winter time sulphate mass using pH 5.0 generally compares better (lower

bias factor) against observations than in 2005-09 whereas, using pH 6.5 the simulated concentrations in 2005-09 are more representative of observations than in 1980-84.

This evaluation indicates the importance of accurately representing the in-cloud formation of sulphate aerosol for regions like Europe where a change in cloud water pH can dramatically affect the ability of the model to reproduce observations and also regional particulate air quality. In particular, accounting for temporal changes in cloud water pH is important to improve the comparison of simulated changes in SO<sub>2</sub> and sulphate to observations.

### **4.3.3 Climate Implications**

The increase in cloud water pH and subsequent change in sulphate aerosol formation also modifies the aerosol number concentration and size distribution, which alters the climate relevant properties of aerosols. The increase in pH causes a reduction in the number concentration of particles of all sizes, with largest reductions in the smaller particles (Fig. 4.3a - b). Globally the total number concentration of particles (N total) reduces by 39%, and by 27% for particles larger than 100 nm diameter (N100). The change in the aerosol size distributions for Europe, NE USA, China and North Atlantic indicate that the increase in cloud water pH reduces the number of smaller particles and increases the number of larger ones over these regions (Fig. 4.3c - d). These changes occur because of the increased amount of sulphate mass in the accumulation and coarse modes and a reduction in aerosol nucleation and condensational growth (Table A3). This shift in the aerosol size distribution to larger sizes reduces the number of particles able to act as CCN by ~50% over some areas (Fig. A7).

The difference in the top of atmosphere (TOA) all-sky and clear-sky shortwave ARE due to the increase in cloud water pH from 5.0 to 6.5 is shown in Figures 4.4a and 4.4b. Under all-sky conditions (considering both ari and aci effects) the increase in cloud water pH causes a positive change in the ARE over the majority of the globe. The decrease in the number of smaller particles (Fig. 4.3), CCN concentrations (Fig. A7) and also therefore cloud droplet number (CDN) concentrations from the increase in pH have reduced the magnitude of the aerosol cloud albedo effect. The global annual mean all-sky ARE at the TOA increases by 2.4 W m<sup>-2</sup> in 1985, with the largest increase of 5.8 W m<sup>-2</sup> occurring over the North Atlantic region. The largest regional increase in the all-sky ARE occurs over the north Atlantic as CCN and CDN concentrations are initially lower, which makes the cloud albedo effect particularly susceptible to any increase in them. In addition,

large relative changes in CCN and CDN concentrations also occur over this region (Fig. A7), which in combination with the high susceptibility of the region results in a large change to their cloud albedo radiative effect.

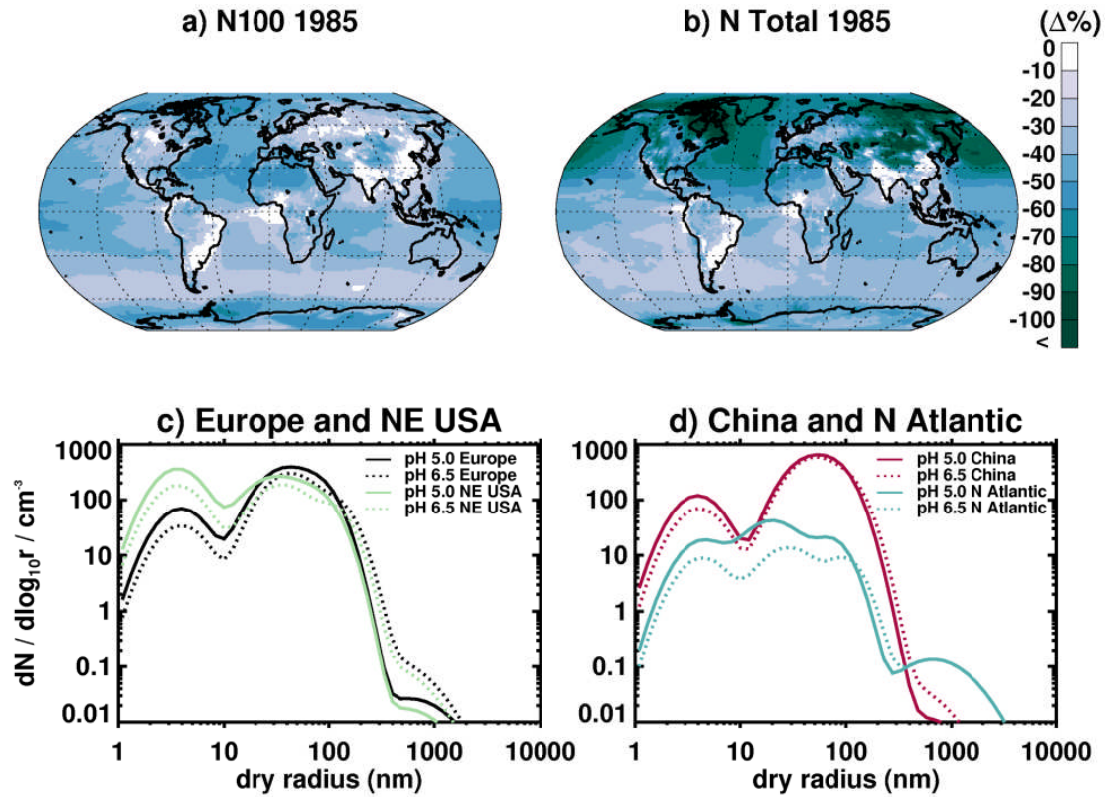


**Figure 4.3** Percentage difference between pH 6.5 and pH 5.0 simulations for 1985 (mid-year of the period) in surface number concentrations of particles with a dry diameter larger than a) 100 nm (N100) and b) all sizes (N Total). Surface aerosol number size distributions in 1985 averaged across the regions c) Europe (black) and NE USA (pale green), and d) China (red) and North Atlantic (blue), as defined in Figure S4. Solid and dashed lines show the simulated aerosol size distribution using a pH of 5.0 and 6.5 respectively.

An increase in cloud water pH causes a negative change in the clear-sky ARE of  $1.7 \text{ W m}^{-2}$  over Europe,  $0.8 \text{ W m}^{-2}$  over NE USA and  $0.6 \text{ W m}^{-2}$  over China in 1985 due to the larger sulphate mass concentrations over these regions in the pH 6.5 simulations. These changes reduce in magnitude from 1985 to 2009 across Europe and NE USA but increase across China, corresponding with the temporal change in sulphate aerosol mass and also anthropogenic emissions of  $\text{SO}_2$  across these regions (Fig 4.1b). Small positive changes in clear-sky ARE occur in other areas of the world due to the slight reduction in sulphate aerosol mass in the atmospheric column (Fig. 4.1b).

We calculate the ARF as the difference in ARE between 1970 and 2009 for all-sky and clear-sky conditions (Fig. 4.4c and 4.4d). The global all-sky ARF is  $+0.4 \text{ W m}^{-2}$  in the pH 5.0 simulation and only slightly lower ( $+0.3 \text{ W m}^{-2}$ ) in

the pH 6.5 simulation (Table A4). This means that the aerosol forcing is essentially independent of cloud water pH, provided that the pH remains constant in both time periods. To explore the potential impact of a time varying cloud water pH on simulated ARF we calculate the difference between ARE in 2009 with a pH of 6.5 to those in 1970 with a pH of 5.0. This scenario considers an increase in cloud water pH of 1.5 units from 1970 to 2009 and results in a global all-sky ARF of  $+2.7 \text{ W m}^{-2}$ . In contrast, a decrease in pH between 1970 (pH 6.5) and 2009 (pH 5.0) results in a global all-sky ARF of  $-2.0 \text{ W m}^{-2}$ . However, applying a global 1.5 unit change in pH is unlikely but relatively large changes in pH are observed at a regional scale (e.g. USA and Europe; Aleksic et al., (2009); Murray et al., (2013); Vet et al., (2014); Schwab, (2016)).

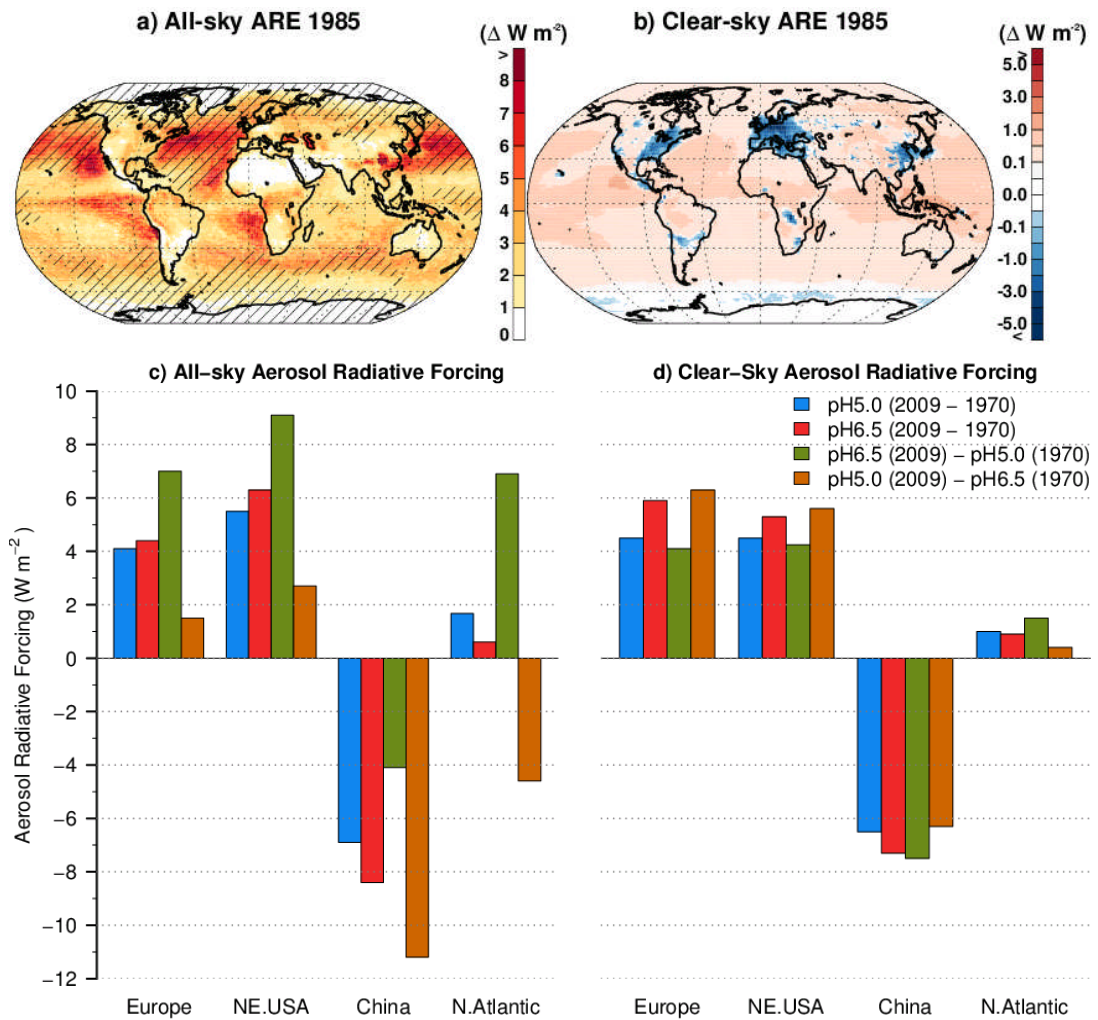


**Figure 4.4** Differences in all-sky a) and clear-sky b) shortwave top of atmosphere aerosol radiative effects between the pH 6.5 and pH 5 simulations for the year 1985. Hatching in a) shows where the differences in cloud drop number concentrations are more than 40%. Calculated c) all-sky and d) clear-sky aerosol radiative forcings between 1970 and 2009 over Europe, NE USA, China and North Atlantic (regions defined in Fig. A4) using four different start and end point combinations from the pH 5.0 and pH 6.5 simulations.

The impacts on all-sky ARF are even larger on regional scales where such a change in pH might occur. Over Europe, the regional all-sky ARF is +4.4 to +4.5 W m<sup>-2</sup> if pH is assumed to be unchanged, but +7.0 W m<sup>-2</sup> if we assume pH has increased over this period (Fig. 4.4c). Over China, the all-sky ARF is -6.9 to -8.4 W m<sup>-2</sup> if pH has not changed, but -11.2 W m<sup>-2</sup> if pH is assumed to have reduced and -4.1 W m<sup>-2</sup> if pH increases. The sign of the pH change is particularly important over a region such as the North Atlantic due to its large susceptibility to changes in cloud albedo. An assumed increase in pH over this region results in an ARF of +6.9 W m<sup>-2</sup> whereas, for a decrease in pH the ARF is -4.6 W m<sup>-2</sup>. The non-implementation of temporal changes in pH (and other such parameters) could result in large errors in the calculated aerosol radiative forcing across regions over the last few decades (Fig. 4.4c - d) and also over the industrial period. The analysis of the uncertainty in aerosol cloud radiative forcing by Carslaw et al., (2013) and Regayre et al., (2014) assumed that uncertainties in pH for the start and end time period were correlated and therefore neglected any errors associated with a temporal change in cloud water pH.

#### 4.4 Conclusions

This study highlighted the importance of accounting for spatial and temporal variability in a parameter such as cloud water pH when considering its impact on sulphate aerosol formation and aerosol radiative effects over recent decades. Our analysis suggests that regions with large SO<sub>2</sub> emissions and also limited oxidants (at certain times of years) are sensitive to changes in cloud water pH. The increase of cloud water pH from 5.0 to 6.5 reduced the SO<sub>2</sub> mass burden over Europe, north eastern United States and East Asia by ~60% and increased the sulphate mass burden over these regions by up to 20% due to enhanced in-cloud oxidation of SO<sub>2</sub> with O<sub>3</sub>. Whilst a 1.5 unit change in pH is large, observations have indicated that smaller changes are possible on a regional basis (Vet et al., 2014; Schwab et al., 2016). However, for an increase in pH the global sulphate mass burden decreased by ~30% due to reductions in nucleation and condensational growth as well as in the atmospheric lifetime of sulphate from increased deposition rates. Regionally the largest increase in the column burden of sulphate mass from an increase in pH occurred in the 1970s and 1980s over Europe and NE USA, whereas it was largest over China in the 2000s. The large spatial and temporal differences in sulphate show the importance of accounting for variations in pH over regions of the

world that are sensitive to these changes and have experienced large changes in anthropogenic emissions of SO<sub>2</sub> over recent decades.

In evaluating the model, the majority of the bias that was present when comparing observed sulphate and SO<sub>2</sub> mass concentrations to values simulated using a pH of 5.0, and also in other studies (Feichter et al., 1996; Kasibhatla et al., 1997; Roelofs et al., 2001; Textor et al., 2006), was removed by using values simulated at a higher pH. Additionally, the evaluation across Europe highlighted that temporal variations in pH were important to improve the model comparison to observations. A lower model bias was produced in the 1980s with a lower pH value whereas in the 2000s the model reproduced observations better when using a higher value of pH.

The calculated regional aerosol radiative effects and also aerosol radiative forcing over recent decades was shown to be particularly sensitive to the choice of cloud water pH used. The all-sky aerosol radiative forcing over the period 1970 to 2009 was found to vary by a factor of 5 depending on the value cloud water pH used to calculate the ARE at each end point. Such errors from a temporally varying cloud water pH were not taken into account in recent studies on the uncertainty in aerosol cloud radiative forcing where the uncertainties in such parameters were assumed to correlate over the time period in question (Carslaw et al., 2013; Regayre et al., 2014). Here we find that taking account of such changes are important when considering the aerosol cloud albedo forcing over regions that are highly susceptible to changes in this effect e.g. the North Atlantic. Over this region the all-sky aerosol radiative forcing was +6.9 W m<sup>-2</sup> if an increase in pH was assumed between 1970 and 2009 whereas for a decrease in pH over this period it was -4.6 W m<sup>-2</sup>. Therefore using a fixed cloud water pH to represent sulphate aerosol formation in global composition climate models could lead to uncertainties in the calculated aerosol radiative effect that have not been previously accounted for.

Here we show that accounting for the spatial and temporal variation in cloud water pH over recent decades is important to accurately simulate sulphate aerosol formation and also to account for changes in aerosol radiative effects over this period. In light of these findings it is recommended that global composition climate models ensure that they are able to calculate a spatially and temporally variable cloud water pH to improve the simulation of aerosols and their impacts.

## Acknowledgments and Data

Steven Turnock would like to acknowledge the funding for his PhD studentship from the Natural Environment Research Council (NERC) and Met Office. For making their data available to be used in this study we would like to acknowledge the EMEP measurement networks along with any data managers involved in data collection. We acknowledge use of the MONSooN system, a collaborative facility supplied under the Joint Weather and Climate Research Programme, a strategic partnership between the Met Office and the Natural Environment Research Council.

## References

- Aleksic, N., Roy, K., Sistla, G., Dukett, J., Houck, N. & Casson, P. (2009). Analysis of cloud and precipitation chemistry at Whiteface Mountain, {NY}. *Atmospheric Environment*. 43 (17). p.pp. 2709–2716.
- Banzhaf, S., Schaap, M., Kerschbaumer, A., Reimer, E., Stern, R., van der Swaluw, E. & Builtjes, P. (2012). Implementation and evaluation of pH-dependent cloud chemistry and wet deposition in the chemical transport model REM-Calgrid. *Atmospheric Environment*. 49. p.pp. 378–390.
- Barrie, L. A., Yi, Y., Leaitch, W.R., Lohmann, U., Kasibhatla, P., Roelofs, G.J., Wilson, J., McGovern, F., Benkovitz, C., Melieres, M. A, Law, K., Prospero, J., Kritz, M., Bergmann, D., Bridgeman, C., Chin, M., Christensen, J., Easter, R., Feichter, J., Land, C., Jeuken, A, Kjellstrom, E., Koch, D. & Rasch, P. (2001). A comparison of large-scale atmospheric sulphate aerosol models (COSAM): overview and highlights. *Tellus Series B-Chemical and Physical Meteorology*. 53 (5). p.pp. 615–645.
- Barth, M.C., Rasch, P.J., Kiehl, J.T., Benkovitz, C.M. & Schwartz, S.E. (2000). Sulfur chemistry in the National Center for Atmospheric Research Community Climate Model: Description, evaluation, features, and sensitivity to aqueous chemistry. *Journal of Geophysical Research*. 105 (D1). p.p. 1387.
- Bellouin, N., Mann, G.W., Woodhouse, M.T., Johnson, C., Carslaw, K.S. & Dalvi, M. (2013). Impact of the modal aerosol scheme GLOMAP-mode on aerosol forcing in the Hadley Centre Global Environmental Model. *Atmospheric Chemistry and Physics*. 13 (6). p.pp. 3027–3044.
- Benedict, K.B., Lee, T. & Collett, J.L. (2012). Cloud water composition over the southeastern Pacific Ocean during the VOCALS regional experiment. *Atmospheric Environment*. 46. p.pp. 104–114.

- Berglen, T.F. (2004). A global model of the coupled sulfur/oxidant chemistry in the troposphere: The sulfur cycle. *Journal of Geophysical Research*. 109 (D19). p.p. D19310.
- Budhavant, K.B., Rao, P.S.P., Safai, P.D., Granat, L. & Rodhe, H. (2014). Chemical composition of the inorganic fraction of cloud-water at a high altitude station in West India. *Atmospheric Environment*. 88. p.pp. 59–65.
- Carslaw, K.S., Lee, L. A., Reddington, C.L., Pringle, K.J., Rap, A., Forster, P.M., Mann, G.W., Spracklen, D. V., Woodhouse, M.T., Regayre, L. A. & Pierce, J.R. (2013). Large contribution of natural aerosols to uncertainty in indirect forcing. *Nature*. 503 (7474). p.pp. 67–71.
- Chin, M., Jacob, D.J., Gardner, G.M., Foreman-Fowler, M.S., Spiro, P.A. & Savoie, D.L. (1996). A global three-dimensional model of tropospheric sulfate. *Journal of Geophysical Research*. 101 (D13). p.p. 18667.
- Collett, J., Oberholzer, B. & Staehelin, J. (1993). Cloud chemistry at Mt Rigi, Switzerland: Dependence on drop size and relationship to precipitation chemistry. *Atmospheric Environment. Part A. General Topics*. 27 (1). p.pp. 33–42.
- Edwards, J.M. & Slingo, A. (1996). Studies with a flexible new radiation code. I: Choosing a configuration for a large-scale model. *Quarterly Journal of the Royal Meteorological Society*. 122 (531). p.pp. 689–719.
- Ervens, B. (2015). Modeling the Processing of Aerosol and Trace Gases in Clouds and Fogs. *Chemical Reviews*. 115. p.pp. 4157–4198.
- Fahey, K.M. (2003). Size-resolved aqueous-phase atmospheric chemistry in a three-dimensional chemical transport model. *Journal of Geophysical Research*. 108 (D22). p.p. 4690.
- Faloona, I. (2009). Sulfur processing in the marine atmospheric boundary layer: A review and critical assessment of modeling uncertainties. *Atmospheric Environment*. 43 (18). p.pp. 2841–2854.
- Feichter, J., Kjellström, E., Rodhe, H., Dentener, F., Lelieveld, J. & Roelofs, G.-J. (1996). Simulation of the tropospheric sulfur cycle in a global climate model. *Atmospheric Environment*. 30 (10-11). p.pp. 1693–1707.
- Granier, C., Bessagnet, B., Bond, T.C., D'Angiola, A., Denier van der Gon, H., Frost, G.J., Heil, A., Kaiser, J.W., Kinne, S., Klimont, Z., Kloster, S., Lamarque, J.-F., Liousse, C., Masui, T., Meleux, F., Mieville, A., Ohara, T., Raut, J.-C., Riahi, K., Schultz, M.G., Smith, S.J., Thompson, A., Aardenne, J., Werf, G.R. & Vuuren, D.P. (2011). Evolution of anthropogenic and biomass burning emissions of air

pollutants at global and regional scales during the 1980–2010 period. *Climatic Change*. 109 (1-2). p.pp. 163–190.

Gurciullo, C.S. & Pandis, S.N. (1997). Effect of composition variations in cloud droplet populations on aqueous-phase chemistry. *Journal of Geophysical Research*. 102 (D8). p.p. 9375.

IPCC (2013). Summary for Policymakers. In: *Climate Change 2013: The Physical Science Bases*. Contribution of Working Group 1 to the Fifth Assessment Report of the Intergovernmental Panel on Climate Change. T. F. Stocker, D. Qin, G.-K. Plattner, M. Tignor, S. K. Allen, J. Boschung, A. Nauels, Y. Xia, Y. Bex, & P. M. Midgley (eds.). Cambridge University Press, Cambridge, United Kingdom and New York, NY, USA.

Kasibhatla, P., Chameides, W.L. & John, J. St. (1997). A three-dimensional global model investigation of seasonal variations in the atmospheric burden of anthropogenic sulfate aerosols. *Journal of Geophysical Research*. 102 (D3). p.pp. 3737–3759.

Kreidenweis, S.M. (2003). Modification of aerosol mass and size distribution due to aqueous-phase SO<sub>2</sub> oxidation in clouds: Comparisons of several models. *Journal of Geophysical Research*. 108 (D7). p.p. 4213.

Lee, L.A., Pringle, K.J., Reddington, C.L., Mann, G.W., Stier, P., Spracklen, D. V., Pierce, J.R. & Carslaw, K.S. (2013). The magnitude and causes of uncertainty in global model simulations of cloud condensation nuclei. *Atmospheric Chemistry and Physics*. 13 (17). p.pp. 8879–8914.

Lohmann, U., Leaitch, W.R., Barrie, L., Law, K., Yi, Y., Bergmann, D., Bridgeman, C., Chin, M., Christensen, J., Easter, R., Feichter, J., Jeuken, a, Kjellstrom, E., Koch, D., Rasch, P. & Roelofs, G.J. (2001). Vertical distributions of sulfur species simulated by large scale atmospheric models in COSAM: Comparison with observations. *Tellus Series B-Chemical and Physical Meteorology*. 53 (5). p.pp. 646–672.

Mann, G.W., Carslaw, K.S., Spracklen, D. V., Ridley, D. a., Manktelow, P.T., Chipperfield, M.P., Pickering, S.J. & Johnson, C.E. (2010). Description and evaluation of GLOMAP-mode: a modal global aerosol microphysics model for the UKCA composition-climate model. *Geoscientific Model Development*. 3 (2). p.pp. 519–551.

Murray, G.L.D., Kimball, K.D., Hill, L.B., Hislop, J.E. & Weathers, K.C. (2013). Long-Term Trends in Cloud and Rain Chemistry on Mount Washington, New Hampshire. *Water, Air, & Soil Pollution*. 224 (9). p.p. 1653.

- O'Connor, F.M., Johnson, C.E., Morgenstern, O., Abraham, N.L., Braesicke, P., Dalvi, M., Folberth, G.A., Sanderson, M.G., Telford, P.J., Voulgarakis, A., Young, P.J., Zeng, G., Collins, W.J. & Pyle, J.A. (2014). Evaluation of the new UKCA climate-composition model – Part 2: The Troposphere. *Geoscientific Model Development*. 7 (1). p.pp. 41–91.
- Pandis, S.N. & Seinfeld, J.H. (1989). Sensitivity analysis of a chemical mechanism for aqueous-phase atmospheric chemistry. *Journal of Geophysical Research*. 94 (D1). p.pp. 1105–1126.
- Plessow, K., Acker, K., Heinrichs, H. & Möller, D. (2001). Time study of trace elements and major ions during two cloud events at the Mt. Brocken. *Atmospheric Environment*. 35. p.pp. 367–378.
- Rasch, P.J., Barth, M.C., Kiehl, J.T., Schwartz, S.E. & Benkovitz, C.M. (2000). A description of the global sulfur cycle and its controlling processes in the National Center for Atmospheric Research Community Climate Model, Version 3. *Journal of Geophysical Research: Atmospheres* (1984–2012). 105 (1999). p.pp. 1367–1385.
- Redington, A.L., Derwent, R.G., Witham, C.S. & Manning, A.J. (2009). Sensitivity of modelled sulphate and nitrate aerosol to cloud, pH and ammonia emissions. *Atmospheric Environment*. 43 (20). p.pp. 3227–3234.
- Regayre, L.A., Pringle, K.J., Booth, B.B.B., Lee, L.A., Mann, G.W., Browse, J., Woodhouse, M.T., Rap, A., Reddington, C.L. & Carslaw, K.S. (2014). Uncertainty in the magnitude of aerosol-cloud radiative forcing over recent decades. *Geophysical Research Letters*. 41 (24). p.pp. 9040–9049.
- Rodhe, H., Dentener, F. & Schulz, M. (2002). The Global Distribution of Acidifying Wet Deposition. *Environmental Science & Technology*. 36 (20). p.pp. 4382–4388.
- Roelofs, G.J., Kasibhatla, P., Barrie, L., Bergmann, D., Bridgeman, C., Chin, M., Christensen, J., Easter, R., Feichter, J., Jeuken, a, Kjellstrom, E., Koch, D., Land, C., Lohmann, U. & Rasch, P. (2001). Analysis of regional budgets of sulfur species modeled for the COSAM exercise. *Tellus Series B-Chemical and Physical Meteorology*. 53 (5). p.pp. 673–694.
- Roelofs, G.J., Stier, P., Feichter, J., Vignati, E. & Wilson, J. (2006). Aerosol activation and cloud processing in the global aerosol-climate model ECHAM5-HAM. *Atmospheric Chemistry and Physics*. 6 (9). p.pp. 2389–2399.
- Schwab, J.J., Wolfe, D., Casson, P., Brandt, R., Demerjian, K.L., Husain, L., Dutkiewicz, V.A., Civerolo, K.L. & Rattigan, O. V. (2016). *Atmospheric Chemistry Measurements at Whiteface Mountain, NY: Cloud Water Chemistry, Precipitation*

Chemistry, and Particulate Matter. *Aerosol and Air Quality Research*. 16. p.pp. 827–840.

Scott, C.E., Rap, A., Spracklen, D. V., Forster, P.M., Carslaw, K.S., Mann, G.W., Pringle, K.J., Kivekäs, N., Kulmala, M., Lihavainen, H. & Tunved, P. (2014). The direct and indirect radiative effects of biogenic secondary organic aerosol. *Atmospheric Chemistry and Physics*. 14. p.pp. 447–470.

Seinfeld, J.H. & Pandis, S.N. (2006). *Atmospheric Chemistry and Physics From Air Pollution to Climate Change*. Second. Wiley-Interscience.

Spracklen, D. V., Carslaw, K.S., Kulmala, M., Kerminen, V.-M., Mann, G.W. & Sihto, S.-L. (2006). The contribution of boundary layer nucleation events to total particle concentrations on regional and global scales. *Atmospheric Chemistry and Physics*. 6 (12). p.pp. 5631–5648.

Spracklen, D. V., Pringle, K.J., Carslaw, K.S., Chipperfield, M.P. & Mann, G.W. (2005). A global off-line model of size-resolved aerosol microphysics: I. Model development and prediction of aerosol properties. *Atmospheric Chemistry and Physics*. 5 (1). p.pp. 2227–2252.

Sun, M., Wang, Y., Wang, T., Fan, S., Wang, W., Li, P., Guo, J. & Li, Y. (2010). Cloud and the corresponding precipitation chemistry in south China: Water-soluble components and pollution transport. *Journal of Geophysical Research Atmospheres*. 115. p.p. D22303.

Textor, C., Schulz, M., Guibert, S., Kinne, S., Balkanski, Y., Bauer, S., Bernsten, T., Berglen, T., Boucher, O., Chin, M., Dentener, F., Diehl, T., Easter, R., Feichter, H., Fillmore, D., Ghan, S., Ginoux, P., Gong, S., Grini, a., Hendricks, J., Horowitz, L., Huang, P., Isaksen, I., Iversen, T., Kloster, S., Koch, D., Kirkevåg, a., Kristjansson, J.E., Krol, M., Lauer, a., Lamarque, J.F., Liu, X., Montanaro, V., Myhre, G., Penner, J., Pitari, G., Lamarque, J.F., Liu, X., Montanaro, V., Myhre, G., Penner, J., Pitari, G., Reddy, S., Seland, Ø., Stier, P., Takemura, T. & Tie, X. (2006). Analysis and quantification of the diversities of aerosol life cycles within AeroCom. *Atmospheric Chemistry and Physics*. 6. p.pp. 1777–1813.

Turnock, S.T., Spracklen, D. V., Carslaw, K.S., Mann, G.W., Woodhouse, M.T., Forster, P.M., Haywood, J., Johnson, C.E., Dalvi, M., Bellouin, N. & Sanchez-Lorenzo, a. (2015). Modelled and observed changes in aerosols and surface solar radiation over Europe between 1960 and 2009. *Atmospheric Chemistry and Physics*. 15. p.pp. 9477–9500.

Vet, R., Artz, R.S., Carou, S., Shaw, M., Ro, C.U., Aas, W., Baker, A., Bowersox, V.C., Dentener, F., Galy-Lacaux, C., Hou, A., Pienaar, J.J., Gillett, R., Forti, M.C.,

Gromov, S., Hara, H., Khodzher, T., Mahowald, N.M., Nickovic, S., Rao, P.S.P. & Reid, N.W. (2014). A global assessment of precipitation chemistry and deposition of sulfur, nitrogen, sea salt, base cations, organic acids, acidity and pH, and phosphorus. *Atmospheric Environment*. 93. p.pp. 3–100.

Wang, S.X., Zhao, B., Cai, S.Y., Klimont, Z., Nielsen, C., McElroy, M.B., Morikawa, T., Woo, J.H., Kim, Y., Fu, X., Xu, J.Y., Hao, J.M. & He, K.B. (2014). Emission trends and mitigation options for air pollutants in East Asia. *Atmospheric Chemistry and Physics*. 14. p.pp. 6571–6603.

Woodward, S. (2001). Modeling the atmospheric life cycle and radiative impact of mineral dust in the Hadley Centre climate model. *Journal of Geophysical Research*. 106 (D16). p.pp. 18155–18166.

Zhang, Q., Jimenez, J.L., Canagaratna, M.R., Allan, J.D., Coe, H., Ulbrich, I., Alfarra, M.R., Takami, A., Middlebrook, A.M., Sun, Y.L., Dzepina, K., Dunlea, E., Docherty, K., DeCarlo, P.F., Salcedo, D., Onasch, T., Jayne, J.T., Miyoshi, T., Shimono, A., Hatakeyama, S., Takegawa, N., Kondo, Y., Schneider, J., Drewnick, F., Borrmann, S., Weimer, S., Demerjian, K., Williams, P., Bower, K., Bahreini, R., Cottrell, L., Griffin, R.J., Rautiainen, J., Sun, J.Y., Zhang, Y.M. & Worsnop, D.R. (2007). Ubiquity and dominance of oxygenated species in organic aerosols in anthropogenically-influenced Northern Hemisphere midlatitudes. *Geophysical Research Letters*. 34 (13). p.p. L13801.

**Chapter 5**  
**The impact of European legislative and technology measures**  
**to reduce air pollutants on air quality, human health and**  
**climate**

## Environmental Research Letters



## LETTER

## The impact of European legislative and technology measures to reduce air pollutants on air quality, human health and climate

## OPEN ACCESS

## RECEIVED

18 September 2015

## REVISED

23 January 2016

## ACCEPTED FOR PUBLICATION

25 January 2016

## PUBLISHED

12 February 2016

Original content from this work may be used under the terms of the [Creative Commons Attribution 3.0 licence](#).

Any further distribution of this work must maintain attribution to the author(s) and the title of the work, journal citation and DOI.



S T Turnock<sup>1</sup>, E W Butt<sup>1</sup>, T B Richardson<sup>1</sup>, G W Mann<sup>1,2</sup>, C L Reddington<sup>1</sup>, P M Forster<sup>1</sup>, J Haywood<sup>3</sup>, M Crippa<sup>4</sup>, G Janssens-Maenhout<sup>4</sup>, C E Johnson<sup>3</sup>, N Bellouin<sup>5</sup>, K S Carslaw<sup>1</sup> and D V Spracklen<sup>1</sup>

<sup>1</sup> Institute of Climate and Atmospheric Science, School of Earth and Environment, University of Leeds, Leeds, UK

<sup>2</sup> National Centre for Atmospheric Science, University of Leeds, Leeds, UK

<sup>3</sup> Met Office, Fitzroy Road, Exeter, Devon, UK

<sup>4</sup> European Commission, Joint Research Centre, Institute for Environment and Sustainability, Air and Climate Unit, Via Fermi, 2749, I-21027 Ispra, Italy

<sup>5</sup> Department of Meteorology, University of Reading, Reading, UK

E-mail: [s.t.turnock12@leeds.ac.uk](mailto:s.t.turnock12@leeds.ac.uk)

**Keywords:** air quality, health, climate, aerosols, emissions, mitigation

Supplementary material for this article is available [online](#)

**Abstract**

European air quality legislation has reduced emissions of air pollutants across Europe since the 1970s, affecting air quality, human health and regional climate. We used a coupled composition-climate model to simulate the impacts of European air quality legislation and technology measures implemented between 1970 and 2010. We contrast simulations using two emission scenarios; one with actual emissions in 2010 and the other with emissions that would have occurred in 2010 in the absence of technological improvements and end-of-pipe treatment measures in the energy, industrial and road transport sectors. European emissions of sulphur dioxide, black carbon (BC) and organic carbon in 2010 are 53%, 59% and 32% lower respectively compared to emissions that would have occurred in 2010 in the absence of legislative and technology measures. These emission reductions decreased simulated European annual mean concentrations of fine particulate matter (PM<sub>2.5</sub>) by 35%, sulphate by 44%, BC by 56% and particulate organic matter by 23%. The reduction in PM<sub>2.5</sub> concentrations is calculated to have prevented 80 000 (37 000–116 000, at 95% confidence intervals) premature deaths annually across the European Union, resulting in a perceived financial benefit to society of US\$232 billion annually (1.4% of 2010 EU GDP). The reduction in aerosol concentrations due to legislative and technology measures caused a positive change in the aerosol radiative effect at the top of atmosphere, reduced atmospheric absorption and also increased the amount of solar radiation incident at the surface over Europe. We used an energy budget approximation to estimate that these changes in the radiative balance have increased European annual mean surface temperatures and precipitation by  $0.45 \pm 0.11$  °C and by  $13 \pm 0.8$  mm yr<sup>-1</sup> respectively. Our results show that the implementation of European legislation and technological improvements to reduce the emission of air pollutants has improved air quality and human health over Europe, as well as having an unintended impact on the regional radiative balance and climate.

**1. Introduction**

Air pollutants have a detrimental effect on atmospheric visibility (Vautard *et al* 2009, Stjern *et al* 2011), ecosystems (Fowler *et al* 2009) and human health (Seaton *et al* 1995, Brunekreef and Holgate 2002). The World Health Organization (WHO) attributed 3.7

million annual premature deaths worldwide to the effects of ambient air pollution in 2012 (WHO 2014). Air pollutants can either be gas phase species (e.g. ozone) or particulate matter. This study will focus solely on particulate matter air quality. Exposure to fine particulate matter (PM<sub>2.5</sub>) is responsible for ~3.3 million deaths worldwide each year (Cohen *et al* 2005,

Lelieveld *et al* 2015), with in excess of 400 000 premature deaths annually across Europe (EEA 2014). Particulate matter (also known as aerosols) also influences climate by altering the radiation budget at both the top of atmosphere (TOA) and surface (Boucher *et al* 2013). Aerosols scatter and absorb radiation, termed as aerosol radiation interactions (ari), and can also alter the properties of clouds, termed as aerosol cloud interactions (aci) (Boucher *et al* 2013). Both interactions caused a negative radiative forcing of the Earth's radiation budget over the industrial period resulting in a cooling effect on climate (IPCC 2013).

Europe and North America implemented legislation from the 1970s to reduce emissions of air pollutants (UNECE 2004). Emissions of sulphur dioxide (SO<sub>2</sub>) fell by 73% across Europe over the period 1980–2004 and by 70% in the United States from 1980 to 2010 (Vestreng *et al* 2007, US EPA 2011). Consequently, European surface concentrations of sulphate aerosol mass decreased by between 65% and 78% over the period 1980–2010 (Tørseth *et al* 2012, Turnock *et al* 2015). In addition to the beneficial health effects from improved air quality, such reductions in particulate matter will also have changed the regional radiative balance and climate (Turnock *et al* 2015).

The benefits to human health from reductions in anthropogenic emissions have been highlighted in a number of studies (Anenberg *et al* 2011, 2012, Shindell *et al* 2012). Reducing PM<sub>2.5</sub> concentrations across more than 20 European cities to 15 µg m<sup>-3</sup> was calculated to reduce the number of annual premature deaths by nearly 17 000 (Boldo *et al* 2006), with larger PM<sub>2.5</sub> reductions to the WHO annual mean guideline value of 10 µg m<sup>-3</sup> estimated to avoid 19 000 premature deaths (Pascal *et al* 2013). Considering specific emission reductions from power plants over the United States, Levy *et al* (2007) calculated that 17 000–21 000 annual premature deaths could be avoided. These studies highlight the large potential benefit to human health that can be achieved from reducing the emissions of air pollutants.

Policies that reduce anthropogenic emissions of aerosols may cause inadvertent impacts on climate (Andreae *et al* 2005, Arneth *et al* 2009, Fiore *et al* 2012, 2015, von Schneidemesser *et al* 2015). The air quality and climate impact of reductions in particulate matter depends on the contribution from purely scattering (sulphate) and more absorbing (black carbon (BC)) components (Shindell and Faluvegi 2009), as well as the complex interactions between aerosols and clouds.

Increased surface temperatures over Europe since the 1980s have been attributed to a combination of reductions in aerosols and increases in greenhouse gases (Ruckstuhl *et al* 2008, Philipona *et al* 2009). Increased surface radiation over Europe (solar brightening) has been observed since the 1980s across the continent (Wild 2009 and references within). This

solar brightening was simulated in all of the Fifth Coupled Model Intercomparison Project (CMIP5) models from 1990 to 2005 and was attributed to a reduction in aerosol optical depth caused by decreases in sulphate aerosols (Cherian *et al* 2014). Changes to aerosols over Europe between the 1980s and 2000s are estimated to have led to a positive change in the TOA aerosol radiative effect (RE) of 1–2 W m<sup>-2</sup> and increased surface radiation by 2 W m<sup>-2</sup> (Marrner *et al* 2007, Pozzoli *et al* 2011). The associated changes in cloud albedo are estimated to have caused a positive change in the RE of 1.5 W m<sup>-2</sup> over central Europe from the late 1980s to late 1990s (Krüger and Graßl 2002). In the United States, a reduction in anthropogenic aerosol precursor emissions between 1990 and 2010 coincided with RE<sub>ari</sub> and RE<sub>aci</sub> decreasing by 0.8 W m<sup>-2</sup> and 1.0 W m<sup>-2</sup> respectively (Leibensperger *et al* 2012a). The observed rapid warming over this period of 0.5 °C was potentially attributed in part to a reduction in anthropogenic aerosols (Leibensperger *et al* 2012b). Gan *et al* (2014) analysed the effect of air pollution controls in the US and found that an increase in the surface shortwave radiation occurred over the same time period as negative trends in AOD and PM<sub>2.5</sub>.

Previous studies have assessed the impact of changes in historical (Colette *et al* 2011, Koch *et al* 2011, Turnock *et al* 2015) and future emissions (Kloster *et al* 2008, Unger *et al* 2008, Colette *et al* 2013) on air quality and climate. Changes in historical emissions have resulted from the combined effects of legislation, abatement technology, economic situation and makeup of the national energy supply (Vestreng *et al* 2007). However, it is not known what fraction of the changes in historical emissions and associated impacts on air quality, climate and human health can be attributed to the implementation of legislation and technological developments. Such studies are needed to understand the efficacy of historical policy. In recent work, Crippa *et al* (2015) studied the impact of historical European air pollution mitigation measures on emissions of SO<sub>2</sub>, BC and organic carbon (OC). They found that emissions of SO<sub>2</sub> and PM<sub>2.5</sub> in 2010 would have been substantially higher over Europe if technology improvements and end of pipe abatement measures had not been implemented since 1970.

Here we use emissions scenarios from Crippa *et al* (2015), combined with a global composition climate model to assess the effect of historical legislative and technology measures on particulate matter air quality, climate and human health. The effect of these emission changes on ozone concentrations will be the subject of a future study. The achievements from past policy initiatives are highlighted and will aid in the design of future emission mitigation measures to improve air quality and climate across other regions of the globe.

## 2. Methods

### 2.1. HadGEM3-UKCA composition-climate model

We used the composition-climate model HadGEM3-UKCA, as described in Turnock *et al* (2015), to simulate surface aerosol mass concentrations as well as the impact on aerosol REs. HadGEM3-UKCA is similar in complexity to other models that have participated in the Atmospheric Chemistry and Climate Model Intercomparison Project (ACCMIP, (Lamarque *et al* 2013)) and the AeroCom initiative (Mann *et al* 2014). Simulations had a horizontal resolution of  $1.875^\circ$  by  $1.275^\circ$  ( $\sim 140$  km at mid latitudes). Our previous work has demonstrated that HadGEM3-UKCA is able to capture the regional changes in annual mean surface aerosol mass concentrations and surface solar radiation observed over Europe in response to changes in anthropogenic emissions during the period 1980–2010 (Turnock *et al* 2015). Our simulations therefore capture regional changes in  $PM_{2.5}$  (at the scale of  $\sim 100$  km) and are suitable for isolating the effects of policy driven changes in regional aerosol precursor emissions. Our model underestimates  $PM_{2.5}$  concentrations in urban areas; we estimate the impact of this in section 2.3. Further details on the model description and experimental set-up are in supplementary methods section 1.

### 2.2. Anthropogenic emission scenarios

Monthly mean anthropogenic emissions of  $CO$ ,  $SO_2$ ,  $NO_x$ , NMVOC, OC and BC are based on version v4.3 of the Emission Database for Global Atmospheric Research (EDGAR) (EC-JRC/PBL 2015). The emissions used in this study are described in Crippa *et al* (2015) and are summarised below. Emission fields are provided at  $0.5^\circ$  by  $0.5^\circ$  resolution for the energy, industry, transport, agriculture, residential, waste and other sources sectors (<http://edgar.jrc.ec.europa.eu/pegasos>).

We compare two simulations with different anthropogenic emissions. All other factors in the model are the same. The reference simulation (REF) uses actual 2010 emissions. The NO-AQ simulation uses anthropogenic emissions that would have occurred in 2010 if measures to reduce air pollutant emissions between 1970 and 2010 did not occur. The NO-AQ scenario is based on 2010 economic activity data but assumes 1970 emission factors to simulate the stagnation of technological improvements in the energy, industry and road transport sectors. It also assumes that no further end-of-pipe abatement measures (e.g., particle filter traps, fuel desulphurisation) occurred in the energy and road transportation sectors after 1970 (Crippa *et al* 2015). The NO-AQ scenario does however account for changes in the makeup of the national energy supply (e.g. coal to gas) that occurred without specific legislation. These assumptions

alter emissions globally, since stagnation of technology improvements are applied globally and some European emission standards are used outside Europe (Crippa *et al* 2016). However, we focus on the impact of these measures over Europe (defined here as the domain  $10^\circ W$ – $36^\circ E$  and  $36^\circ N$ – $61^\circ N$ ).

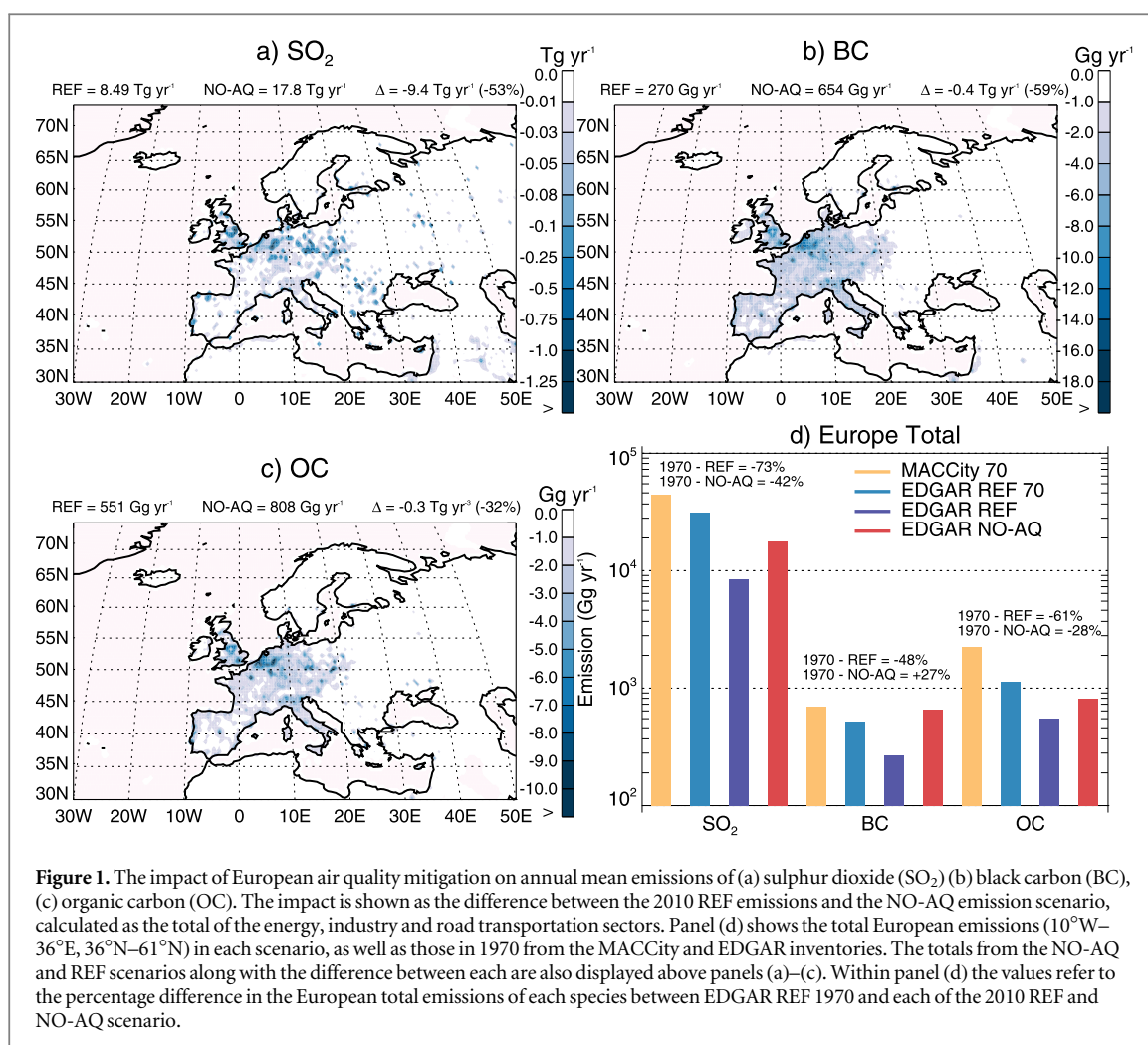
Figures 1(a)–(c) shows the spatial distribution of the difference in emissions between the two scenarios (REF minus NO-AQ). This difference represents the emissions that were averted in 2010 due to the implementation of technology improvements and end-of-pipe abatement measures. The largest difference in emissions occurs over central and eastern Europe and the UK. Total European  $SO_2$ , BC and OC emissions over all sectors are reduced, compared to what would have occurred, by  $9.4$  Tg  $SO_2$   $yr^{-1}$  (53%),  $0.4$  Tg BC  $yr^{-1}$  (59%) and  $0.3$  Tg OC  $yr^{-1}$  (32%) (figure 1(d)). Reductions in  $SO_2$  emissions are dominated by changes in the energy sector, whereas reductions in BC and OC are dominated by changes in the transport sector (table S1).

Figure 1(d) compares total European emissions in the NO-AQ scenario against the actual 2010 (REF) and 1970 emissions from the EDGAR and MACCity inventories. The emissions of  $SO_2$  and OC in both the 2010 REF and NO-AQ scenarios are lower than emissions in 1970. In contrast, BC emissions from the 2010 NO-AQ scenario are larger than in 1970 but are lower in the 2010 REF scenario. This suggests that in the absence of technological improvements and end-of-pipe abatement measures, emissions of  $SO_2$  and OC would still have declined substantially due to changes in the makeup of the energy supply and consumption rates whereas emissions of BC would have been larger than in 1970. This highlights the large impact of legislation and technological improvements on reducing BC emissions compared to  $SO_2$  and OC and that historical changes to anthropogenic emissions are determined by the combined effect of legislation, technology and economic factors.

### 2.3. Human health and economic impacts

Concentration response functions (CRFs) for long-term exposure to  $PM_{2.5}$  have been used here to quantify the adverse health effects in terms of excess premature mortality from ischemic heart disease, stroke, chronic obstructive pulmonary disease, lung cancer and acute lower respiratory infection in infants. Here, the link between  $PM_{2.5}$  concentrations and relative risk of the above diseases is based on the integrated exposure-response functions developed by Burnett *et al* (2014), which also uses the baseline rate of disease and spatial distribution of the population.

The resolution of global aerosol models means that they typically underestimate urban  $PM_{2.5}$  concentrations. To estimate the impact of this underestimation on simulated human health impacts, we complete another calculation where we increase the



**Figure 1.** The impact of European air quality mitigation on annual mean emissions of (a) sulphur dioxide (SO<sub>2</sub>) (b) black carbon (BC), (c) organic carbon (OC). The impact is shown as the difference between the 2010 REF emissions and the NO-AQ emission scenario, calculated as the total of the energy, industry and road transportation sectors. Panel (d) shows the total European emissions (10°W–36°E, 36°N–61°N) in each scenario, as well as those in 1970 from the MACCity and EDGAR inventories. The totals from the NO-AQ and REF scenarios along with the difference between each are also displayed above panels (a)–(c). Within panel (d) the values refer to the percentage difference in the European total emissions of each species between EDGAR REF 1970 and each of the 2010 REF and NO-AQ scenario.

PM<sub>2.5</sub> concentrations in European urban areas in both the REF and NO-AQ simulations. We then apply the CRFs to these modified concentrations. We estimate that the underprediction of PM<sub>2.5</sub> in urban areas in our global model (Turnock *et al* 2015) causes a bias in our mortality estimates of 13%–16%, substantially less than the uncertainty in the CRF (see supplementary methods). Our method is outlined fully in supplementary methods section 2.

The impact on human health from poor air quality can also have a perceived economic effect on society. The methods and data within WHO Regional Office for Europe (2015) have been used to calculate the perceived economic benefit to society that result from the health benefits associated with the reduction in particulate matter concentrations due to the implementation of air pollution mitigation measures (see supplementary methods section 3).

#### 2.4. Climate response

Based on the climate response to regional radiative forcing (Shindell and Faluvegi 2009), and the atmospheric energy budget (Andrews *et al* 2010, Richardson *et al* 2015), we estimate the temperature and precipitation response due to changes in the radiative balance

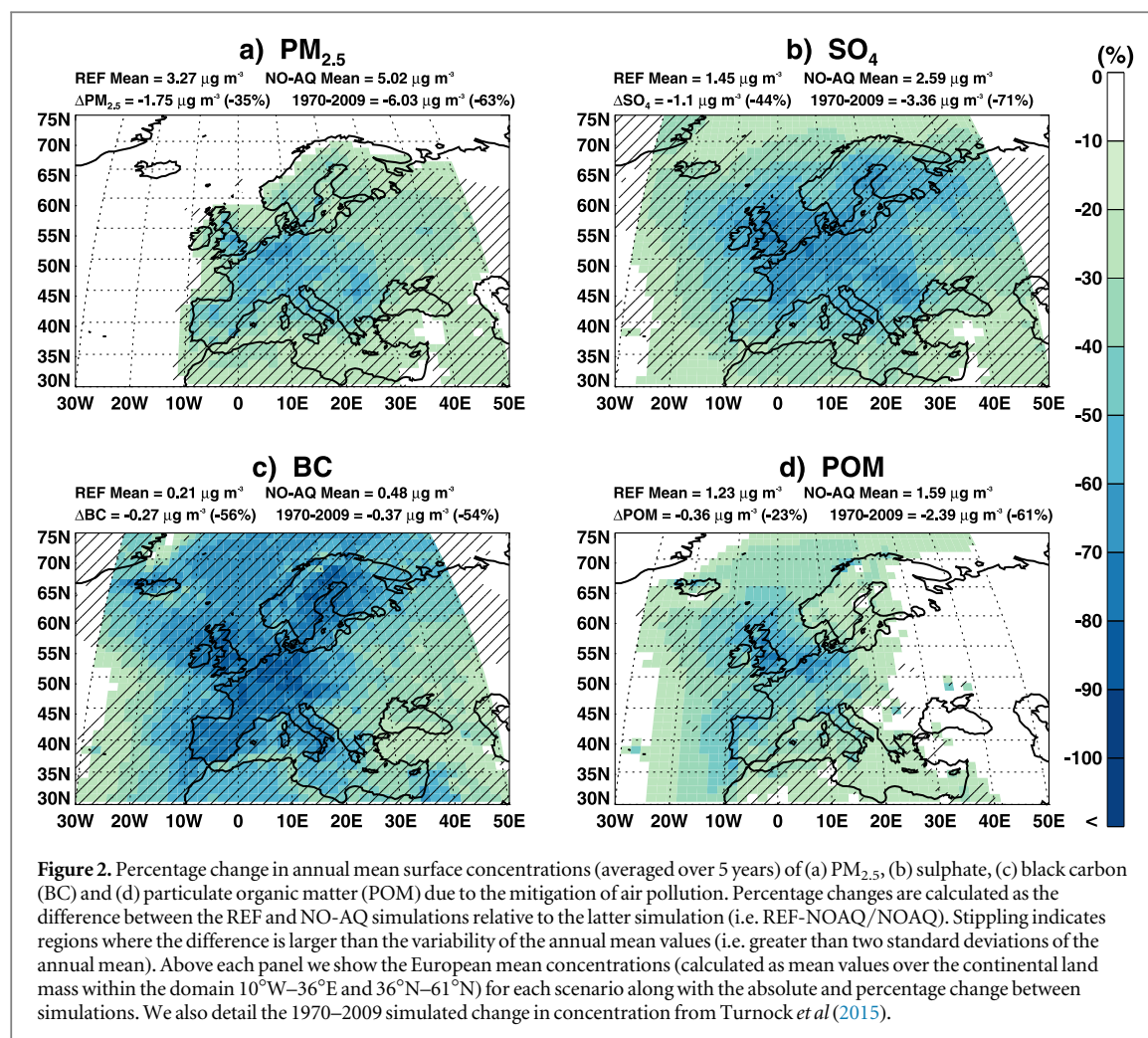
from the implementation of air pollutant (particulate matter) mitigation measures (see supplementary methods section 4).

### 3. Results and discussion

#### 3.1. Effects on air quality

Figure 2 shows the simulated change in surface annual mean PM<sub>2.5</sub> concentrations due to the implementation of European air pollutant emission reduction measures (REF versus NO-AQ simulations). European average concentrations are calculated as the 5 year annual mean ( $\pm$  standard deviation) over the continental land mass within the domain 10°W–36°E and 36°N–61°N. Across Europe, annual mean PM<sub>2.5</sub> concentrations reduce by  $1.75 \pm 0.04 \mu\text{g m}^{-3}$  (35%), sulphate by  $1.1 \pm 0.03 \mu\text{g m}^{-3}$  (44%), BC by  $0.27 \pm 0.01 \mu\text{g m}^{-3}$  (56%) and particulate organic matter (POM) by  $0.36 \pm 0.01 \mu\text{g m}^{-3}$  (23%).

Reductions in PM<sub>2.5</sub> mass concentration of 40%–50% occur across much of central, eastern and parts of southern Europe (figure 2(a)). Sulphate mass concentrations decrease by more than 50% across most of central Europe and south eastern Europe (figure 2(b)), mainly due to the substantial decrease in SO<sub>2</sub>

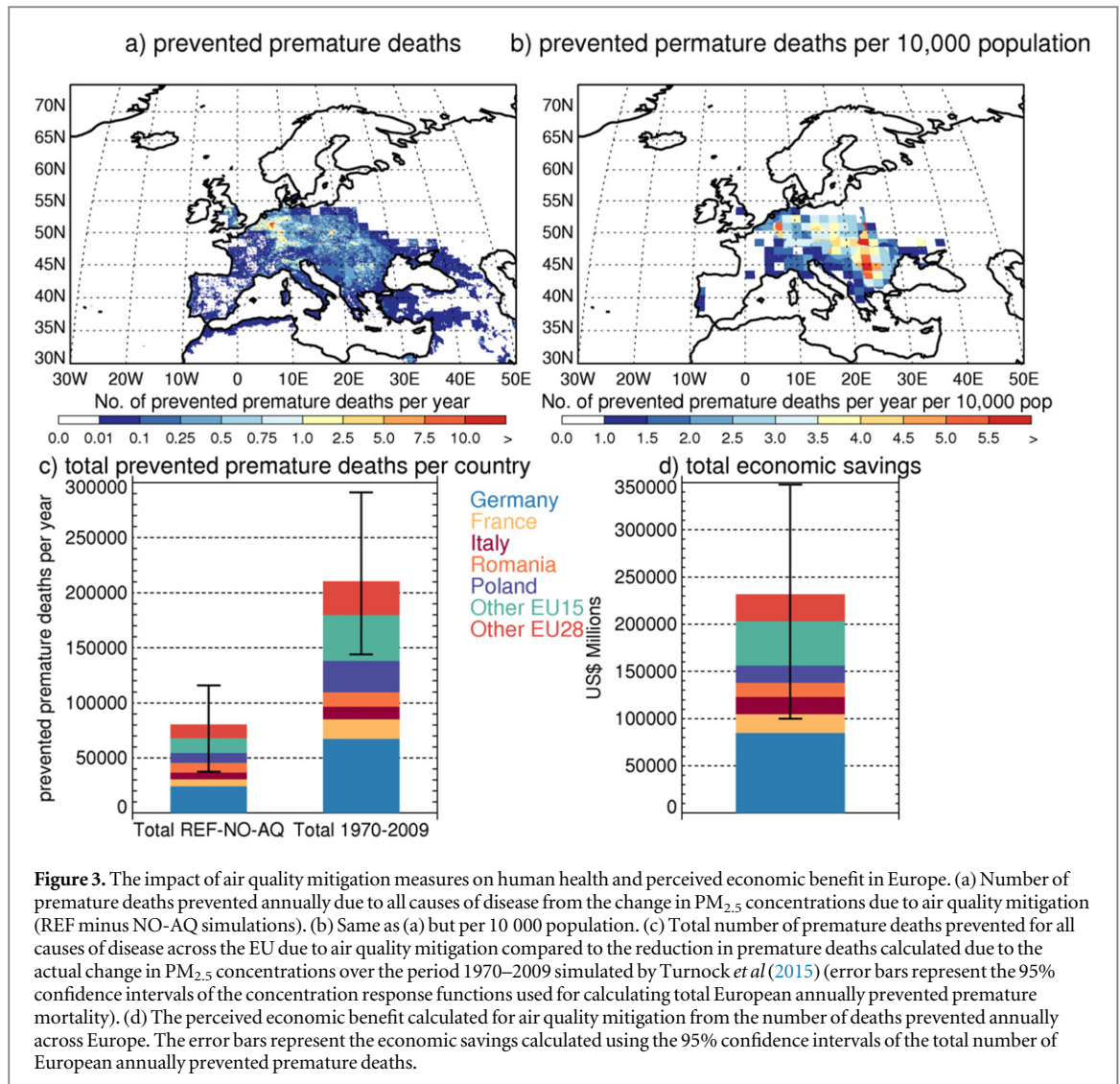


emissions in these regions (figure 1(a)) that mostly occurs in the energy sector (table S1). The largest absolute reduction in sulphate mass concentrations (of  $>5 \mu\text{g m}^{-3}$ ) occurs in south-eastern Europe (figure S1). This is attributed to large reductions in SO<sub>2</sub> emissions from the energy sector combined with atmospheric conditions that enhance the efficiency of sulphate formation (higher oxidant concentrations and temperatures than northern Europe). Reductions in BC mass concentrations of more than 70% occur across all of western Europe and Scandinavia (figure 2(c)), mainly due emissions reductions over Europe from the road transport sector (table S1). Fractional reductions in POM mass concentrations are typically less than 40% (figure 2(d)), despite a similar absolute reduction compared to BC (figure S1). The smaller fractional change in POM concentrations are due to the larger background concentrations of POM from natural emissions, which are the same in both simulations.

Legislative and technology measures have therefore led to reduced aerosol mass concentrations across Europe, with potential impacts for both regional climate and human health. We compared the change in aerosol concentration calculated due to these air

quality mitigation measures against the change in aerosol concentrations that actually occurred over the period 1970–2009 simulated by Turnock *et al* (2015) using the same model. Using this method we estimate that air pollutant mitigation measures are responsible for 29% of the actual reductions in PM<sub>2.5</sub> that occurred over the same period. Air pollutant mitigation contributes the most to changes in BC concentrations (73%) compared to sulphate (33%) or POM (15%). This difference reflects the different causes behind the changes in anthropogenic emissions and highlights the important effect of enacted European legislation on air quality.

Ammonium nitrate aerosol (absent from our simulations) has increased by 15%–30% over Europe since the 1980s due to the reduction in SO<sub>2</sub> and sulphate aerosols (Fagerli and Aas 2008). The increase in ammonium nitrate aerosol concentrations would partially offset some of our simulated improvements to air quality and health but would not alter the overall net decrease in European mean particulate matter concentrations ( $1.75 \mu\text{g m}^{-3}$ ) due to the larger declines in sulphate (44%), BC (56%) and POM (23%) simulated here.



### 3.2. Health and economic effects

Figure 3 shows the impacts of improvements in regional air quality from air pollutant mitigation measures on public health. The simulated reduction in  $PM_{2.5}$  concentrations due to air pollutant mitigation measures reduces the number of premature deaths across Europe, with the largest numbers prevented across central Europe (Germany and The Netherlands) (figure 3(a)). Air pollutant mitigation measures prevent 3 to 4 premature deaths annually per 10 000 people in central and eastern Europe (figure 3(b)) and 5 to 6 premature deaths annually per 10 000 people in south eastern Europe (Romania and Bulgaria), where the largest reductions in  $PM_{2.5}$  occurred (figures 2(a) and S1(a)).

Across all the European Union (EU), reductions in  $PM_{2.5}$  due to air pollutant mitigation measures prevented 80 250 (37 380–115 840, at 95% confidence intervals of the CRFs) premature deaths annually (individual country totals on figure 3(c) and table S2), which is 19% of the estimated premature deaths due to present-day (2011)  $PM_{2.5}$  concentrations across Europe.

We compared the improved public health due to these air quality mitigation measures against an estimate of the improved public health due to the actual change in  $PM_{2.5}$  concentrations that occurred over the same period. Using the change in simulated  $PM_{2.5}$  concentrations between 1970–74 and 2005–2009 from Turnock *et al* (2015), we estimate that 210 000 annual premature deaths were prevented over this period. Therefore European policies to reduce air pollutants and technological improvements can be considered responsible for ~38% of the total number of premature deaths prevented due to the improved air quality across the EU from 1970 to 2009 (figure 3(c)).

We estimate that the improvement in human health from implementing air pollutant mitigation measures results in a perceived economic benefit to society of US\$232 billion across the EU (individual country totals on figure 3(d) and table S3), 1.4% of the EU's GDP in 2010. In particular, the perceived economic benefits to society for some countries in eastern Europe, such as Hungary and Bulgaria, are relatively more important and represent a greater percentage of their national GDP (>5%). The WHO calculated that

**Table 1.** Changes in the European annual mean all-sky aerosol radiative effects due to air pollutant mitigation measures. Clear-sky and cloudy-sky RE at the TOA and surface between the REF and NO-AQ simulations over the European continental land mass within the domain 10°W–36°E and 36°N–61°N. Values in parentheses are changes over the period 1970–2009 from Turnock *et al* (2015).

	All sky ( $\text{W m}^{-2}$ )	Clear sky ( $\text{W m}^{-2}$ )	Cloudy sky ( $\text{W m}^{-2}$ )
TOA	2.26 (3.1)	1.67 (2.0)	0.59 (1.1)
Surface	3.30	2.70	0.60
Atmosphere	−1.04	−1.03	−0.01

in 2010, premature mortality due to ambient concentrations of particulate matter was costing the EU US\$700 billion, or 4% of the EU's GDP (WHO Regional Office for Europe 2015). We therefore suggest that the perceived economic costs of poor air quality would be 33% greater than they are currently if European legislation and technological improvements had not been implemented.

### 3.3. Effects on climate

Table 1 shows the difference in European annual mean aerosol RE at the TOA and at the surface due to the implementation of the air pollutant emission mitigation measures. The reduction of aerosol concentrations in the atmosphere over Europe (figure 2) causes a positive change in the aerosol RE at the TOA, reduces the atmospheric absorption of radiation (mainly due to reductions in BC) and also increases the shortwave radiation incident at the surface. The annual European mean all-sky aerosol RE at the TOA increases by  $2.3 \pm 0.06 \text{ W m}^{-2}$  with clear-sky TOA radiation increasing by  $1.7 \pm 0.05 \text{ W m}^{-2}$ . The shortwave radiation incident at the surface increases under both all-sky ( $3.3 \pm 0.07 \text{ W m}^{-2}$ ) and clear-sky conditions ( $2.7 \pm 0.05 \text{ W m}^{-2}$ ). Air pollutant mitigation measures have reduced atmospheric absorption of radiation over Europe by  $\sim 1 \text{ W m}^{-2}$  in both all-sky and clear-sky conditions (table 1 and figure 4) due to the large reductions in BC aerosols. Our model shows that air pollution mitigation has resulted in a warming effect on climate compared to what would have occurred, dominated by changes in the direct aerosol RE (clear-sky). This occurs from a combination of warming due to reductions in scattering aerosols (sulphate and POM) and the cooling response from the reduction in absorbing BC aerosols.

We can compare the change in aerosol RE calculated here against an estimate of the RE that actually occurred over the period 1970–2009 (table 1). In transient simulations with historical emissions, Turnock *et al* (2015) estimated that the annual European mean all-sky aerosol RE increased by  $3.1 \text{ W m}^{-2}$  between 1970 and 2009. The larger change in RE over the period 1970–2009 reflects the similar changes in BC but larger reductions in sulphate and POM that occurred in reality. Therefore our model simulations show that

European legislation and technological improvements to reduce air pollutants are responsible for approximately 74% of the change in all-sky TOA aerosol RE from the 1970s to present day.

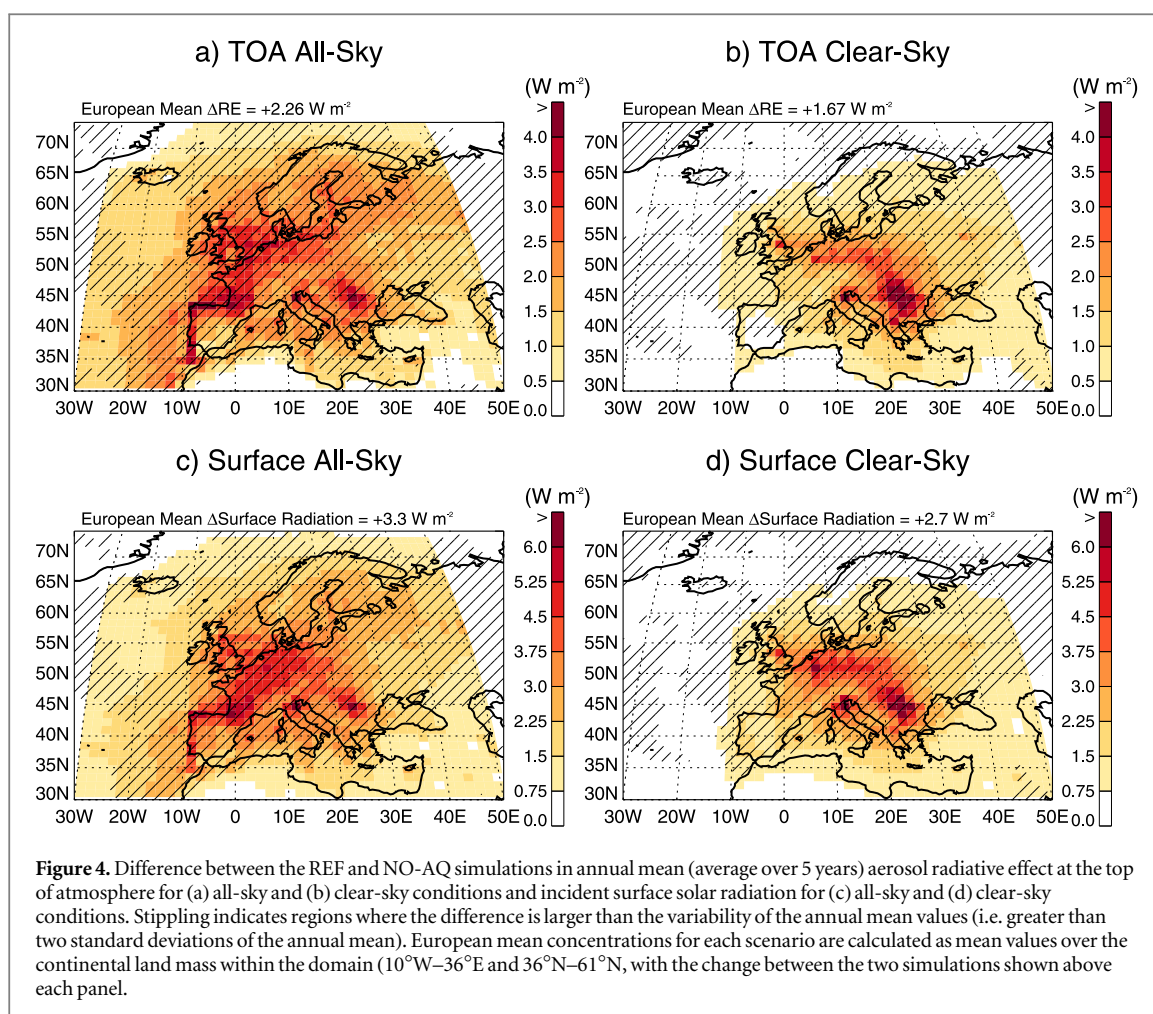
Over the 20th Century nitrate aerosols (not present within our model) were shown by Bellouin *et al* (2011) to have had a relatively small impact on the negative global aerosol forcing, enhancing it by less than 20%. The calculated changes in aerosol REs in this study will have been overestimated due to the absence of the negative aerosol REs from ammonium nitrate.

Figure 4 shows the spatial pattern of changes to the aerosol RE at the TOA and at the surface. The largest increase in TOA clear-sky aerosol RE occurs over south-east and central Europe (figure 4(b)), corresponding with the largest reduction in sulphate mass (figures 2(b) and S1). The largest reductions in atmospheric absorption (TOA minus surface) occur over The Netherlands and Germany where the largest reductions in BC aerosols occurs (figure 2(c)). The TOA warming response over these areas would have been even larger without the reductions of the absorbing BC aerosols (cooling response).

The all-sky changes are also caused by changes to cloud properties (aci). Air pollution mitigation reduces concentrations of cloud condensation nuclei (CCN) (figure S3(a)) leading to larger, less numerous cloud droplets (figure S3(b)), increasing shortwave all-sky radiation at the TOA and surface (figures 4(a) and (c)). Air pollutant mitigation causes the largest increase in all-sky radiation (both TOA and surface) over coastal areas of western Europe (figures 4(a) and (c)), corresponding with the largest reduction in CCN, cloud droplet number concentrations and larger cloud fractions (figures S3 and S4). Over central Europe, CCN and cloud drop concentrations are larger (shown by larger total number concentrations in figure S2), meaning air pollutant mitigation causes smaller fractional changes and a smaller RE here. The difference between all-sky and clear-sky radiation changes (figure S3(d)) gives an indication of the cloudy sky RE, which is greatest over north west Europe.

Overall reductions in aerosols from the implementation of air pollutant mitigation measures resulted in a positive change in the aerosol RE at the TOA and also increased the amount of solar radiation incident at the surface under both all-sky and clear-sky conditions. The simulated change in European all-sky TOA aerosol RE due to air pollutant mitigation is 2.5 times the change in global mean  $\text{CO}_2$  radiative forcing over the period 1970–2009 (Myhre *et al* 2013), indicating the large regional impact of air pollutant mitigation measures. Such changes to the radiative balance over Europe could have non-negligible effects on the climate, impacting both surface temperature and precipitation patterns.

Using the change in TOA aerosol RE between the two simulations, we estimate that the reduction in



particulate matter from the implementation of air pollutant mitigation measures have increased European mean surface temperatures by  $0.45 \pm 0.11 \text{ }^{\circ}\text{C}$  compared to temperatures that would have occurred without mitigation measures (for methods see section 4 of supplementary methods). This change in European surface temperature is anticipated to be slightly smaller than that presented here due to the absence of ammonium nitrate from the simulations. In addition, the reduced atmospheric absorption of radiation caused by mitigation measures will induce a rapid adjustment to increase European precipitation by  $13 \pm 0.8 \text{ mm yr}^{-1}$ . Future work is needed to contrast the human health and economic costs associated with these changes in climate against those quantified here due to air quality improvements.

#### 4. Conclusions

Air quality legislation and technology improvements implemented over Europe have reduced the emission of air pollutants. Here we used a coupled composition-climate model to assess the impact of these reduced emissions on air quality, human health and the Earth's radiative balance.

We used two simulations to quantify the impact of air pollutant mitigation measures on emissions across the energy, industry and road transport sectors over the period 1970–2010 (Crippa *et al* 2015). One simulation used actual 2010 emissions whereas the other simulation used a 2010 emission scenario in which air pollutant mitigation measures were not implemented, represented by the absence of improvements to end-of-pipe abatement measures and technology between 1970 and 2010. The implementation of these air pollutant mitigation measures is estimated to have reduced European anthropogenic emissions of  $\text{SO}_2$  (53%), BC (59%) and OC (32%) compared to what would have occurred in the absence of legislative and technology measures.

We estimate that this reduction in emissions improved regional air quality over Europe by reducing concentrations of fine particulate matter ( $\text{PM}_{2.5}$  by 35%) and their component masses (sulphate by 44%, BC by 56% and POM by 23%). We estimate that these policy measures and technology changes are responsible for  $\sim 29\%$  of the actual reductions in  $\text{PM}_{2.5}$  that occurred from 1970 to 2009.

The improvement in air quality from the implementation of European air pollutant mitigation measures has benefitted human health by preventing

80 000 premature deaths (37 000–116 000, at 95% confidence intervals of the CRF) annually across Europe. These improvements to health have had a perceived economic benefit to society estimated to be US \$232 billion annually, representing 1.4% of the EU's GDP in 2010.

The spatial resolution of our global model (~140 km) means that our results apply to regional changes in PM<sub>2.5</sub>. For this reason our model typically underestimates PM<sub>2.5</sub> concentrations in urban areas of Europe, leading to a ~15% bias in our premature mortality estimates (based on calculations where we adjust simulated PM<sub>2.5</sub> concentrations in urban areas to match observed concentrations). This error is substantially smaller than the factor 3 uncertainty in estimated premature mortality calculated using the 95% confidence intervals of the CRF. Better understanding of the health impacts of PM<sub>2.5</sub>, in addition to studies using higher resolution models would improve future calculations of the impact of air pollutants on human health.

Changes in fine particulate matter concentrations from measures to reduce air pollutants can have an unintended impact on climate by altering the radiative balance. The reduction in aerosol concentrations has caused a positive change to the all-sky aerosol RE at the TOA ( $2 \text{ W m}^{-2}$ ), reduced the absorption of radiation in the atmosphere ( $-1 \text{ W m}^{-2}$ ) and increased the amount of shortwave radiation incident at the surface ( $3 \text{ W m}^{-2}$ ). Changes are largest over central and eastern Europe for clear sky conditions, indicating that aerosol radiation interactions are dominant here, but for all-sky conditions the changes are largest over western Europe, signifying that aerosol cloud interactions are more important here.

We have estimated that these changes in the radiative balance from air pollutant mitigation measures would have caused European mean surface temperatures to increase by  $\sim 0.45 \pm 0.11 \text{ }^\circ\text{C}$  and precipitation by  $\sim 13 \pm 0.8 \text{ mm yr}^{-1}$  compared to those that would have occurred without mitigation measures.

Implementing measures to reduce emissions of air pollutants has led to an improvement in air quality and reduced the impact on human health over Europe. However, the reduction in aerosol concentrations has also had an unintended warming (positive) response on the Earth's radiative balance. The calculated effect on air quality, climate and human health from European legislation and technological improvements implemented over the last 40 years should be used to help inform the design of future multi-pollutant mitigation strategies.

## Acknowledgments

Steven Turnock would like to thank the Natural Environment Research Council (NERC) and Met Office for providing the funding for this PhD

studentship. This work was also made possible by participation in the EU Framework 7 PEGASOS project (no: 265148). We acknowledge the use of the MONSooN system, a collaborative facility supplied under the Joint Weather and Climate Research Programme, a strategic partnership between the Met Office and NERC. We would like to acknowledge the use of the EDGAR anthropogenic emissions inventory and the scenarios used in this study provided by the Joint Research Centre, Italy. Edward Butt is funded by the United Bank of Carbon.

## References

- Andreae M O, Jones C D and Cox P M 2005 Strong present-day aerosol cooling implies a hot future *Nature* **435** 1187–90
- Andrews T, Forster P M, Boucher O, Bellouin N and Jones A 2010 Precipitation, radiative forcing and global temperature change *Geophys. Res. Lett.* **37** L14701
- Anenberg S C, Talgo K, Arunachalam S, Dolwick P, Jang C and West J J 2011 Impacts of global, regional, and sectoral black carbon emission reductions on surface air quality and human mortality *Atmos. Chem. Phys.* **11** 7253–67
- Anenberg S C *et al* 2012 Global air quality and health co-benefits of mitigating near-term climate change through methane and black carbon emission controls *Environ. Health Perspect.* **120** 831–9
- Arnett A, Unger N, Kulmala M and Andreae M O 2009 Clean the air, heat the planet? *Science* **326** 672–3
- Bellouin N, Rae J, Jones A, Johnson C, Haywood J and Boucher O 2011 Aerosol forcing in the climate model intercomparison project (CMIP5) simulations by HadGEM2-ES and the role of ammonium nitrate *J. Geophys. Res.* **116** D20206
- Boldo E, Medina S, LeTertre A, Hurley F, Mücke H-G, Ballester F, Aguilera I and Eilstein D 2006 Apehis: health impact assessment of long-term exposure to PM(2.5) in 23 European cities *Eur. J. Epidemiology* **21** 449–58
- Boucher O *et al* 2013 Clouds and aerosols *Climate Change 2013: The Physical Science Basis Contribution of Working Group I to the Fifth Assessment Report of the Intergovernmental Panel on Climate Change* (Cambridge: Cambridge University Press)
- Brunekreef B and Holgate S T 2002 Air pollution and health *Lancet* **360** 1233–42
- Burnett R T *et al* 2014 An integrated risk function for estimating the global burden of disease attributable to ambient fine particulate matter exposure *Environ. Health Perspect.* **122** 397–403
- Cherian R, Quaas J, Salzmann M and Wild M 2014 Pollution trends over Europe constrain global aerosol forcing as simulated by climate models *Geophys. Res. Lett.* **41** 2176–81
- Cohen A J *et al* 2005 The global burden of disease due to outdoor air pollution *J. Toxicology Environ. Health A* **68** 1301–7
- Colette A *et al* 2011 Air quality trends in Europe over the past decade: a first multi-model assessment *Atmos. Chem. Phys.* **11** 11657–78
- Colette A *et al* 2013 European atmosphere in 2050, a regional air quality and climate perspective under CMIP5 scenarios *Atmos. Chem. Phys.* **13** 7451–71
- Crippa M, Janssens-Maenhout G, Dentener F, Guizzardi D, Sindelarova K, Muntean M, Dingenen R V and Granier C 2015 Forty years of improvements in European air quality: the role of EU policy-industry interplay *Atmos. Chem. Phys. Discuss.* **15** 20245–85
- Crippa M, Janssens-Maenhout G, Guizzardi D and Galmarini S 2016 Understanding the rapid precipitation response to CO<sub>2</sub> and aerosol forcing on a regional scale *J. Climate* **29** 583–94
- EC-JRC/PBL 2015 *EDGAR version 4.3*. (online) 2015 Available from: <http://edgar.jrc.ec.europa.eu/>

- European Environment Agency (EEA) 2014 *Air Quality in Europe—2014 Report* (<http://eea.europa.eu/publications/air-quality-in-europe-2014>)
- Fagerli H and Aas W 2008 Trends of nitrogen in air and precipitation: model results and observations at EMEP sites in Europe, 1980–2003 *Environ. Pollut.* **154** 448–61
- Fiore A M, Naik V and Leibensperger E M 2015 Air quality and climate connections *J. Air Waste Manage. Assoc.* **65** 645–85
- Fiore A M *et al* 2012 Global air quality and climate *Chem. Soc. Rev.* **41** 6663–83
- Fowler D *et al* 2009 Atmospheric composition change: ecosystems–atmosphere interactions *Atmos. Environ.* **43** 5193–267
- Gan C-M, Pleim J, Mathur R, Hogrefe C, Long C N, Xing J, Roselle S and Wei C 2014 Assessment of the effect of air pollution controls on trends in shortwave radiation over the United States from 1995 through 2010 from multiple observation networks *Atmos. Chem. Phys.* **14** 1701–15
- IPCC 2013 Summary for policymakers *Climate Change 2013: The Physical Science Basis. Contribution of Working Group I to the Fifth Assessment Report of the Intergovernmental Panel on Climate Change* ed T F Stocker *et al* (Cambridge: Cambridge University Press)
- Kloster S, Dentener F, Feichter J, Raes F, van Aardenne J, Roekner E, Lohmann U, Stier P and Swart R 2008 Influence of future air pollution mitigation strategies on total aerosol radiative forcing *Atmos. Chem. Phys.* **8** 6405
- Koch D *et al* 2011 Coupled aerosol–chemistry–climate twentieth-century transient model investigation: trends in short-lived species and climate responses *J. Clim.* **24** 2693–714
- Krüger O and Graßl H 2002 The indirect aerosol effect over Europe *Geophys. Res. Lett.* **29** 3–6
- Lamarque J-F *et al* 2013 The atmospheric chemistry and climate model intercomparison project (ACCMIP): overview and description of models, simulations and climate diagnostics *Geosci. Model Dev.* **6** 179–206
- Leibensperger E M, Mickley L J, Jacob D J, Chen W-T, Seinfeld J H, Nenes A, Adams P J, Streets D G, Kumar N and Rind D 2012a Climatic effects of 1950–2050 changes in US anthropogenic aerosols: I. Aerosol trends and radiative forcing *Atmos. Chem. Phys.* **12** 3333–48
- Leibensperger E M, Mickley L J, Jacob D J, Chen W-T, Seinfeld J H, Nenes A, Adams P J, Streets D G, Kumar N and Rind D 2012b Climatic effects of 1950–2050 changes in US anthropogenic aerosols: II. Climate response *Atmos. Chem. Phys.* **12** 3349–62
- Lelieveld J, Evans J S, Fnais M, Giannadaki D and Pozzer A 2015 The contribution of outdoor air pollution sources to premature mortality on a global scale *Nature* **525** 367–71
- Levy J I, Wilson A M and Zwack L M 2007 Quantifying the efficiency and equity implications of power plant air pollution control strategies in the United States *Environ. Health Perspect.* **115** 743–50
- Mann G W *et al* 2014 Intercomparison and evaluation of global aerosol microphysical properties among AeroCom models of a range of complexity *Atmos. Chem. Phys.* **14** 4679–713
- Marmar E, Langmann B, Fagerli H and Vestreng V 2007 Direct shortwave radiative forcing of sulfate aerosol over Europe from 1900 to 2000 *J. Geophys. Res.* **112** D23S17
- Myhre G *et al* 2013 Anthropogenic and natural radiative forcing *Climate Change 2013: The Physical Science Basis Contribution of Working Group I to the Fifth Assessment Report of the Intergovernmental Panel on Climate Change* ed T F Stocker *et al* (Cambridge: Cambridge University Press)
- Pascal M *et al* 2013 Assessing the public health impacts of urban air pollution in 25 European cities: results of the Aphekom project *Sci. Total Environ.* **449** 390–400
- Philipona R, Behrens K and Ruckstuhl C 2009 How declining aerosols and rising greenhouse gases forced rapid warming in Europe since the 1980s *Geophys. Res. Lett.* **36** L02806
- Pozzoli L, Janssens-Maenhout G, Diehl T, Bey I, Schultz M G, Feichter J, Vignati E and Dentener F 2011 Re-analysis of tropospheric sulfate aerosol and ozone for the period 1980–2005 using the aerosol–chemistry–climate model ECHAM5–HAMMOZ *Atmos. Chem. Phys.* **11** 9563–94
- Richardson T, Forster P, Andrews T and Parker D 2015 Understanding the rapid precipitation response to CO<sub>2</sub> and Aerosol forcing on a regional scale *J. Clim.* in press
- Ruckstuhl C *et al* 2008 Aerosol and cloud effects on solar brightening and the recent rapid warming *Geophys. Res. Lett.* **35** L12708
- Seaton A, Godden D, MacNee W and Donaldson K 1995 Particulate air pollution and acute health effects *Lancet* **345** 176–8
- Shindell D and Faluvegi G 2009 Climate response to regional radiative forcing during the twentieth century *Nat. Geosci.* **2** 294–300
- Shindell D T *et al* 2012 Simultaneously mitigating near-term climate change and improving human health and food security *Science* **335** 183–9
- Stjern C W, Stohl A and Kristjánsson J E 2011 Have aerosols affected trends in visibility and precipitation in Europe? *J. Geophys. Res.* **116** D02212
- Tørseth K, Aas W, Breivik K, Fjæraa A M, Fiebig M, Hjellbrekke A G, Lund Myhre C, Solberg S and Yttri K E 2012 Introduction to the European Monitoring and Evaluation Programme (EMEP) and observed atmospheric composition change during 1972–2009 *Atmos. Chem. Phys.* **12** 5447–81
- Turnock S T *et al* 2015 Modelled and observed changes in aerosols and surface solar radiation over Europe between 1960 and 2009 *Atmos. Chem. Phys.* **15** 9477–500
- US Environmental Protection Agency 2011 *Technology Transfer Network Clearinghouse for Inventories and Emission Factors, National Emissions Inventory (NEI) Air Pollutant Emissions Trends Data* ([www.epa.gov/air-emissions-inventories](http://www.epa.gov/air-emissions-inventories)) (accessed 23 July 2015)
- Unger N, Shindell D T, Koch D and Streets D G 2008 Air pollution radiative forcing from specific emissions sectors at 2030 *J. Geophys. Res.* **113** D02306
- United Nations Economic Commission for Europe 2004 *Clearing the Air: 25 years of the Convention on Long-Range Transboundary Air Pollution* ed J Sliggers and W Kakebeke ([www.unece.org/fileadmin/DAM/env/lrtap/ExecutiveBody/BOOKscreen.pdf](http://www.unece.org/fileadmin/DAM/env/lrtap/ExecutiveBody/BOOKscreen.pdf))
- Vautard R, Yiou P and van Oldenborgh G J 2009 Decline of fog, mist and haze in Europe over the past 30 years *Nat. Geosci.* **2** 115–9
- Vestreng V, Myhre G, Fagerli H, Reis S and Tarrasón L 2007 Twenty-five years of continuous sulphur dioxide emission reduction in Europe *Atmos. Chem. Phys.* **7** 3663–81
- von Schneidmesser E *et al* 2015 Chemistry and the linkages between air quality and climate change *Chem. Rev.* **115** 3856–97
- WHO Regional Office for Europe 2015 *Economic Cost of the Health Impact of Air Pollution in Europe: Clean Air, Health and Wealth* (Copenhagen: WHO Regional Office for Europe) ([www.euro.who.int/en/media-centre/events/events/2015/04/ehp-mid-term-review/publications/economic-cost-of-the-health-impact-of-air-pollution-in-europe](http://www.euro.who.int/en/media-centre/events/events/2015/04/ehp-mid-term-review/publications/economic-cost-of-the-health-impact-of-air-pollution-in-europe))
- Wild M 2009 Global dimming and brightening: a review *J. Geophys. Res.* **114** D00D16
- World Health Organization 2014 *Burden of Disease from Ambient Air Pollution for 2012* ([http://who.int/phe/health\\_topics/outdoorair/databases/AAP\\_BoD\\_results\\_March2014.pdf](http://who.int/phe/health_topics/outdoorair/databases/AAP_BoD_results_March2014.pdf)) (accessed 3 May 2015)

## **Chapter 6**

### **Discussion and Conclusion**

Anthropogenic emissions have altered significantly over the last 50 years across regions such as Europe where air pollution control legislation has played a large part in reducing emissions since the 1980s. This has altered the concentrations and properties of aerosols across this time period, which has important consequences for their contribution to air quality and also their impact on climate. It is important to quantify if a composition climate model is able to reproduce the impact of past measures to improve air quality (on both air pollutants and climate), prior to using such models in estimating the impact from future emission reduction measures.

A coupled composition climate model, HadGEM3-UKCA, was used to study the effect of changes in anthropogenic emissions on aerosols and their impact on air quality and climate across Europe over the period 1960 to 2009. HadGEM3-UKCA simulates the interaction between chemistry, aerosols and the radiative balance, thus linking any changes in emissions to impacts on predicted air quality and climate.

The following sections provide a summary of the results from each chapter and refer back to the aims of the thesis in Chapter 1.

#### **6.1 Modelled and Observed Changes in aerosols and surface solar radiation over Europe between 1960 and 2009**

HadGEM3-UKCA was used to simulate the changes in European aerosol components and their effect on the radiative balance over a period of substantial change in anthropogenic emissions. The model was also evaluated against long term observations of aerosol properties over Europe to ascertain the ability of such models to reproduce long term changes in aerosol properties. A summary of the findings from this study in relation to the research questions posed is presented below:

- a. Observed European sulphate aerosol mass concentrations reduced by 68% over the period 1978 to 2009 with the model simulating a 78% reduction. Total suspended particulate matter reduced by 50% between 1978 and 1998, whilst a 20% reduction was simulated by the model. Over the period 1997 to 2009, both observed and simulated

PM<sub>10</sub> concentrations reduced by 9% and 8% respectively. Observed and simulated AOD reduced by 11-14% over the period 2000 to 2009 across Europe. SSR was observed and simulated to have increased over Europe between 1990 and 2009 by 4 – 6 W m<sup>-2</sup>. A decrease in SSR occurred in both the observations and model simulations from 1960 to 1974. However, over the period 1975 to 1989 observed SSR increased whilst that simulated by the model decreased.

- b. The model is able to reproduce the annual mean changes in sulphate aerosol mass over a 30 year period, although the magnitude of the linear trend in winter is underestimated. In addition, the model is able to reproduce the more recent changes in PM<sub>10</sub> (1997 – 2009), AOD (2000 – 2009) and SSR (1990 – 2009). However, the model is not able to reproduce the magnitude of the changes in total suspended particulate matter (1978 – 1998) or the sign and magnitude of changes in SSR before 1990.

The model also consistently underpredicts aerosol mass concentrations of sulphate, total suspended particulate matter and PM<sub>10</sub> concentrations across their respective measurement periods of 1978-2009, 1978-1998 and 1998-2009. In particular, the model exhibited a large underprediction of sulphate aerosol mass in winter over northern Europe. Present day aerosol number concentrations are also underpredicted across all size ranges, with a slightly better representation of smaller sized particles than larger ones. The model had a smaller bias when compared to ground based AOD observations than for surface mass concentrations but to calculate AOD requires additional information (e.g. relative humidity) so it can't be directly compared to surface observations.

- c. A number of possible reasons have been suggested for the model underestimation including:
  - o Uncertainties in observations;
  - o Overestimation of deposition processes;
  - o Underestimation of aerosols from missing sources of nitrate, anthropogenic SOA, dust, domestic primary biomass combustion and primary biological aerosols.

The large underestimation of wintertime sulphate across Europe could be due to an underrepresentation of the in-cloud oxidation reaction route to sulphate aerosol formation or an overestimation of deposition processes. The former is the subject of Chapter 4 in this thesis.

- d. The European all-sky TOA shortwave aerosol radiative forcing (relative to a 1980-2000 mean) has increased by  $> 3.0 \text{ W m}^{-2}$  over the period 1973 to 2009. This change has occurred concurrently with a period of large reductions in anthropogenic emissions and aerosol concentrations leading to a reduction in their cooling effect on climate. A similar change was also simulated for the change in clear-sky TOA aerosol radiative forcing across Europe.
- e. The model evaluation highlighted that whilst absolute concentrations of aerosols tended to be underestimated, the change in both sulphate and SSR over the period 1990 to 2009 are relatively well reproduced. This is also the period when most of the change in TOA aerosol radiative forcing occurs. Therefore the model evaluation of long term changes in aerosols can provide a degree of confidence in the magnitude of the simulated changes in aerosol radiative effects.

## **6.2 The spatial and temporal importance of pH to sulphate aerosols and radiative forcing over the period 1960 to 2009**

A similar experimental set up as described above was used to ascertain the sensitivity of sulphate aerosol formation and its radiative effects to spatial and temporal variations in cloud water pH over a period of substantial change in anthropogenic emissions. A summary of the findings from this study in relation to the research questions posed is presented below:

- a. An increase in cloud water pH increased the total column burden of sulphate aerosol mass across regions with high anthropogenic  $\text{SO}_2$  emissions and oxidant limited conditions (Europe, north eastern United States and east Asia). Across other areas of the globe a slight reduction in the total column burden of sulphate aerosols was predicted due to the decreased importance of other routes to sulphate aerosol formation (namely the gas-phase oxidation route) and a decreased global atmospheric lifetime of sulphate from increased deposition rates.
- b. The model evaluation against ground based observations of sulphate aerosol mass was generally improved across Europe when using an increased value of cloud water pH, particularly in wintertime. In addition, simulated sulphate mass concentrations using a lower value of pH in the 1980s compared better to observations whereas, in the period 2005 to 2009 simulated concentrations using a higher pH were

more representative of observations. The modelled representation of wintertime temporal trends in sulphate aerosol mass across Europe was improved by increasing cloud water pH. However, the increase in cloud water pH resulted in an overestimation of summertime trends in sulphate mass.

- c. The increase in cloud water pH also affected the aerosol size distribution by reducing the number of smaller sized particles in the nucleation and Aitken modes, whilst increasing the number of larger particles within the accumulation and coarse modes. The number of particles at CCN relevant sizes was reduced by the increase in cloud water pH.
- d. By reducing the number of particles able to act as CCN, the increase in cloud water pH has effectively reduced the magnitude of the aerosol cloud albedo effect. A positive response of up to  $5 \text{ W m}^{-2}$  locally was found as the difference between the aerosol radiative effects in the pH 6.5 and pH 5.0 simulations. However, under clear skies a negative response of up to  $3.0 \text{ W m}^{-2}$  occurred over Europe, north east USA and east Asia due to the increased sulphate aerosol mass produced. Calculated aerosol radiative forcings (1970 to 2009) were found to be independent of cloud water pH, provided that the pH is the same for both time periods. However, large regional differences in aerosol radiative forcings were calculated if pH was allowed to vary between the two time periods. Over Europe an assumed pH increase between 1970 and 2009 resulted in an aerosol radiative forcing of  $+7.0 \text{ W m}^{-2}$  whereas, for a pH decrease over the same time it was  $+1.5 \text{ W m}^{-2}$ . Similarly over the North Atlantic aerosol radiative forcing was calculated to vary between  $-4.6 \text{ W m}^{-2}$  and  $+6.9 \text{ W m}^{-2}$  depending on whether an increase or decrease in pH was assumed.
- e. The use of a fixed global value of cloud water pH is not sufficient to represent the spatial and temporal changes in sulphate aerosol formation that would have occurred due to the anticipated changes in cloud water pH. This could lead to uncertainties in the calculation of the aerosol radiative effects and also the impact on particulate air quality, particularly over regions that are sensitive to in-cloud aqueous phase sulphate formation (e.g. Europe, north east USA and east Asia).

### **6.3 The impact of European legislative and technology measures to reduce air pollutants on air quality, human health and climate**

An emission scenario was used to consider the impact from the implementation of specific European air quality policy measures and technology changes on air quality, human health and climate. A summary of the findings from this study in relation to the research questions posed is presented below:

- a. The application of European air quality policy measures for the end-of-pipe treatment of emissions, as well as improvements in technology since the 1970s has resulted in a substantial reduction in European emissions of aerosol precursor species. Compared to what would have occurred without these mitigation measures, total European emissions of SO<sub>2</sub>, BC and OC are 53%, 59% and 32% lower. These reductions are dominated by changes in the energy and transportation sectors.
- b. The implementation of these air quality policy measures has improved particulate air quality across Europe. European fine particulate matter (PM<sub>2.5</sub>) reduced by 35%, along with its constituent components of sulphate by 44%, BC by 56% and POM by 23%.
- c. The reduction in fine particulate matter from the implementation of the air quality policy measures and technology improvements has been calculated as preventing 80,250 premature deaths annually across Europe. This represents 19% of the calculated premature deaths due to the current concentrations of PM<sub>2.5</sub> across Europe, showing that measures to reduce the emissions of air pollutants have benefitted the health of citizens of the European Union. This improvement in health has also been calculated to have a perceived economic benefit to society of US\$ 232 billion across the EU, 1.4% of the EU's GDP in 2010.
- d. As well as the benefits to air quality and human health, the implementation of air quality policy measures and technology improvements has had an unintended impact on climate via changes to the radiative balance. The reduction in aerosol concentrations causes a positive change in the aerosol radiative effect at the TOA of 2.3 W m<sup>-2</sup> across Europe. This change occurs from the combined effect of a warming response due to reductions in scattering aerosols (sulphate and POM) and a cooling response from a reduction in

absorbing BC aerosols. In addition, the atmospheric absorption reduces (due to decreases in BC) and the amount of radiation incident at the surface increases. Using the change in aerosol radiative effects at the TOA, European surface temperatures are calculated to have increased by 0.45°C when compared to what would have occurred without the mitigation measures. The reduction in atmospheric absorption of radiation is anticipated to induce a rapid adjustment in European precipitation and increase it by 13 mm yr<sup>-1</sup>.

## 6.4 Summary

The large changes in anthropogenic emissions over the last 40 years across Europe induced considerable variations in the concentrations, properties and processes of aerosols, as well as in their impact on air quality and climate. Chapter 3 of this thesis evaluated the composition climate model HadGEM3-UKCA (microphysical treatment of both aerosol mass and number) over Europe for the period 1978 to 2009 against a number of different observations of aerosol properties (sulphate, total mass, aerosol number concentrations, AOD and surface solar radiation). Compared to previous studies this analysis represents a more detailed model evaluation of the changes in aerosol properties over a relatively long timescale across Europe (a region experiencing large changes in anthropogenic emissions) by using a larger number and type of observations, a detailed treatment of aerosols within the model and monthly output over a multi-decadal period (Berglen et al., 2007; Koch et al., 2011; Skeie et al., 2011; Shindell et al., 2013). The results from Chapter 3 also complement other such detailed evaluation studies (Leibensperger et al., 2012a; Chin et al., 2014) by showing that HadGEM3-UKCA is able to reproduce the temporal trends but not the absolute magnitude of aerosol properties over the last 30 years across Europe. Understanding the ability of the model to reproduce historical changes of aerosol properties in response to changing anthropogenic emissions is important when using the same model to simulate the future response to emissions.

The long term model evaluation highlighted that the absence of aerosol sources (e.g. nitrate aerosols, emissions of domestic combustion and primary biological aerosols) and the underrepresentation of aerosol processes (e.g. cloud pH and anthropogenic SOA formation) could account for some of the identified model bias and are potentially topics for future model development. Additionally the model was able to reproduce the

observed increase in incoming surface solar radiation since 1990 ('brightening') but was unable to simulate the decrease ('dimming') in the 1980s in accordance with other studies (Folini & Wild, 2011; Allen et al., 2013; Chiacchio et al., 2015). The double-call radiation setup used in this thesis was able to show that the inclusion of aerosols is necessary to reproduce the increasing trend in SSR since the 1990s, which provided confidence in the simulated positive response of aerosol radiative effects across Europe over this period as anthropogenic emissions declined.

The underrepresentation of cloud water pH in the model was a process identified within chapter 3 and other studies (Roelofs et al., 2001; Berglen, 2004; Textor et al., 2006) that could have caused some of the underestimation of observed wintertime sulphate mass concentrations across Europe. Cloud water pH is known to be important for in-cloud aqueous phase sulphate aerosol formation (Roelofs et al., 2001; Faloon, 2009) but its treatment varies between global climate model (Ervens, 2015). Chapter 4 improves on previous studies (Redington et al., 2009; Banzhaf et al., 2012) by assessing the sensitivity of sulphate aerosol formation and aerosol radiative effects to changes in cloud water pH over the period 1960 to 2009, when anthropogenic emissions and concentrations of oxidants have varied.

An increase in cloud water pH caused sulphate aerosol formation to increase over regions with a seasonal limitation in oxidants and also large sources of SO<sub>2</sub>. The strength of aerosol radiation interactions also increased over these regions (negative response in clear-sky aerosol radiative effects). Over Europe, the increase in cloud water pH was able to virtually eliminate the model bias against observed sulphate mass concentrations, indicating the importance of including both temporal and spatial variations in pH. Across other regions an increase in cloud water pH shifted the aerosol size distribution to larger sizes, reducing the lifetime of aerosols in the atmosphere and resulting in a positive response in all-sky aerosol radiative effects.

Previous studies into the uncertainty of aerosol cloud radiative forcing assumed that uncertainties in pH are correlated between the start and end point, therefore neglecting any impact from temporal changes in pH (Carslaw et al., 2013; Regayre et al., 2014). It was found in chapter 4 that the magnitude of the aerosol radiative forcing calculated over the period 1970 to 2009 was particularly sensitive to the value of pH selected at the start and end point of the time period. Over Europe an increase in cloud

water pH (from 5.0 to 6.5) between 1970 and 2009 resulted in an aerosol radiative forcing that was  $5.5 \text{ W m}^{-2}$  larger than if a decrease was assumed over the same period. Uncertainties in the current estimates of aerosol radiative forcing could be even larger if these spatial and temporal changes in cloud water pH are not taken into account.

Whilst varying pH by 1.5 units globally is a relatively extreme sensitivity study, observations have indicated that similar changes are possible at the regional scale. The results in Chapter 4 highlight the regional importance of taking into account such spatial and temporal changes in cloud water pH for simulating sulphate aerosol formation and aerosol radiative effects. The results show that a fixed representation of cloud water pH in models is not adequate to represent the effects from such changes.

Chapters 3 and 4, along with previous studies (Colette et al., 2011; Koch et al., 2011), have considered the impact of total emission changes over recent decades on aerosol properties, air quality and climate via aerosol radiative effects. Historical anthropogenic emissions have changed due to the combined effects of economic factors, makeup of the national energy supply, legislation and abatement technology. It is not known what fraction of emission reductions and their impact on air quality, human health and climate can be attributed to the implementation of previous air quality legislation and emission abatement technology as no studies have previously analysed this. When considering the design of future emission mitigation measures it is important to consider how effective past legislation and technology measures have been.

Chapter 5 showed that historical European air quality policy measures and technology improvements reduced anthropogenic emissions of aerosol precursor species. European particulate air quality was improved by the implementation of these measures, with annual mean  $\text{PM}_{2.5}$  concentrations reducing by  $1.75 \mu\text{g m}^{-3}$  (35%). This represents 29% of the actual changes in  $\text{PM}_{2.5}$  that occurred in Chapter 3. The reduction in  $\text{PM}_{2.5}$  concentrations improved human health over Europe by preventing 80,250 premature deaths annually, which is 19% of the prevented deaths attributed to European  $\text{PM}_{2.5}$  concentrations in 2011. However, the implementation of the measures to improve air quality has had an unintended impact on the radiative balance. The reduction in aerosol concentrations induced a positive change in all-sky aerosol radiative effects at the top of atmosphere of  $+2.3 \text{ W m}^{-2}$ , compared to a change in Chapter 3 of  $+3.1 \text{ W m}^{-2}$ . Based on these changes to the radiative balance, European annual mean surface temperatures are

calculated to have increased by 0.45 °C when compared to what would have occurred without the mitigation measures.

The reduction in PM<sub>2.5</sub> concentrations and the change in aerosol radiative effects calculated in Chapter 5 are smaller than the changes calculated in Chapter 3 but indicate the contribution of policy and technology induced changes to that of the total. The results in Chapter 5 quantify the efficacy of European air quality legislative and technology measures by linking them directly to changes in anthropogenic emissions and the resultant effect on air quality, human exposure to air pollutants and inadvertent climate impacts.

Overall it is important to understand and evaluate model simulations of historical changes in aerosols and their radiative effects over a period of substantial change in anthropogenic emissions (in part due to legislative measures) prior to developing future mitigation measures to improve air quality.

## **6.5 Implications for Future Work**

The results of this thesis show that the large change in anthropogenic emissions over Europe, in part due to the implementation of air pollutant emission reduction legislation, has had a considerable impact on the concentrations of aerosols and also their radiative effects. The model evaluation within Chapter 3 highlighted that whilst HadGEM3-UKCA was able to simulate the changes in aerosols relatively well over the last 30 years, a number of potentially important model biases occurred. In particular, aerosol mass and number concentrations were consistently underestimated by the model, implying that aerosol sources and/or processes are underrepresented. Therefore to be able to simulate temporal changes in aerosols across regions within global composition climate models, it is important that future model development attempts to address some of these biases.

Future work to improve the model evaluation against observations should focus on a number of potentially important processes that are missing within the current version of HadGEM3-UKCA. Nitrate is an important aerosol component that needs to be included within the model to be able to accurately simulate both past and future changes in aerosols and their radiative effects (Bellouin et al., 2011). This could be particularly important when simulating sulphate aerosol formation and also for predicting future air quality effects across regions (e.g. Europe), as the two aerosol species

compete with each other for ammonia. Here large reductions in sulphate and uncontrolled increases in ammonia emissions mean that nitrate will be an important future component of fine particulate matter (Fagerli & Aas, 2008; Pozzer et al., 2012; Wang et al., 2013). This is an active area of model development within the UKCA community but future work should focus on evaluating the ability of the model to reproduce temporal changes in aerosol mixtures that include nitrate.

The calculation of SOA and the proportion from biogenic and anthropogenic sources is a large uncertainty within global models, with most underpredicting the quantity of organic aerosols (Volkamer et al., 2006; Farina et al., 2010; Spracklen et al., 2011; Tsigaridis et al., 2014). The inclusion of additional SOA from both biogenic and anthropogenic sources could improve the model representation of organic aerosol and its comparison against observations. The large model bias in total suspended particulate matter over the period 1978 to 1998 and the improved comparison against PM<sub>10</sub> observations between 1997 and 2009 indicate that larger sized particles e.g. dust or biological material, are underrepresented in the model. Including sources of re-suspended mineral dust, primary biological particles (Heald & Spracklen, 2009), domestic wood burning and wildfires over Europe (Hodzic et al., 2007; Langmann et al., 2008; Manders et al., 2012) within emission inventories could improve the model-observational comparison.

The model evaluation of long term changes in aerosols could be extended to include additional datasets of long term observations such as satellite products and also ground based observations from across other regions e.g. North America. This could extend the model evaluation to outside Europe and include other methods of measuring aerosols to ascertain if the model biases exist in other regions and for other measurement techniques.

Whilst the focus of Chapter 3 has been on the changes in anthropogenic emissions and the effect on aerosols over the period 1960 to 2009, natural emissions of aerosols and their precursor species could also have changed. The importance of any temporal trends in natural sources of dust or sea salt could be investigated to ascertain their influence on European air quality and aerosol radiative effects.

Chapter 3 showed that to be able to capture observed spatial and temporal changes in aerosols within the model, certain aerosol processes are not adequately represented. Chapter 4 explored the sensitivity of sulphate aerosol formation to spatial and temporal changes in cloud water pH. This

showed that global composition climate models need to simulate a spatially and temporally varying cloud water pH to be able to accurately represent sulphate aerosol formation.

Future developments to HadGEM3-UKCA could include the incorporation of an online calculation of cloud water pH, such as those within other models (Berglen, 2004; Redington et al., 2009; Ervens, 2015). This model development should be tested against the sulphate and SO<sub>2</sub> observations over Europe used within this thesis. The model evaluation can be extended to include observations from north America and other regions that are sensitive to aqueous phase chemistry to provide a thorough validation of the new pH parameterisation. In particular, it would be important to use the version of the model that includes nitrate chemistry to take account of the effect of changes in sulphate aerosol on nitrate. The version of HadGEM3-UKCA utilising an “online” pH calculation could then be compared to the results within this thesis, as well as the work down on uncertainty estimation by Lee et al., (2013). All of which could provide an indication of how much a temporal change in such a parameter that is important for aerosol formation could affect aerosol radiative forcing. Additionally a pre-industrial simulation could be conducted to include the online pH calculation and ascertain any difference in the pre-industrial to present day aerosol radiative forcing.

Chapter 5 showed the impact of air pollutant mitigation measures and technology improvements on air quality, human health and climate using a double call configuration of the radiation scheme. This allowed the changes in the radiative balance to be diagnosed and used in a simple calculation of the effect on surface temperatures and precipitation. To improve on this the same set of emissions could be used within a version of the model that is coupled to an ocean, set up to generate its own meteorology (so called “free-running”) and has a single call to the radiation scheme. This would allow radiative changes from aerosols to feedback onto the meteorology and calculate the impact on climate from air quality measures. Using an updated version of the model that also incorporates the ACTIVATE scheme for aerosol cloud interactions would allow for aerosols to induce rapid adjustments on clouds. A comparison between two simulations using the reference and no air quality emissions would ascertain the effect on temperature and precipitation from the implementation of the air quality mitigation measures and technology changes. The analysis could be extended further to the impact of such measures on the hydrological cycle and in particular the ‘acid rain’ problems across northern Europe in the

1980s. This would provide a more robust estimation of the climate response to air quality mitigation measures.

As the emission scenarios provided also include changes to gas-phase air pollutants, the analysis could be easily extended from the focus on particulate air quality to include that of gas phase species e.g. O<sub>3</sub>. The air quality, health and radiative impacts from gas-phase species such as O<sub>3</sub> could be considered under the same scenario as was done for particulate air quality.

Using the understanding gained from Chapter 5 it would be a natural step to analyse how future air quality mitigation measures could affect climate and also the impact of a future climate (from CO<sub>2</sub> driven changes) on air pollutants. This could also be extended to future impacts on human health from air pollutants. Using an earth system model, the air quality, chemistry climate interactions and feedbacks (Figure 1.10) could be investigated by using future emission pathways of air pollutants. Using such a setup, the impact on other areas of the Earth system such as the carbon/nitrogen cycle could also be investigated. This is important as understanding the various aerosol-chemistry-climate mechanisms from different aerosol components is essential to comprehend changes to the past and present day prior to making any future climate predictions (Hansen et al., 2007; Kloster et al., 2008).

## 6.6 References

- Allen, R.J., Norris, J.R. & Wild, M. (2013). Evaluation of multidecadal variability in CMIP5 surface solar radiation and inferred underestimation of aerosol direct effects over Europe, China, Japan, and India. *Journal of Geophysical Research: Atmospheres*. 118 (12). p.pp. 6311–6336.
- Banzhaf, S., Schaap, M., Kerschbaumer, A., Reimer, E., Stern, R., van der Swaluw, E. & Builtjes, P. (2012). Implementation and evaluation of pH-dependent cloud chemistry and wet deposition in the chemical transport model REM-Calgrid. *Atmospheric Environment*. 49. p.pp. 378–390.
- Bellouin, N., Rae, J., Jones, A., Johnson, C., Haywood, J. & Boucher, O. (2011). Aerosol forcing in the Climate Model Intercomparison Project (CMIP5) simulations by HadGEM2-ES and the role of ammonium nitrate. *Journal of Geophysical Research*. 116 (D20). p.p. D20206.

- Berglen, T.F. (2004). A global model of the coupled sulfur/oxidant chemistry in the troposphere: The sulfur cycle. *Journal of Geophysical Research*. 109 (D19). p.p. D19310.
- Berglen, T.F., Myhre, G., Isaksen, I.S.A., Vestreng, V. & Smith, S.J. (2007). Sulphate trends in Europe: are we able to model the recent observed decrease? *Tellus B*. 59 (4). p.pp. 773–786.
- Carslaw, K.S., Lee, L. a., Reddington, C.L., Pringle, K.J., Rap, a., Forster, P.M., Mann, G.W., Spracklen, D. V., Woodhouse, M.T., Regayre, L. a. & Pierce, J.R. (2013). Large contribution of natural aerosols to uncertainty in indirect forcing. *Nature*. 503 (7474). p.pp. 67–71.
- Chiacchio, M., Solmon, F., Giorgi, F., Stackhouse, P. & Wild, M. (2015). Evaluation of the radiation budget with a regional climate model over Europe and inspection of dimming and brightening. *Journal of Geophysical Research: Atmospheres*. 120 (5). p.pp. 1951–1971.
- Chin, M., Diehl, T., Tan, Q., Prospero, J.M., Kahn, R.A., Remer, L.A., Yu, H., Sayer, A.M., Bian, H., Geogdzhayev, I. V., Holben, B.N., Howell, S.G., Huebert, B.J., Hsu, N.C., Kim, D., Kucsera, T.L., Levy, R.C., Mishchenko, M.I., Pan, X., Quinn, P.K., Schuster, G.L., Streets, D.G., Strode, S.A., Torres, O. & Zhao, X.-P. (2014). Multi-decadal aerosol variations from 1980 to 2009: a perspective from observations and a global model. *Atmospheric Chemistry and Physics*. 14 (7). p.pp. 3657–3690.
- Colette, A., Granier, C., Hodnebrog, Ø., Jakobs, H., Maurizi, A., Nyiri, A., Bessagnet, B., D'Angiola, A., D'Isidoro, M., Gauss, M., Meleux, F., Memmesheimer, M., Mieville, A., Rouïl, L., Russo, F., Solberg, S., Stordal, F. & Tampieri, F. (2011). Air quality trends in Europe over the past decade: a first multi-model assessment. *Atmospheric Chemistry and Physics*. 11 (22). p.pp. 11657–11678.
- Ervens, B. (2015). Modeling the Processing of Aerosol and Trace Gases in Clouds and Fogs. *Chemical Reviews*. 115. p.pp. 4157–4198.
- Fagerli, H. & Aas, W. (2008). Trends of nitrogen in air and precipitation: Model results and observations at EMEP sites in Europe, 1980–2003. *Environmental Pollution*. 154 (3). p.pp. 448–461.
- Faloona, I. (2009). Sulfur processing in the marine atmospheric boundary layer: A review and critical assessment of modeling uncertainties. *Atmospheric Environment*. 43 (18). p.pp. 2841–2854.

- Farina, S.C., Adams, P.J. & Pandis, S.N. (2010). Modeling global secondary organic aerosol formation and processing with the volatility basis set: Implications for anthropogenic secondary organic aerosol. *Journal of Geophysical Research*. 115 (D9). p.p. D09202.
- Folini, D. & Wild, M. (2011). Aerosol emissions and dimming/brightening in Europe: Sensitivity studies with ECHAM5-HAM. *Journal of Geophysical Research*. 116 (D21). p.p. D21104.
- Hansen, J., Sato, M., Ruedy, R., Kharecha, P., Lacis, A., Miller, R., Nazarenko, L., Lo, K., Schmidt, G.A., Aleinov, I., Russell, G., Baum, E., Bauer, S., Canuto, V., Cairns, B., Cheng, Y., Chandler, M., Cohen, A., Del Genio, A., Fleming, E., Faluvegi, G., Hall, T., Friend, A., Jonas, J., Jackman, C., Kelley, M., Koch, D., Kiang, N.Y., Lerner, J., Labow, G., Novakov, T., Menon, S., Perlwitz, J., Oinas, V., Perlwitz, J., Romanou, A., Rind, D., Shindell, D.T., Schmunk, R., Sun, S., Stone, P., Tausnev, N., Streets, D., Thresher, D., Zhang, S., Unger, N. & Yao, M. (2007). Climate simulations for 1880 – 2003 with GISS modelE. *Climate Dynamics*. 29 (7-8). p.pp. 661–696.
- Heald, C.L. & Spracklen, D. V. (2009). Atmospheric budget of primary biological aerosol particles from fungal spores. *Geophysical Research Letters*. 36 (April). p.p. L09806.
- Hodzic, A., Madronich, S., Bohn, B., Massie, S., Menut, L. & Wiedinmyer, C. (2007). Wildfire particulate matter in Europe during summer 2003: meso-scale modeling of smoke emissions, transport and radiative effects. *Atmospheric Chemistry and Physics*. 7 (15). p.pp. 4043–4064.
- Koch, D., Bauer, S.E., Del Genio, A., Faluvegi, G., McConnell, J.R., Menon, S., Miller, R.L., Rind, D., Ruedy, R., Schmidt, G. a. & Shindell, D.T. (2011). Coupled Aerosol-Chemistry–Climate Twentieth-Century Transient Model Investigation: Trends in Short-Lived Species and Climate Responses. *Journal of Climate*. 24 (11). p.pp. 2693–2714.
- Kloster, S., Dentener, F., Feichter, J., Raes, F., van Aardenne, J., Roeckner, E., Lohmann, U., Stier, P. & Swart, R. (2008). Influence of future air pollution mitigation strategies on total aerosol radiative forcing. *Atmospheric Chemistry and Physics*. 8 (21). p.pp. 6405–6437.
- Langmann, B., Varghese, S., Marmer, E., Vignati, E., Wilson, J., Stier, P. & O'Dowd, C. (2008). Aerosol distribution over Europe: a model evaluation study with detailed aerosol microphysics. *Atmospheric Chemistry and Physics*. 8 (6). p.pp. 1591–1607.

- Lee, L.A., Pringle, K.J., Reddington, C.L., Mann, G.W., Stier, P., Spracklen, D. V., Pierce, J.R. & Carslaw, K.S. (2013). The magnitude and causes of uncertainty in global model simulations of cloud condensation nuclei. *Atmospheric Chemistry and Physics*. 13 (17). p.pp. 8879–8914.
- Leibensperger, E.M., Mickley, L.J., Jacob, D.J., Chen, W.-T., Seinfeld, J.H., Nenes, A., Adams, P.J., Streets, D.G., Kumar, N. & Rind, D. (2012a). Climatic effects of 1950–2050 changes in US anthropogenic aerosols – Part 1: Aerosol trends and radiative forcing. *Atmospheric Chemistry and Physics*. 12 (7). p.pp. 3333–3348.
- Manders, A. M.M., van Meijgaard, E., Mues, A. C., Kranenburg, R., van Ulft, L.H. & Schaap, M. (2012). The impact of differences in large-scale circulation output from climate models on the regional modeling of ozone and PM. *Atmospheric Chemistry and Physics*. 12 (20). p.pp. 9441–9458.
- Pozzer, A., Zimmermann, P., Doering, U.M., van Aardenne, J., Tost, H., Dentener, F., Janssens-Maenhout, G. & Lelieveld, J. (2012). Effects of business-as-usual anthropogenic emissions on air quality. *Atmospheric Chemistry and Physics*. 12 (15). p.pp. 6915–6937.
- Redington, A.L., Derwent, R.G., Witham, C.S. & Manning, A.J. (2009). Sensitivity of modelled sulphate and nitrate aerosol to cloud, pH and ammonia emissions. *Atmospheric Environment*. 43 (20). p.pp. 3227–3234.
- Regayre, L.A., Pringle, K.J., Booth, B.B.B., Lee, L.A., Mann, G.W., Browse, J., Woodhouse, M.T., Rap, A., Reddington, C.L. & Carslaw, K.S. (2014). Uncertainty in the magnitude of aerosol-cloud radiative forcing over recent decades. *Geophysical Research Letters*. 41 (24). p.pp. 9040–9049.
- Roelofs, G.J., Kasibhatla, P., Barrie, L., Bergmann, D., Bridgeman, C., Chin, M., Christensen, J., Easter, R., Feichter, J., Jeuken, a, Kjellstrom, E., Koch, D., Land, C., Lohmann, U. & Rasch, P. (2001). Analysis of regional budgets of sulfur species modeled for the COSAM exercise. *Tellus Series B-Chemical and Physical Meteorology*. 53 (5). p.pp. 673–694.
- Shindell, D.T., Lamarque, J.-F., Schulz, M., Flanner, M., Jiao, C., Chin, M., Young, P.J., Lee, Y.H., Rotstayn, D., Mahowald, N., Milly, G., Faluvegi, G., Collins, W.J., Conley, A.J., Dalsoren, S., Easter, R., Ghan, S., Horowitz, L., Liu, X., Myhre, G., Nagashima, T., Naik, V., Rumbold, S.T., Skeie, R., Sudo, K., Szopa, S., Takemura, T., Voulgarakis, A., Yoon, J.-H. & Lo, F. (2013). Radiative forcing in the ACCMIP historical and future climate simulations. *Atmospheric Chemistry and Physics*. 13. p.pp. 2939–2974.

- Skeie, R.B., Berntsen, T.K., Myhre, G., Tanaka, K., Kvalevåg, M.M. & Hoyle, C.R. (2011). Anthropogenic radiative forcing time series from pre-industrial times until 2010. *Atmospheric Chemistry and Physics*. 11 (22). p.pp. 11827–11857.
- Spracklen, D. V., Jimenez, J.L., Carslaw, K.S., Worsnop, D.R., Evans, M.J., Mann, G.W., Zhang, Q., Canagaratna, M.R., Allan, J., Coe, H., McFiggans, G., Rap, A. & Forster, P. (2011). Aerosol mass spectrometer constraint on the global secondary organic aerosol budget. *Atmospheric Chemistry and Physics*. 11 (23). p.pp. 12109–12136.
- Textor, C., Schulz, M., Guibert, S., Kinne, S., Balkanski, Y., Bauer, S., Berntsen, T., Berglen, T., Boucher, O., Chin, M., Dentener, F., Diehl, T., Easter, R., Feichter, H., Fillmore, D., Ghan, S., Ginoux, P., Gong, S., Grini, a., Hendricks, J., Horowitz, L., Huang, P., Isaksen, I., Iversen, T., Kloster, S., Koch, D., Kirkevåg, a., Kristjansson, J.E., Krol, M., Lauer, a., Lamarque, J.F., Liu, X., Montanaro, V., Myhre, G., Penner, J., Pitari, G., Lamarque, J.F., Liu, X., Montanaro, V., Myhre, G., Penner, J., Pitari, G., Reddy, S., Seland, Ø., Stier, P., Takemura, T. & Tie, X. (2006). Analysis and quantification of the diversities of aerosol life cycles within AeroCom. *Atmospheric Chemistry and Physics*. 6. p.pp. 1777–1813.
- Tsigaridis, K., Daskalakis, N., Kanakidou, M., Adams, P.J., Artaxo, P., Bahadur, R., Balkanski, Y., Bauer, S.E., Bellouin, N., Benedetti, A., Bergman, T., Berntsen, T.K., Beukes, J.P., Bian, H., Carslaw, K.S., Chin, M., Curci, G., Diehl, T., Easter, R.C., Ghan, S.J., Gong, S.L., Hodzic, A., Hoyle, C.R., Iversen, T., Jathar, S., Jimenez, J.L., Kaiser, J.W., Kirkevåg, A., Koch, D., Kokkola, H., Lee, Y.H., Lin, G., Liu, X., Luo, G., Ma, X., Mann, G.W., Mihalopoulos, N., Morcrette, J.-J., Müller, J.-F., Myhre, G., Myriokefalitakis, S., Ng, N.L., O'Donnell, D., Penner, J.E., Pozzoli, L., Pringle, K.J., Russell, L.M., Schulz, M., Sciare, J., Seland, Ø., Shindell, D.T., Sillman, S., Skeie, R.B., Spracklen, D., Stavrakou, T., Steenrod, S.D., Takemura, T., Tiitta, P., Tilmes, S., Tost, H., van Noije, T., van Zyl, P.G., von Salzen, K., Yu, F., Wang, Z., Zaveri, R.A., Zhang, H., Zhang, K., Zhang, Q. & Zhang, X. (2014). The AeroCom evaluation and intercomparison of organic aerosol in global models. *Atmospheric Chemistry and Physics*. 14 (19). p.pp. 10845–10895.
- Volkamer, R., Jimenez, J.L., San Martini, F., Dzepina, K., Zhang, Q., Salcedo, D., Molina, L.T., Worsnop, D.R. & Molina, M.J. (2006). Secondary organic aerosol formation from anthropogenic air pollution: Rapid and higher than expected. *Geophysical Research Letters*. 33 (17). p.p. L17811.
- Wang, Y., Zhang, Q. Q., He, K., Zhang, Q. and Chai, L.: Sulfate-nitrate-ammonium aerosols over China: response to 2000–2015 emission changes of sulfur dioxide,

nitrogen oxides, and ammonia, *Atmos. Chem. Phys.*, 13(5), 2635–2652, doi:10.5194/acp-13-2635-2013, 2013.

## Appendix A Supplementary material for Chapter 4

### Supplementary Figures

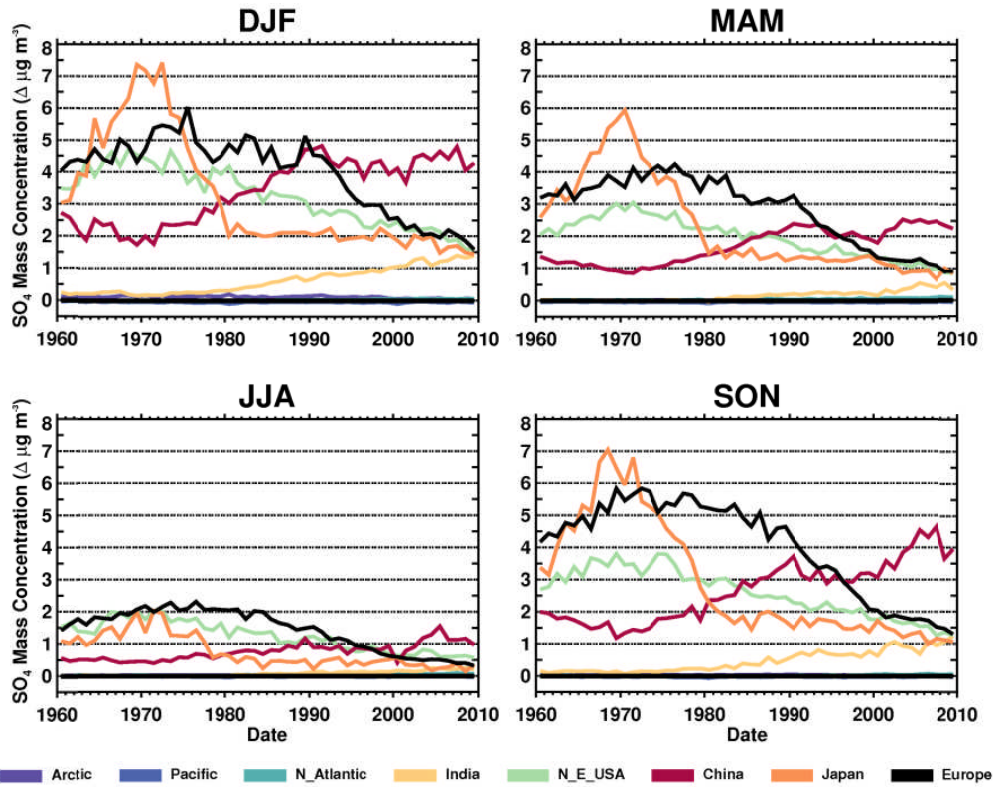


**Figure A1** – Seasonal mean values of the difference in the total column burden of SO<sub>4</sub> between the pH 6.5 and pH 5.0 simulations across different regions, as defined in Figure A4

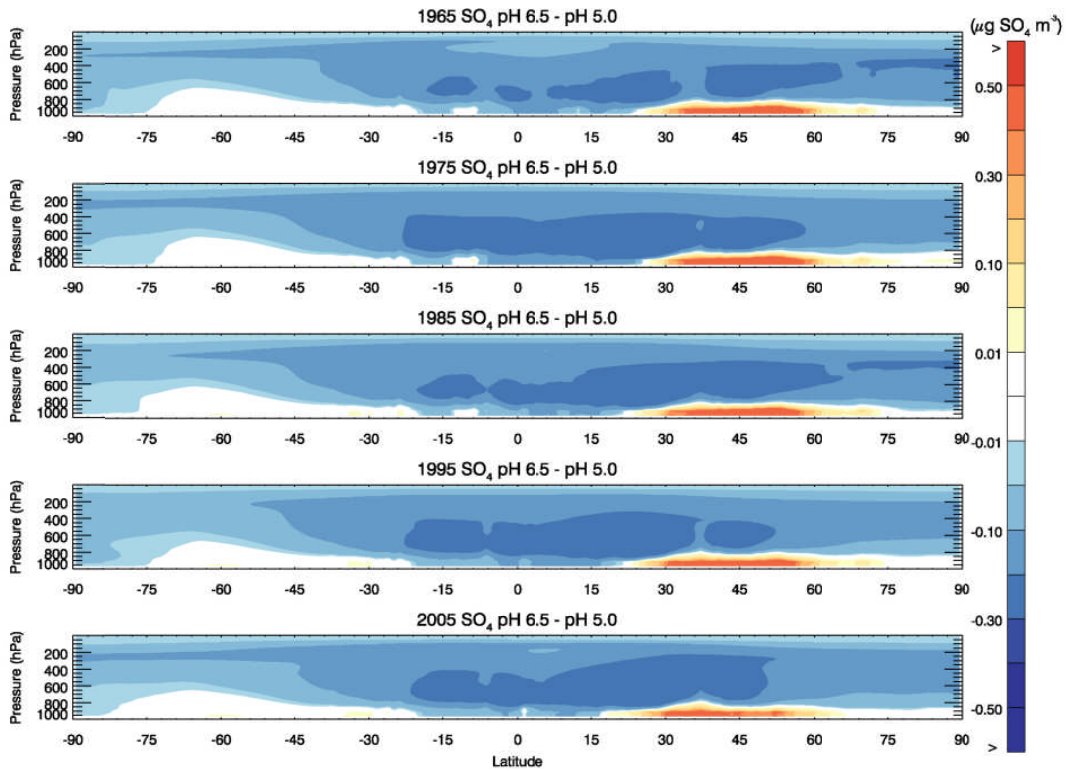


**Figure A2** – Zonal mean plot of the difference between the sulphate aerosol mass concentrations in the pH 6.5 and pH 5.0 simulations

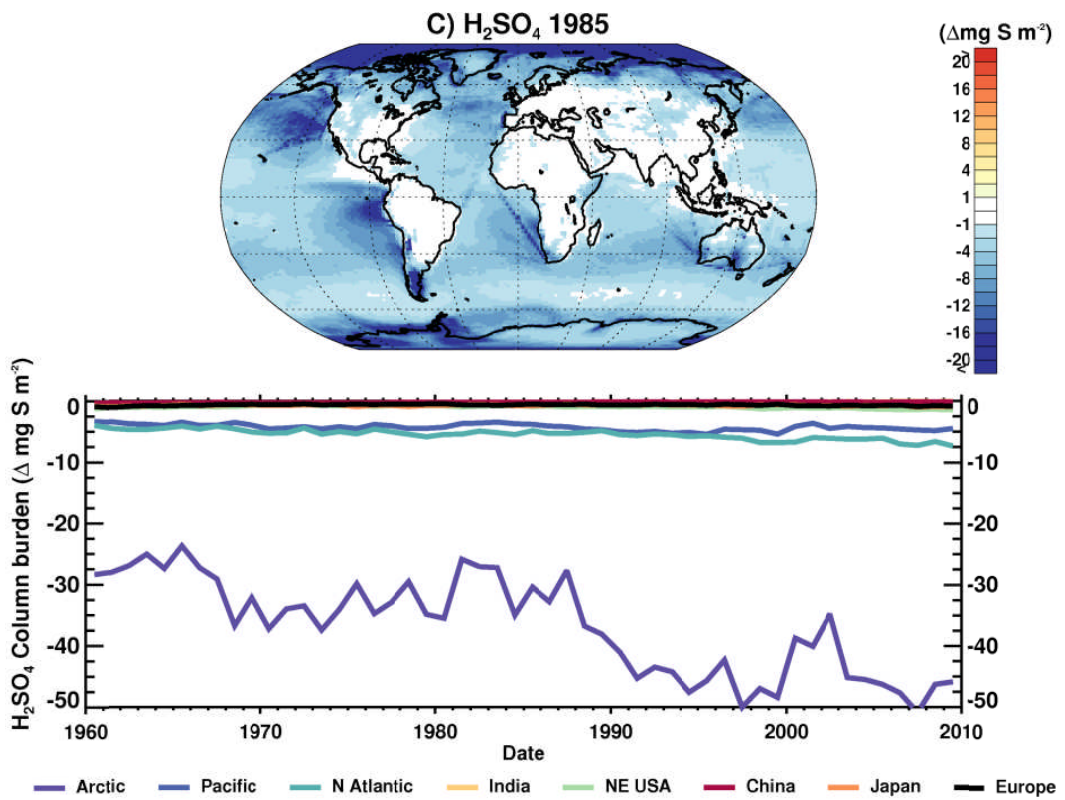


**Figure A3** – Difference in column burden of sulfuric acid vapour ( $\text{H}_2\text{SO}_4$ ) between the pH 6.5 and pH 5.0 simulations for 1985. The time series shows the temporal evolution of the difference in column burdens over the regions defined in Figure A4.

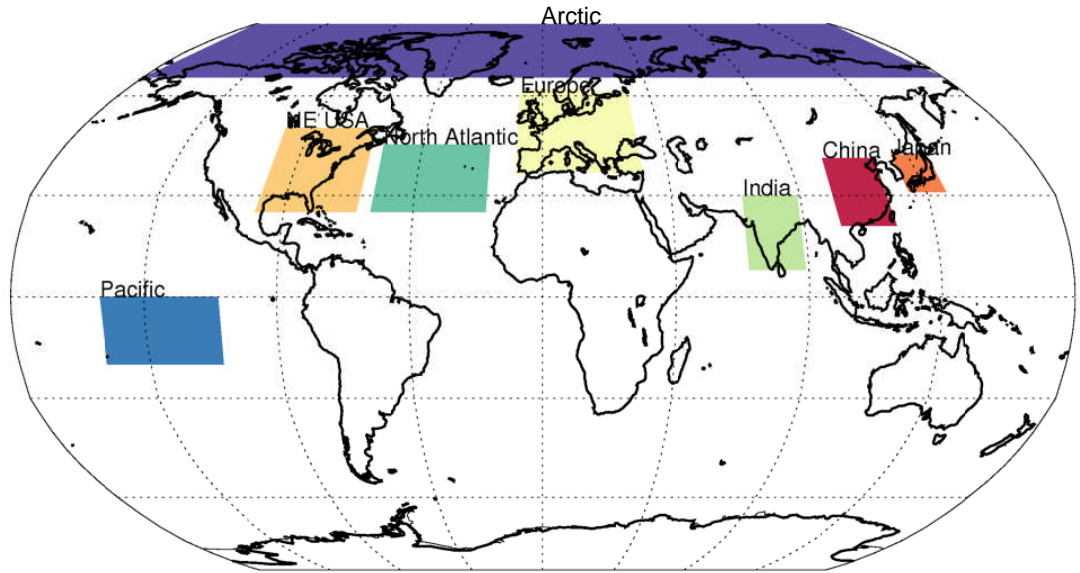


Figure A4 – Regional domains

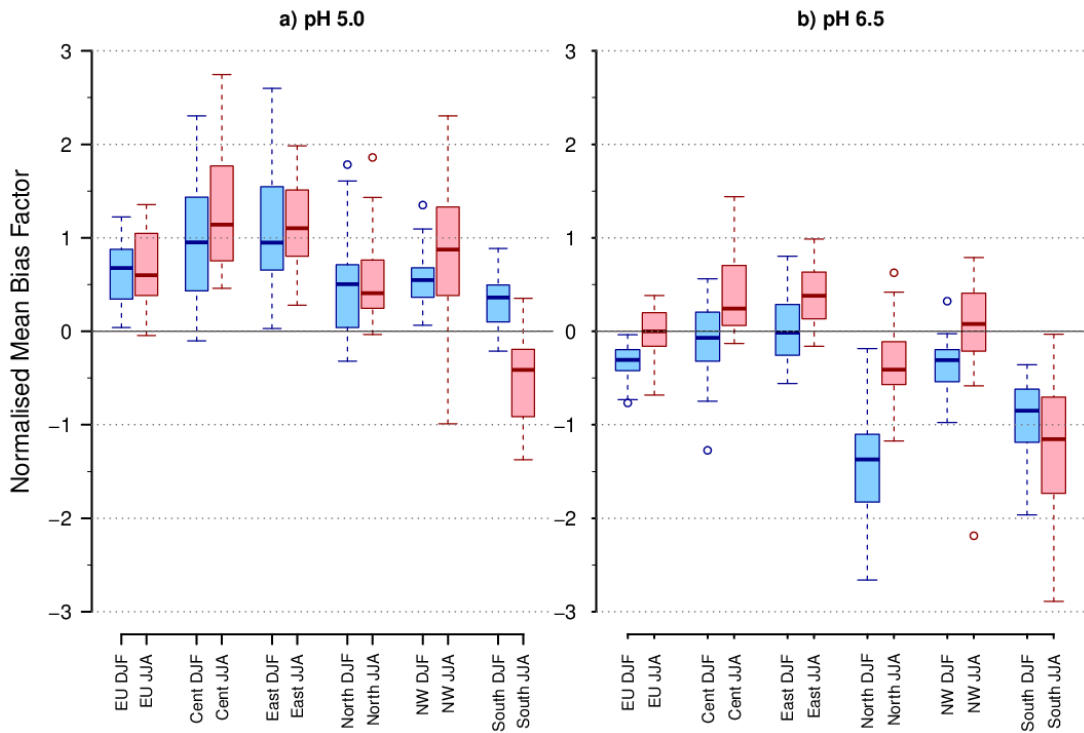
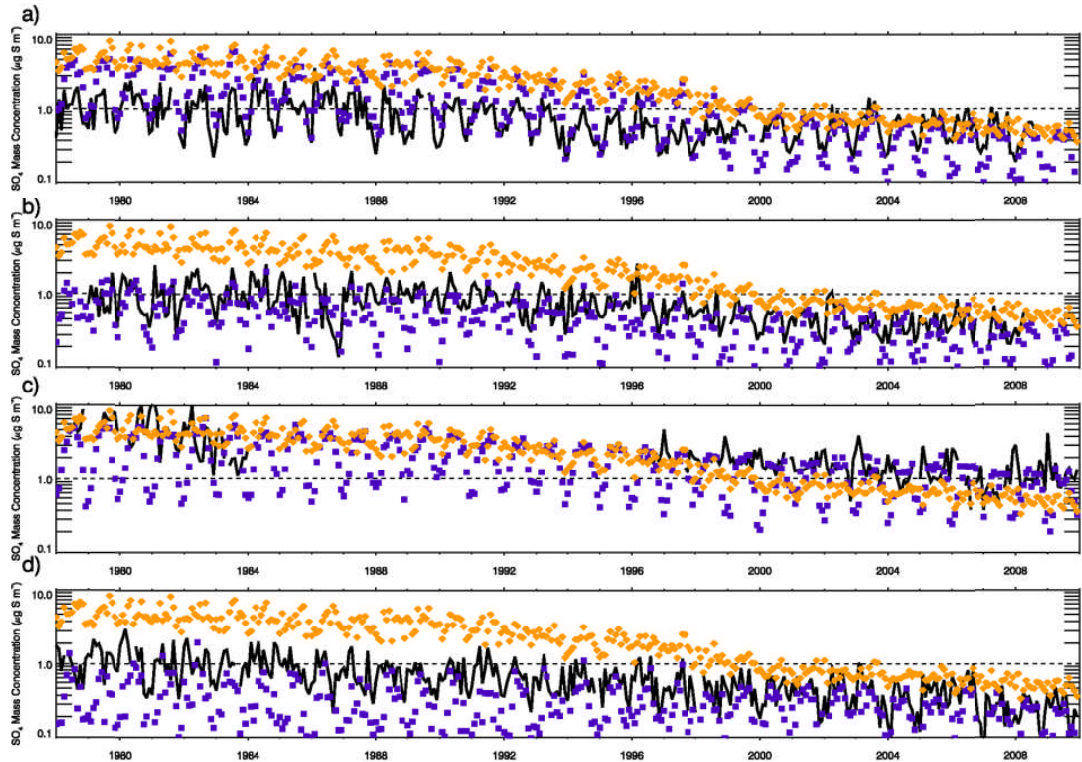
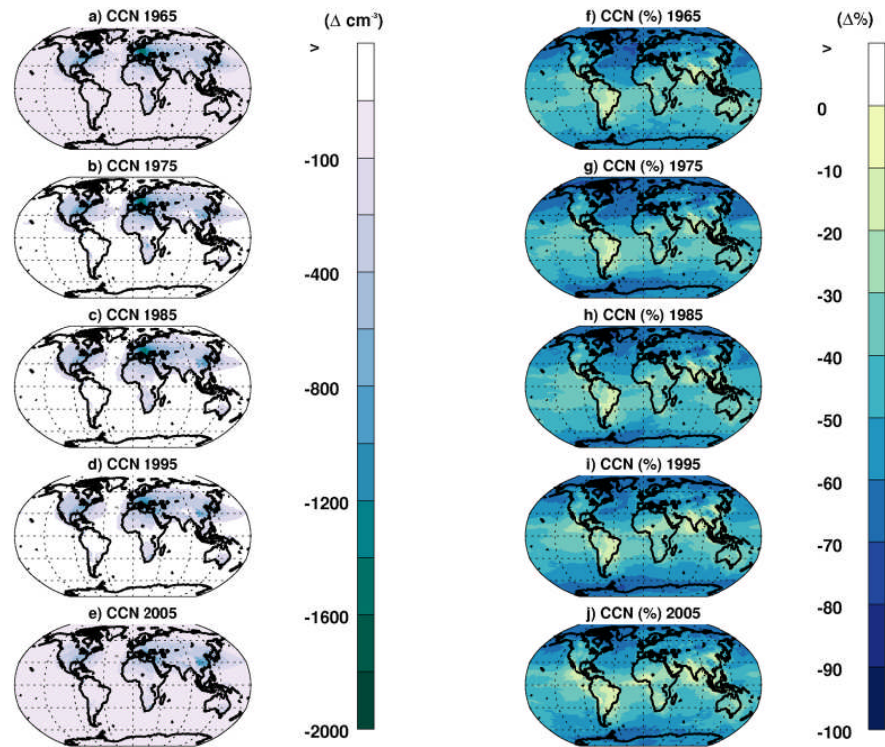


Figure A5 – NMBF of modelled vs observed SO<sub>2</sub> mass concentrations across EMEP sites between 1978 and 2010 for the two different simulations.



**Figure A6** – Observed and simulated (pH 5.0, purple and pH 6.5, orange) SO<sub>4</sub> at a) Schauinsland (Germany), b) Eskdalemuir (UK), c) K-pusztá (Hungary) and d) Birkenes (Norway) monitoring locations.



**Figure A7** – Absolute and percentage change in CCN concentrations (defined as particles greater than 50 nm diameter at 850 hPa in the atmosphere) between the pH 6.5 and pH 5 simulations for the years 1965, 1975, 1985, 1995 and 2005

## Supplementary Tables

**Table A1** –Summary of the representation of aqueous phase oxidation in numerous global composition climate models (information reproduced from Ervens, 2015)

Model	S(IV) Oxidants	Assumptions on partitioning, pH	Cloud properties	Resolution	Chem/Met Coupling
GEOS-CHEM	H <sub>2</sub> O <sub>2</sub> , O <sub>3</sub>	Thermodynamic eqm, pH=4.5	LWC = f(T)	2° lon X 2.5° lat; 48 vertical; chem sims on 4° X 5° grid; aerosol on 2° X 2.5°	Coupled aerosol/oxidant simulations
GOCART	H <sub>2</sub> O <sub>2</sub>	SO <sub>4</sub> formation – f([H <sub>2</sub> O <sub>2</sub> ]gas, cloud fraction)	LWC derived based on cloud fraction	2° lon X 2.5° lat; 46 vertical (0.1 mbar)	Online
Oslo CTM2	H <sub>2</sub> O <sub>2</sub> , O <sub>3</sub> , HNO <sub>4</sub>	Thermodynamic eqm, pH=4.5	Liquid water from Met fields	5.626° X 5.625°; 19 vertical up to 10 hPa	5 min chem; 60 min for transport; can be run online or offline
GISS	H <sub>2</sub> O <sub>2</sub>	Thermodynamic eqm, semi-prognostic H <sub>2</sub> O <sub>2</sub>	Prognostic cloud water prediction, cloud fraction diagnostically determined	4° lon X 5° lat; 9 vertical;	Decoupled chem with semi prognostic H <sub>2</sub> O <sub>2</sub>
MOZART	H <sub>2</sub> O <sub>2</sub> , O <sub>3</sub>	pH based on charge balance	Cloud water content prognostically predicted	2.8° lon X 2.8° lat	Couple aerosol module; offline photolysis rates
NARCM	H <sub>2</sub> O <sub>2</sub> , O <sub>3</sub>	Thermodynamic eqm, pH based on charge balance	Prognostic LWC prediction, Nd is related to sulphate mass; simulated aerosol size distribution	145Km spacing; 22 vertical levels up to 14 hPa	Offline

Model	S(IV) Oxidants	Assumptions on partitioning, pH	Cloud properties	Resolution	Chem/Met Coupling
ECHAM5 -HAM	H <sub>2</sub> O <sub>2</sub> , O <sub>3</sub>	pH based on initial aerosol in small and large drops respectively	Average drop sizes (2 classes) based on LWC and drop number concentration; 7 internally and externally mixed aerosol modes	300km X 300km; 5.6° X 5.6°; 19 vertical layers to 10 hPa	Online, fully coupled
TM4 and TM5	H <sub>2</sub> O <sub>2</sub> , O <sub>3</sub>	Thermodynamic eqm, pH=5.0	Fixed drop size (8µm); 7 aerosol modes	Standard resolution 3° X 2°; nested chem 1° X 1°	Offline
ECHAM5 /MESSy1	H <sub>2</sub> O <sub>2</sub> , O <sub>3</sub> , CH <sub>3</sub> OOH – details aqueous phase chem	Kinetic uptake; pH based on explicit aqueous phase chem	Monodisperse drop distribution	2.8° lon X 2.8° lat; 90 vertical layers up to 0.01 hPa	offline

**Table A2** – Global burdens of SO<sub>2</sub>, H<sub>2</sub>SO<sub>4</sub> and SO<sub>4</sub> in the pH 5.0 and pH 6.5 simulations

Year	SO <sub>2</sub> (Tg S)			H <sub>2</sub> SO <sub>4</sub> (Tg S)			SO <sub>4</sub> (Tg S)		
	pH 5.0	pH 6.5	pH 6.5 – pH 5.0	pH 5.0	pH 6.5	pH 6.5 – pH 5.0	pH 5.0	pH 6.5	pH 6.5 – pH 5.0
1965	0.34	0.12	-0.22 (-65%)	4.3E-5	3.1E-5	-1.2E-5 (-28%)	0.52	0.37	-0.15 (-29%)
1975	0.35	0.12	-0.23 (-66%)	4.7E-5	3.2E-5	-1.5E-5 (-32%)	0.60	0.41	-0.19 (-32%)
1985	0.35	0.12	-0.23 (-66%)	4.3E-5	3.1E-5	-1.2E-5 (-28%)	0.60	0.43	-0.17 (-28%)
1995	0.31	0.11	-0.20 (-65%)	4.4E-5	3.0E-5	-1.4E-5 (-32%)	0.64	0.46	-0.18 (-28%)
2005	0.31	0.12	-0.19 (-61%)	4.5E-5	3.1E-5	-1.4E-5 (-31%)	0.65	0.45	-0.20 (-31%)

**Table A3** – Difference between the pH 6.5 and pH 5.0 simulations in the fluxes of the sulphur budget (Tg S) within each mode for the mid-year of the hindcast period, 1985. Values in parenthesis are percentage difference.

Mode	Total	Nucl	Cond	In-cloud H <sub>2</sub> O <sub>2</sub>	In-cloud O <sub>3</sub>	Cloud Processing	Coagulation	Mode Merging	Dry Deposition	Nucl Scav	Impact Scav	Lifetime (days)
Nucleation	-0.001 (-58)	-0.03 (-77)	-0.1 (-69)	N/A	N/A	N/A	To Acc -0.03 (-73) To Cor -0.01 (-49)	-0.04 (-62)	-0.001 (-58)	N/A	N/A	+0.8
Aitken Soluble	-0.17 (-64)	N/A	-2.3 (-63)	N/A	N/A	-1.4 (-64)	To Acc -0.19 (-66) To Cor -0.001 (-34)	-0.56 (-59)	-0.17 (-55)	N/A	N/A	-1.2
Accumulation	-0.007 (-2)	N/A	-1.7 (-51)	-4.7 (-96)	+12.1 (+299)	-1.4 (-64)	To Cor +0.001 (+119)	+1.2 (+1055)	+0.25 (+24)	+2.0 (+14)	+0.11 (+44)	-1.4
Coarse	+0.012 (+312)	N/A	-0.03 (-23)	-0.02 (-83)	+0.4 (+2660)	N/A	N/A	N/A	+0.16 (+162)	+1.3 (+492)	+0.02 (+143)	-0.3

Nucl – Nucleation, Cond – condensation, Scav – Scavenging, Acc – Accumulation, Cor - Coarse

**Table A4** – Mean values of Aerosol Radiative Effect (ARE) and Aerosol Radiative Forcings (ARF) from pH 5.0 and pH 6.5 simulations and over different time periods.

	Region	1970 ARE		$\Delta$ 1970 ARE pH 6.5 – pH 5.0	2009 ARE		$\Delta$ 2009 ARE pH 6.5 – pH 5.0	$\Delta$ ARF pH 5.0 2009 - 1970	$\Delta$ ARF pH 6.5 2009 - 1970	$\Delta$ ARF 2009 pH 6.5 – 1970 pH 5.0	$\Delta$ ARF 2009 pH 5.0 – 1970 pH 6.5
		pH 5.0	pH 6.5		pH 5.0	pH 6.5					
All-Sky	Global	+ 3.6	+ 6.0	+ 2.4	+ 4.0	+ 6.3	+ 2.3	+0.4	+0.3	+ 2.7	- 2.0
	Europe	- 4.3	- 1.7	+ 2.6	- 0.2	+ 2.7	+ 2.9	+4.1	+4.4	+ 7.0	+ 1.5
	NE USA	-3.6	-0.8	+2.8	+1.9	+5.5	+3.6	+5.5	+6.3	+9.1	+1.8
	N Atlantic	+ 0.03	+ 6.3	+ 6.3	+ 1.7	+ 6.9	+ 5.2	+1.67	+0.3	+ 6.9	- 4.6
	Arctic	+4.6	+5.5	+0.9	+6.0	+6.8	+0.8	+1.4	+1.3	+2.2	+0.5
	China	+ 2.9	+ 7.2	+ 4.3	- 4.0	- 1.2	+ 2.8	-6.9	-8.4	- 4.1	- 11.2
Clear-Sky	Global	- 3.2	- 3.0	+ 0.2	- 3.2	- 2.9	+ 0.3	0.0	+0.1	+ 0.2	- 0.3
	Europe	- 9.9	- 11.7	- 1.8	- 5.4	- 5.8	- 0.4	+4.5	+5.9	+ 4.1	+6.3
	NE USA	-9.0	-10.0	-1.0	-4.5	-4.7	-0.2	+4.5	+5.3	+4.3	+5.5
	N Atlantic	- 5.4	- 4.8	+ 0.6	- 4.4	- 3.9	+ 0.5	+1.0	+0.9	+ 1.5	+ 0.4
	Arctic	-1.1	-0.8	+0.3	-0.8	-0.6	+0.2	+0.3	+0.2	+0.5	0.0
	China	- 6.2	- 6.4	- 0.2	- 12.7	- 13.7	- 1.0	-6.5	-7.3	- 7.5	- 6.3

**Appendix B**  
**Supplementary Material for Chapter 5**

# The impact of European legislative and technology measures to reduce air pollutants on air quality, human health and climate

S T Turnock<sup>1</sup>, E W Butt<sup>1</sup>, T B Richardson<sup>1</sup>, G W Mann<sup>1,2</sup>, C L Reddington<sup>1</sup>, P M Forster<sup>1</sup>, J Haywood<sup>3</sup>, M Crippa<sup>4</sup>, G Janssens-Maenhout<sup>4</sup>, C. E. Johnson<sup>3</sup>, N. Bellouin<sup>5</sup>, K S Carslaw<sup>1</sup> and D V Spracklen<sup>1</sup>

<sup>1</sup> Institute of Climate and Atmospheric Science, School of Earth and Environment, University of Leeds, Leeds, UK

<sup>2</sup> National Centre for Atmospheric Science, University of Leeds, Leeds, UK

<sup>3</sup> Met Office, Fitzroy Road, Exeter, Devon, UK

<sup>4</sup> European Commission, Joint Research Centre, Institute for Environment and Sustainability, Air and Climate Unit, Via Fermi, 2749. 21027 Ispra, Italy

<sup>5</sup> Department of Meteorology, University of Reading, Reading, UK

## SUPPLEMENTARY MATERIAL

### METHODS

#### 1 HadGEM3-UKCA Model Set up

We used the HadGEM3-UKCA chemistry-climate model to simulate the impact of different emission scenarios on global aerosol concentrations and their interaction with the Earth's radiative balance. The simulations were performed using an atmosphere only configuration of the model at a resolution of 1.875° by 1.275° in the horizontal (approximately 140 km at mid latitudes) and 63 vertical levels (up to 40 km). 3-D monthly mean fields of aerosols and radiation were output over a 5 year period to account for meteorological variability, but using the same single year of emissions in each. The ERA-Interim reanalysis fields (Dee et al., 2011) for 2005-2009 were used to nudge the 3-D meteorological fields within HadGEM3-UKCA at 6-hourly intervals. The sea ice and sea surface temperature are prescribed from CMIP5 (Hurrell et al., 2008).

The coupling of chemistry and aerosols into HadGEM3-UKCA is described by Morgenstern et al. (2009) and O'Connor et al. (2014). Tropospheric chemistry reactions involving O<sub>3</sub>-HO<sub>x</sub>-NO<sub>x</sub>-VOC (O'Connor et al., 2014) and sulphur species (Mann et al., 2010) are included in the model. The aerosol size distribution is simulated using a two-moment modal scheme with five log-normal modes and four chemical components (sulphate, BC, POM and sea salt). The model simulates the interactions of various aerosol processes including particle formation, cloud processing, hygroscopic growth, coagulation, condensation, deposition and scavenging. Mineral dust aerosol is simulated using the 6 bin Woodward (2001) scheme. There is no representation of ammonium nitrate in this model version.

Changes in the Earth's radiative balance are calculated using the Edwards & Slingo (1996) radiation code within HadGEM3-UKCA. A 'double-call' radiation configuration has been used in these simulations, where the radiation scheme is called twice; once with modelled aerosol fields included and the other with an aerosol-free atmosphere (an aerosol climatology is used to define cloud drop concentrations) (Bellouin et al., 2013; Turnock et al., 2015). An aerosol

radiative effect (RE), from aerosol radiation interactions (ari, direct effect) and aerosol cloud interactions (aci, 1<sup>st</sup> indirect effect), is calculated as the difference between monthly mean values in each call at both top-of-atmosphere (TOA) and surface. The change in aerosol RE due to the inclusion of air pollutant mitigation is calculated as the difference in aerosol RE between the two simulations using the different anthropogenic emissions. The ‘double-call’ radiation configuration does not allow changes to the radiative balance to feed back onto the meteorology and therefore rapid adjustments of the atmosphere and clouds due to changes in aerosols are not accounted for. However, based on the transient climate response to forcing and the atmospheric energy budget we have estimated the temperature and precipitation response due to the calculated difference in aerosol radiative effect between the two simulations (see supplementary methods section 4).

Natural emissions of aerosols from sea-salt, tropospheric volcanoes and dimethyl sulphide are calculated using interactive parameterisations or represented as monthly mean fields (see Turnock et al. 2015 for details). These emissions, along with the meteorological fields, are the same in both simulations such that any changes in aerosols can be attributed to the different anthropogenic emissions used within each simulation.

The model has been previously shown to be able to adequately simulate changes in European annual mean surface concentrations of aerosol mass (Turnock et al., 2015), making it an appropriate model to use in assessing the regional impact of policy driven changes in anthropogenic emissions.

## 2 Health Effects Calculations

Concentration response functions (CRFs) for long-term exposure to PM<sub>2.5</sub> have been used to quantify the adverse health effects in terms of excess annual premature mortality. These functions provide assumed shape relationships between changes in long-term PM<sub>2.5</sub> concentration exposure and relative risk (RR) of disease within a given population. Until recently CRFs have previously been determined from North American epidemiological studies (e.g. Pope III, (2002)) where annual mean PM<sub>2.5</sub> concentrations were typically below 30 µg m<sup>-3</sup>. However, in densely populated areas of the world annual mean PM<sub>2.5</sub> concentrations regularly exceed 30 µg m<sup>-3</sup>. CRFs have traditionally been extrapolated using linear (Cohen et al., 2004) and log-linear (Ostro, 2004) models to capture RRs for populations across the full range of PM<sub>2.5</sub> exposures. However, these extrapolation models simulated RRs above the observed maximum which cannot be constrained using empirical evidence. Burnett et al., (2014) developed integrated exposure-response functions (IERs) to constrain the concentration response relationship at high PM<sub>2.5</sub> concentrations (>30 µg m<sup>-3</sup>) by using observed epidemiological meta-data of exposure from different combustion sources (e.g., ambient air pollution, household air pollution, second hand smoking and active smoking). We use the results of this study to simulate RRs for five different diseases (for adults ≥ 25 years of age: stroke, ischemic heart disease (IHD), chronic obstructive pulmonary disease (COPD) and lung cancer (LC); for infants ≤ 5 years of age: acute lower respiratory infection (ALRI)).

The IER of Burnett et al. (2014) describes the relative risk, RR, based on the PM<sub>2.5</sub> concentration, C:

$$RR(C) = 1 + \alpha \left[ 1 - \exp(-\gamma(C - C_0)^\delta) \right] \quad (1)$$

$$\text{for } C \leq C_0 \quad RR = 1$$

Where  $C_0$  is the minimum-risk  $PM_{2.5}$  concentration above which there is evidence indicating detrimental health impacts (range: 5.8–8.0  $\mu\text{g m}^{-3}$ ) and parameters  $\alpha$ ,  $\gamma$  and  $\delta$  determine the shape of the concentration response function for each disease.

Burnett et al., (2014) provides 1000 point estimates of  $C_0$ ,  $\alpha$ ,  $\gamma$  and  $\delta$  with age-specific estimates for both IHD and stroke. We developed a lookup table for each disease using the mean value RR corresponding to  $PM_{2.5}$  concentrations in the range of 0–200  $\mu\text{g m}^{-3}$  at 0.1  $\mu\text{g m}^{-3}$  increments. We also produce the median, 5<sup>th</sup>, 95<sup>th</sup> percentile RRs in order to capture the uncertainty range in the RR.

To calculate premature mortality for a baseline simulation, we used the attributable-fraction type relationship provided by Apte et al., (2015):

$$M_{i,j} = P_i \times \hat{I}_{j,k} \times (RR_j(C_i) - 1), \text{ where } \hat{I}_{j,k} = \frac{I_{j,k}}{\overline{RR}_{j,k}} \quad (2)$$

where,  $M$  is premature mortality in a particular age stratum ( $z$ ) for disease  $j$  due to  $PM_{2.5}$  in grid box  $i$  within country  $k$ . Note that as in Apte et al. (2015), we also omit population age stratum  $z$  for compaction of notation.  $P_i$  represents the population within each grid box  $i$ ,  $I_{j,k}$  is the baseline mortality rate for disease  $j$  in country  $k$ ,  $C_i$  represents the annual mean  $PM_{2.5}$  concentration within grid box  $i$  and  $RR_j(C_i)$  is the RR at concentration  $C_i$ .  $\overline{RR}_{j,k}$  represents the average population-weighted RR for disease  $j$  within country  $k$ , defined by Apte et al., (2015):

$$\overline{RR}_{j,k} = \frac{\sum_{i=1}^N P_i \times RR_j(C_i)}{\sum_{i=1}^N P_i} \quad (3)$$

The grouping of  $\hat{I}_{j,k} = I_{j,k} / \overline{RR}_{j,k}$  indicates the hypothetical underlying baseline mortality rate for country  $k$  if  $PM_{2.5}$  concentrations are reduced to that of the minimum risk within country  $k$ .

To calculate the change in mortality ( $\Delta M$ ) in grid box  $i$  and within country  $k$  under an emission scenario where  $PM_{2.5}$  concentrations are changed from  $C_i$  to an alternative concentration  $C_i^*$  without altering the underlying baseline mortality rate for disease  $j$ , we apply the relationship defined by Apte et al., (2015):

$$\Delta M_{i,j} = P_i \times \hat{I}_{j,k} \times (RR_j(C_i^*) - RR_j(C_i)) \quad (4)$$

The total change in mortality is obtained by summing over all the individual disease end points for each grid box within a region. Here  $C_i$  is the annual mean  $PM_{2.5}$  mass concentration ( $\mu\text{g m}^{-3}$ ) calculated using the REF 2010 emissions and  $C_i^*$  is the annual mean  $PM_{2.5}$  mass concentration ( $\mu\text{g m}^{-3}$ ) calculated using the NO-AQ emission scenario. For use in the calculation of human health effects the  $PM_{2.5}$  concentrations provided from the global model are assumed to represent the regional concentrations of an area when interpolated onto the finer resolution of the population grid data (~5 km). The global gridded population count data ( $P$ ) is obtained from the Gridded Population of the World Version 3 for the year 2010 (CIESIN, 2015). For year 2010 age specific population data, we use country level results taken from the United Nations World Population Prospects (UN, 2015). For year 2010 mortality data, we use country level results from the Global Burden of Disease study (GBD, 2012) that provides age- and cause-specific mortality data ( $I_{j,k}$ ) for the five diseases IHD, stroke, COPD, LC, ALRI.

The total change in mortality between 1970-74 and 2005-2009 was calculated by using equation (4) and the difference between annual mean  $PM_{2.5}$  concentrations over the period 1970-74 and 2005-2009 from Turnock et al. (2015).

An additional sensitivity scenario calculated the change in mortality between the PM<sub>2.5</sub> concentrations in the REF and NO-AQ simulations including an estimate of the enhanced contribution to PM<sub>2.5</sub> from urban areas over Europe. A comparison between the observed and simulated (REF) annual mean PM<sub>2.5</sub> concentrations across the capital cities of the 28 EU member states was undertaken. The magnitude of the discrepancy between the observations and model was used to enhance the amount of simulated PM<sub>2.5</sub> (in both the REF and NO-AQ) within the urban areas of the particular country (defined based on grid cells within the population data having a population density of larger than 1,000 people per km<sup>2</sup>) by either 5, 10, 15 or 20 µg m<sup>-3</sup>. The sensitivity of the calculated health impacts to the inclusion of the additional urban area PM<sub>2.5</sub> has been obtained by comparing the annual prevented premature mortalities from the difference between these simulations to that calculated without the urban PM<sub>2.5</sub> fraction included.

### **3 Economic Savings Calculations**

The impact on human health from poor air quality can also have a perceived economic effect on society. The concept of “value of a statistical life” (VSL) is used to calculate the economic benefit achieved from preventing premature deaths due to the improvements in air quality. The VSL is derived from surveys of individual’s willingness to pay (WTP) to maintain the current standard of life in the event of an increased level of risk to mortality (OECD, 2012; WHO Regional Office for Europe, 2015). The VSL is the WTP divided by the change in risk to mortality. This allows society to assign a monetary value to a particular health impact and the VSL is the aggregation of individual monetary values for small changes in the risk of mortality across an entire population.

The perceived economic benefits to society from the implementation of air pollution mitigation measures has been carried out in accordance with the methods and data within WHO Regional Office for Europe, (2015). The perceived economic benefits to society are calculated by multiplying country specific average adult VSL values for each of the EU member states in 2010 by the number of premature deaths prevented annually for each country due to air pollutant mitigation measures. The country specific VSL are based on studies by the Organisation for Economic Co-operation and Development (OECD), which provide a baseline VSL figure of US\$3 million as a starting point and are then adjusted for specific country differences in per capita income (per-capita GDP) and best-estimated income elasticity (Braathen, 2012; OECD, 2012, 2014; WHO Regional Office for Europe, 2015). The total economic benefits to society have also been calculated as a percentage of each country’s 2010 GDP values (World Bank, 2015).

## **4 Calculation of Climate response**

### *4.1 Temperature*

The change in European mean surface air temperature induced by the radiative forcing at the TOA over Europe from the reduction in aerosols due to air pollution mitigation measures is calculated using the values of regional climate response per unit local radiative forcing, as determined by Shindell & Faluvegi (2009). These values represent the change in surface air temperature in response to an applied radiative forcing over a defined latitudinal banding. They have recently been applied by Sand et al., (2015) in calculating the Arctic surface temperature response to regional changes in anthropogenic emissions. Shindell & Faluvegi (2009) investigated the sensitivity of regional climate to different types of radiative forcings (e.g. CO<sub>2</sub>,

aerosols, ozone) applied at different spatial locations and found that the extratropics have an increased sensitivity to applied local forcing.

Local climate response values of  $\sim 0.15 \text{ }^\circ\text{C}(\text{W m}^{-2})^{-1}$  for black carbon aerosols and  $\sim 0.25 \text{ }^\circ\text{C}(\text{W m}^{-2})^{-1}$  for sulphate aerosols are obtained over the latitudinal banding of  $28^\circ\text{N}$  to  $60^\circ\text{N}$  (values obtained from Figure 1 of Shindell & Faluvegi (2009)). Here we use a mean value of  $0.2 \pm 0.05 \text{ }^\circ\text{C}(\text{W m}^{-2})^{-1}$  to represent the local climate response (LCR) to an applied TOA aerosol radiative forcing ( $F_{TOA}$ ) over Europe. The change in European mean surface temperature ( $\Delta T$ ) is calculated in equation (5) by multiplying LCR by the TOA forcing ( $F_{TOA}$ ).

$$\Delta T = TCR \times F_{TOA} \quad (5)$$

The European aerosol all-sky TOA radiative forcing between the REF and NO-AQ simulations of  $+2.26 \text{ W m}^{-2}$  was used within equation 5 along with the LCR of  $0.2 \pm 0.05 \text{ }^\circ\text{C}(\text{W m}^{-2})^{-1}$  to calculate the response in European surface air temperature to this forcing. This represents the difference in European surface temperature that has occurred due to the changes in particulate matter from the implementation of air pollution mitigation measures.

#### 4.2 Precipitation

The estimated precipitation changes are calculated based on changes in the atmospheric energy budget. Global mean precipitation is tightly constrained by tropospheric cooling (Andrews et al., 2010; Richardson et al., 2015). Therefore, in response to an applied forcing over the troposphere (calculated as the RE at TOA minus RE at the surface,  $\Delta F_{atm}$ ) there is a rapid adjustment in precipitation due to the near-instantaneous change in tropospheric cooling, and an additional feedback driven by changes in surface air temperature (Andrews et al., 2010).

The rapid precipitation response to forcing in the mid-latitudes is dominated by changes in tropospheric cooling as circulation changes are small (Richardson et al., 2015). Therefore the European rapid precipitation response can be estimated based solely on the change in tropospheric cooling over Europe. This method neglects changes in sensible heat flux from the surface which would affect the atmospheric energy balance, and therefore also precipitation. The rapid adjustment in precipitation ( $\Delta P_{fast}$ ) is calculated using equation (6).

$$\Delta P_{fast} = \Delta F_{atm} \times C \quad (6)$$

The conversion factor (C) converts the atmospheric radiative forcing to precipitation units ( $\text{mm yr}^{-1}$ ) using the density of water ( $\rho_{water}$ ) and the latent heat of condensation for water ( $L_c$ ), and is given by:

$$C = \frac{365 \times 86400 \times 1000 / \rho_{water}}{L_c} \approx \frac{365}{29} \text{ mm yr}^{-1} \text{ W}^{-1} \text{ m}^2$$

Assuming no significant changes in circulation, the rapid precipitation response over Europe of  $13 \pm 0.8 \text{ mm yr}^{-1}$  is calculated by multiplying the  $\Delta F_{atm}$  over Europe ( $-1.04 \pm 0.06 \text{ W m}^{-2}$ ) by the conversion factor C.

Precipitation would be expected to further increase due to the radiative feedback response ( $\Delta P_{fb}$ ) induced by the temperature increase from the reduction in aerosols (Andrews et al., 2010). This is calculated using equation (7) by multiplying the precipitation feedback response per unit kelvin ( $\Delta P_{fb/k}$ ) value of  $2.49\% \text{ K}^{-1}$  from Andrews et al., (2010) by the estimated temperature change ( $\Delta T$ ). The error in the feedback response is based on the average regression error in Andrews et al., (2010) of  $0.5\% \text{ K}^{-1}$ . It is difficult to estimate how the precipitation

feedback response would manifest regionally without knowing the regional pattern of temperature change and therefore this has not been calculated for Europe.

$$\Delta P_{fb} = \Delta T \times \Delta P_{fb/k} \quad (7)$$

The calculated values of temperature and precipitation changes are fairly crude theoretical estimates. However, based on our physical understanding of how the climate responds to an applied radiative forcing it is highly likely that both temperature and precipitation have increased over Europe as a result of the aerosol reductions from the implemented air quality mitigation measures.

## SUPPLEMENTARY FIGURES

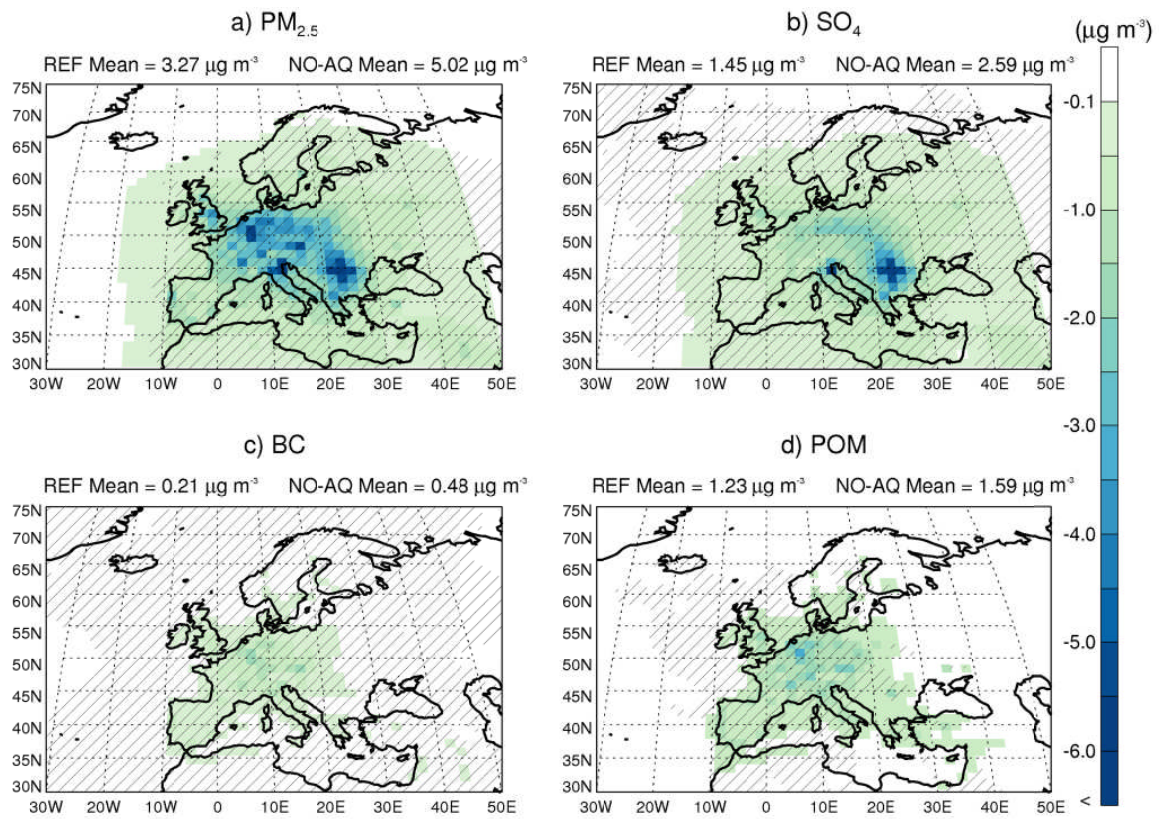


**Figure S1.** Absolute change in surface annual mean concentrations (averaged over 5 years) of a)  $\text{PM}_{2.5}$ , b) sulphate, c) black carbon and d) POM due to mitigation of air pollution. Absolute changes are calculated as the difference between the REF and NO-AQ simulations (i.e. REF-NOAQ). Stippling indicates regions where the difference is larger than the variability of the annual mean values (i.e. greater than two standard deviations of the annual mean). European mean concentrations for each scenario are calculated as mean values over the continental land mass within the domain  $10^\circ\text{W} - 36^\circ\text{E}$  and  $36^\circ\text{N} - 61^\circ\text{N}$ , and are detailed above each panel.

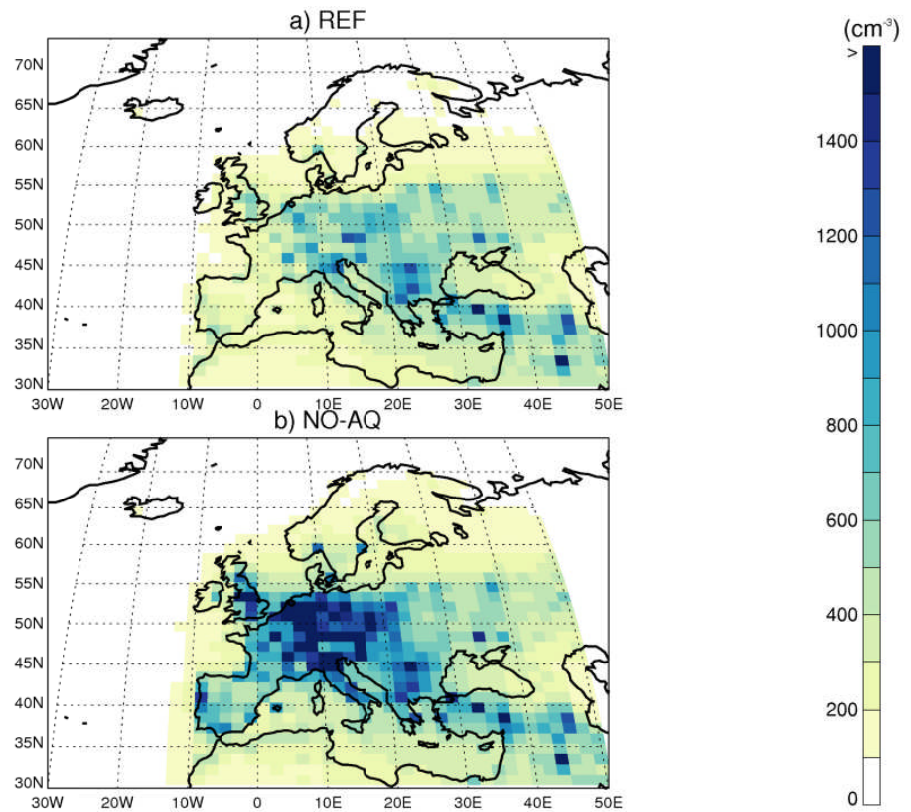


**Figure S2.** Total particle number concentration over Europe in the a) REF and b) NO-AQ scenarios.

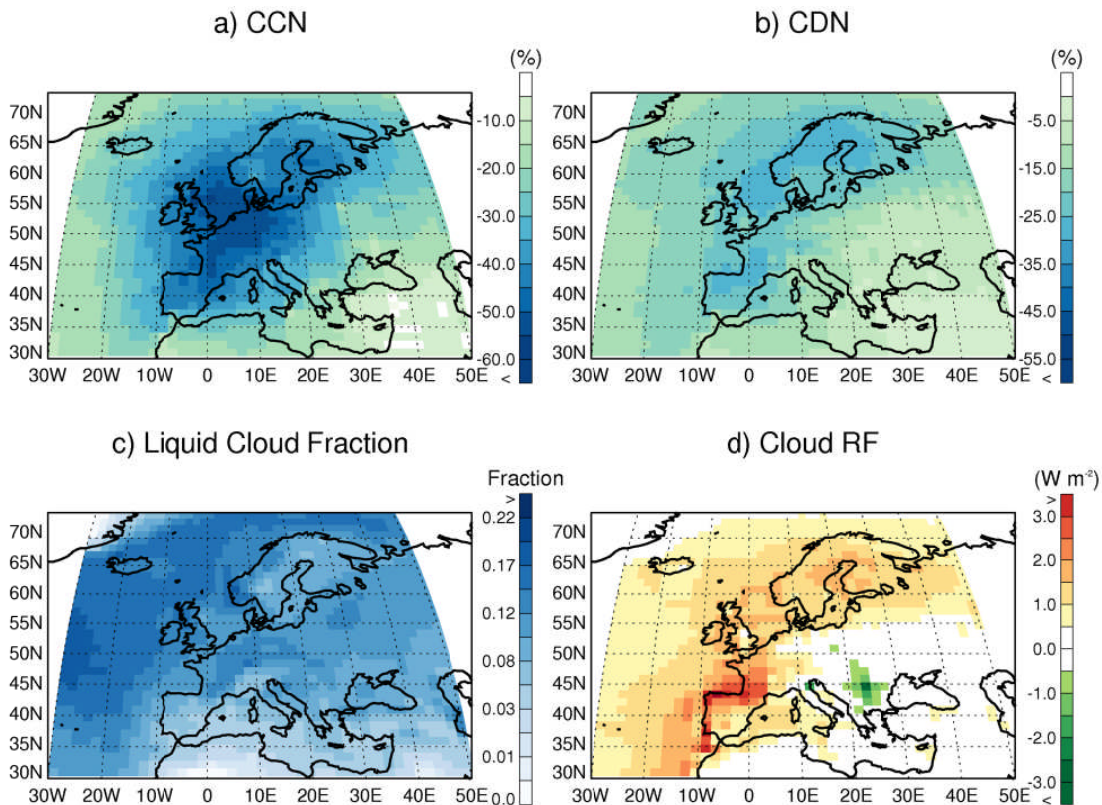


**Figure S3.** Percentage difference between the REF and NO-AQ simulations of annual mean (averaged over 5 years) a) cloud condensation nuclei concentrations (CCN) and b) cloud droplet number (CDN) concentrations at 850 hPa. c) annual mean liquid cloud fraction over the period 2005-2009 at 850 hPa. d) The change in annual mean cloud radiative effect at TOA (all-sky minus clear-sky) between the REF and NO-AQ simulations.

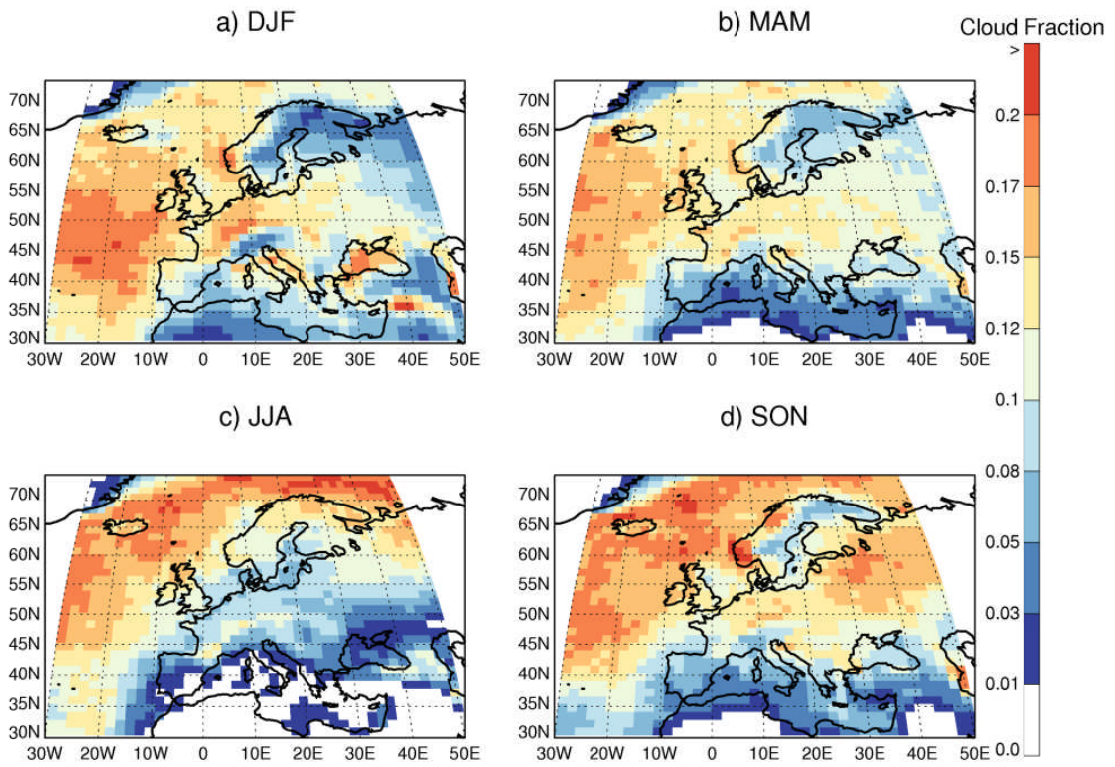


**Figure S4.** Simulated seasonal mean liquid cloud fraction at 850 hPa over Europe in the REF scenario for a) December January February, b) March April May, c) June July August and d) September October November

**SUPPLEMENTARY TABLES**

**Table S1.** Total European emissions of air pollutants from the energy, industrial, transport sectors (Crippa et al., 2015) in the REF and NO-AQ simulations. The total of all three sectors is calculated for each scenario. The absolute and relative differences in emissions between each scenario are calculated for each sector.

Air Pollutant	Sector	Total European Emission (Gg yr <sup>-1</sup> )		Absolute change (REF – NO-AQ) (Gg yr <sup>-1</sup> )	Percentage Change (%)
		REF	NO-AQ		
SO <sub>2</sub>	Total	6214	15570	-9356	-60
	Energy	5311	13021	-7710	-59
	Industrial	875	1570	-695	-44
	Transport	29	978	-949	-97
	Total	148	532	-384	-72
BC	Energy	7	48	-41	-85
	Industrial	18	36	-18	-50
	Transport	124	449	-325	-72
	Total	90	347	-257	-74
OC	Energy	6	43	-37	-86
	Industrial	21	52	-31	-60
	Transport	63	252	-189	-75

**Table S2.** Number of annually prevented premature deaths from all causes of disease across the 28 EU member states due to the reduction in PM<sub>2.5</sub> concentrations between the NO-AQ and REF simulations. The number of prevented premature deaths is also calculated using PM<sub>2.5</sub> concentrations that include an estimate of urban contribution to PM<sub>2.5</sub> in each country (+ Urban). Uncertainty estimates are represented by the 5th and 95<sup>th</sup> percentile values in the concentration response functions of each disease considered.

Country	Number of annual prevented premature deaths per year (all causes of disease)					
	Mean	Mean + Urban	5% C.I.	5% C.I. + Urban	95% C.I.	95% C.I. + Urban
<b>EU 15 Countries</b>						
Germany	24,450	14,372	7,664	4,971	45,315	26,933
France	6,209	4,011	1,592	1,663	12,141	7,256
Italy	6,268	4,928	4,573	3,343	6,641	6,300
Netherlands	3,254	1,710	1,110	792	4,946	2,725
Belgium	2,518	1,333	645	560	4,936	2,363
Luxembourg	110	79	44	37	193	128
Denmark	111	127	0	49	571	321
Ireland	0	53	0	40	0	58
UK	2,353	5,539	0	5,029	1,023	6,252
Greece	760	675	424	367	1,190	1,059
Spain	1,595	1,247	875	774	2,084	1,675
Portugal	1,094	767	559	494	1,018	798
Austria	1,826	1,407	1,317	866	2,173	1,926
Finland	0	26	0	17	0	40
Sweden	39	146	0	105	200	221
EU15 Total	50,587	36,420	18,803	19,105	82,431	58,056
<b>Additional Countries to make up EU Member States</b>						
Bulgaria	2,264	2,015	1,595	1,346	2,926	2,612
Croatia	685	564	670	445	652	699
Cyprus	9	8	6	5	16	13
Czech Republic	3,624	2,265	1,493	1,009	4,389	3,019
Estonia	0	18	0	19	0	19
Hungary	3,116	2,437	2,529	1,731	2,711	2,653
Latvia	0	45	0	20	0	79
Lithuania	14	93	0	48	16	157
Malta	3	3	2	1	5	4
Poland	8,660	5,763	4,691	2,866	10,390	8,128
Romania	8,986	7,883	6,166	4,973	10,359	10,276
Slovakia	2,034	1,382	1,181	790	1,691	1,363
Slovenia	267	219	239	163	254	268
Additional Total	29,661	22,693	18,573	13,415	33,407	29,290
EU28 Total	80,248	59,112	37,376	32,520	115,838	87,347

The impact of European measures to reduce air pollutants

**Table S3.** Economic savings across the EU member states from the value of a statistical life for each country (WHO Regional Office for Europe, 2015) and annual prevented premature deaths calculated from air pollution mitigation measures. These savings have been converted to a percentage of each country's 2010 GDP (World Bank, 2015). %5 C.I. and 95% C.I. are calculated based on the annual prevented premature deaths calculated using the respective confidence intervals in Table S2.

Country	Country Specific VSL (2010) US\$ (millions)	Economic cost of premature deaths from change in PM <sub>2.5</sub> Exposure 2010 US \$			Economic cost of premature deaths from change in PM <sub>2.5</sub> Exposure as a % of GDP (2010)
		Mean	5% C.I.	95% C.I.	
Austria	3.67	6,702	4,833	7,976	1.7
Belgium	3.50	8,812	2,258	17,276	1.8
Bulgaria	1.77	4,007	2,824	5,178	8.2
Croatia	2.07	1,418	1,387	1,349	2.4
Cyprus	2.87	27	16	45	0.1
Czech Republic	2.75	9,966	4,107	12,070	4.8
Denmark	3.46	384	0	1,976	0.1
Estonia	2.27	0	0	0	0.0
Finland	3.32	0	0	0	0.0
France	3.16	19,620	5,030	38,367	0.7
Germany	3.48	85,085	26,671	157,697	2.5
Greece	2.82	2,142	1,195	3,355	0.7
Hungary	2.32	7,228	5,866	6,288	5.6
Ireland	3.75	0	0	0	0.0
Italy	2.92	18,303	13,354	19,391	0.9
Latvia	2.10	0	0	0	0.0
Lithuania	2.15	29	0	34	0.1
Luxembourg	6.28	693	277	1,211	1.3
Malta	2.65	9	4	13	0.1
Netherlands	3.76	12,236	4,173	18,596	1.5
Poland	2.10	18,186	9,852	21,820	3.8
Portugal	2.50	2,734	1,398	2,544	1.1
Romania	1.67	15,006	10,298	17,299	9.1
Slovakia	2.42	4,922	2,858	4,092	5.5
Slovenia	2.90	774	694	736	1.6
Spain	3.06	4,882	2,676	6,377	0.3
Sweden	3.50	136	0	700	0.0
United Kingdom	3.55	8,353	1	3,632	0.3
Total	3.60	231,654	99,772	348,022	1.4

## Supplementary References

Andrews, T., Forster, P. M., Boucher, O., Bellouin, N. and Jones, A.: Precipitation, radiative forcing and global temperature change, *Geophys. Res. Lett.*, 37(14), L14701, doi:10.1029/2010GL043991, 2010.

Apte, J. S., Marshall, J. D., Cohen, A. J. and Brauer, M.: Addressing Global Mortality from Ambient PM 2.5, *Environ. Sci. Technol.*, 49, 8057–8066, doi:10.1021/acs.est.5b01236, 2015.

Bellouin, N., Mann, G. W., Woodhouse, M. T., Johnson, C., Carslaw, K. S. and Dalvi, M.: Impact of the modal aerosol scheme GLOMAP-mode on aerosol forcing in the Hadley Centre Global Environmental Model, *Atmos. Chem. Phys.*, 13(6), 3027–3044, doi:10.5194/acp-13-3027-2013, 2013.

Braathen, N. A.: Valuation of human lives. Presentation at an informal joint workshop of the regulatory committee and the annual meeting of sustainable development experts on the role of impact assessments in policy making, Paris: Organisation for Economic Co-operation and Development. [online] Available from: ([www.oecd.org/gov/](http://www.oecd.org/gov/)), 2012.

Burnett, R. T., Arden Pope, C., Ezzati, M., Olives, C., Lim, S. S., Mehta, S., Shin, H. H., Singh, G., Hubbell, B., Brauer, M., Ross Anderson, H., Smith, K. R., Balmes, J. R., Bruce, N. G., Kan, H., Laden, F., Prüss-Ustün, A., Turner, M. C., Gapstur, S. M., Diver, W. R. and Cohen, A.: An integrated risk function for estimating the global burden of disease attributable to ambient fine particulate matter exposure, *Environ. Health Perspect.*, 122, 397–403, doi:10.1289/ehp.1307049, 2014.

CIESIN: Socioeconomic Data and Applications Centre, Gridded Population of the World (GPW), v3 [online] Data Collection, [online] Available from: <http://sedac.ciesin.columbia.edu/data/collection/gpw-v3> (Accessed 12 July 2013), 2015.

Cohen, A. J., Anderson, H. R., Ostro, B., Pandey, K. D., Krzyzanowski, M., Künzli, N., Gutschmidt, K., Iii, C. A. P., Romieu, I., Samet, J. M. and Smith, K. R.: Mortality Impacts of Urban Air Pollution, in *Comparative Quantification of Health Risks*, vol. 77, pp. 1353–1434., 2004.

Crippa, M., Janssens-Maenhout, G., Dentener, F., Guizzardi, D., Sindelarova, K., Muntean, M., Dingenen, R. Van and Granier, C.: Forty years of improvements in European air quality: the role of EU policy–industry interplay, *Atmos. Chem. Phys. Discuss.*, 15(14), 20245–20285, doi:doi:10.5194/acpd-15-20245-2015, 2015.

Dee, D. P., Uppala, S. M., Simmons, A. J., Berrisford, P., Poli, P., Kobayashi, S., Andrae, U., Balmaseda, M. A., Balsamo, G., Bauer, P., Bechtold, P., Beljaars, A. C. M., van de Berg, L., Bidlot, J., Bormann, N., Delsol, C., Dragani, R., Fuentes, M., Geer, A. J., Haimberger, L., Healy, S. B., Hersbach, H., Hólm, E. V., Isaksen, L., Kållberg, P., Köhler, M., Matricardi, M., McNally, A. P., Monge-Sanz, B. M., Morcrette, J.-J., Park, B.-K., Peubey, C., de Rosnay, P., Tavolato, C., Thépaut, J.-N. and Vitart, F.: The ERA-Interim reanalysis: configuration and performance of the data assimilation system, *Q. J. R. Meteorol. Soc.*, 137(656), 553–597, doi:10.1002/qj.828, 2011.

Edwards, J. M. and Slingo, A.: Studies with a flexible new radiation code. I: Choosing a configuration for a large-scale model, *Q. J. R. Meteorol. Soc.*, 122(531), 689–719, doi:10.1002/qj.49712253107, 1996.

GBD: Global Burden of Disease Study 2010 (GBD 2010) Results by Cause 1990–2010, Seattle, United States. [online] Available from: <http://ghdx.healthdata.org/record/global-burden-disease-study-2010-gbd-2010-results-cause-1990-2010>, 2012.

Hurrell, J. W., Hack, J. J., Shea, D., Caron, J. M. and Rosinski, J.: A New Sea Surface Temperature and Sea Ice Boundary Dataset for the Community Atmosphere Model, *J. Clim.*, 21(19), 5145–5153, doi:10.1175/2008JCLI2292.1, 2008.

Mann, G. W., Carslaw, K. S., Spracklen, D. V., Ridley, D. a., Manktelow, P. T., Chipperfield, M. P., Pickering, S. J. and Johnson, C. E.: Description and evaluation of GLOMAP-mode: a modal global aerosol microphysics

model for the UKCA composition-climate model, *Geosci. Model Dev.*, 3(2), 519–551, doi:10.5194/gmd-3-519-2010, 2010.

Morgenstern, O., Braesicke, P., O'Connor, F. M., Bushell, A. C., Johnson, C. E., Osprey, S. M. and Pyle, J. A.: Evaluation of the new UKCA climate-composition model – Part 1 : The stratosphere, *Geosci. Model Dev.*, 2, 43–57 [online] Available from: [www.geosci-model-dev.net/2/43/2009](http://www.geosci-model-dev.net/2/43/2009), 2009.

O'Connor, F. M., Johnson, C. E., Morgenstern, O., Abraham, N. L., Braesicke, P., Dalvi, M., Folberth, G. A., Sanderson, M. G., Telford, P. J., Voulgarakis, A., Young, P. J., Zeng, G., Collins, W. J. and Pyle, J. A.: Evaluation of the new UKCA climate-composition model – Part 2: The Troposphere, *Geosci. Model Dev.*, 7(1), 41–91, doi:10.5194/gmd-7-41-2014, 2014.

OECD: Mortality risk evaluation in environment, health and transport policies, Paris: Organisation for Economic Co-operation and Development., 2012.

OECD: The cost of air pollution: health impacts of road transport, Paris: Organisation for Economic Co-operation and Development., 2014.

Ostro, B.: Outdoor air pollution Assessing the environmental burden of disease at national and local levels, 2nd ed., edited by A. Prüss-Üstün, D. Campbell-Lendrum, C. Corvalán, and A. Woodward, World Health Organization (WHO Environmental Burden of Disease Series, No. 5), Geneva., 2004.

Pope III, C. A.: Lung Cancer, Cardiopulmonary Mortality, and Long-term Exposure to Fine Particulate Air Pollution, *JAMA*, 287(9), 1132, doi:10.1001/jama.287.9.1132, 2002.

Richardson, T., Forster, P., Andrews, T. and Parker, D.: Understanding the rapid precipitation response to CO<sub>2</sub> and Aerosol forcing on a regional scale, *J. Clim.*, in press, doi:10.1175/JCLI-D-15-0174.1, 2015.

Sand, M., Berntsen, T. K., von Salzen, K., Flanner, M. G., Langner, J. and Victor, D. G.: Response of Arctic temperature to changes in emissions of short-lived climate forcers, *Nat. Clim. Chang.*, advance on, doi:10.1038/nclimate2880, 2015.

Shindell, D. and Faluvegi, G.: Climate response to regional radiative forcing during the twentieth century, *Nat. Geosci.*, 2(4), 294–300, doi:10.1038/ngeo473, 2009.

Turnock, S. T., Spracklen, D. V., Carslaw, K. S., Mann, G. W., Woodhouse, M. T., Forster, P. M., Haywood, J., Johnson, C. E., Dalvi, M., Bellouin, N. and Sanchez-Lorenzo, a.: Modelled and observed changes in aerosols and surface solar radiation over Europe between 1960 and 2009, *Atmos. Chem. Phys.*, 15, 9477–9500, doi:10.5194/acp-15-9477-2015, 2015.

UN: World Population Prospects, the 2015 Revision. United Nations, Department of Economic and Social Affairs, Population Division, New York, USA. [online] Available from: <http://www.un.org/en/development/desa/population/events/other/10/index.shtml>, 2015.

WHO Regional Office for Europe, O.: Economic cost of the health impact of air pollution in Europe: Clean air, health and wealth., Copenhagen: WHO Regional Office for Europe., 2015.

Woodward, S.: Modeling the atmospheric life cycle and radiative impact of mineral dust in the Hadley Centre climate model, *J. Geophys. Res.*, 106(D16), 18155, doi:10.1029/2000JD900795, 2001.

World Bank: World Databank. World Development Indicators, Washingt. DC [online] Available from: <http://data.worldbank.org/indicator/NY.GDP.MKTP.CD> (Accessed 24 June 2015), 2015.